2008

JAEA R&D Review

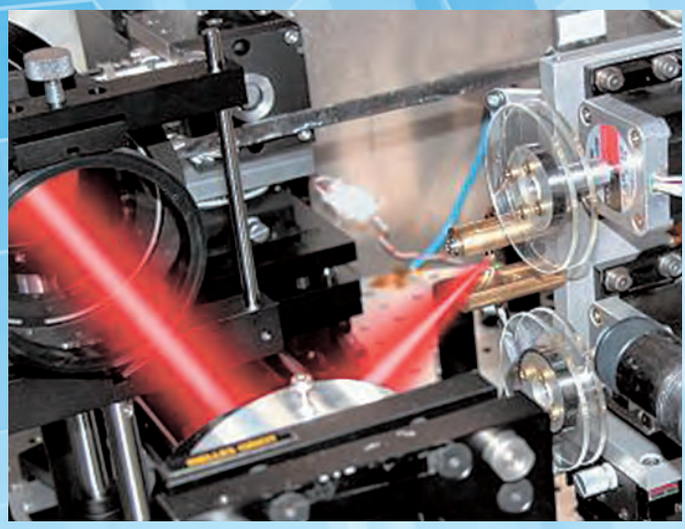

Compact Laser-driven Ion Accelerator

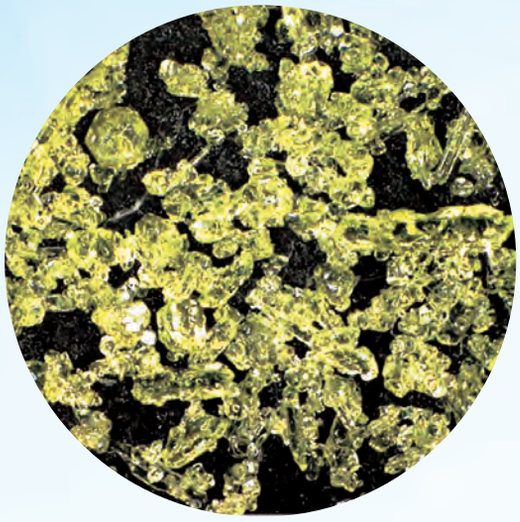

Crystals of Uranyl Nitrate

Message from the President

岡嶋俊雄

President Toshio Okazaki

Welcome to the third issue of the “JAEA R&D Review”, which will inform you of the current R&D activities of the Japan Atomic Energy Agency (JAEA).

Three years have passed since the establishment of JAEA. We are now reaching a very important stage for the achievement of our goals for our R&D activities in the first mid-term plan. In addition, the importance of nuclear energy was recognized at the G8 Summit held in Tohyako, Hokkaido, Japan in July, 2008, because of its stable supply of energy and potential to solve global environmental problems. JAEA is the sole comprehensive R&D institution aiming at facilitating both basic research and practical application with regard to nuclear energy in Japan. In other words, our research areas cover a wide range of sciences and technologies needed for peaceful and safe uses of nuclear energy. Through our activities, JAEA has been contributing significantly to creating and improving various innovative technologies related to nuclear energy.

In the field of Fast Breeder Reactor (FBR) cycle technology designated as a “Key Technology of National Importance” by the government of Japan, JAEA has been making great efforts to restart “MONJU” (a prototype FBR) and also has been promoting R&D of the FBR cycle for commercialization. In the field of R&D for utilization of applied quantum beams, JAEA continues to put great effort into the operation of “J-PARC” (high-intensity proton accelerator project) which utilizes the most advanced quantum beam technologies. In the field of fusion energy, JAEA is strongly pursuing the ITER Project and Broader Approach Project which are recognized as a science and technology of strategic priority. Furthermore, JAEA is constructing two underground research laboratories where R&D projects for disposal of high-level radioactive waste are being undertaken. In addition, JAEA is steadily executing a new mission, for disposal of radioactive wastes which are generated by research facilities.

The mission of JAEA is to improve the quality of life for all people by innovative advancements in nuclear energy. I strongly believe that JAEA will achieve this goal and become one of the world’s most authoritative and comprehensive institutes, what we call a Center of Excellence (COE), for creative and reliable nuclear energy R&D.

This publication constitutes a review of our achievements in the fiscal year 2007. It provides you with a flavor of some of the work that has been carried out, and also invites you to check the references listed and contact the researchers if there are any topics that you wish to learn more about. I hope that you will take a few minutes to peruse some of the following pages. I would be most gratified if I could hear from you with any comments on this publication.

I hope that you enjoy this publication. Thank you very much for your interest.

JAEA R&D Review 2008

1 Research and Development of Advanced Nuclear System

2 Research and Development on Geological Disposal of High-Level Radioactive Waste

3 Nuclear Fusion Research and Development

4 Quantum Beam Science Research

Steady Implementation of FaCT Project
–Assessing Innovative FBR Cycle Technology–

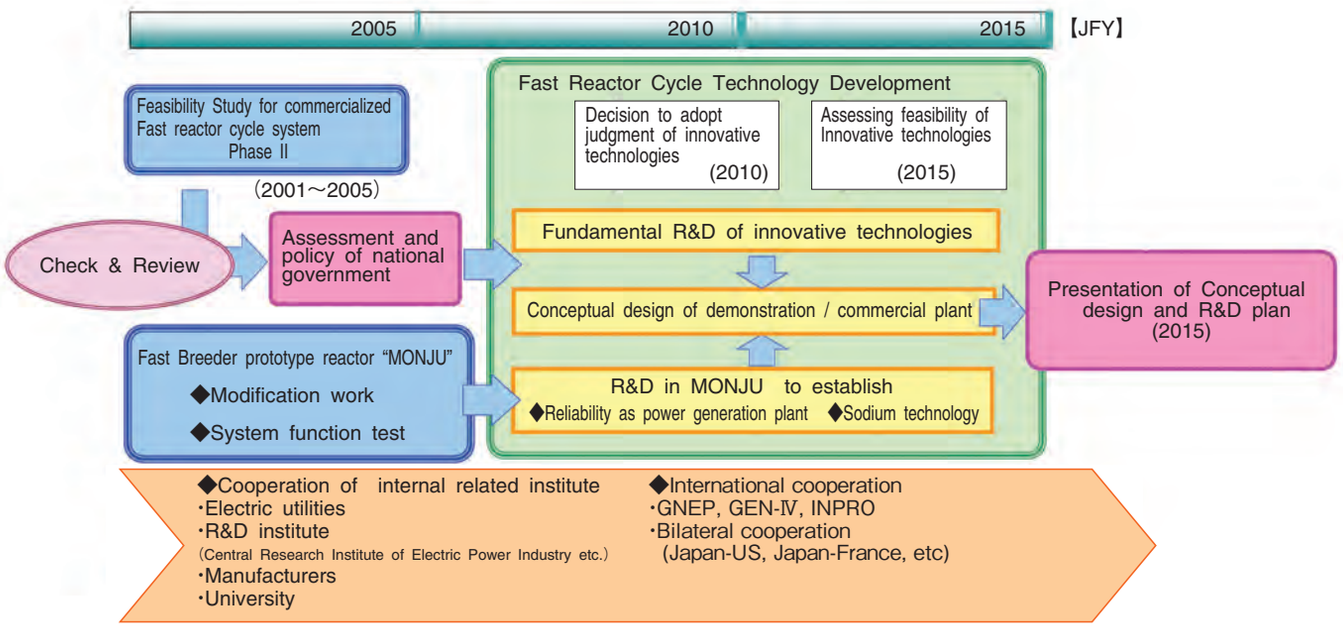

Fig.1-1 Fast Reactor Cycle Technology Development - FaCT Project -

The fast breeder reactor (FBR) cycle is designated as a key technology of national importance in the The Third Science and Technology Basic Plan, this being a technology that contributes to political objectives such as compatibility between the environment and economic growth, and the enhancement of industrial competitiveness to survive in international markets. Aiming for the start-up of a demonstration fast reactor (FR) around 2025 and its introduction on a commercial basis before 2050, Japan Atomic Energy Agency (JAEA) is now promoting its "Fast Reactor Cycle Technology Development (FaCT)" project, supported by the government's assessments and policy, specifically now carrying out a "Feasibility Study on commercialized fast breeder cycle system (FS)" (Fig.1-1).

This FaCT project is developing a combination of the sodium-cooled FBR utilizing oxide fuel, advanced aqueous reprocessing, and the simplified pelletizing fuel fabrication, the technologies presently seen to have the best practical prospects for fostering economic competitiveness, safety, efficient use of resources, reduction of environment load, and non-proliferation, based on their performance in existing facilities.

To scales these technologies up to commercial levels, it is necessary to realize innovative technologies within the above conceptual framework and to assess their performance. In the FaCT project, design studies reflecting the R&D results of the prototype FBR "Monju" and experimental studies for the innovating technologies will be implemented in order to decide on which of the innovative technologies to adopt by 2010 and to present conceptual designs of commercial and demonstration fast reactor cycle facilities along with development plans to realize them by 2015.

FBR System

The commercialization of FBR system still faces challenges; it needs to improve its economy, safety and reliability.

These challenges are, for example, the development of high-performance materials, structures and components which will reduce the facility volume and component size, simplify cooling systems, make the reactor vessel compact, optimize thermal hydraulic properties, and decisively ensure recriticality prevention in case of core disruption. The frontline of this R&D will be introduced in Topic 1-1 to Topic 1-7.

Fuel Cycle System

Major issues facing the fuel cycle system include the safety and controllability of innovative processes, and the development of components with outstanding performance in operation, durability, and repairability Issues facing fuel reprocessing include the development of crystallization technology that enables most uranium in a solution of spent fuel to be recovered in solid form and a recovering process for minor actinides. Issues facing fuel fabrication that have just recently arisen include the development of denitration and conversion techniques, fundamental technology to simplify the pellets fabricating processes, as well as technologies to remotely treat thermogenic substances. The achievements of this R&D will be introduced in Topic 1-8 to Topic 1-11.

Plan for Execution of the Project

A domestic development framework for R&D of the demonstration reactor, in which responsibility, authority, and engineering functions are concentrated, was established in 2007 to implement effective development. Under this framework, the R&D and the design study have been performed with the collaboration of electric utilities and manufacturers. Further, for the fuel cycle, JAEA has conducted preliminary examination and investigation a second fuel reprocessing plant from around 2010 sponsored by the Japanese government.

To lessen development risks and achieve global standardization, an R&D collaboration agreement was concluded by three nations: Japan, France, and the US, for the sodium-cooled FBR demonstration/prototype reactors. Furthermore, multilateral international partnerships such as GNEP are being vigorously pursued.

1-1 Coolant Pipes Made Economically Competitive by Shortening
–Development of High Chromium Steel for FBR Components Which Has Excellent High Temperature Strength, Toughness and Microstructural Stability–

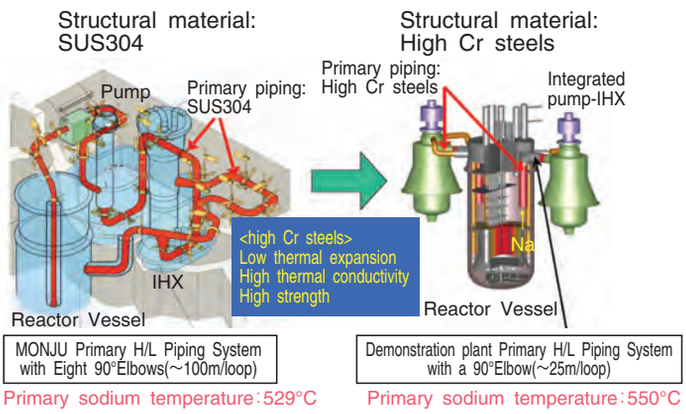

Fig.1-2 Pipe shortening by employing high Cr steel

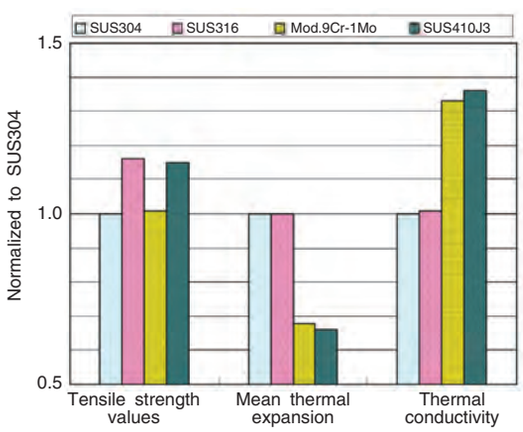

Fig.1-3 Material properties of stainless steels and high Cr steels
FBR structural materials require high strength, low thermal expansion, and high thermal conductance.
12% Cr steel has high potential as a FBR structural material, because it has almost the same tensile strength as SUS316 and thermal properties superior to stainless steels.

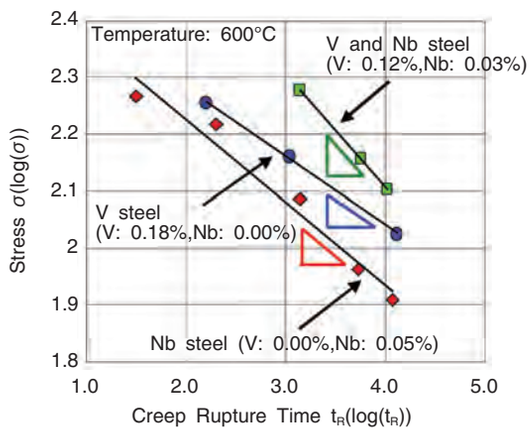

Fig.1-4 Effects of vanadium and/or niobium on creep strength
Creep strength obtained by V alone is more stable than that obtained by Nb alone.

Applicability of high chromium (Cr) steel as a main structural material in FBR has been explored to enhance the economic competitiveness of the FBR. Since this steel has excellent high temperature strength and thermal properties, the coolant pipes can be shortened and a compact plant design can be achieved (Fig.1-2). Applicability of Mod. 9Cr-1Mo steel has been investigated for the demonstration plant because the steel has proven performance in thermal power boilers. For a commercial plant, however, development of innovative high Cr steel is required to enhance the economic competitiveness. Some conventional high Cr steels have properties superior to those of Mod. 9Cr-1Mo steel, as shown in Fig.1-3. However, such steels cannot be used in the FBR components directly, because their long term stability at elevated temperature has not demonstrated yet. In addition, excellent creep-fatigue strength and fracture toughness are required in the FBR structural material. Therefore, prior to employing the steels in the FBR components, it is required that these properties be improved.

Though high temperature strength of the high Cr steel has been achieved by adding some strengthening elements such as vanadium (V) and niobium (Nb), long term efficiency and stability of strengthening elements has not been confirmed yet. Therefore, the long term effectiveness and stability of V and Nb were investigated.

Generally, both V and Nb contribute to improve the high temperature strength of high Cr steels by precipitating as fine carbides and/or nitrides (VX and NbX, where X is C or N; all of these termed “MX”). Several trial products in which the V and Nb contents were varied were made, and mechanical tests and metallurgical examinations were conducted to investigate the long term effectiveness and stability of the precipitation strengthening. As shown in Fig.1-4, both creep strength and long term stability depend on the V and Nb content. Metallurgical examinations revealed that VX was stable after long term creep and aging. This result shows that precipitation of VX in high Cr steel is an efficient strengthening method for FBR components. Based on the above investigations, the stability of precipitation strengthening can be enhanced by controlling the V and Nb content.

Reference
Onizawa, T., Ando, M., Wakai, T., Asayama, T. et al., Long Term Efficiency and Stability of MX Precipitation Strengthening of High Chromium Steel (Transformations and Microstructures), Tetsu To Hagane, vol.94, no.3, 2008, p.91-98 (in Japanese).

1-2 Evaluation of the Structural Integrity of Reactor Vessels –Measurement of the Thermal Deformation near the Fluid Surface Using the Laser Speckle Method–

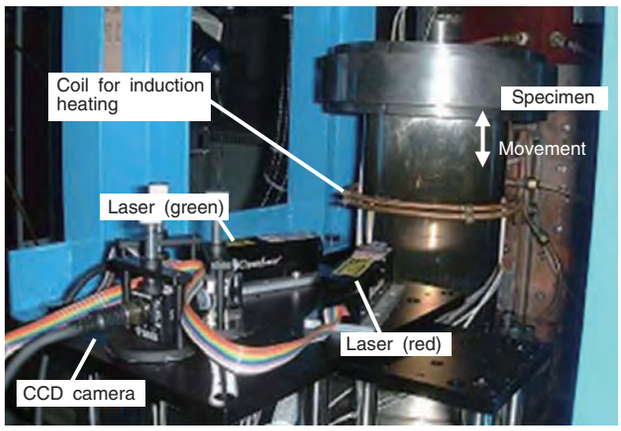

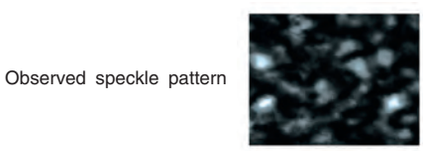

Fig.1-5 Laser speckle system and its measurement of a specimen

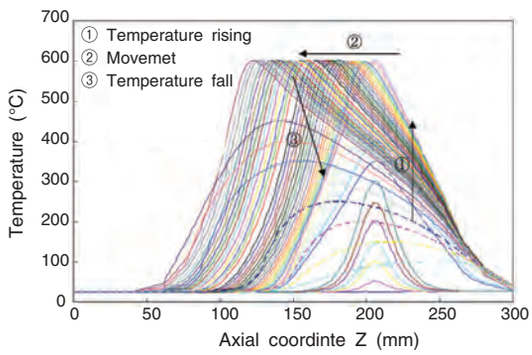

Fig.1-6 Time history of temperature distribution along the axis of the specimen

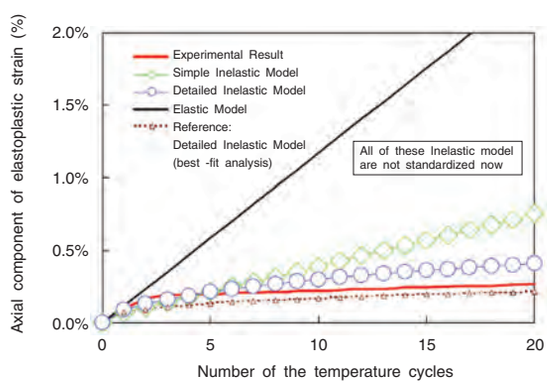

Fig.1-7 Comparison of the strain found in experiments and analyses (Z=150mm in Fig.1-6)

A main vessel in the FBR is subjected to a severe cyclic thermal load due to cyclic movement of longitudinal temperature distribution with a large gradient. This is generated by the combination of heating of the lower part by hot liquid sodium and cooling of upper part by ambient gas during start-up and shut down of the system. As a result, inelastic strain accumulates near the sodium liquid surface. Since excessive inelastic strain breaks down the structural integrity, precise prediction of this strain is important for structural design of the reactor vessels. To understand the actual behavior of the inelastic strain and so evaluate an inelastic strain analysis, tests of the strain on a reactor vessel model were carried out.

Fig.1-5 shows the tested cylindrical specimen (material: 316FR steel, height: 300mm, outer diameter: 55mm, thickness 3.5mm). This specimen was given the temperature distribution shown in Fig.1-6, which imitates an actual reactor vessel. In this experiment, the following factors were measured: (1) temperature, (2) radial deformation, and (3) axial strain. In the past it has been difficult to measure local strain on a high temperature structure with high precision. For the measurement of this strain, we developed a non-contact measurement system based on the laser speckle method. This system measured the speckle pattern (Fig.1-5 lower right) of diffuse reflection of a laser. Through the image processing of the change of this pattern, the strain on the structure surface can be estimated.

The experiments showed that movements of the longitudinal temperature gradient caused axial strain, especially in the early stage. With succeeding repetitions of the temperature movement, less incremental axial strain is caused. As shown in Fig.1-7, upon 3 or more cycles of the temperature movement, the traditional elastic analysis overestimates the axial strain. Although the elastic analysis is on the safe side, the strain prediction should be based on inelastic analysis to rationalize the reactor vessel design.

The strain measured here is important and useful for improvement of inelastic analysis needed to make the structural model. In the future, using this data we will develop a more detailed model to explain actual behavior such as temperature dependency, non-linear hardening, and cyclic hardening. This model will improve the prediction of the inelastic strain, and enable design of compact reactor vessels.

Reference

Watanabe, D., Chuman, Y., Otani, T., Shibamoto, H., Inoue, K., Kasahara, N., An Experimental Validation of the Guideline for Inelastic Design Analysis through Structural Model Tests, Nuclear Engineering and Design, vol.238, issue 2, 2008, p.389-398.

1-3 Determining Transfer / Damping of Temperature Fluctuation of Fluid to Structure
–Evaluation of High Cycle Thermal Fatigue at Core Outlet in FBR–

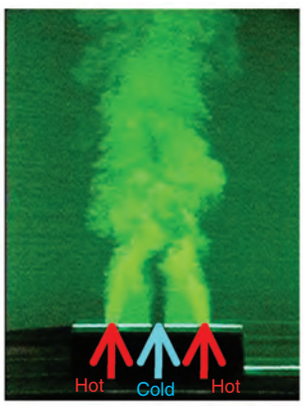

Fig.1-8 Visualized convective mixing of jets
Only hot jets are colored. The jets oscillate as they mix together.

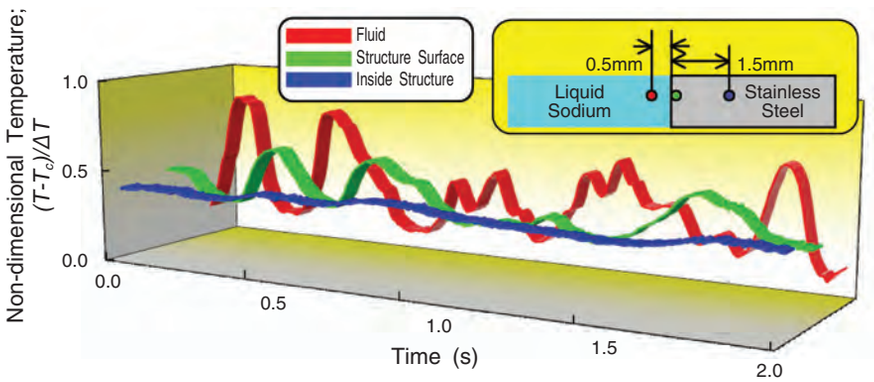

Fig.1-9 Attenuation of temperature fluctuation during transfer from fluid to structure
The vertical axis is normalized to the discharged temperature difference between jets.
(*T*: fluid temperature, *Tc*: temperature of cold jet at nozzle exit, ΔT: discharged temperature difference)

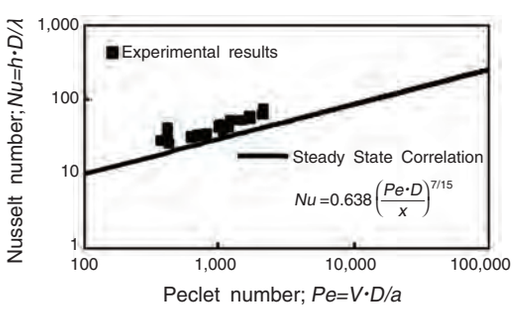

Fig.1-10 Comparison of heat transfer correlation between steady state and non-stationary conditions
The Vertical axis is the Nusselt number, the ratio of the heat convection to the heat conduction. The horizontal axis is the Peclet number, the ratio of heat transportation based on flow velocity to thermal diffusivity. (*h*: heat transfer coefficient, *D*: representative length, λ: thermal conductivity of fluid, *V*: velocity of jet discharge, *a*: thermal diffusivity in fluid, *x*: distance from nozzle exit)

At the core outlet of an FBR, hot fluid is mixed with cold fluid near the reactor structure. Thermal stress is induced due to the thermal expansion of the structure where the temperature fluctuation is transferred from the fluid. A large temperature fluctuation may cause thermal fatigue damage if applied several million times (high cycle thermal fatigue). In a previous study, the relation of the frequency of temperature fluctuation to the vulnerability of a structure to damage was evaluated under special experimental conditions in which this fluctuation could be controlled (see JAEA R&D Review 2007 Topic 1-8). In this study, a sodium jet experimental system was constructed to evaluate the characteristics of the transfer of temperature fluctuation from fluid to structure.

The experimental test apparatus had three parallel jets passing along a stainless steel wall. The center was a cold jet, with hot jets on both sides. This experimental setup models a simplified two dimensional configuration of the reactor core outlet which has cold flow channels of control rods surrounded by hot channels of fuel subassemblies. Fig.1-8 shows convective mixing of the three jets obtained from a water experiment with the same geometry as the sodium experiment. It was observed that the jets at either side inclined toward the center jet. The temperature fluctuation was large at the region where the center jet contacted with the side jets. In the sodium experiment, thermocouples were embedded in the wall at this region. The transfer of temperature fluctuation from fluid to structure was evaluated by the simultaneous measurement of temperatures in fluid and structure. Fig.1-9 shows the temperature histories in fluid near the structure, on the structural surface, and in the structure. The fluid temperature fluctuated with large amplitude. On the structural surface, on the other hand, the amplitude of temperature fluctuation was much smaller than that in fluid. Furthermore, the fluctuation amplitude in the structure was still smaller than that on the structural surface.

This quantitative evaluation of the attenuation makes it possible to efficiently evaluate high cycle thermal fatigue. This attenuation had dependency on temperature fluctuation. This was expressed as a theoretical power curve function. We developed a new method of determining the transfer coefficient of temperature fluctuation from fluid to structure by fitting measured results to this function. Fig.1-10 shows a comparison of the calculated heat transfer coefficients and the heat transfer coefficients under the steady state condition (Poppendiek's correlation equation). It was found that the transfer coefficient of temperature fluctuation could be evaluated using a constant heat transfer correlation equation including the flow velocity dependency (Peclet number dependency). Further experimental study using a mockup model is planned to develop an evaluation method of the high cycle thermal fatigue, and to investigate structural integrity.

Reference
Kimura, N. et al., Experimental Investigation on Transfer Characteristics of Temperature Fluctuation from Liquid Sodium to Wall in Parallel Triple-Jet, International Journal of Heat and Mass Transfer, vol.50, issues 9-10, 2007, p.2024-2036.

1-4 Development of a Fuel Handling Method for a Compact Reactor Vessel
–Fuel Handling Machine Bearing Endurance Test in Sodium Vapor–

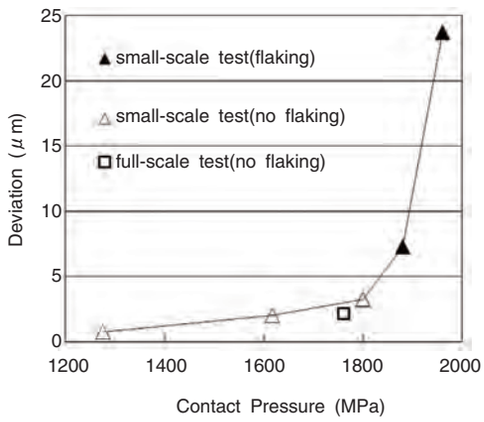

Fig.1-11 Bearing ring roundness

Fig.1-12 Full-scale fuel handling machine bearing

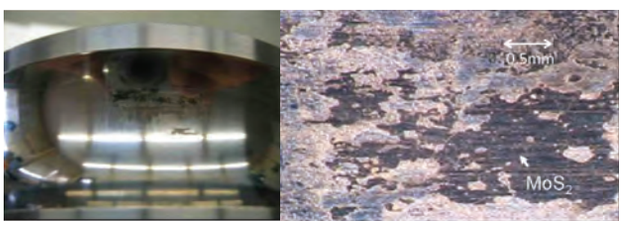

(Over View) **(Magnified Surface)**

Fig.1-13 Bearing ring after endurance test

(Over View) **(Magnified Surface)**

Fig.1-14 Bearing ball after endurance test

Our commercial-use sodium cooled reactor design includes a compact reactor vessel with a new in-vessel fuel exchange system. The upper inner core (UIS) structure has a slit for a fuel handling machine (FHM). The FHM removes and inserts each fuel subassembly through the UIS slit without removing the UIS from above the core.

The FHM has to function in sodium and in the gas inside the reactor vessel cover including sodium vapor. The usual lubrication materials such as grease are not usable with sodium, since sodium is chemically active and the greases could pollute coolant sodium. Therefore the FHM bearing requires a special lubrication. Besides, the FHM uses ball bearings, to avoid interference of the UIS slit with the FHM during an earthquake. Since ball bearings generally are subject to high contact pressure, endurance of the FHM bearings is one of the issues for the FHM development.

In this study, 1/10-scale and full-scale bearing endurance tests were conducted. In the 1/10-scale test, several ring and ball materials were tested to find a suitable material combination for the FHM bearing. The relation between endurance and contact pressure was determined. The 1/10-scale tests were conducted at 250 ºC, applying 20000 vibration cycles in the air. The temperature was a little higher than the FHM operation temperature and the number of vibrations was equivalent to ten refueling operations. Based on the 1/10-scale test results, a bearing with stainless steel rings and ceramic balls was selected. To enhance lubrication, MoS_2 coating on the bearing rings was adopted. The results also showed that surface flaking would start at a contact pressure of approximately 1800 MPa. Deviation of the inner ring grew larger as the contact pressure became larger. When the deviation went beyond 3.5 to 7 μm, the deviation increment rapidly grew larger, as shown in Fig.1-11.

In the full scale test, a full-scale FHM bearing was manufactured and an endurance test was conducted in argon gas with sodium vapor simulating the FHM operating conditions. The full-scale bearing is shown in Fig.1-12. The contact pressure was controlled to be 1745 MPa, considering the surface pressure that can be maintained. The other test conditions are similar to the 1/10-scale tests. Fig.1-13 and Fig.1-14 show surface conditions of rings and balls after tests. There is sign of some MoS_2 transfer between ring and ball but overall surface conditions were maintained well without any flaking. The deviation of the inner rings was observed to be 2 μm, which is lower than the limit suggested by the 1/10-sacle tests. Those results show that this bearing is suited for the FHM operating conditions.

In future studies, a full scale FHM test in the air and a gripper mechanism test in sodium are planned as part of JSFR FHM development.

Reference

Chikazawa, T. et al., Development of a New Fuel Handling Machine Suitable for an Upper Inner Structure with a Slit-The Performance Test of a Large-Sized Bearing in Argon Gas Atmosphere-, JAEA-Research 2007-001, 2007, 91p. (in Japanese).

1-5 Improved Analysis of Hypothetical Core Disruption Behavior in FBRs –3-D Simulation of Complex Thermal-Hydraulic Phenomena under Very High Temperature–

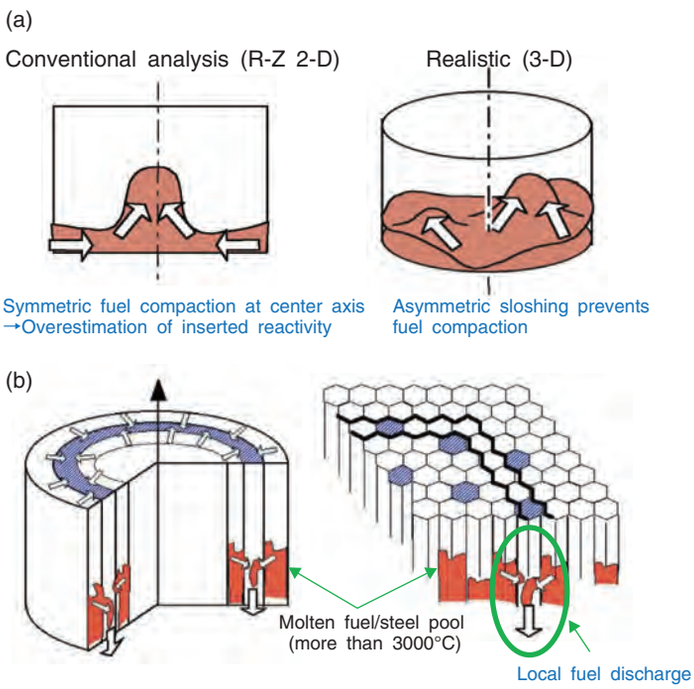

Fig.1-15 Need for a three-dimensional analytical method
3-D analytical method enables realistic simulation.
(a) Reactivity insertion by radial sloshing of whole-core scale
(b) Fuel discharge from the core through control rod guide tubes (CRGTs)

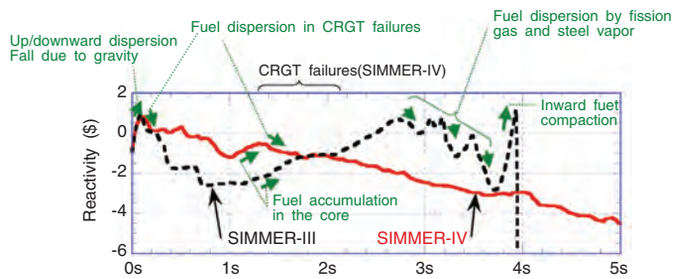

Fig.1-16 Comparison of reactivity histories
2-D (SIMMER-III) analysis predicts recriticality due to fuel compaction, while 3-D (SIMMER-IV) analysis predicts reactivity decrease due to fuel discharge from the core.

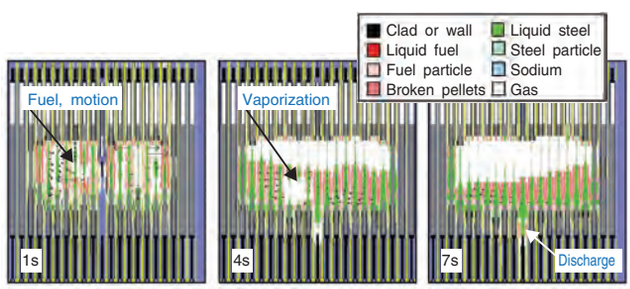

Fig.1-17 Core material dynamic behavior (SIMMER-IV)
3-D core-disruption behavior accompanying melting/freezing, vaporization/condensation, etc. at around 3000°C.

One of the major issues in FBR development is dealing with a core disruptive accident (CDA), which might rapidly release radioactive materials due to its thermal and mechanical consequences, although its occurrence frequency is negligibly low. A high-temperature molten fuel above 3000°C allows forming molten fuel pool, where molten core materials can move between fuel assemblies with molten wrapper tube wall.

A safety analysis code, SIMMER-III, has been utilized for past safety evaluations. This code has been developed in Japan for a multi-phase, multi-component fluid-dynamics model coupled with structural materials models and neutronics models. SIMMER-III, however, is a two-dimensional code. Due to this dimensionality, this code tended to overestimate the reactivity increase resulting from fuel compaction into the core center because it could not simulate motion around the axis (Fig.1-15). Further, the reactivity reduction by fuel discharge through control rod guide tubes (CRGTs) could not be calculated, because the tubes which are dispersed throughout the core could not be simulated. This deficiency has forced the past evaluations to be conservative, since fuel discharge through CRGTs etc. had to be ignored. To reasonably reduce the conservativeness of the evaluation, we have developed the SIMMER-IV code, extending the SIMMER-III framework to three-dimensions. This code clarifies the significance of 3-D simulation by comparing it to the conventional 2-D simulation. In this study, SIMMER-IV has been applied to 3-D simulation of a CDA in an FBR for the first time in the world.

In the SIMMER-III analysis, after output power exceeds the limit for 2.4s, the fuel melts and increases in mobility, and the reactivity reaches prompt criticality in 3.9s due to inward fuel compaction. In the SIMMER-IV analysis, CRGTs failed at different times around 2s cooling the fuel so that it did not become a mobile pool, so that the fuel was not compacted and reactivity did not rise (Fig.1-16). 3-D motion of complex phenomena with phase changes, etc. could be simulated (Fig.1-17).

This study has shown the effectiveness of the 3-D simulation in making reasonable evaluation of accidents.

Reference

Yamano, H. et al., Development of a Three-Dimensional CDA Analysis Code: SIMMER-IV and Its First Application to Reactor Case, Nuclear Engineering and Design, vol.238, no.1, 2008, p.66-73.

1-6 Experimental Study on Molten Core Material Behavior –The EAGLE Project as a Collaborative Study with the Republic of Kazakhstan–

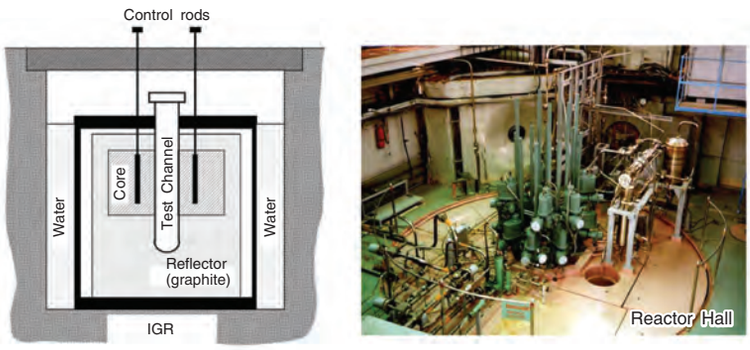

Fig.1-18 IGR and test channel

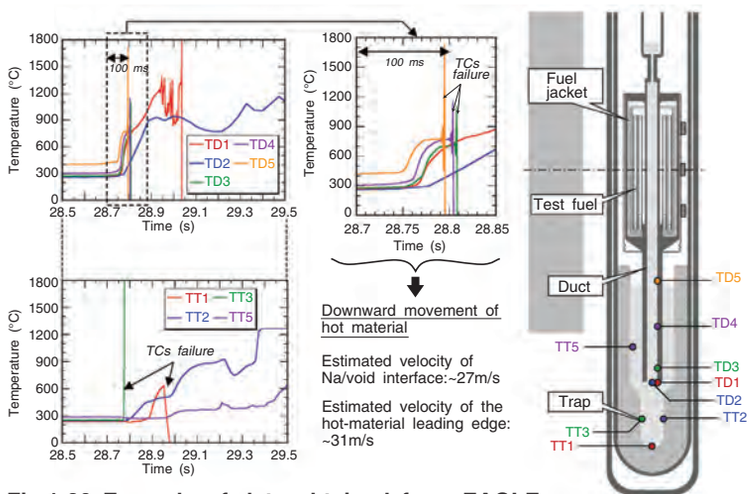

Fig.1-20 Example of data obtained from EAGLE

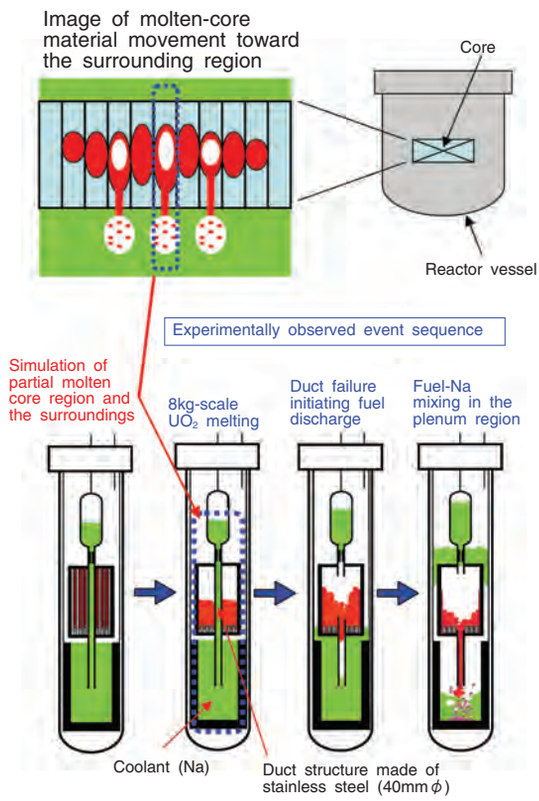

Fig.1-19 Concept of molten core accident simulation

JAEA is conducting an experimental project called EAGLE in order to clarify molten-core-material behavior in hypothetical core-melt accidents of FBR and to confirm that the consequences of such an accident can be mitigated appropriately, although the possibility of such accidents is extremely small. This experimental program is a collaboration between JAEA and National Nuclear Center of Republic of Kazakhstan using its IGR (Impulse Graphite Reactor) specifically designed for experiments.

IGR has a central hole as illustrated in Fig.1-18 to accommodate the test channel equipped with double-layer pressure vessels enclosing fuel for testing. Three experiments in which about 8kg of UO_2 is melted have been performed up to now simulating accident conditions. These tests provided information on accident progress behavior (Fig.1-19). Fig.1-20 shows an example of the data obtained from the experiments. In this experiment, molten fuel broke through the stainless steel (SS) duct structure and discharged through the duct toward the cold region filled with sodium (downward in this experiment), and was cooled down through mixing with sodium. Besides thermocouple (TC) data shown in this figure, various data from void-sensors (detecting bubbles in sodium), pressure gauges, microphones, etc. were obtained, and they elucidated the series of physical processes which occurred, such as the duct-structure failure, contact with molten fuel pushing sodium downward from the core (TCs at upper, middle and lower levels detected temperature increases with time lags with this order) and the fuel discharge through the duct.

In the conventional safety evaluation of FBR core-melt accidents, it was assumed that a large amount of molten-fuel remained within the core region which could potentially cause a rapid power excursion with massive molten-fuel movement. However, through the EAGLE experiments, it was shown that molten fuel tends to discharge out of the core region so that massive amounts of molten fuel remaining within the core region is very unlikely. The new findings obtained through the EAGLE project indicate that the conventional safety evaluations are conservative, and that core design features enhancing fuel-discharge characteristics can prevent severe power excursions.

Reference

Konishi, K., Toyooka, J., Kamiyama, K., Sato, I. et al., The Result of a Wall Failure In-Pile Experiment under the EAGLE Project, Nuclear Engineering and Design, vol.237, issue 22, 2007, p.2165-2174.

1-7 Analysis of Complex Phenomena upon Tube Failure in SG –Development of a Numerical Simulation Program Evaluating Sodium-Water Reaction Phenomena for Safety Assessment–

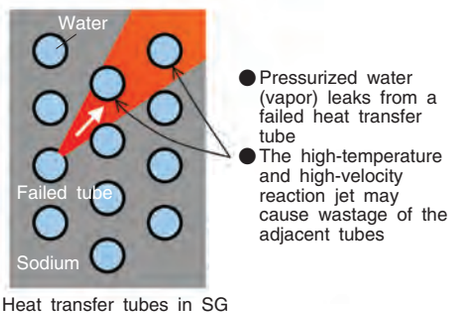

Fig.1-21 Sodium-water reaction phenomena upon tube failure

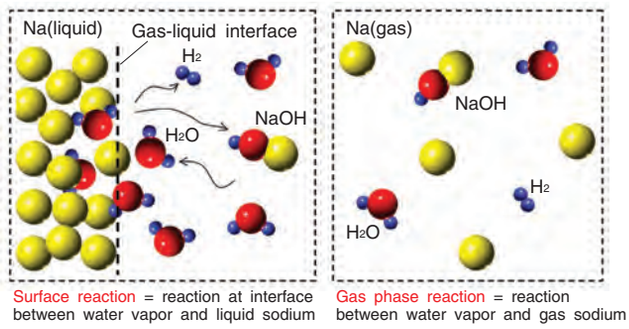

Fig.1-22 Two chemical reaction mechanisms

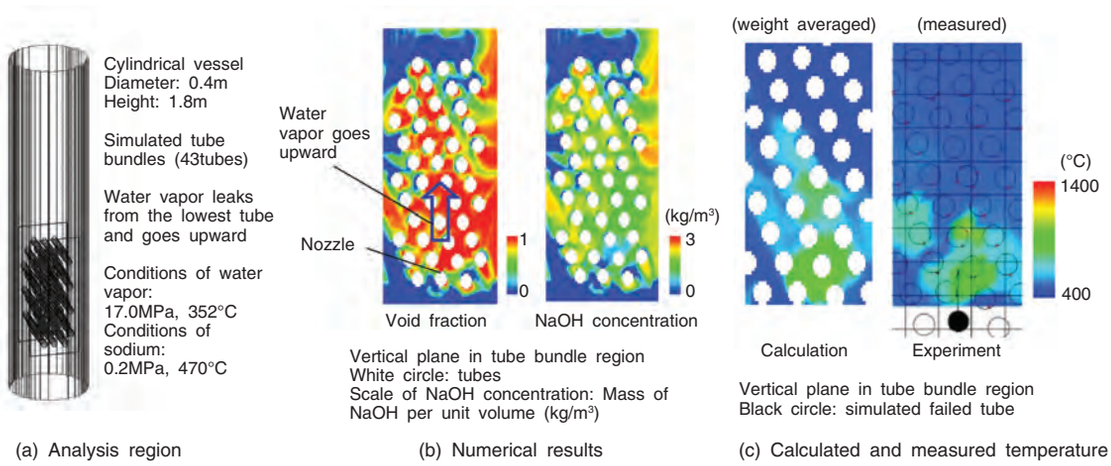

Fig.1-23 Numerical analysis of sodium-water reaction experiment

When pressurized water leaks from a failed heat transfer tube in a steam generator (SG) of a sodium cooled fast breeder reactor, the water vapor reacts with the liquid sodium outside the tube. It is known that in some cases the high-temperature and high-velocity reaction jet may cause wastage of the adjacent tubes (Fig.1-21). Evaluation of these phenomena under anticipated conditions is a key issue in safety assessment of the SG. In this study, a numerical analysis code SERAPHIM analyzing compressible multi-phase flows with sodium-water chemical reaction has been developed.

A multi-fluid model was adopted to calculate multi-phase flows of water, liquid sodium and multi-component gas. Advection and diffusion of the gaseous species is also considered in our method. Two chemical reaction mechanisms were modeled (Fig.1-22). One is a surface reaction model for the reaction at the interface between the water vapor and the liquid sodium. The surface reaction rate is assumed to be diffusion-controlled in our model. Another is a gas-phase reaction model for the reaction between the water vapor and the gas sodium generated by evaporation. In this model the reaction rate constant is estimated based on the Arrhenius law.

Applicability of the SERAPHIM code has been validated through the analysis of an experiment on the sodium-water reaction (Fig.1-23(a)). By using the SERAPHIM code, profiles of void fractions, concentrations (Fig.1-23(b)), and temperature and velocity fields can be obtained. As shown in Fig.1-23(c), the temperature field calculated by the SERAPHIM code shows good agreement with the experimental result.

Reference

Takata, T., Yamaguchi, A., Uchibori, A., Ohshima, H., Numerical Investigation of Sodium-Water Reaction Phenomenon in a Tube Bundle Configuration, Proceedings of 2007 International Congress on Advances in Nuclear Power Plants (ICAPP 2007), Nice, France, 2007, Paper 7510, 8p., in CD-ROM.

1-8 Development of Uranium Recovery System by Crystallization Technologies

–R&D Status on Uranium Crystallization System for Future FBR Recycle System–

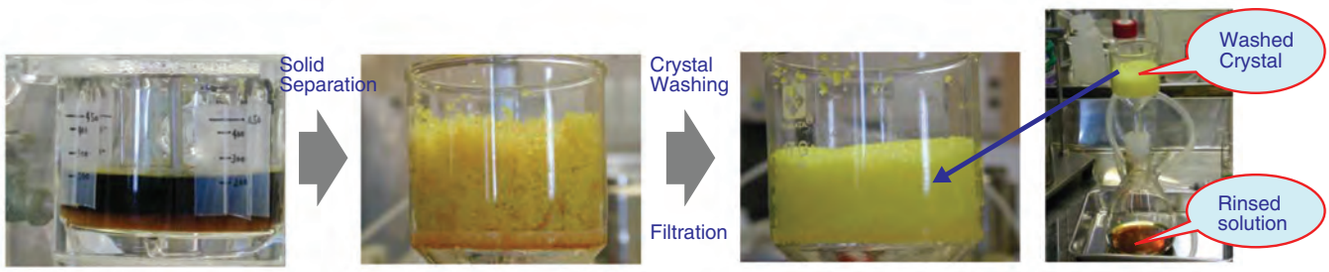

Fig.1-24 Steps in uranium crystallization from uranium and ruthenium nitrate solution
The solution in the vessel is cooled to lower temperature as e.g. 0°C. The crystal and mother solution are separated by suction filtration by a glass filter, the crystal is washed to remove mother solution remained.

Fig.1-25 Development of Engineerring Scale Crystallizer
Crystallizer tank (about 300mm(ID) × 900mm(L), hold-up volume is about 5 liters) has a cooling jacket made of transparent plastic to allow internal observation. The crystal size is about 700 to 800 μm.

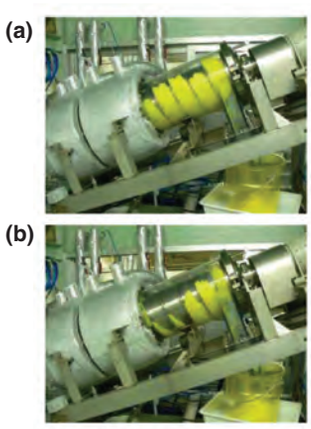

Fig.1-26 Appearance of non-steady state simulation test
(a) Crystal blockade is intentionally caused by reducing the rotation speed.
(b) The crystal blockage is removed by manually.

The crystallization is considered one of the key technologies for uranium recovery from the spent fuel in the future reprocessing plant, because it promises much desired safety and economical efficiency.

The crystallization is a separation technology based on differences in solubility, executed by changing temperature and concentration, with no organic reagent needed, so that the separation system can be simple (Fig.1-24) .

Since 1990s, JAEA has been carrying out small scale hot experiments at the Chemical Processing Facility (CPF), and development of an engineering-scale system is being carried out.

In the hot experiments, the uranium recovery rate, the decontamination factors of plutonium, and fission products (FPs) have been confirmed, and the crystal purification technology have been investigated.

In research for practical application, we selected a rotary driven type crystallizer which has the advantages of criticality safety, high throughput, and remote maintenance, etc. (Fig.1-25).

The uranium crystal is generated in the cooled solution in the crystallizer, and the crystal is isolated from residual solution (mother solution) by the cylinder rotation and is discharged from the device.

In the system development of the engineering scale system, we fabricated an engineering scale crystallizer system, and have been investigating the properties of steady and non-steady state operations. In these investigations, the operation conditions for stable crystallization, the crystal accumulation and blockage phenomena during crystal discharge, and the outlet of mother solution are being confirmed. The crystal accumulation can be monitored by a cylinder torque meter, and the event can be overcome by the stoppage of feed solution and stepwise increment of the screw speed (Fig.1-26). Development of the instrumentation and control system also is progressing.

This work was financed by the Ministry of Economy Trade and Industry of Japan (METI), and the Ministry of Education, Culture, Sports, Science and Technology of Japan (MEXT).

Reference

Ohyama, K., Nomura, K. et al., Development of Uranium Crystallization System in "NEXT" Reprocessing Process, Proceedings of International Conference on Advanced Nuclear Fuel Cycles and Systems, Boise, USA, 2007, p.1461-1466, in CD-ROM.

1-9 Toward Engineering Scale Minor Actinides Recovery
–Development of Extraction Chromatography Techniques–

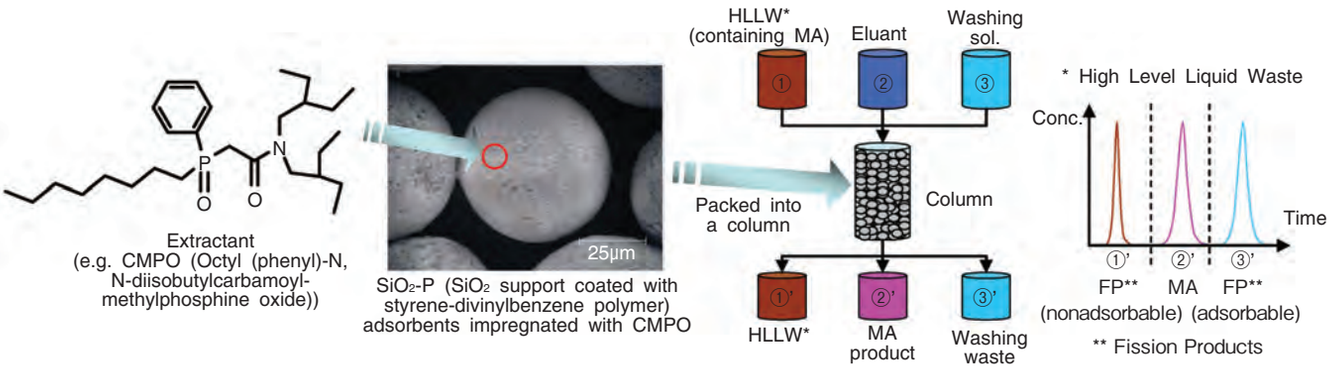

Fig.1-27 MA recovery by extraction chromatography
SiO_2-P adsorbent material impregnated with an extractant is packed into a column. Solution containing MA (①) is fed into this column, and MA is adsorbed. The adsorbed MA is eluted by a suitable eluant (②), and recovered into a solution (②'). Several columns with different adsorbents (extractants) may be used for better separation of MA from other elements.

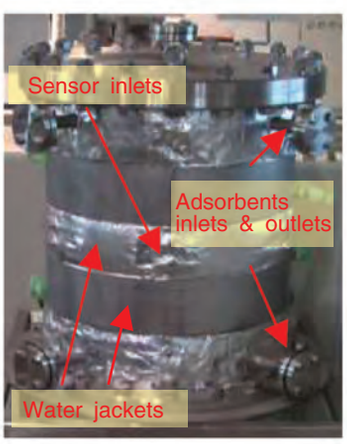

Fig.1-28 Engineering scale column
Stainless steel column with 48cm inner diameter, which has water jackets for temperature control and sensor inlets for experiments.

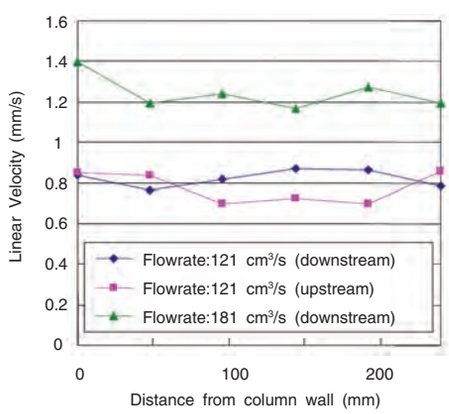

Fig.1-29 Linear velocity in a column
The uniform flow through a column with 48cm diameter can be obtained with flow of 121cm³/s (downstream).
About 1.7kg of MA is supported to be recovered in this flowrate condition.

Studies on minor actinide (MA) recovery by solvent extraction have been carried out in several countries. These processes use extractants with diluents, which cause various kinds of liquid waste in large amounts. In the extraction chromatography technique, in which extractants are impregnated into support particles, no diluent is used, and higher MA loading can be achieved, so this is potentially more economical. We developed a process and system of MA recovery by extraction chromatography which can be expanded to an engineering scale.

We selected a SiO_2 support coated with styrene-divinylbenzene polymer (SiO_2-P) (Fig.1-27), which has superior safety and handling properties, and started assessing SiO_2-P adsorbent materials impregnated with several kinds of extractants, e.g. CMPO; adsorption/elution of MA, acid and radiation resistance, and ease of after-treatment of these adsorbents. These properties are now being measured, and several process flows for MA recovery will be designed and evaluated based on these data.

In our development of an engineering scale system, we fabricated an engineering scale column system (Fig.1-28) and have been investigating the fluidics and thermal control properties in actual operation, and the durability through long-term operation. Through these investigations, we determined the operational conditions necessary for uniform flow through the column, which is indispensable for steady MA recovery (Fig.1-29).

We also investigated remote control and instrumentation for the column operation, and we will have overall assessments of separation performance, safety, instrumentation and control, and remote handling based on these results and engineering scale experiments.

This work was financed by the Ministry of Education, Culture, Sports, Science and Technology of Japan (MEXT) under the framework of "The Development of Innovative Nuclear Technologies."

Reference

Koma, Y., Watanabe, S., Sano, Y. et al., Extraction Chromatography for Am and Cm Recovery in Engineering Scale, Proceedings of 3rd International ATALANTE Conference (ATALANTE 2008), Montpellier, France, 2008, O1-19, p.8, in CD-ROM.

1-10 Toward Innovative MOX Fuel Production by Simplified Process –Developing a Unified Process Combining De-Nitration by Microwave Heating with Granulation–

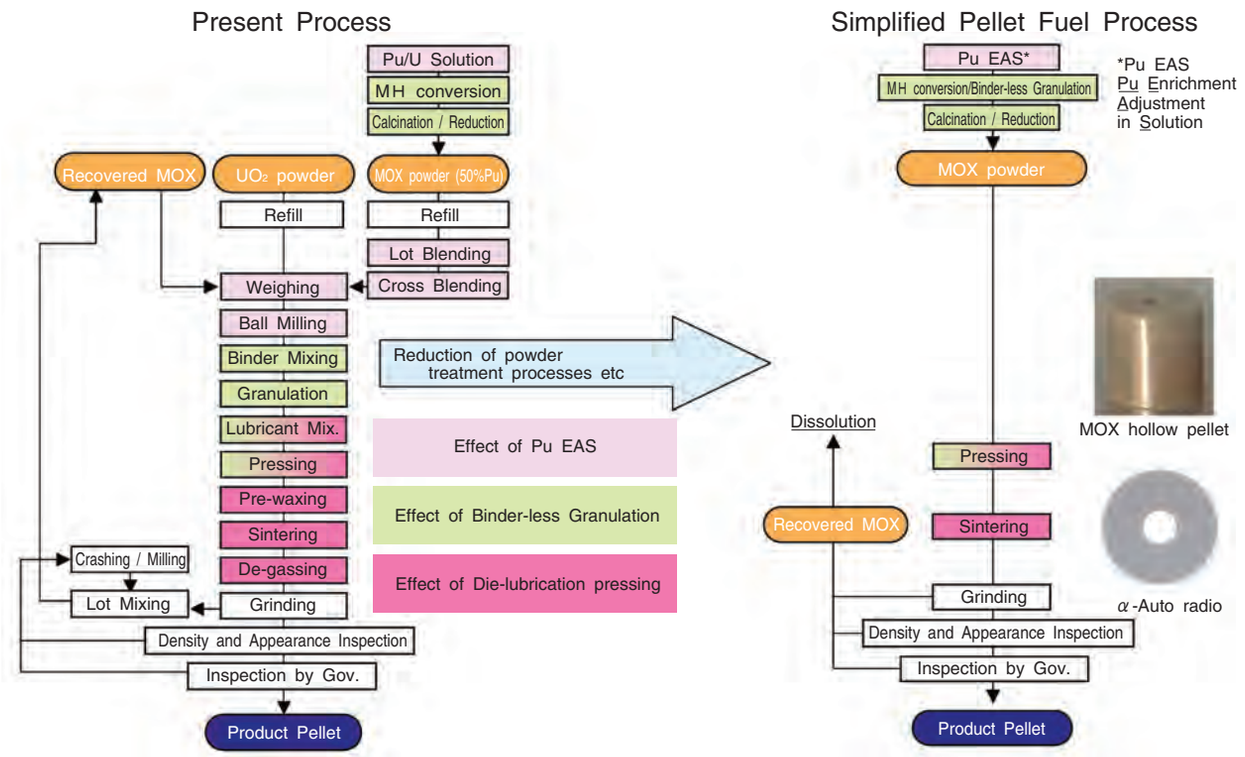

Fig.1-30 Simplified pellet fuel production process
Simplified pellet fuel making process (right) compared with present process (left)

The key for the industrial production of MOX fuel to be burned in the FBR is the reduction of its manufacturing cost. The most promising method for meeting this requirement is the simplified technology shown in Fig.1-30. The key ideas behind this method are (1) adjustment of mixing rate of PuO_2/UO_2 in the liquid state, (2) combining de-nitration with granulation, and (3) fabricating a hollow-pellet with a lubricated die. The details are as follows.

Apart from its simplicity, the distinctive characteristic of the simplified technology is its accuracy in adjustment of mixing rate of PuO_2/UO_2, since the job is carried out in the liquid state. By this means, complicated powder mixing processes needed in the conventional solid state mechanical mixing system were greatly improved. In simulation experiments employing a mockup system and typical liquids, a mixing accuracy of ±2.5% was attained. The overflow type fixed quantity service cylinder and an air lift separator which supplies air free liquid into the service cylinder played important roles in this success. In laboratory experiments employing real fuel liquids (Pu/U=3/7), we observed the mixing state of the powder products which were de-nitrated by microwave heating, and confirmed that non uniform distribution of Pu was not appeared in the hollow-pellet. The results clearly show that the uniformity of MOX powder products obtained by the liquid phase mixing method is better than that by the conventional method.

Another distinctive characteristic of the simplified technology is the granulation done in process of adjusting the U/Pu mixing rate. In this method, high speed agitation with rotating blades is efficiently employed, and not an organic binder but rather water is sprayed, resulting in slippery particles. Thus, the flowability of particles is improved (over 60 in Carr coefficient), a great benefit. The density of MOX hollow-pellets, which were filled with these particles and compressed by the usual press in a die, reached over 95% TD after sintering.

Further, a hollow-pellet was fabricated utilizing the same MOX particles as above, and compressed in a die which was lubricated. These results demonstrated the feasibility of this simplified technology for MOX fuel production on the laboratory scale.

Hereafter, we would like to carry out larger scale experiments to attain the target production rate by 2010 when the adoption of innovative technology will be made. The improvement of production efficiency is the key for this innovative technology, we believe.

Reference

Suzuki, M. et al., Development of FR Fuel Cycle in Japan(3) -Current State on Unified Technology of Denitration Conversion and Granulation for Simplified Pellet Fuel Fabrication Based on Microwave Heating- , Proceedings of 2008 International Congress on Advances in Nuclear Power Plants (ICAPP '08), Anaheim, CA, USA, 2008, p.2036-2045, in CD-ROM.

1-11 Heat Removal during TRU Fuel Fabrication
–Design Study of Heat Removal for TRU Fuel Fabrication System–

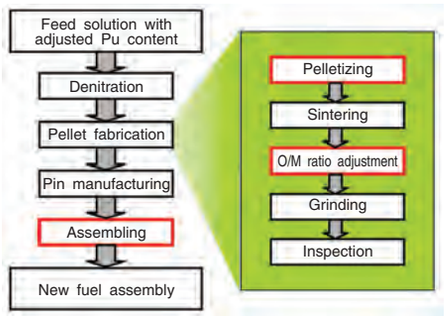

Fig.1-31 Process flow of simplified pelletizing fuel fabrication
The processes in which heat removal is important is shown in red.

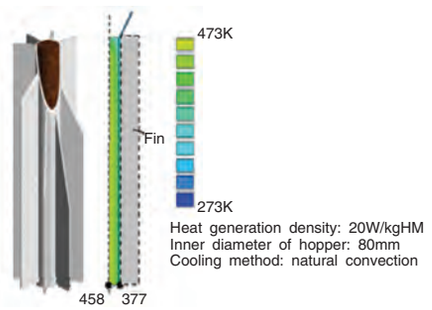

Fig.1-32 Powder supply hopper and temperature distribution
To prevent accumulation of decay heat, hopper is designed with narrow shape and fins is installed. An inner diameter with which the temperature of powder doesn't exceed 473K was obtained by heat flow calculation.

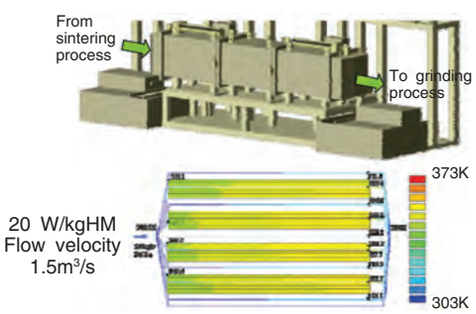

Fig.1-33 O/M ratio adjustment furnace and temperature distribution
The furnace is designed to be separated into batches to keep oxygen partial pressure very low. When pellets are unloaded, cooling air is fed to keep pellet temperature below 358K.

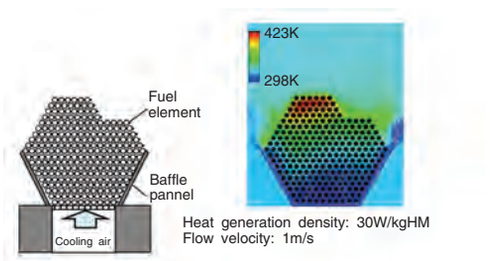

Fig.1-34 Concept of fuel assembling equipment and temperature distribution
Fuel elements are layered horizontally. Cooling air is fed from under the bundle.

TRU fuel is being considered as a future FBR fuel because it can decrease the environmental burden by closing in minor actinides (MA) such as americium and curium in the nuclear fuel cycle. The TRU fuel generates high heat on the order of tens of W/kgHM (kgHM means weight of heavy metal element in the fuel material) by the decay of the contained MA. Heat generation by the fuel causes oxidation of MOX powder and pellets, oxidation of the cladding tube, and mechanical interference between the cladding tube and wrapper tube. Therefore, it is necessary to cool the fuel during the fuel fabrication process. In the fuel assembling process, the powder supply hopper in pelletizing process, the pellet unloading from the O/M (atomic ratio of oxygen and the metal in the oxide) ratio adjustment furnace and the fuel bundle in the fuel assembling process are considered to have overheating problems.

Concepts of a heat removal system for these areas were examined, and the temperature limit for each was evaluated through heat flow calculations. Fig.1-31 shows the process flow of a simplified pelletizing method.

For the examination, provisional temperature limits were set at 358K for powder and pellet in the air, 473K for powder in inert gas, and 573K for fuel elements and the fuel assembly.

The powder supply hopper is designed to substitute the inside contents with the inert gas and has heat radiation fins were installed outside to cool the hopper naturally (Fig.1-32). The O/M adjustment furnace is designed to cool down pellets to 358K in a reduction atmosphere, and then to unload pellets while cooling them with air (Fig.1-33). The fuel assembling equipment is designed so that cooling air is blown from under the fuel element bundle (Fig.1-34).

Based on these designs, temperature distribution was evaluated with heat flow calculations (Fig.1-32, Fig.1-33 and Fig.1-34). Especially for fuel element bundle, because there are complex passages with many cladding tubes and wrapping wires, evaluation with a model of 20,000 meshes and evaluation with a detailed model of up to five million meshes were combined. Temperature distribution was calculated for various heat generation densities and cooling conditions, and the size of container and/or cooling conditions with which the maximum temperature of the fuel doesn't exceed the temperature limit were confirmed.

From these examinations and evaluations, the prospect of keeping below the temperature limit by combining natural cooling and forced cooling was confirmed for fuel with heat generation density 20W/kgHM.

Reference
Kawaguchi, K. et al., Conceptual Study of Measures against Heat Generation for TRU Fuel Fabrication System, Proceedings of International Conference on Advanced Nuclear Fuel Cycles and Systems (GLOBAL 2007), Boise, USA, 2007, p.290-295, in CD-ROM.

R&D Supporting the Technology and Reliability of Geological Disposal in Japan

High-level radioactive waste (hereafter, HLW) is generated when we utilize nuclear power. In Japan, reprocessing is done to recover uranium and plutonium remaining in spent fuel from power generating reactors, for recycling into useful fuel. The liquid remaining after such retrieval is finished is vitrified to produce a chemically and physically stable glass, which is HLW. International consensus has been reached that HLW can be disposed of in stable deep geological strata (geological disposal) so as to be isolated from human environments for a long term. Waste glass inserted in an over pack (e.g. carbon steel) with a bentonite buffer around that will be placed at a depth below 300 m in the Japanese proposal (Fig.2-1).

To initiate repository operation in the late 2030s, the Nuclear Waste Management Organization of Japan (NUMO), which has the responsibility for geological disposal of HLW, is now calling for municipalities to volunteer as candidate site areas and be surveyed, which is the first stage in the final disposal project.

Geological disposal of HLW will be a long term project of more than one hundred years from siting to construction, operation and closing. Therefore, continuous strengthening of the technical foundations of these activities is very important. To support such a national project technically, we have conducted research and development in various fields, e.g. geoscientific research, engineering development, and performance assessment (PA) of the geological disposal system.

A particular focus of our research and development activity at present involves projects at two Underground Research Laboratories (URLs) to establish techniques for characterizing the geological environment: one at Mizunami city in crystalline rock and the other at Horonobe town in sedimentary rock (Fig.2-2). The investigations from the surface (phase1) have been completed. The results from this phase of both URL projects were reported at an open symposium in September 2007. The research of the excavation phase is ongoing currently to verify and refine the results of phase1 such as methodology of investigation and modelling of geological environments. Research on geological phenomena such as faults and volcanic activities in order to evaluate the long-term stability of deep geological environments also has progressed (Topic 2-7, Topic 2-8).

At the same time, we are conducting laboratory experimental studies at the Tokai research center. Relatively large-scale and non-radioactive experiments, performance assessment of the multibarrier system supported by extensive computer analysis, and research to obtain basic data concerning the chemical properties and migration behavior of radionuclides under geological disposal conditions has been carried out. These studies are linked with the geological environment data obtained from URLs. In 2007, the data for long-term stability of overpack were complied (Topic 2-3) and "FepMatrix" was released on the Web to serve as an important supporting tool for scenario development in safety assessment (Topic 2-4).

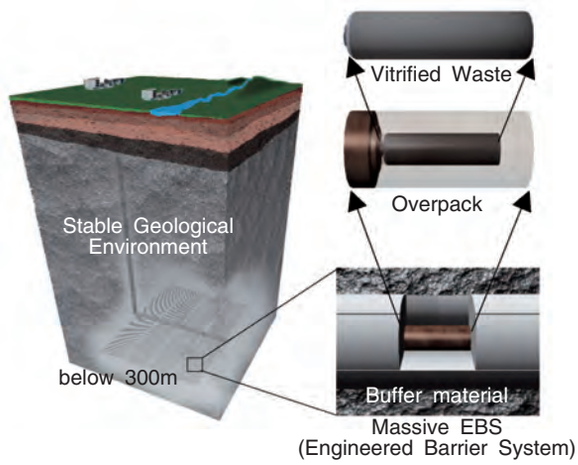

Fig.2-1 Basic Concept of HLW Disposal in Japan

Based on such research and development activities, we have conducted a project to develop the next generation novel knowledge management system (KMS) to systematically manage multiple lines of evidence and scientific results relevant to safety in the form of a knowledge base. The design of KMS was completed in March 2008. System integration is underway at present (Topic 2-1).

In April 2008, the basic policy and plan for implementation of geological disposal of HLW were revised by government. It was apparent that research and development organizations should contribute to understanding by the nation of these efforts through publicity on their research and development facilities by means such as URL. In this revision, the implementation schedule was also changed. We will make steady progress in improving technology and reliability of geological disposal in Japan, taking advantage of trends in business and planning our R&D to be optimally effective.

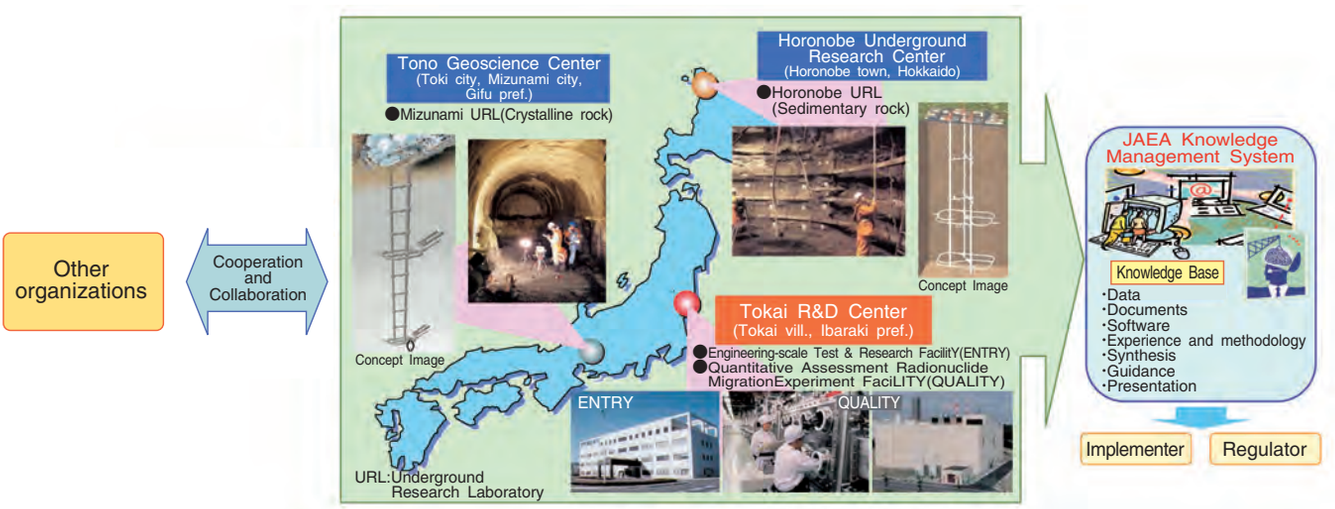

Fig.2-2 R&D Facilities

2-1 For the Utilization of Knowledge on Geological Disposal Technology
–Detailed Design of Knowledge Management System–

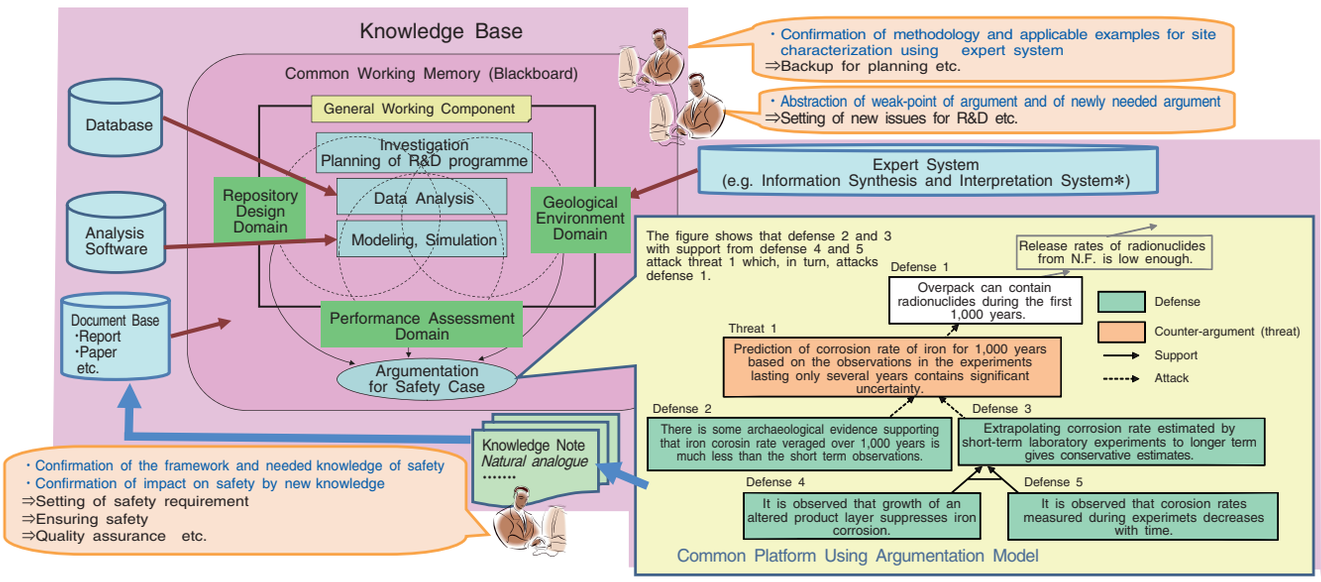

Fig.2-3 Schematic detailed design of knowledge management system
(*: performed under a contract with ANRE)

The unique feature of geological disposal of radioactive waste is that safety needs to be ensured for an extremely long time, tens of thousands of years in the future. It is necessary to have society accept explanations of the safety of geological disposal based on a variety of evidence, because it is impossible to actually demonstrate safety for such a long term. A reliable knowledge base on geological disposal is indispensable to give a trustworthy explanation. The objective of R&D on geological disposal technology is to accumulate knowledge and to enhance the reliability of the technology.

Explanation of the safety of geological disposal is complicated, drawing on an enormous amount of knowledge in multiple fields. The main body of a safety report alone runs to several thousand pages. In addition, the amount of knowledge related is anticipated to increase exponentially during the next few decades as waste disposal is implemented. It is important to continue to systematically collect such new knowledge in order to demonstrate safety.

The results of R&D, such as a database, software for analysis and technical report, are organized into a knowledge base. The knowledge base is updated with new knowledge provided through the R&D. The results of R&D are evaluated as to how they contribute to explanation of safety. Newly gained knowledge is examined carefully as to whether it supports the reliability of procedures or creates doubt. The evaluation of knowledge is a very time-consuming task. Therefore, it is necessary to build a new system in order to share the information among those concerned. A framework of knowledge management that optimizes production, dissemination, and use of the relevant knowledge has been proposed, based on a concept that regards development of the safety case as a chain of arguments and counter-arguments (argumentation model) regarding the design.

Our Knowledge Management System (KMS) enables those concerned to understand the effect of new knowledge upon safety, identify issues in use of knowledge, and make plans for the necessary investigations and analyses to solve the identified issues. In many cases these activities depend on “tacit knowledge” of the experts which has been accumulated over decades. In our KMS, the tacit knowledge, including technical know-how on application of complex investigation techniques and experience gained in the past, is synthesized as an expert system in order to improve the efficiency and quality of the safety case and to transfer the knowledge to the next generations (Fig.2-3). The detailed design of an intelligent KMS that utilizes state of the art technology in knowledge engineering has been completed. A prototype of a novel KMS will be developed by the end of the current five-year R&D program (2005 - 2010), taking into account both present requirements and possible future needs of users.

Reference

Osawa, H. et al., Design Concept of a Knowledge Management System of Geological Disposal Technology, Karyoku Genshiryoku Hatsuden, vol.621, no.6, p.26-33 (in Japanese).

2-2 Development of Buffer Material Database –Compilation of Characteristic Data of Buffer Material–

(a) Top page of the database website

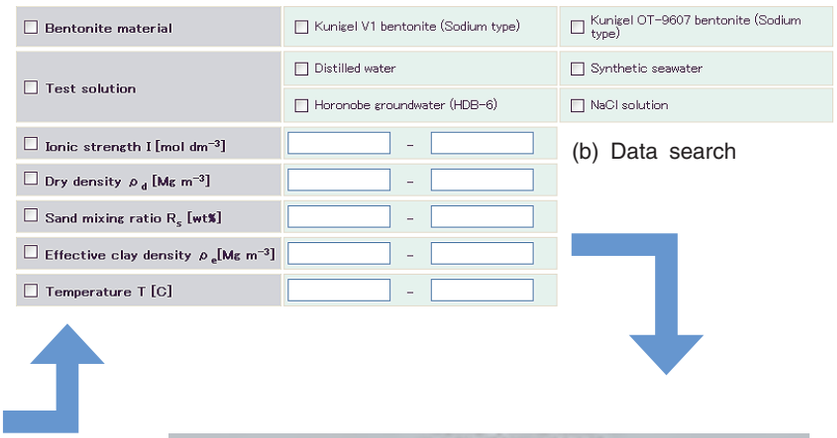

(b) Data search

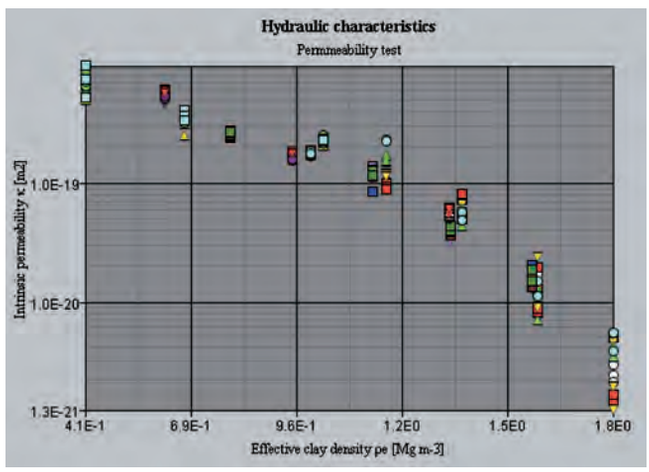

(c) Example of graph-plotting

Fig.2-4 Screen displays of the buffer material database

The basic characteristics of the buffer material such as hydraulic, swelling, mechanical and thermal properties are essential in designing and long-term behavior/performance assessment of a engineered barrier system of the HLW repository. It is beneficial to systematically compile these basic buffer data to allow both the implementing company and regulators to easily access data for their use in future stages. Therefore, we have developed the Buffer Material Database focusing on the basic properties of Japanese bentonite. A Japanese version of the database has been on the JAEA Website since Mar. 2006, and an English version since Mar. 2007 (http://bufferdb.jaea.go.jp/bmdb/).

The basic characteristics of the buffer material have been collected mainly through experiments since 1989. All of the data are now available at the above database website (Fig.2-4 (a)). Some functions such as data search (Fig.2-4 (b)) and graph-plotting (Fig.2-4 (c)) are built in the database system. The data is searchable by selecting variable items such as dry density, sand mixtures ratio, test temperature, water content, test solution (distilled water, synthetic seawater, Horonobe groundwater and NaCl solution), and ionic strength of the test solution. The searched data can be downloaded from the website in CSV format. In addition, information on the experiments such as composition of the bentonite material, sand material and test solution are also available. At present, data of about 1,820 cases are stored in the database, and the data related to bentonite extrusion behavior into rock fractures was added at the end of last year. Up to now, the buffer material database has been used by research institutes, universities, private companies and the nuclear waste management organizations at home and abroad such as NUMO, SKB, NAGRA and POSIVA. The number of user registrations has now reached 145, and there have been 427 data downloads and 625 uses of the graph-plotting function. Updating of the database is continuously conducted and also the system will be improved in response to users' opinions and requests.

Reference

Kikuchi, H., Tanai, K. et al., Database Development of Fundamental Properties for the Buffer Material in Japan, Proceedings of International Conference on Nuclear Energy System for Future Generarion and Global Sustainability (GLOBAL2005), Tsukuba, Japan, paper no.238, 2005, 6p., in CD-ROM.

2-3 Estimation of Long-Term Metallic Corrosion Using Archaeological Sample –Application of Analogize Phenomena in Nature on Geological Isolation Research–

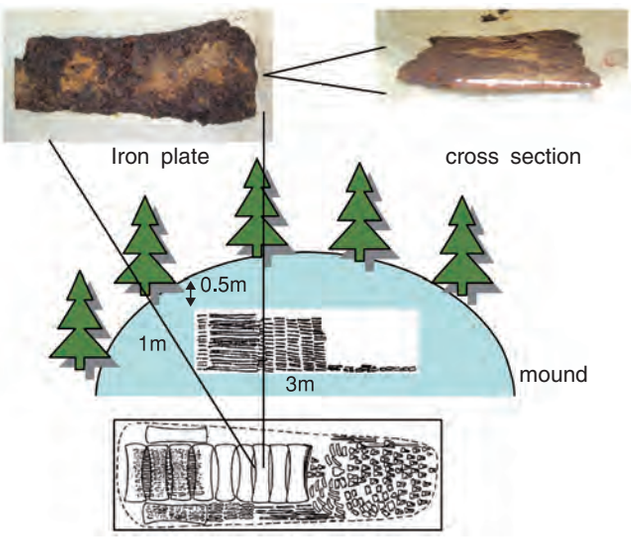

Fig.2-5 Condition of iron plate buried for 1500 years and its excavation site

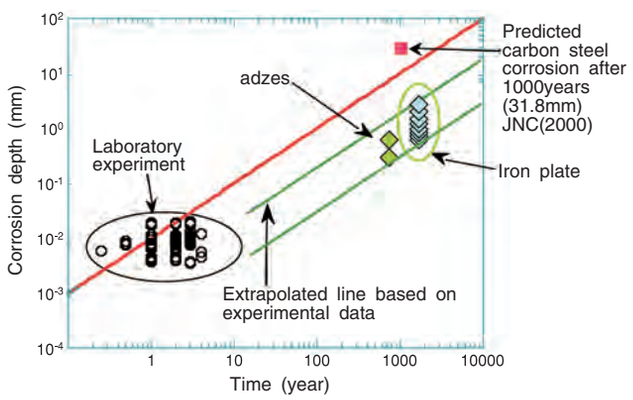

Fig.2-6 Conservatism of prediction of corrosion after 1000 years based on data of excavated artifacts

Carbon steel material being considered for use as an engineered barrier system (overpack) is expected to keep its strength for more than 1000 years. We estimated maximum corrosion depth of the overpack as 31.8 mm for 1000 years in the case of vertical setting in rock. For the purpose to obtain some data as second evidence for the long stability estimation, we investigated corrosion phenomena for iron material of archaeological sample which buried for more 1000 years and their corroded environmental condition.

Two adzes buried in clay for 750 years were dug out from the Izumo-Oyashiro-keidai ruins (Taisha-machi, Shimane). One of candidate metal material of the overpack is carbon steel which will be surrounded by clay in a proposed concept of Japanese high-level waste disposal. The environment of these excavated samples is similar to the proposed Japanese disposal environment.

Yamato 6th tumulus is famous as a ruin from which 872 iron plate artifacts were excavated. We examined the corrosion depth of these samples using X-ray CT. Although they were buried for 1500 years, they had metallic brightness in their cross sections (Fig.2-5).

Corrosion data for these artifacts such as thickness and density of the rust were analyzed non-destructively using a high-power X-ray computer tomography system, because of their historical importance. The density distribution was obtained from the X-ray CT image, and thickness of the rust was determined by the density difference between the base iron material (ρ=8.0) and their rust (magnetite: ρ=4.0). In Fig.2-6, the corrosion data of the artifacts is shown together with data from laboratory experiments with corrosion periods of several years. The red square symbol ■ is carbon steel corrosion depth, 31.8 mm, after 1000 years predicted by extrapolation of the laboratory data (red line). Two green lines extrapolations based on experimental corrosion data under slightly oxidizing or reducing conditions. The upper line corresponds to a 0.001 mm/y corrosion rate. It is clear from these results that the predicted corrosion data is conservative.

We will continue to obtain corrosion data of iron artifacts as secondary evidence for the long term stability estimation of carbon steel and work to develop a high reliability estimation method.

Reference

Yoshikawa, H. et al., Application of Archaeological Analogues for a Repository Safety Case : Arguments Supporting the Waste Container Lifetime, Safety Cases for Deep Geological Diposal of Radioactive Waset : Where Do We Stand ? , Symposium Proceedings, Paris, France, 2007, OECD-NEA, 2008, p.365-371.

2-4 Realistic Application of Safety Assessment Methodology to Disposal Environments
–Arrangement and Development of Basic Information Using FepMatrix Tools–

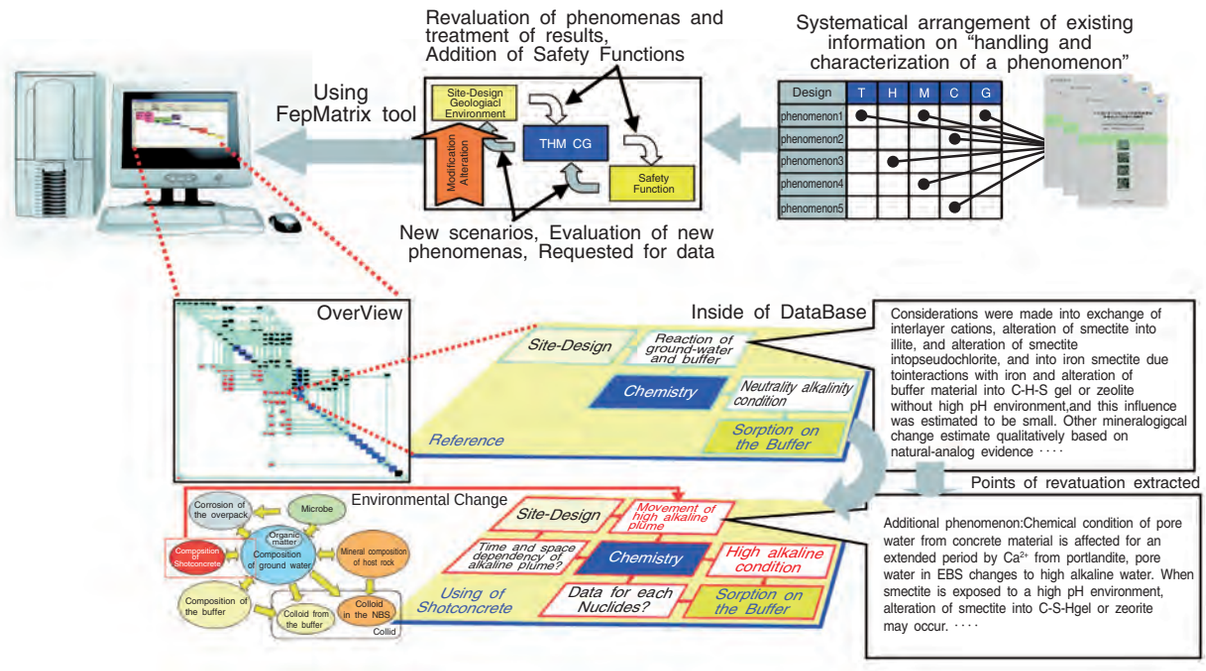

Fig.2-7 Example of information flow in safety assessment

In the safety assessment of radioactive waste geological disposal, there are wide-ranging characteristic features and phenomena to deal with, and it is also essential to consider those features and phenomena in the time scale of hundreds of thousands of years and in the space scale of an enormous natural host-rock. For the safety assessment, it is very important to accurately take in these uncertainties, hence, investigation of the uncertainty comprises several stages, such as the stage of understanding the relevant phenomena classifiable into various specialized fields and the stage of the model building based on this understanding. Therefore, a method to easily understand the process of creating the safety assessment procedure and to improve the tracking of this process are considered in this project.

The characteristic features and phenomena to deal with in the assessment can broadly be classified into four categories, Thermal (T), Hydrological (H), Mechanical (M), and Chemical (C). It is important to organize them considering geometric (G) time change. (Hereinafter "THMCG".) This is because operation of a barrier function (safety function) giving concrete form to the long-term behavior and the safety assessment thought to result from the geological disposal system based on the geological environment as interpreted by THMCG and a design suited to that environment can be systematically characterized. By organizing the above information, it will be possible to review scenarios considering the interaction of the phenomena which should be assessed. To confirm the effectiveness of this concept, we tried organizing the process of making the safety assessment of a reference case which was used for the H12 report's second evaluation of geological disposal R&D using FepMatrix which is a scenario analysis tool (http://www.jaea.go.jp/02/press2007/p07061901/index.html). FepMartix is a publicly available tool developed for organizing the mutual relation functions of vast numbers of characteristics and phenomena in chart form in a computer. With this method, the conditions of geological environment, design of the disposal, and the phenomena of concern and how they are dealt with are reflected in the safety assessment of H12 in an organized fashion.

For instance, in investigating the impact on the environment of the alkaline component of cement in the rock which needs concrete support, this method enables us to extract easily points of the current safety assessment which have been modified or added, by following the modification history of the information (in the balloon boxes of Fig.2-7). Moreover, it was found that when settings which were made according to quantitative assessment of safety functions are too conservative or oversimplified and were to be removed, by tracing back the flow of information from the safety function, we could extract easily the phenomena which should be considered in more detail and the scenario that should be given attention. Thus, the prospect for the extraction of scenarios and the modification of analysis cases looks brighter, even though the results are updated and the designs are modified in future geological research.

Reference
Inagaki, M. et al., A Study of Methodology and It's Applications for the Evaluation of Total System Performance which Considered the Site-Information and the Design-Information, JAEA-Research 2008-022, 2008, 37p. (in Japanese).

2-5 Development of Knowledge Base for HLW Disposal Technology –Technical Know-How and Analysis of Decision Criteria for Characterization of Geological Environment–

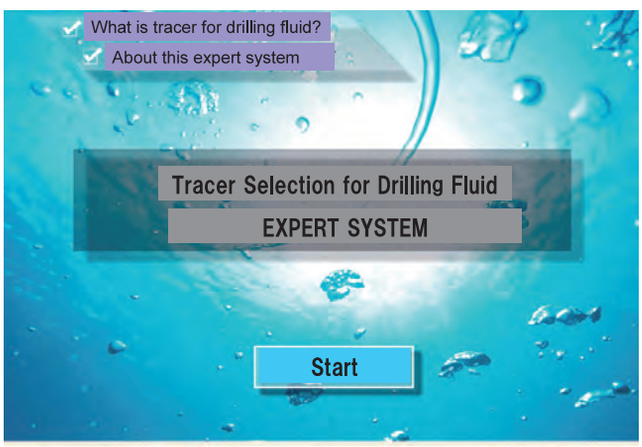

Fig.2-8 Start page of expert system to aid in selection of tracer for drilling fluid

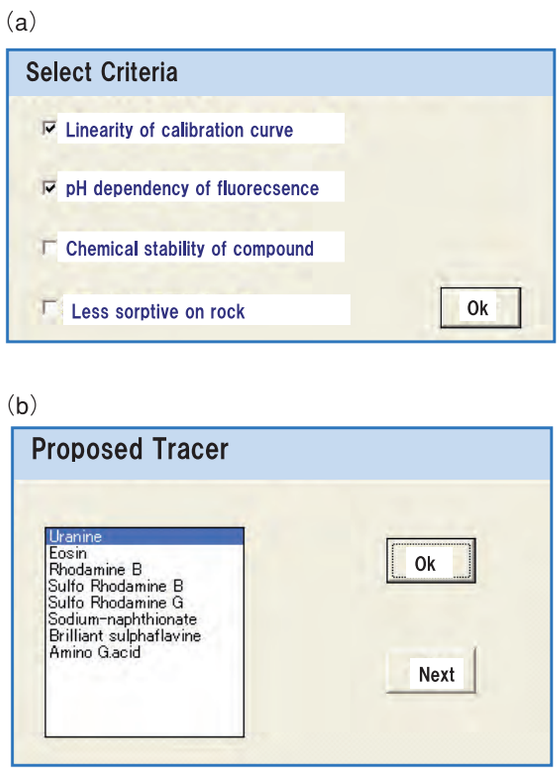

Fig.2-9 Proposed tracers for drilling fluid
In this example, two criteria were chosen by the user. Then, the expert system proposed eight compounds.

The Mizunami Underground Research Laboratory Project (MIU Project) has been carried out since 1996 in Mizunami city, Gifu prefecture, as a part of R&D for HLW disposal. A report giving all results of the surface-based investigation phase (Phase I) was published in 2007. In this report, methodology for the characterization of geological environments was summarized. On the other hand, the decision making process leading to the modification of the investigation program and the setting of input parameters to be used for modeling was not described. The experiences and knowledge gained during investigations of geological environment are only preserved in the program specifications. The above decision making process, experiences, and knowledge are however important for the implementation of HLW disposal.

In this study, we tried to clarify these decision making process, experiences and knowledge obtained through the Phase I investigations. For example, the decision making process can be expressed as following rules of an “if-then” format. In total, seven types of expert system have been developed. Fig.2-8 shows an expert system for the selection of tracer for drilling fluid. Suitable tracers are proposed by the expert system based on the experience obtained through the MIU Project (Fig.2-9). Additionally, basic information (chemical structure etc.) of each compound is available.

We found that so-called “expert judgment” can be expressed as rules. In this way, knowledge and experiences dealing with characterization of geological environments can be passed on to the next generation. This approach is desired for the implementation of HLW disposal project because the target duration of this project is several decades

This work was carried out by JAEA under the contract with the Natural Resources and Energy Agency, Ministry of Economy, Trade and Industry.

Reference

Saegusa, H. et al., Final Report on the Surface-based Investigation (Phase I) at the Mizunami Underground Laboratory Project, JAEA-Research 2007-043, 2008, 337p. (in Japanese).

2-6 Development of Quality Assessment Method for Hydrochemical Data
–Proposal of Methodology Based on Evidence Support Logic–

1. pH measurement is of adequate quality
   - 2. Drilling fluid contamination sufficiently low
     - 3. Degree of contamination by drilling water, as indicated by artificial tracers
     - 4. Degree of contamination by drilling water, as indicated by natural tracers
   - 5. Evidence other than drilling fluid contamination
     - 6. Analytical evidence indicates that pH has not changed significantly from in-situ value
       - 7. pH measurement is of adequately high quality
       - 17. Stability of physico-chemical parameters
       - 18. Chemical preservation of sample adequately preserved in-situ pH
       - 19. CO2 not lost or gained by the sample
     - 25. Indirect evidence indicates that pH has not changed significantly from in-situ value
       - 26. Contamination by untraced formation water affected pH insignificantly
       - 27. Indirect geochemical evidence indicates that pH has not changed significantly
       - 35. Hydrogeological evidence indicates that pH has not changed significantly
       - 43. Evidence that quality of equipment and material is adequate
       - 55. Methodological information indicates that pH has not changed significantly

Fig.2-10 A part of process model for assessing accuracy of measured pH value
Process model is constructed based on classification of all items needed to decide a quality evaluation proposition (in this case, on the accuracy of measured pH). Probability that the proposition is true, false or uncertain is calculated based on the values input to the end nodes of the process model.

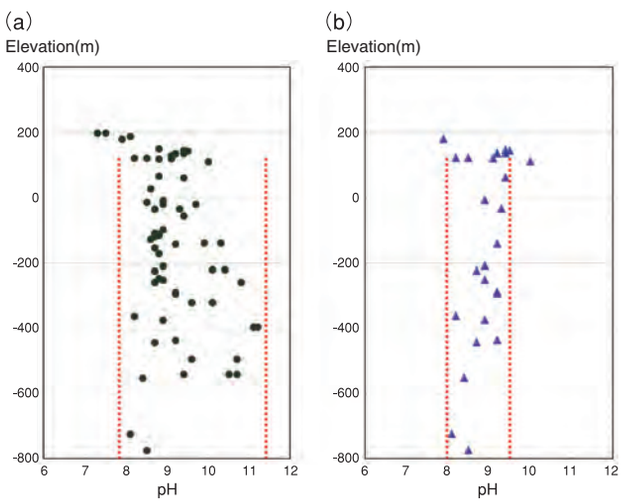

Fig.2-11 Result of quality assessment of measured pH value
The plot of data obtained by borehole investigations is evaluated to have a certain degree of accuracy (b) fall within a narrower range than the plot of all data (a).

Hydrochemical investigations of deep geological environments for the study of water resources, high-level radioactive waste disposal, etc. have become frequent in recent years. However, the methodology of the hydrochemical investigation and of the quality control differs with each investigation. Therefore, there is a possibility that some problems will occur due to difference of data quality when we use the hydrochemical data of different investigations in common. Development of methodology for selecting hydrochemical data that have enough quality to meet user needs will be useful for solving this problem. This study is aimed at establishing a methodology for quality assessment of chemical data obtained from groundwater samples using a method known as Evidence Support Logic.

The basic operations of ESL are similar to Boolean operations. However, the element “uncertainty” is also used in ESL in addition the “true” and “false” in Boolean operations. Uncertainty in ESL means the probability that a proposition cannot be judged either true or false. One of the main characteristics of ESL is its process model (Fig.2-10). This process model is a hierarchical structure extracting evidence and classifying related items needed to prove a hypothesis. In the case of Fig.2-10, the hypothesis is “measured pH value is the true pH value of groundwater”. The process model searches and organizes all elements related to quality of the data given in the proposition. Therefore, it is useful not only for elucidating the process of quality assessment but also for improvement of investigation method by detection of problems with the investigation. The results showed that 23 out of 63 samples satisfied the applied quality criteria. The plotted data from the 23 samples (Fig.2-11 (b)) have a more constant value from the top to the bottom of investigation area (from 8 to 9) than the data from all samples (Fig.2-11 (a)). After low quality data was identified, it was verified that sufficient quality control was not applied, and there was contamination during borehole drilling and on groundwater sampling. These results show that the data which meet the chosen criterion express pH of each depth more precisely.

This study indicates that the quality assessment method demonstrated is applicable to hydrochemical studies and that by thus confirming the sample quality it will be possible to develop a clearer interpretation of the deep underground geochemical environment.

Reference

Mizuno, T. et. al., Proposal for Quality Assessment Method of Groundwater Chemistry for Hydrochemical Investigation, Nihon Chikasui Gakkaishi, vol.49, no.2, 2007, p.139-152 (in Japanese).

2-7 Study of Features of Active Faults Based on Measurement of Hydrogen Gas Emission from the Underground
–Development and Application of Portable Hydrogen Gas Equipment–

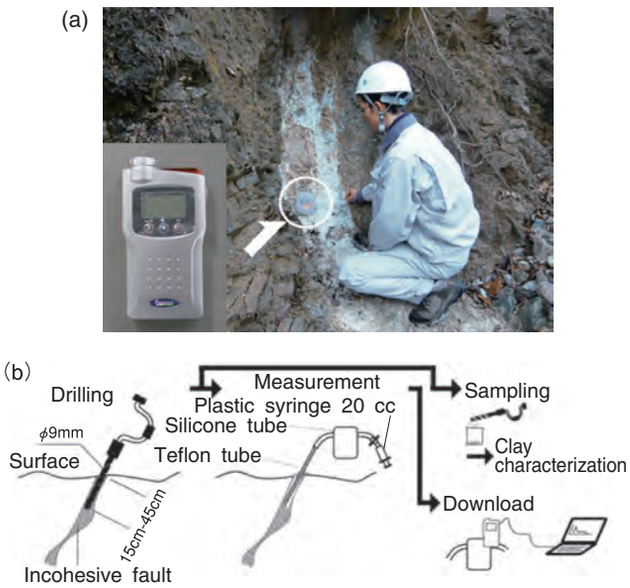

Fig.2-12 Hydrogen measurement in fault zone (a) and process flow of hydrogen measurement (b)
(a) Data logger with H_2 sensor. The key part of the new equipment is a light, compact hydrogen gas sensor which can make measurements easily.
(b) A Teflon tube is fixed in the hole using clay recovered from the hole. The equipment is left logging on the site for approximately three hours or more.

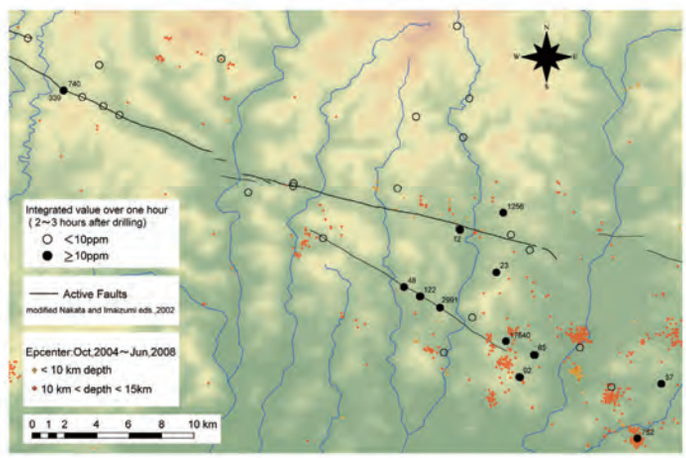

Fig.2-13 Distribution of density of hydrogen gas around Yamazaki fault zone
The integrated value over one hour (2-3 hours after drilling); ○ is less than 10ppm, ● is 10ppm or more.

Research on the influence of fault activity on deep geological environments contributes to the reliability of geological disposal systems for high level radioactive wastes. The permeability of a fault zone tends to be higher than the surrounding bedrock. Thus, it is important to understand the long-term changes of regional groundwater flow around the fault zone, where a wide crushed bedrock zone frequently exists. We are examining the applicability of an investigation technique using hydrogen gas emission from fracture zone.

It has been observed that the hydrogen gas emitted from underground along the active fault exceeds the atmospheric concentration (ca.0.5ppm). Various laboratory experiments have shown that hydrogen gas is generated during fracturing of rocks in deep underground near the hypocenter of an earthquake. It is reported that the hydrogen gas migrates to ground surface along the same fractures through which groundwater flows. Therefore, we expected that in this way we could estimate hydraulic properties such as the groundwater pathways and the continuity of fractured rock zones around the fault.

To determine hydraulic flow properties around an active fault, it is necessary to measure the concentration distribution of hydrogen gas over a wide area. However, the conventional hydrogen gas measurement tool is a large device requiring a day or more to accurately measure concentration of hydrogen gas discharged from underground. Therefore, we developed a new measuring tool using portable hydrogen gas detectors which enables measurement of many points in a short time (Fig.2-12). We investigated the concentration of hydrogen gas emitted from the Yamasaki fault zone, in southeast Japan. The Yamasaki fault zone is one of the major active faults in Japan which caused the A.D. 868 Harima Earthquake. In our survey, the points where high concentrations of hydrogen gas emission was detected were unevenly distributed along the active fault, and in the southeast portion of the study area where small earthquakes frequently occurred (Fig.2-13).

Based on these results, we will carry out the measurement of hydrogen gas emission in many study areas to obtain basic information on hydraulic flow properties around the fault by and also to understand the relationship between emitted gas concentration distribution and properties of the geologic structure.

Reference
Shimada, K., Tanaka, H., Saito, T., Rapid and Simple Measurement of H_2 Emission from Active Faults Using Compact Sampling Equipments, Resource Geology, vol.58, no.2, 2008, p.196-202.

2-8 Strategy for Long-Term Predictions for Geological Disposal R&D –Long Term Prediction of Groundwater Flow Changes Based on the Geological History–

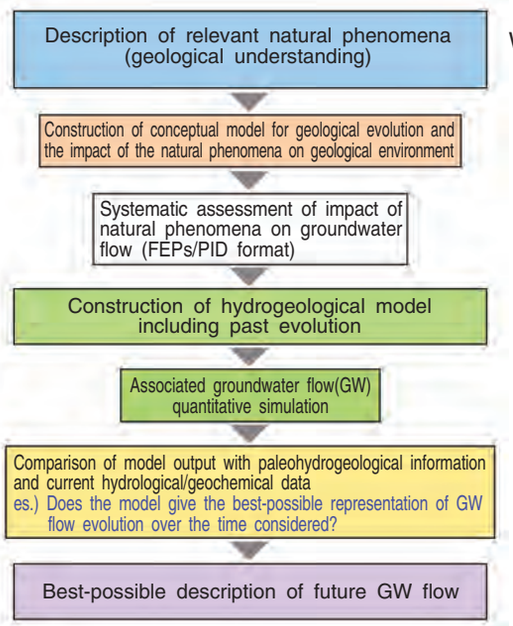

Fig.2-14 Basic framework for long-term prediction of groundwater (GW) flow changes
Understanding of evolution of the groundwater (GW) flow from the past to the present was used to develop descriptions of likely future evolution of GW flow.

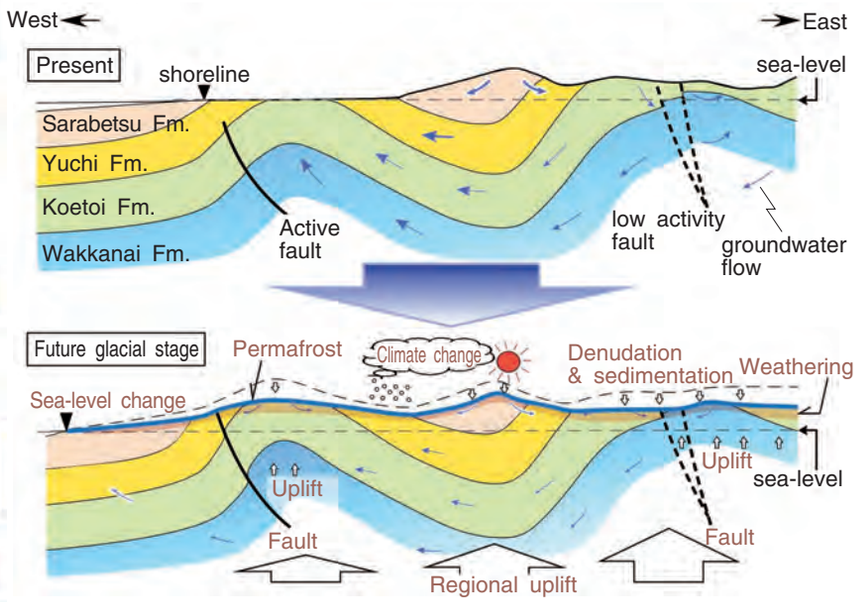

Fig.2-15 A conceptual model of likely future evolution of GW flow in the Horonobe area
The figure represents the situation in a future glacial stage, with some exaggeration, some 100,000 years in the future. The conceptual sketches of the future GW flow are based on an evaluation of the expected impact of natural phenomena, such as permafrost and shoreline and topographic changes, on the present GW flow.

A representative scenario for a human environment to be affected by waste disposed in a deep geological formation, is the groundwater scenario, where radionuclides are transported to the surface along with flowing groundwater (GW). The GW flow will be changed by natural phenomena such as precipitation/shoreline changes due to a climatic/sea-level change, and changes of topography/geological structures due to uplift, subsidence, and denudation on the geological timescale. Therefore, a critical issue for improvement of confidence in the long-term safety of the geological disposal is assessment of the safety taking into account expected long-term evolution of GW flow. We have been doing R & D of prediction of the GW flow evolution in the Horonobe area, northern Hokkaido as a case study, taking into consideration the impact of natural phenomena.

Basic methods of geological prediction are classified into two groups: (1) prediction by extrapolation of the tendencies and regularities of natural phenomena in the past, (2) prediction by analogy based on a study of the effects phenomena which resemble those expected in the study area. In any method, studying the past geological history is the key to predicting the future. We have developed a methodology for describing future GW flow using various site investigation technologies (Fig.2-14). Future likely evolution of the GW flow is described on the basis of past GW flow evolution determined by the geological history; it assumes that future natural phenomena will occur under much the same conditions as they did in the past.

The GW recharge will be reduced in a future glacial stage due to development of permafrost and precipitation reduction, and the flux and pathway of GW flow also will change due to a change of hydraulic gradient caused by topographic changes and lowering of sea-level (Fig.2-15).

We have been carrying out GW flow simulation for estimation of the past GW flow evolution taking account of the impact of natural phenomena. The results will be confirmed by comparison with the groundwater chemistry obtained by borehole surveys etc.

Reference

Niizato, T. et al., Paleogeography and Geological Evolution Since the Late Pliocene in and around the Horonobe Area, Northern Hokkaido, Chishitsugaku Zasshi, vol.113, suppl., 2007, p.119-135 (in Japanese).

2-9 Tracing Water Movement from Surface to Underground
–Surface Hydrological Investigation at Horonobe Area, Hokkaido, Japan–

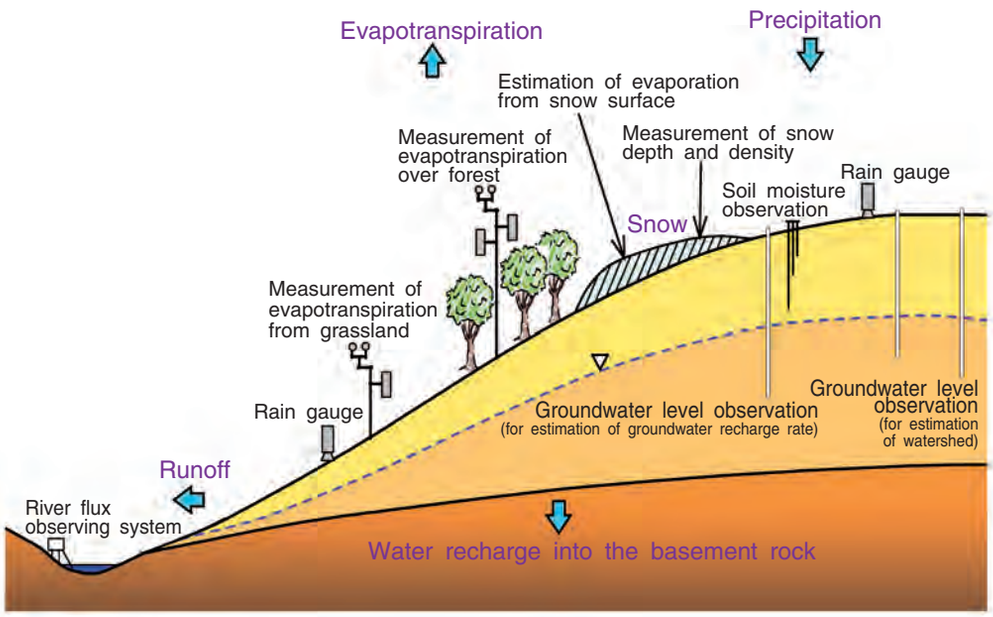

Fig.2-16 Schematic view of the surface hydrological investigation
Groundwater recharge rate from surface into underground is estimated by subtraction of evapotranspiration and runoff from amount of precipitation.

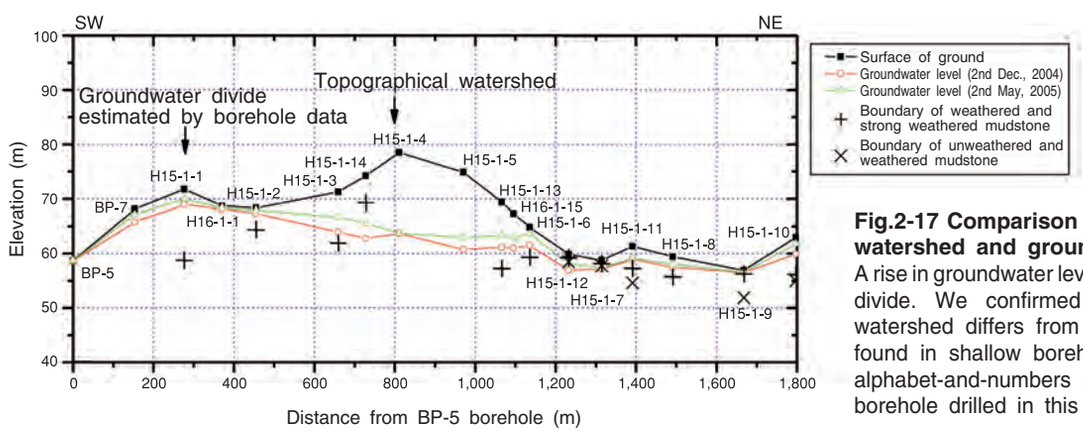

Fig.2-17 Comparison between topographical watershed and groundwater divide
A rise in groundwater level indicates a groundwater divide. We confirmed that the topographical watershed differs from the groundwater divides found in shallow borehole data. (In this figure, alphabet-and-numbers is a name of a shallow borehole drilled in this area.)

After rain and snow fall, there is evapotranspiration from plants and the ground surface, and runoff into rivers and lakes. The rest seeps underground through the soil. Knowing this recharge rate is necessary for groundwater flow analysis which in turn is important to evaluate the safety of geological disposal. Recharge rate is estimated by considering the above water balance of precipitation, runoff and evapotranspiration because it is difficult to measure directly.

In the Horonobe Underground Research Laboratory Project, we carry out surface hydrological investigations which consist of meteorological observation, observation of river flux and water quality, soil moisture observation and groundwater level observation in shallow boreholes extending several meters below the ground surface. These investigations aim to aid in developing the methodology to understand water balance and groundwater flow properties, by application of the series of research techniques used for these observations specifically to the estimation of recharge rate (Fig.2-16) .

From the current investigation, recharge rate of this whole area can be estimated as about 120 mm a year, which corresponds to 10% of precipitation (about 1,375mm a year) in this area. We also confirmed that the topographical watershed differs from the groundwater divide found in shallow borehole data. These results provide significant information for setting the boundary and initial conditions for groundwater flow analysis (Fig.2-17) .

We plan to evaluate the validity of these methodologies and the results of these investigations, including the appropriateness of the size of the observation areas, by comparison of observations up to now with data of the distribution of water quality and age, etc. and precise observations of precipitation and evapotranspiration taking account of snow accumulation.

Reference

Tomura, G. et al., Surface hydrological Investigation of Horonobe Underground Research Laboratory Project, JAEA-Research 2007-063, 2007, 46p. (in Japanese).

2-10 Tunneling Underground to Investigate Initial Stress Conditions –3-D Initial Underground Stress Measurement by Hydraulic Fracturing–

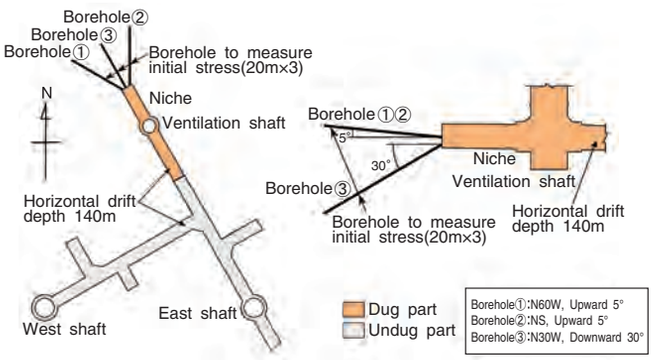

(a) 140m deep horizontal tunnel (niche) plane view

(b) 140m deep level tunnel (niche) side view

(c) Borehole ① drilling situation

Fig.2-18 Borehole drilling at initial stress measurement position

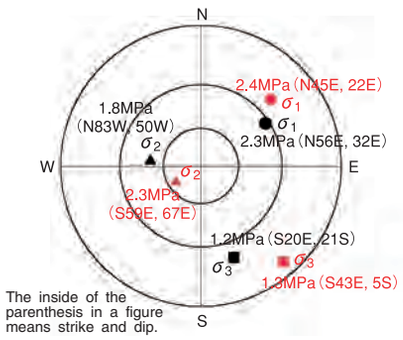

Fig.2-19 Measured initial stress (Schmidt net lower hemisphere of the principal stress)

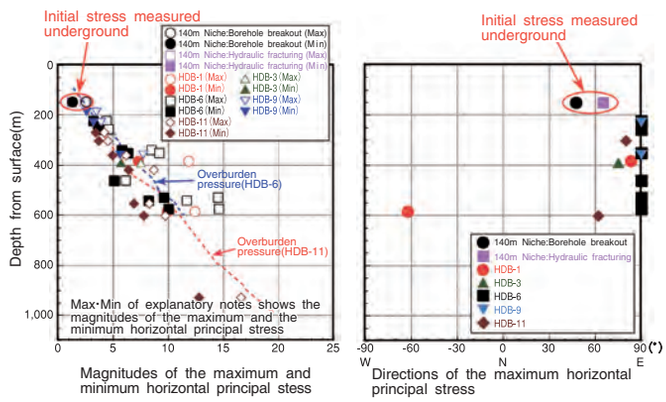

(d) Relation between the maximum/minimum horizontal principal stress and depth

(e) Relation between the direction of the maximum horizontal principal stress and depth

Fig.2-20 Comparison with the initial stress estimated in Phase1

The Underground Research Laboratory (URL) has been conducting a research project in Horonobe-cho, Hokkaido. This project aims at improvement of the reliability of technologies for geological disposal of high level radioactive wastes. It started in 2000, and the surface-based investigation phase was completed in 2005. Now it has shifted to the construction phase2 (investigation during construction of the underground facilities).

In the surface-based investigation phase1, the area of about 3 km × 3 km around URL in the Hokushin district, Horonobe-cho was selected as the main research area, and geophysical exploration, geological survey, borehole survey, etc. were carried out in this area. In general, initial stress due to crustal movement and overburden pressure has been taking place underground here. In designing underground structures, it is necessary to measure initial stress around underground structures. Therefore, estimation of initial stress distributed in the URL area has been attempted during surface-based investigations in order to design URL.

In investigation during construction of the underground facilities, the updating and check of the validity of initial stress estimations made during surface-based investigations is one of the main issues. Thus, three boreholes were made from the niche (GL-140 m) of ventilation shaft shown in Fig.2-18, and a three-dimensional evaluation of the initial stress in Koetoi Formation was done by the method called hydraulic fracturing. Breakout (spalling) of the walls of the boreholes due to the stress concentration was detected on plastic films wrapped on an impression packer inserted in the borehole. Then, analysis of the borehole breakout was performed to estimate in situ the orientation and magnitude of stress.

The measurement result of initial stress is shown in Fig.2-19. Initial stress was broken down into principal stress σ_1 (major principal stress), σ_2 (intermediate principal stress), and σ_3 (minor principal stress), and comparatively good coincidence in distribution of the direction of the principal stress evaluated by the two above methods was observed. Although the magnitudes of principal stress σ_1, σ_2, and σ_3 found by the surface based investigation and the impression packer were 2.3, 1.8, 1.2 MPa and 2.4, 2.3, 1.3 MPa, respectively and σ_2 values were somewhat different, general agreement was obtained. Fig.2-20 shows the result of the horizontal initial stress obtained from the borehole investigation (HDB-1, 3, 6, 9, 11 holes) carried out in the past, and the result obtained from the present underground test. Fig.2-20(d) shows the relation between the magnitudes of the horizontal principal stress, and depth. The Fig.2-20(e) shows the relation between the direction of the maximum horizontal principal stress, and depth. From this result, although the magnitudes of the maximum horizontal principal stress obtained here are mostly in agreement with the overburden pressure, they are slightly smaller than the past results. Moreover, the direction of the maximum horizontal principal stress had been found to be east/west in general. However, the present test showed that the direction was 25° or 43° counterclockwise from east/west. To gain data to explain this difference, initial stress measurements in the pressure at the depth 140 m (not counting the niche) in Koetoi Formation, and pressure at the still deeper depth for the Wakkanai Formation will be carried out.

Reference

Nakamura, T., Sanada, H. et al., Initial Stress Estimation of Diatomaceous Mudstone using Hydraulic Fracturing Test", The 12th Japan Rock Mechanics Symposium, 2008, p.297-303, in CD-ROM (in Japanese).

3 Nuclear Fusion Research and Development

For Practical Use of Fusion Energy

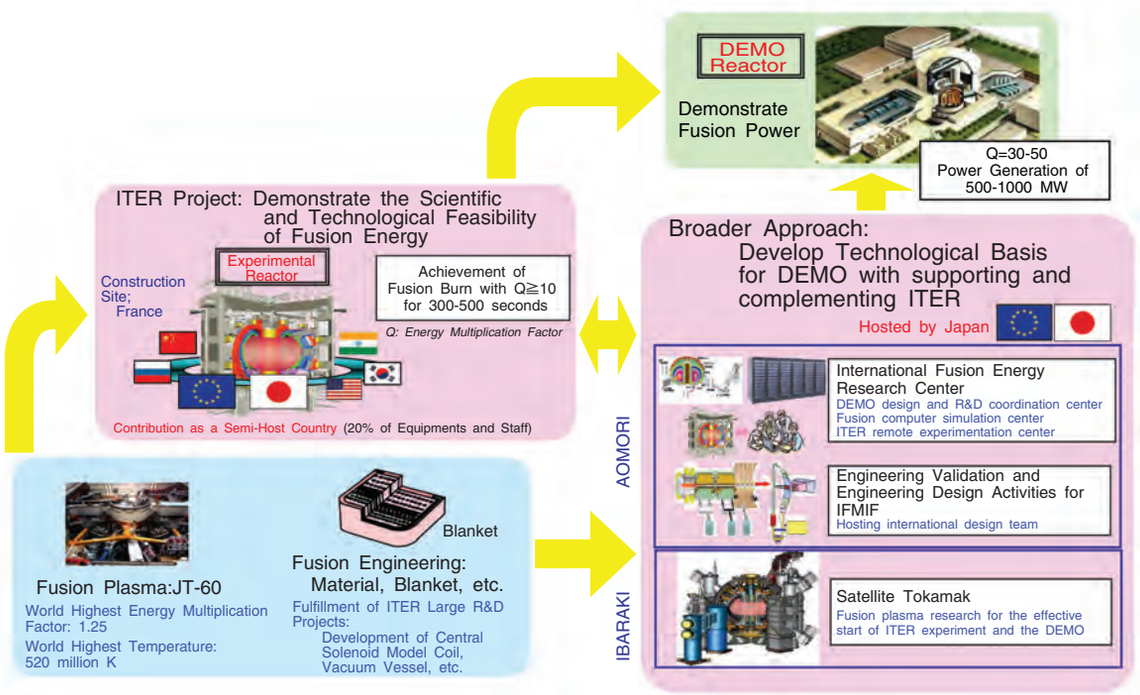

Fig.3-1 Development Steps Toward the Fusion DEMO Reactor

At the Fusion Research and Development Directorate, crucial R&D for practical use of fusion energy (fusion plasma and fusion engineering R&D) is being carried out in wide scale international cooperative projects such as ITER project and Broader Approach, aiming at realization of the fusion DEMO reactor (Fig.3-1).

ITER (International Thermonuclear Experimental Reactor) Project

The ITER project is an international cooperative project to demonstrate the scientific and technical feasibility of fusion energy through construction and operation of an experimental reactor. The participants are Japan, EU, US, Russia, China, Korea, and India. The participants account for more than half of the world population. The experimental reactor, ITER, is being constructed in Cadarache in France. The ITER agreement entered into force in October 2007, and JAEA was designated as the domestic agency of ITER project in Japan. Topic 3-5 and Topic 3-7, "World Record Achievement in Plasma Heating Device" and "Demonstration of Final Installation to within 0.5mm of a 4-ton Blanket by Remote Handling" are research results achieved in the course of preparation for ITER equipment procurement.

Broader Approach (BA) Activity

The BA activity is a joint project by Japan and EU executing research supporting ITER and the research and development for the DEMO reactor, the next step of ITER, aiming at the early realization of fusion energy. It is being implemented in Japan during the period of ITER construction (about 10 years). It consists of three projects; the activities of the International Fusion Energy Research Center, the engineering validation and engineering design activities of the international fusion material irradiation facility (IFMIF), and the research activities of Satellite Tokamak (upgrade of JT-60 to a superconducting machine). The former two is being conducted at Rokkasho village in Aomori Prefecture, and the satellite tokamak project at Naka city in Ibaraki Prefecture. The agreement launching BA entered into force in June 2007, and JAEA was designated as the implementing agency of BA activity in Japan. The BA activity includes a remote experiment of ITER, and Topic 3-3, "Development of the Plasma Movie Database System for JT-60", is a result which contributes to realize it.

Fusion Plasma Research

The critical requirement for the future fusion reactor is to attain a high level of economical efficiency, namely, to sustain a high fusion power in a reactor core of compact size. It is necessary to improve the plasma pressure (temperature × density) to accomplish that. Topic 3-1, "Establishment of Long-Pulse Operation for "ITER" Burning Plasmas", experimentally demonstrated that a high plasma pressure can be maintained stably using JT-60. Furthermore, Topic 3-2, "Finding the Intrinsic Rotation by Plasma Pressure", clarified the guiding principle to achieve high plasma pressure.

Fusion Engineering Research

The fuel of fusion energy is deuterium and tritium. A large quantity of deuterium exists in seawater. The tritium hardly exists naturally at all, but it can be produced from lithium, which is also contained plentifully in seawater. Topic 3-8 and Topic 3-9, "Materials Necessary for Stably Supplying Fuel Tritium to Fusion Reactors" and "Tritium Extraction Using a Fuel Cell" yielded results which contribute to the steady production of tritium.

It is necessary to heat plasma to cause the fusion reaction. Topic 3-4 and Topic 3-6, "Achieving High Power in the JT-60U RF System" and "Development of a Large Negative Ion Source" are results which enable the plasma to be heated more efficiently.

It is necessary to streamline the maintenance of the fusion reactor in order to raise its operation rate and thus improve its economic efficiency. Topic 3-10, "Torus Configuration and Maintenance Concept of Compact Fusion DEMO Reactor" is a result which raises the operation rate of the plant by executing regular maintenance in a short time.

3-1 Establishment of Long-Pulse Operation for "ITER" Burning Plasmas –Steady State Sustainment of High Confinement and High β Plasmas–

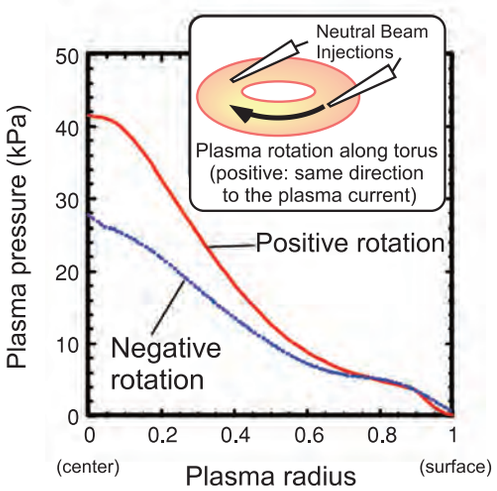

Fig.3-2 Comparison of plasma pressure profile with different plasma rotation
The plasma rotation along the torus was controlled by neutral beam injections providing torque. When the plasma rotated in the positive direction, the plasma confinement was improved. Then, higher plasma pressure was obtained as shown by the red line.

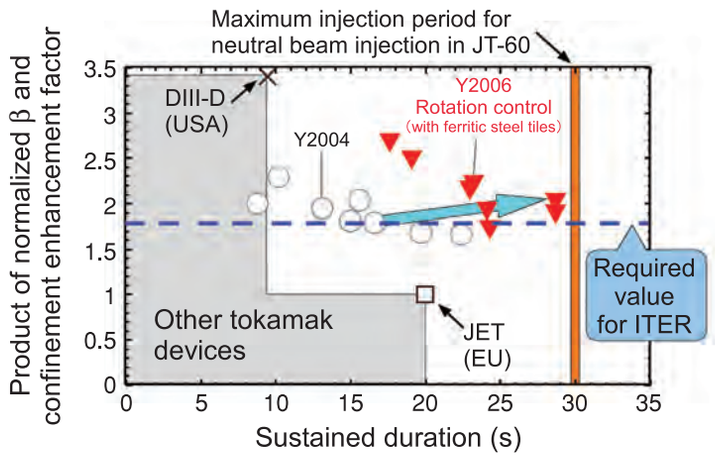

Fig.3-3 Plasma performance and sustained duration in long-pulse plasmas
The controllability of the plasma rotation and the efficiency of neutral beam heating were improved by toroidal magnetic field ripple reduction through use of ferritic steel tiles. As a result, a high product of normalized plasma pressure and confinement enhancement factor exceeding the ITER standard was sustained for 28.6s. This new world record is about 1.7times longer than the previous world record of 16.5s achieved in JT-60U.

One of the major objectives of ITER is to sustain burning plasmas with fusion gain (Q = fusion power output/auxiliary heating power input) larger than 10 for a long time (more than 400s). The fusion power is proportional to the square of the plasma pressure (temperature × density). To obtain such high Q plasmas, both A) High fusion power output, achieved by increasing the plasma pressure, and B) Reduced auxiliary heating power, achieved by improving the plasma confinement, must be satisfied simultaneously. "Normalized plasma pressure (β_N)" is used as the index of plasma pressure and "confinement enhancement factor (H_H)" is used as the index of the quality of the plasma confinement. The product of β_N and H_H, $\beta_N \cdot H_H$, is widely used as a measure of Q, since Q is proportional to $\beta_N \cdot H_H$,

In order to establish long-pulse burning plasma operation in ITER, steady state plasma operation with high value of $\beta_N \cdot H_H$, exceeding the value required for ITER, has been a main target of fusion plasma research. Making use of the good controllability of plasma rotation in JT-60, we found that the achievable β_N and H_H can be increased when the plasma rotation in the core becomes positive (Fig.3-2). In addition, the uniformity of toroidal magnetic field was improved by installing ferritic steel tiles inside the vacuum vessel. As a result of the reduction in the loss of fast ions from neutral beam injections for plasma heating, both the controllability of the plasma rotation and the efficiency of the neutral beam heating were improved successfully.

By optimization of the toroidal rotation profile and the edge plasma density so as to maintain high β and high confinement, steady-state operation of the high performance plasma has been established in JT-60 (Fig.3-3). In this study, high performance plasma with $\beta_N \cdot H_H$ of 2.0 was sustained for 28.6s, the world record. The achieved value of $\beta_N \cdot H_H$ is higher than that required for ITER standard operation of 1.8. The sustained duration is limited by the maximum injection period for the neutral beam heating system in JT-60. Since the pulse duration of the heating system for ITER is longer than the target regime (more than 400s), the long-pulse operation of burning plasmas for ITER seems to have been established.

Reference
Oyama, N. et al., Improved Performance in Long-Pulse ELMy H-Mode Plasmas with Internal Transport Barrier in JT-60U, Nuclear Fusion, vol.47, no.7, 2007, p.689-697.

3-2 Intrinsic Rotation Due to Plasma Pressure Discovered –Toward the Understanding of High Pressure / Highly Self-Regulating Plasma–

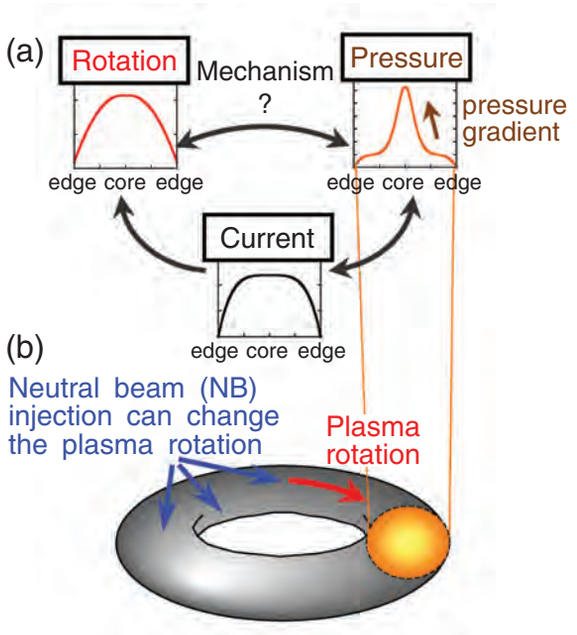

Fig.3-4
(a) Schematic view of self-regulating high pressure plasma
The plasma pressure, rotation, and electric current profiles are strongly linked to each other.
(b) Schematic drawing of JT-60 plasma
JT-60 has various neutral beams (NB) with different injection angles, which can change the direction of the plasma rotation and the rotation profile flexibly.

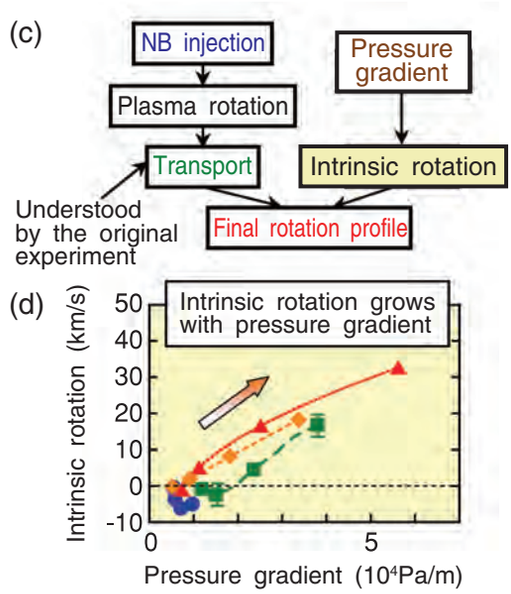

Fig.3-5
(c) Formation mechanism of the rotation profile
The rotation profile is determined by the external momentum input by NBs, momentum transport, and the intrinsic rotation caused by the plasma itself. Using an original experiment and analysis method, we have separately evaluated the externally induced rotation and the intrinsic rotation.
(d) Relation between the intrinsic rotation and the pressure gradient
The intrinsic rotation increases with increasing pressure gradient. The difference in color corresponds to the different NB power and torque.

Burning plasmas for nuclear fusion reactors are highly self-regulating, governed by strong linkage among plasma pressure, electric current, and rotation profiles as shown in Fig.3-4(a). To construct fusion reactors, it is essential to understand and control this self-regulating system. However, it has been an open critical issue for nuclear fusion research worldwide to understand the formation mechanism of the rotation profile and the relation between the rotation and pressure profiles. The rotation profiles are determined by various mechanisms: (1) the external torque input by neutral beams (NBs), (2) the momentum transport, and (3) the intrinsic rotation. However, these terms cannot be evaluated separately by the conventional steady-state-experiment and analysis.

In order to address this issue, we newly developed and applied an experimental method utilizing the modulation of a part of the NBs, and as a result we evaluated the momentum transport correctly. At low plasma pressure, it was found that the rotation profiles are determined by the external torque applied by the NBs and the momentum transport. At higher plasma pressures, the self-regulation appeared. In this case, we found that the measured rotation profiles cannot be explained merely by the momentum transport and the external momentum input from the NBs, and the intrinsic rotation becomes dominant. The relation found between the plasma pressure gradient and the intrinsic rotation in various confinement modes is shown in Fig.3-5(c). It was experimentally found for the first time that the intrinsic rotation grows with increase in the pressure gradient in all cases. This study enables us to understand the mechanism of the intrinsic rotation in high pressure and highly self-regulating plasmas, and gives important information about the prediction and operation of the self-regulation plasmas in ITER and other future fusion reactors.

Reference
Yoshida, M. et al., Role of Pressure Gradient on Intrinsic Toroidal Rotation in Tokamak Plasmas, Physical Review Letters, vol.100, 2008, p.105002-1-105002-4.

3-3 Development of the Plasma Movie Database System for JT-60 –Movie Data Handling Technology for Remote Experiment in the ITER-BA Project–

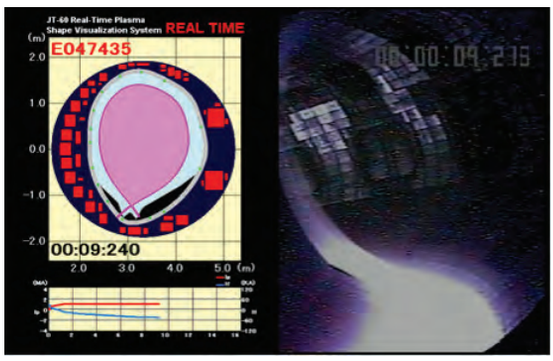

Fig.3-6 An Example View of Plasma Movie
The plasma movie consists of the plasma video camera picture, plasma cross section computer graphics (CG), and the voltage signal from the magnetic field probe input to the sound channel.

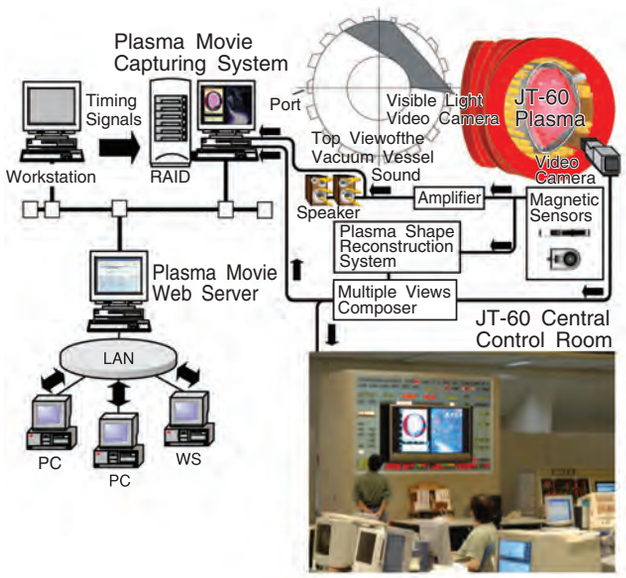

Fig.3-7 Hardware Configuration of the Plasma Movie Database System
Plasma Movie Capturing System (PMCS) automatically records a plasma movie according to the timing signal of JT-60 discharge sequence. This system executes 2 types of compression, MPEG2 and MPEG4, for an effective database handling. A user can download the plasma movie data file from the database through LAN.

A plasma movie is one of the most efficient methods to convey what discharge has been made in the JT-60. This movie on a large TV monitor is able to provide various types of useful information in real time to the physicists; hot spots due to heat flow from a plasma on the vacuum vessel wall, time-evolution of plasma position and shape, change of macroscopic plasma rotation, etc. This innovative technology has contributed to safe, efficient operation, and has added an important chapter to the history of tokamak experiment. This real-time monitor has already be come an indispensable tool in JT-60.

This movie is composed of 4 elements: a video camera picture (right: Fig.3-6), a plasma cross section CG (left: Fig.3-6) generated by physics-based calculations from magnetic field measurements, a sound which is just the magnetic probe oscillation signal converted to audio, and a display of the waveforms of the plasma current and of the poloidal field coil current. This plasma monitoring system for JT-60 was the first developed in the world for tokamaks, and is still a unique feature of JT-60. The sound signal sometimes has a mysterious timbre originating from amplification of the raw voltage signal of a small magnetic field pick-up coil sensor in the vacuum vessel. This sound seems to imply various plasma states; changes in plasma rotation speed appear to cause changes in the tone of sound. A stable plasma produces smooth high tone as it rotates at a high constant speed. On the other hand, an unstable plasma has a noisy low tone as it rotates at an irregular speed.

The plasma movie database system (PMDS) converts analog to digital movie data using 2 compression methods (MPEG2 and MPEG4). The MPEG2 generates a high-resolution (large volume) data file which corresponds to the high definition TV, while the MPEG4, originally developed for the high-speed network broadcasting, generates a low-resolution, data file.

The hardware configuration of PMDS is illustrated in Fig.3-7. The plasma movie capturing system (PMCS) converts a movie to MPEG2 format compressing in real time, and records the resultant MPEG2 movie file automatically. Immediately after the MPEG2 movie is completed, the system starts converting from MPEG2 to MPEG4 format. When all the conversion is completed, the system transfers an MPEG4 movie file to the plasma movie web server (PMWS). Two formatted movie files are stored in corresponding databases. The PMDS checks what new movie files become available for distribution through the network every 10 minutes. A user can download a movie file from the database. This system has been configured using a personal computer with Windows XP and the existing network, which minimized the development cost and time. We solved a technical issue in efficient handling of the huge-volume movie data by employing 2 compression methods newly available in the market, as mentioned above. Since this system creates a movie file for every discharge in the JT-60 experiment sequence, it provides a movie with sound giving sensory support to the conventional understanding of each discharge using waveforms of time-series data. In addition, the physicists can use this system also for search of the latest interesting pulse discharge.

For conducting experiments on ITER and the satellite tokamak fusion device JT-60SA from remote sites, the physicists and operators at the remote site have to know what discharge is going as accurately and immediately as possible. This system could be also the key technology of such future remote experiment since it includes advanced real-time processing and movie data handling technology. It has already been used in a demonstration of JT-60 remote experimentation from Europe in Dec., 2007.

Reference

Sueoka, M. et al., The Plasma Movie Database System for JT-60, Fusion Engineering and Design, vol.82, issues 5-14, 2007, p.1008-1014.

3-4 Achieving High Power in the JT-60U RF System –World Record for Gyrotron Oscillation (1.5MW,1s)–

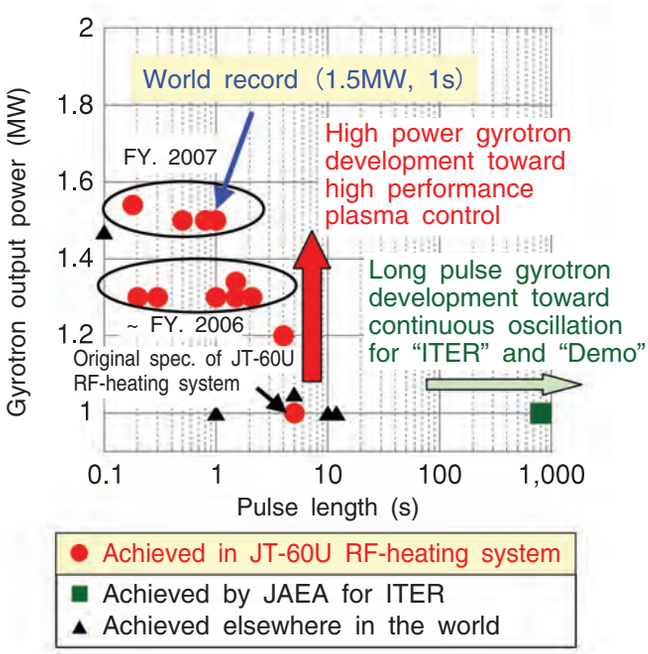

Fig.3-8 Performance of the world's gyrotrons (>1MW)
Remarkable power and pulse length were achieved by the JT-60U RF-heating system.

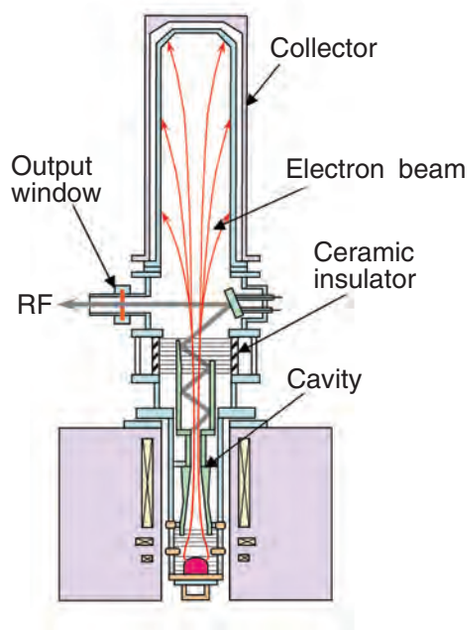

Fig.3-9 Schematic view of gyrotron
Energy of electron beam is converted to RF energy at the cavity, and the RF radiation is output through the output window. The cavity is strongly heated due to the high RF power density of the cavity resonator, and stray-RF radiation heats the ceramic insulator.

Gyrotron oscillation power of 1.5MW with pulse length of 1s, a world record, was achieved by the gyrotron of the JT-60U RF-heating system (Original spec.: 1MW for 5s) (Fig.3-8).

RF injection with pulse length over 1s is an important issue in fusion experiments because the typical time scale of phenomena in plasma is around 1s. Capability to do experiments on controlling high performance plasma strongly depends on the maximum RF power. Therefore, it is essential to improve the oscillation power of each gyrotron and also to develop a long pulse gyrotron, striving for continuous oscillation in future devices such as "ITER" and "DEMO". In a gyrotron system, electron beam and RF power heats up the internal components. That leads to failure of the components, arcing and sudden oscillation termination due to thermal expansion of a cavity, especially during high power operation. Those phenomena had limited oscillation power to 1MW in previous fusion experiments. Oscillation power of over 1.5MW had been achieved only in short pulse tests (less than around 0.1s) with gyrotrons without enough heat removal capability. Important issues are to clarify heat distribution, to improve high-temperature durability, and to improve heat removal capability. It is important to demonstrate stable oscillation with high power and pulse length over 1s.

In previous work, we found that a ceramic insulator was dielectrically heated by stray-RF radiation (Fig.3-9), so we introduced a silicon-nitride ceramic into one of the JT-60U gyrotrons in place of an alumina ceramic. Temperature rises of some internal components were measured and investigated over a wide range of oscillation power up to 1.3MW by means of the gyrotron. If a scaling up of those experimental results is possible there could be higher beam current operation with the improved cooling performance of the cavity. We have achieved stable 1.5MW oscillation for 1s by precise optimization of oscillation conditions using the improved gyrotron. Transmission of this high-power RF has been also demonstrated. Moreover, thermal expansion of the cavity had no significant ill effect on stable oscillation and the cavity temperature reached its maximum in 0.5s and saturated. Therefore, further pulse length extension with high power is possible in the near future when there are improvements in the power supply and transmission line.

Reference

Kobayashi, T. et al., Achievement of 1.5MW, 1s Oscillation by the JT-60U Gyrotron, Plasma and Fusion Research, vol.3, 2008, p.014-1-014-3.

3-5 World Record Achievement in Plasma Heating Device –Demonstrated High-Power and Steady-State Operation in Gyrotron toward ITER Construction–

Fig.3-10 The plasma heating device "gyrotron" for ITER
Height is 3m, and weight is 800kg. The gyrotron is installed in a superconducting magnet of 7T field strength. Synthetic diamond is used as the output window.

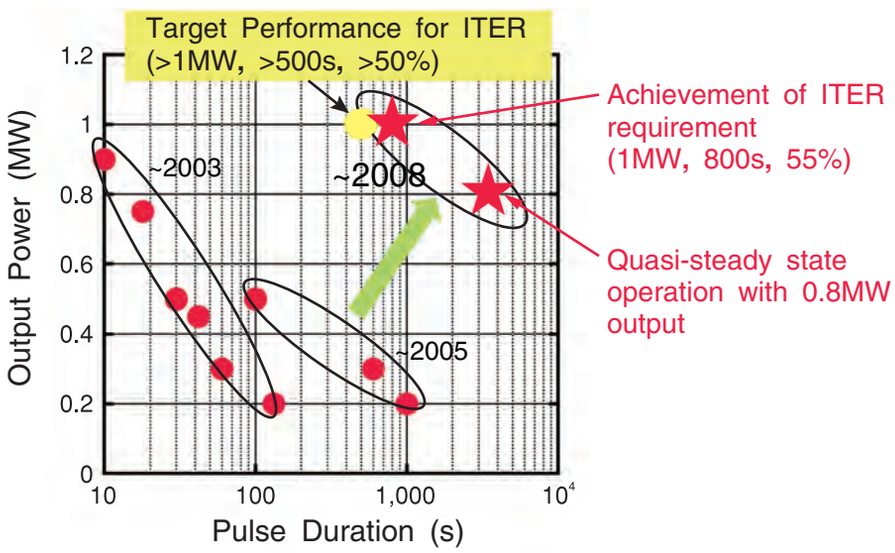

Fig.3-11 The progress of ITER gyrotron development at JAEA
This gyrotron is the first in the world to exceed the requirements of ITER (1MW, 500s, 50% efficiency). (ITER gyrotron is also under development in EU (1.2MW, short pulse) and Russia (1MW, 110s).

A gyrotron is an electron tube which can transduce electron beam energy into electromagnetic wave energy in the range of several GHz ~ THz. It will be used as a plasma heating device in the International Thermonuclear Experimental Reactor (ITER) (Fig.3-10). The high temperature plasma needs to be one hundred million degrees Celsius for the fusion reaction, which can be realized by the injection of RF beams like a microwave oven.

The ITER gyrotron is required to have 170 GHz frequency (70 times as high as that of microwave oven), 1MW output (2000 times as high as that of microwave oven), 50% efficiency (ratio of DC input power to RF power) and 500s pulse duration, which is a typical pulse time of ITER. We started the development of the high power gyrotron for ITER about 15 years ago and have developed advanced technologies of energy recovery, high power oscillation, and synthetic diamond windows ahead of other countries. Furthermore, we combined the technologies of steady state oscillation (to control the beam current) and of changing the rotational frequency of the electron beam and the rotation ratio (the ratio of the rotation speed to the travel speed) during the oscillation, which is a source of RF energy. The gyrotron succeeded in stably-shifting the operating region to the hard-self-excitation region, which achieved higher efficiency than the normal operating region. As a result, the oscillation efficiency of 55% was attained with 1MW power and the pulse duration greatly exceeded the performance required for the ITER gyrotron. Furthermore, quasi-steady state oscillation of 1 hour, which is necessary for the steady state operation phase planned for ITER, was achieved with 0.8MW output power and 57% efficiency (Fig.3-11). These results show that for, the first time in the world, the requirements of the ITER gyrotron have been met. The achievement is a great step forward for the ITER project. The physics mechanism by which high efficiency oscillation in the hard-self-excitation region can occur was clarified experimentally at the same time. This progress will stabilize and heighten gyrotron performance, and it will greatly contribute to the improvement of the plasma heating system in ITER. Application of gyrotrons to other fields, public and private, is also expected.

This study was awarded the Technological Prize (Research Section) in 2008 by the Minister of Education, Culture, Sports, Science and Technology.

Reference

Sakamoto, K., Kasugai, A. et al., Achievement of Robust High-Efficiency 1MW Oscillation in the Hard-Self-Excitation Region by a 170GHz Continuous-Wave Gyrotron, Nature Physics, vol.3, no.6, 2007, p.411-414.

3-6 Development of a Large Negative Ion Source
–R&D for Maintenance Free Ion Source for Uniform Negative Ion Beam–

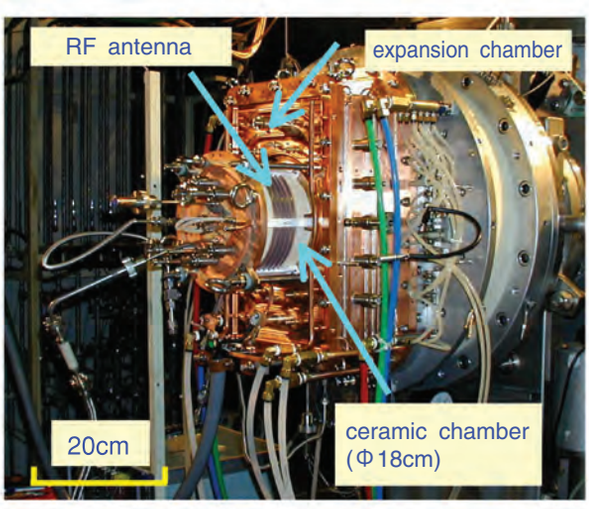

Fig.3-12 RF negative ion source
This source consists of a ceramic chamber (ϕ18 cm) for plasma production and a plasma expansion chamber (48 cm (height) × 24 cm (wide) × 20 cm (depth)). Plasma is produced with the RF antenna wound around the ceramic chamber.

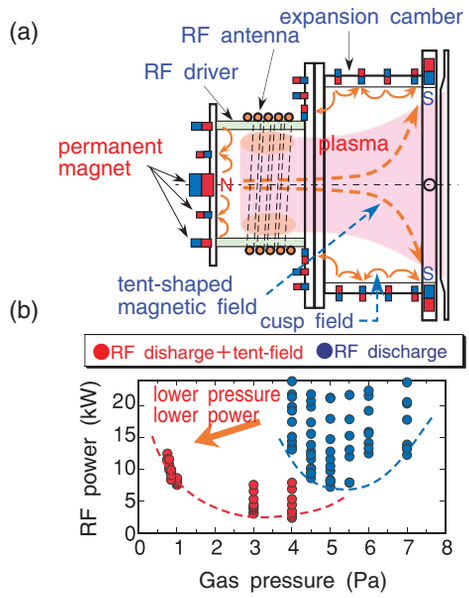

Fig.3-13 (a) Cross section of RF negative ion source and magnetic field lines, (b) operational region of RF negative ion source with and without the tent-shaped magnetic field

In “ITER” and “DEMO”, neutral beam injectors (NBI) play an essential role for heating of the core plasma up to 100 million °C. In NBI, negative ions of hydrogen or deuterium are accelerated in a 1MV-class and are transformed into neutral beams. Such a high energy neutral beam must be stably in the core plasma for a long period. Therefore, the negative ion source must operate at high performance with high power, good uniformity and long lifetime. In NBIs installed in existing large fusion devices, the spatial profile of the negative ion beam is not uniform. This non-uniform beam causes local beam divergence, which results in high heat load on acceleration grids and beam line components. We have discovered that a magnetic field in the negative ion source induces the non-uniformity of negative ion beam. With a modified configuration with a tent-shaped magnetic field, we have achieved uniform negative ion beam extraction.

In conventional negative ion sources, negative ions are extracted from source plasma produced by heating filaments. The filaments often break during high power operation, which prevents a long-term operation of the negative ion source. Since the maintenance period is planned to be twice a year during “ITER” operation, the negative ion source must holdup under repetitive operation for six months.

For a maintenance-free ion source, we have started a development of an RF negative ion source (Fig.3-12) which does not use the filaments for plasma production. An electromagnetic wave is generated with an RF antenna, which ionizes a working gas, thus producing RF plasma. In case of hydrogen gas, plasmas produced with the RF waves of 2MHz could not be sustained under the 4 Pa in the ion source. However, the negative ion source for “ITER” is required to operate at 0.3 Pa to reduce the stripping loss of accelerated negative ions by collisions with residual gases.

Here we have applied a tent-shaped field combined with a cusp field formed by permanent magnets (Fig.3-13). As a result, plasma loss on the wall was suppressed, enabling RF plasma production even when gas pressure is under 1 Pa and with lower RF power. This method is effective for the low pressure operation of a RF negative ion source needed for the ITER NBI.

Reference

Tobari, H. et al., Uniform H^- Ion Beam Extraction in a Large Negative Ion Source with a Tent-Shaped Magnetic Filter, Review of Scientific Instruments, vol.79, 2008, p.02C111-1-02C111-4.

3-7 Demonstration of Final Installation to within 0.5mm of a 4-ton Blanket by Remote Handling
–Improvement in a Robotic Positioning Control Scheme for ITER–

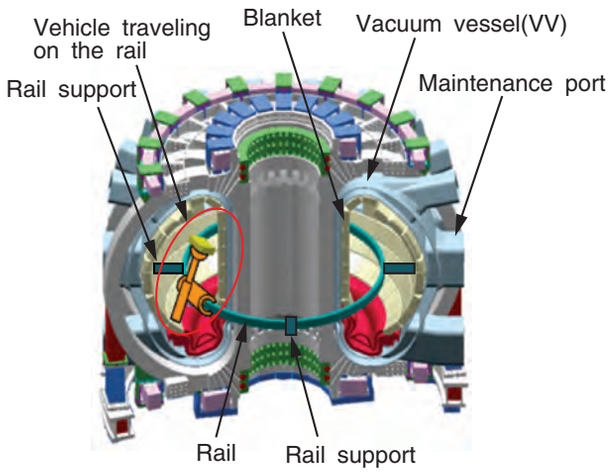

Fig.3-14 The ITER blanket module maintenance robot composed of a vehicle and a rail
We have adopted a modular structure of about 400 parts to enable maintenance of damaged blanket modules only. Blanket maintenance requires the remote manipulation of 4-ton modules, with final installation to within 0.5mm between the module and two keys on the vacuum vessel (VV). Designing a remote maintenance robot that can install modules on 2 keys with a chamfer requires a high degree of positioning accuracy.

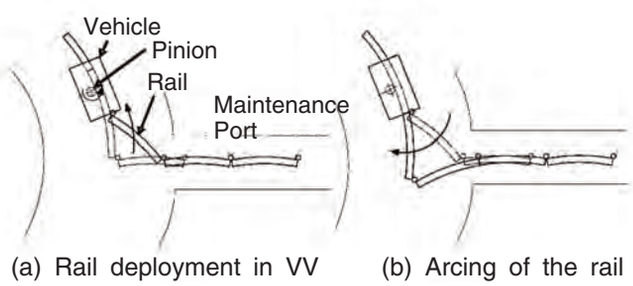

Fig.3-15 Installation of robot in VV (Rail deployment)

Fig.3-16 Blanket handling for high positioning accuracy

The inner lining (termed a “blanket”) of the vacuum vessel (VV) of the International Thermonuclear Experimental Reactor (ITER) will be activated by 14 MeV neutrons generated by fusion reactions. Maintenance of the blanket in the VV thus is carried out under high gamma ray radiation conditions (~0.5 kGy/h). All interventions inside the VV therefore must be performed remotely. The principal features of this maintenance robot are as follows:

- The vehicle travels on a rail and has telescopic arms that can extend up to 6m. The rail is supported every 90° around the annular vessel, which provides sufficient stiffness (Fig.3-14).
- The rail is deployed by the vehicle which will be used for traveling along the rail (Fig.3-15). The rail therefore can be composed of simple structures that are not sensitive to radiation.

We have demonstrated rail deployment into the VV and the basic capabilities needed for blanket handling with a high degree of positioning accuracy.

The most critical issue of sensor-based control of positioning is designing a measurement scheme to compensate for the relative error between the location of the mechanism that grips the blanket and the target position for installing the blanket, thereby minimizing assembly error. A contact method using a force sensor that is uninfluenced by assembly error is employed for positioning. However, a technical problem of measuring via contact sensors is to allow for sensing time so as to be able to measure along each of the six degrees of freedom, rotation about three axes and linear movement along three coordinates. To solve this problem, we invented a new control scheme which initially determines the degree of each rotation. This initial measurement scheme limits the number of possible degrees of freedom to the three linear coordinates. The proposal was tested using a full-scale robot in order to confirm the feasibility of the new control scheme (Fig.3-16). The new control scheme resulted in a positioning accuracy of less than 3mm, within the positioning requirement of 5mm. Sensing time was reduced as well.

In conclusion, we found that the new proposal for improving the control scheme is appropriate for reducing sensing time and achieving the required positioning accuracy. Based on these results, we will proceed toward procuring this remote maintenance robot in order to deliver an efficient, reliable remote handling system to ITER.

Reference

Kakudate, S. et al., Effect on Positioning Accuracy due to Assembly Error of Large Robot for ITER Blanket Maintenance, Purazuma, Kaku Yugo Gakkai-shi, vol.84, no.5, 2008, p.269-278 (in Japanese).

3-8 Materials Necessary for Stably Supplying Fuel Tritium to Fusion Reactors
–Development of Tritium Breeding Materials Resistant to Reduction in Hydrogen–

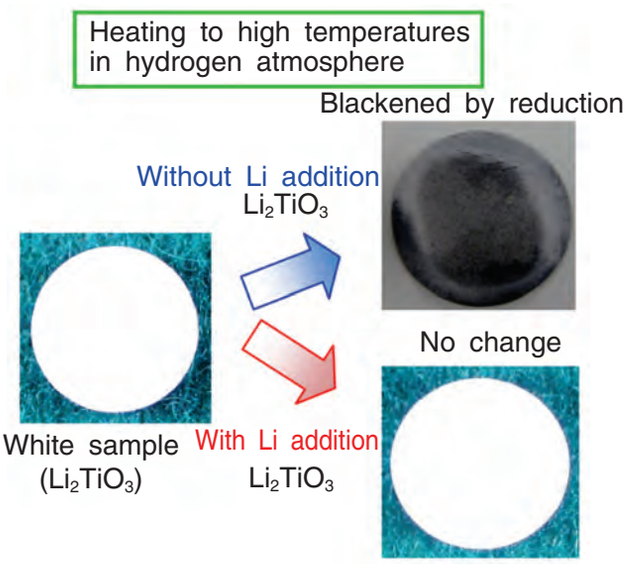

Fig.3-17 Color of Li_2TiO_3 after heating to high temperatures in hydrogen atmosphere
The color of Li_2TiO_3 without added Li changed from white to black in a hydrogen atmosphere at high temperatures. This color-change corresponds to reduction of Li_2TiO_3. In the case of Li_2TiO_3 with added Li, the color did not change, indicating that this sample was not reduced in the hydrogen atmosphere.

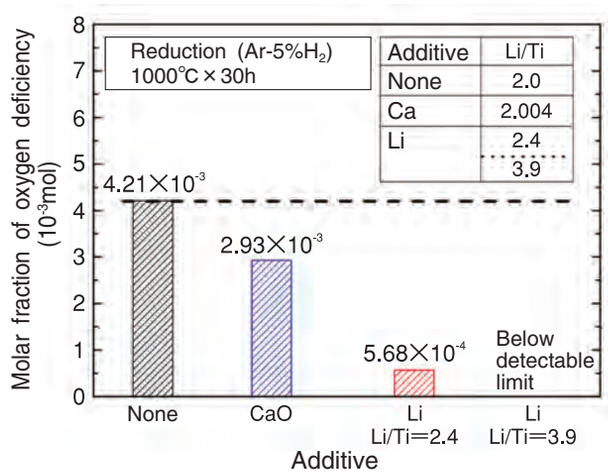

Fig.3-18 Molar fraction of oxygen deficiency of Li_2TiO_3 with different additives
Reduction of Ti in Li_2TiO_3, namely, the valence change from Ti^{4+} to Ti^{3+}, is accompanied by oxygen vacancies in the crystal structure. The Li/Ti = 3.9 sample exhibited no oxygen vacancies, which indicates clearly that it was highly resistant to reduction.

D-T fusion reactors need deuterium (D) and tritium (T) as their fuel. Since tritium does not exist in nature, it is necessary to produce tritium artificially by neutron irradiation of a lithium-filled blanket.

Lithium titanate (Li_2TiO_3) has been recognized as one of the primary candidates for tritium breeding materials because of its good tritium release and its low activation. Addition of H_2 to the inert sweep gas at the blanket has been proposed for enhancing the release of the generated tritium from the breeder material. However, Li_2TiO_3 is reduced in a H_2 atmosphere at an operating temperature above 600°C, which will lead to degradation of the tritium release characteristics. The reduction of Ti in Li_2TiO_3 from Ti^{4+} to Ti^{3+} is accompanied by mass decrease due to decrease in oxygen content of Li_2TiO_3. In a previous study, Li_2TiO_3 (Li/Ti > 2.0) to which CaO was added exhibited smaller oxygen deficiency than Li_2TiO_3 without such addition. As the next research step, development of Li_2TiO_3 with excess Li was attempted to improve its resistance to deoxidization at high temperatures.

Usually, solid state reaction of Li_2CO_3 and TiO_2 is used in the synthesis of Li_2TiO_3. However, Li addition by solid state reaction was found to be difficult. In the present study, we have developed a new process, in which Li alkoxide and Ti alkoxide are mixed to add Li_2O to Li_2TiO_3.

Fig.3-17 shows a photograph of Li_2TiO_3 samples heated in hydrogen atmosphere at high temperatures. The color of a Li_2TiO_3 sample changed black, while that of a Li_2TiO_3 sample with added Li remained white. This black discoloration indicates valence change from Ti^{4+} to Ti^{3+}, which accompanies decrease in the oxygen content of the sample.

Fig.3-18 compares the molar fraction of oxygen deficiency of the Li_2TiO_3 with added Li to Li_2TiO_3 of our previous study with added CaO. The molar fraction of oxygen deficiency increased as the molecular ratio Li/Ti decreased. The result for Li/Ti = 3.9 indicated no oxygen vacancies.

The overall results indicated that Li addition is very effective in suppressing oxygen deficiency. Thus, an advanced tritium breeding material for high temperature use in fusion reactors has been developed through successful synthesis of Li_2TiO_3 with added Li.

Reference
Hoshino, T. et al., Non-Stoichiometory and Vaporization Characteristic of $Li_{2.1}TiO_{3.05}$ in Hydrogen Atmosphere, Fusion Engineering and Design, vol.82, issues 15-24, 2007, p.2269-2273.

3-9 Tritium Extraction Using a Fuel Cell
–Tritium Recovery from Blanket Sweep Gas–

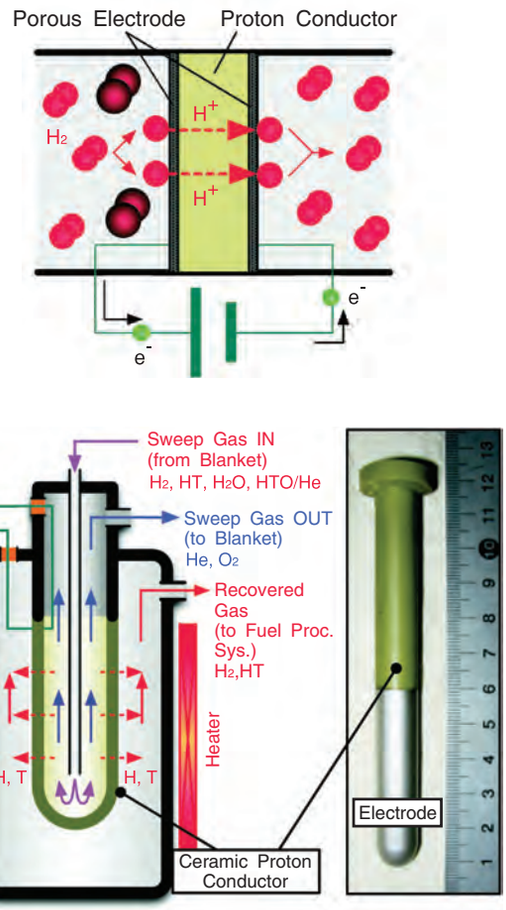

Fig.3-19 The principle of the hydrogen pump (upper), and the schematic of a hydrogen pump using proton conductor ceramic membrane in test tube shape (down)

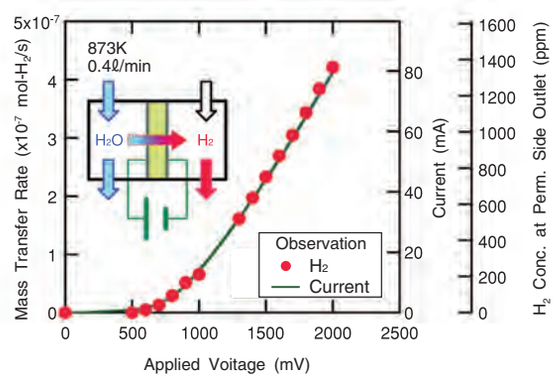

Fig.3-20 Water decomposition and extraction of hydrogen
He with H_2O at 2668 Pa was fed to the anode side, and hydrogen was measured at the cathode (Perm.) side.

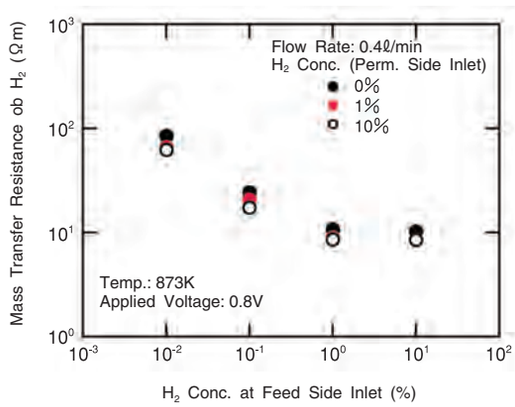

Fig.3-21 Correlation of the mass transfer resistance of hydrogen through the membrane and hydrogen gas concentration
Hydrogen concentrations at both sides were changed.

A fusion reactor is a system extracting the energy of the nuclear fusion reaction between deuterium and tritium. However, tritium is scarce in nature. Therefore, in a fusion reactor, tritium is made by the nuclear reaction between the neutron and the lithium in the blanket. Tritium bred in the blanket is purged out by helium (He) sweep gas, and is separated from He at a recovery system. To operate the fusion reactor, we have to make more tritium than is burned up in the reactor.

Possible tritium recovery method includes metallic film permeation and use of hydrogen storing alloy. However, in a fusion DEMO reactor, the temperature and flow rate of the sweep gas are expected to increase greatly. A more effective method is needed. In response, we directed our attention to the hydrogen pump an apparatus using the principle of the fuel cell in reverse. When electric potential is applied to the proton conductor (fuel cell), hydrogen can move inversely against a hydrogen concentration gradient and can be extracted selectively (Fig.3-19).

We selected a ceramic proton conductor since we would use it at a high temperature. The proton current which can be passed through the ceramic conductor is quite small in comparison with that of a polymer electrolyte, but we could extract hydrogen from water vapor using the ceramic conductor (Fig.3-20). In addition, we found out that the rate of decrease of the mass transfer resistance is unchanged with the increase of hydrogen gas concentration (Fig.3-21).

We thus established the fundamental feasibility of the hydrogen pump. Hereafter, our effort shifts to the practical application of the hydrogen pump, requiring such accomplishments as the enhancement of pumping performance.

Reference

Kawamura, Y. et al., Mass Transfer Process of Hydrogen via Ceramic Proton Conductor Membrane of Electrochemical Hydrogen Pump, Fusion Engineering and Design, vol.82, issue 2, 2007, p.113-121.

3-10 Torus Configuration and Maintenance Concept of Compact Fusion DEMO Reactor
–Torus Configuration for High Operation Rate–

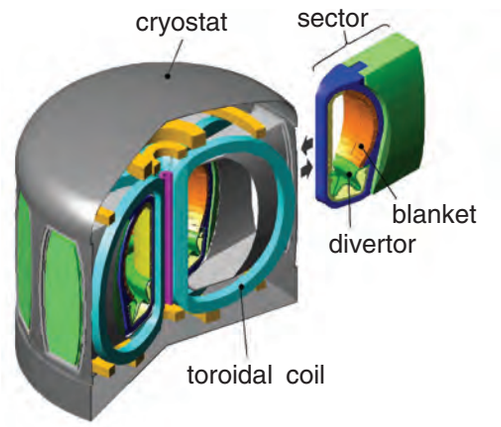

Fig.3-22 Concept of torus configuration and maintenance for fusion DEMO reactor

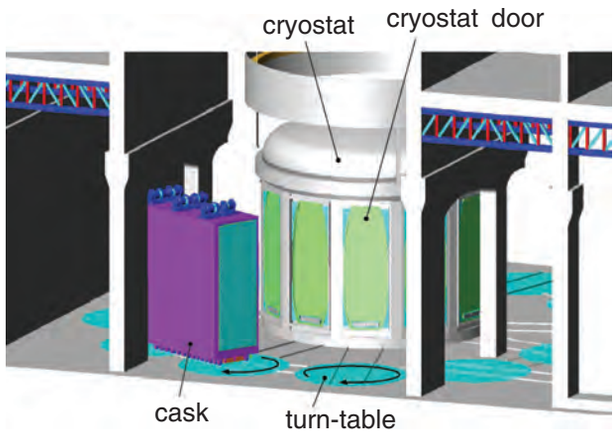

Fig.3-23 Sector transport for maintenance
A cask containing a sector moves on rails placed on the floor and turn-tables.

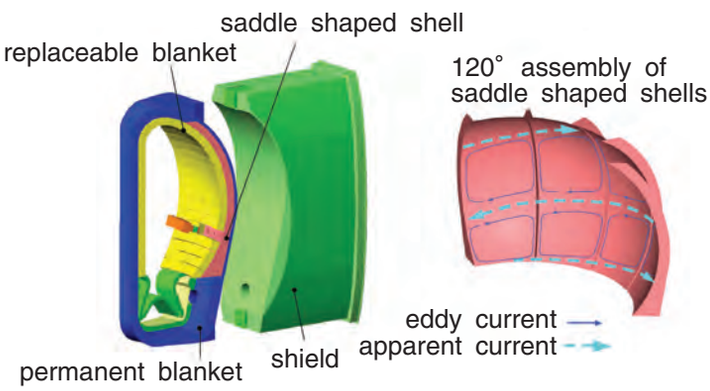

Fig.3-24 Structure of sector and saddle shaped shell
Eddy current on the shell assembly stabilizes the burning plasma.

A conceptual study of compact fusion DEMO reactor design resulted in a torus configuration and maintenance scheme which shortens the time required for periodic replacement of core components such as blanket and divertor. Such shortening of maintenance time can lead to an improvement of plant operation rate, and thus to a reduction of the cost of electricity.

To quicken maintenance, we adopted a “sector maintenance scheme” in which the core components are divided into twelve toroidal sectors and each sector is en bloc removed and transported to a neighboring hot cell for maintenance and replacement of blanket modules (Fig.3-22). Each sector loads about sixty replaceable blanket modules that must be replaced every two or three years. In the replacement, six steel tubes connected to each blanket module (four for cooling and two for tritium fuel recovery) must be cut, re-welded and tested by remote control. When these replacement procedures are carried out in situ in the cryostat, the replacement time is expected to exceed half a year, unacceptable from the point of view of operation rate. With sector maintenance, the required time will be reduced to about three months because, by replacing used sectors with spare sectors, time-consuming procedures (pipe cutting re-welding and testing) can be carried out in the hot cell during tokamak operation. On the other hand, this maintenance scheme raises concern about transport of heavy sectors. This issue is resolved with the use of a wheel and bearing system and turn-tables (Fig.3-23). A saddle shaped conducting shell placed in between replaceable and permanent blankets is one of the key components of DEMO. The assembly of the shells also plays the role of passively stabilizing the plasma by inducing eddy currents, as shown in Fig.3-24.

Reference

Tobita, K. et al., SlimCS − Compact Low Aspect Ratio DEMO Reactor with Reduced-Size Central Solenoid, Nuclear Fusion, vol.47, no.8, 2007, p.892-899.

4 Quantum Beam Science Research

The Future Explored by Quantum Beam Technology

What are quantum beams?

Quantum beams are high quality beams including electromagnetic waves (laser, X-ray, γ-ray, etc.), leptons (electron, positron, etc.) and hadrons (proton, neutron, ion, etc.), which possess both wave characteristics and particle characteristics. At JAEA we are utilizing these quantum beams (neutrons, ions, electrons, γ-rays, high intense ultra-short pulsed lasers and synchrotron radiation) in innovative R&D (Fig.4-1). We thereby aim to contribute to the progress in science and technology and promotion of industry. Specifically, we are dedicated to R&D in the "Four Priority Fields to be Promoted" contained in the "Science and Technology Basic Plan".

These fields are: development of highly durable fuel cell membrane (nanotechnology and materials area), fine structure analysis of proteins aiding drug discovery, analyzing DNA damage and restoration mechanism and the creating new species (life sciences and biotechnology area), development of materials and technologies for environmental protection (environmental sciences and energy area), and development of radiation-resistant semiconductors (information and communication technology area). Further, in the advanced medical treatment area, techniques for miniaturization of particle beam radiotherapy equipment by generating proton beams with high intensity lasers are being developed.

The characteristics of quantum beams

In this R&D, the characteristics of each quantum beam are utilized effectively and organically, leading to various unique achievements only possible for JAEA.

Quantum beams are excellent at revealing structure, allowing us "to see" better, and have new fabricating functions, allowing us "to create" more. High quality beams of atoms or ions enables us to observe and create with nm level precision. Through the observation and fabrication of atomic arrangement, electronic state, and various elements, we can explore the mystery why a substance becomes superconductive, or the various functions and reactions the human body has. We also are contributing to various important tasks such as developing new medicines, catalysts of exhaust gas from automobiles using less noble metal, and post-oil fuels made from plants, which are carbon-neutral.

Recent Accomplishment

As specific examples of our accomplishments, we have experimentally demonstrated the principle of the flying plasma mirror with a high intensity laser, and this result suggests the possibility of generating ato (10^{-18}) second quantum beams from tunable lasers. In Topic 4-1 and Topic 4-5 we show our steady progress in generating high energy particles with lasers, for medical applications. In Topic 4-3 and Topic 4-6, we show the possibility of using quantum beams in basic science by analyzing the mechanism by which a material has a huge negative coefficient of thermal expansion, or a heavy ion that has a special effect on living cells. In Topic 4-4 and Topic 4-9, we applied radiation-induced cross-linking and graft techniques utilizing electron beams and γ-rays to develop a post oil material made from carbon-neutral plants, and to develop an electrolyte film that operates at the high temperatures of a fuel cell. We promote collaboration inside JAEA so as to make basic science contributions to solving problems facing the Fast Breeder Reactor project, for instance residual stress measurement with neutrons and synchrotron radiation.

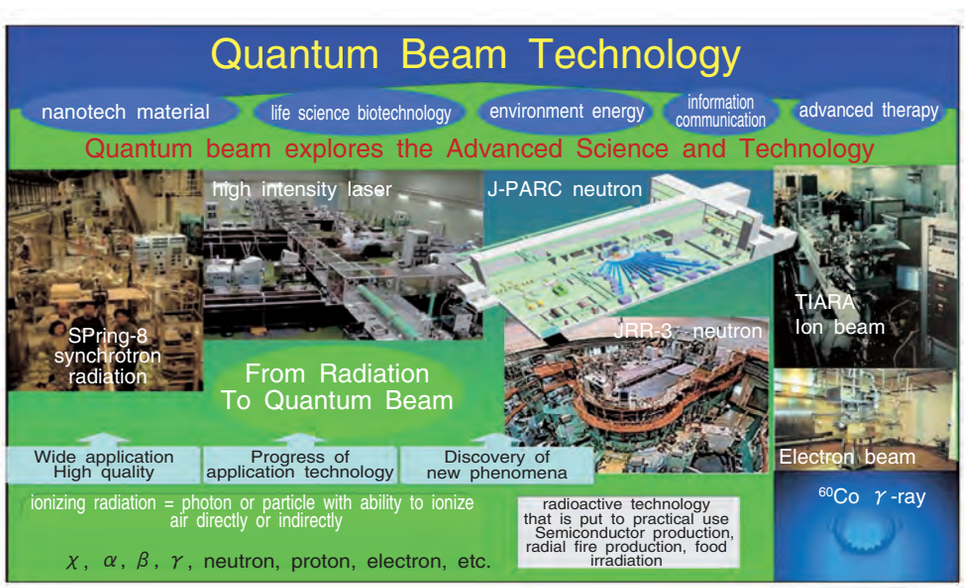

Fig.4-1 The Quantum Beam Facilities at JAEA

4-1 Making a Mirror Moving Nearly at the Speed of Light by Lasers –Demonstration of Light Reflection and Frequency-Upshifting by Electron Density Modulation in Plasmas–

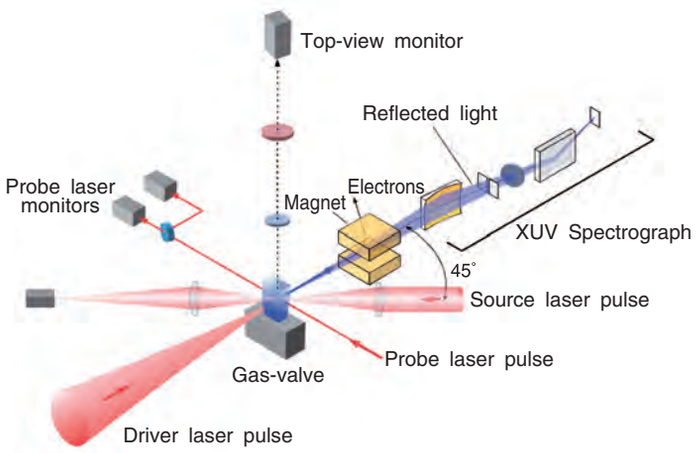

Fig.4-2 A schematic of the proof-of-principle experiment of the flying mirror
The Driver pulse was focused onto a gas-jet to generate flying mirrors. The Source pulse was aimed at the generated mirrors with a crossing angle of 45°. The reflected pulses were in almost the same direction of that of the Driver pulse.

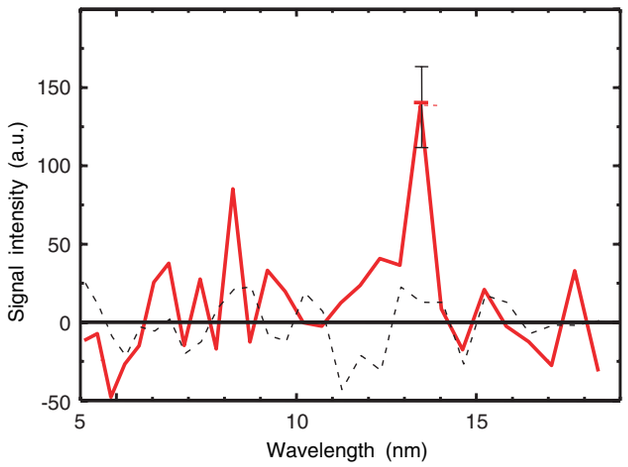

Fig.4-3 The spectrum of the light (X-ray) reflected by flying mirrors generated in the plasma
The signal was observed at the wavelength of 13.4nm.

Recently, focused laser intensity has been increasing dramatically, and such intense lasers enable us to explore various fields of science such as nonlinear optics, quantum beam generation, and so on. However, conventional high power lasers must be made very large to attain intensity higher than 10^{22} W/cm^2. Addressing this issue, a revolutionary idea was proposed at JAEA in 2003 making large-scale lasers unnecessary. In the proposed method, a moderate intensity laser is focused onto a plasma, then some of the plasma electrons start to group together. This agglomeration of electrons acts as a mirror (relativistic-speed flying mirror) which reflects and focuses incoming light partially. The characteristics of this flying mirror are summarized as follows: (1) the mirror is stable against intense lasers because it consists of electrons instead of common optical components such as metals; (2) high focused intensity is possible because the reflected light can be focused to a smaller spot due to the wavelength reduction, or frequency upshifting, caused by the Doppler effect; (3) the pulse duration of the reflected light also is compressed by frequency upshifting, which increases the intensity.

Up to now, a proof of this principle has not been made because of the experimental difficulty of colliding two laser pulses with micrometer accuracy. We succeeded in demonstrating this concept by careful design of the experiment and the fine tuning of the colliding of two laser pulses using crossing Ti:Sapphire lasers. As shown in Fig. 4-2, Ti:Sa laser pulses with a peak power of 2 TW and a pulse duration of 80fs were focused onto helium gas. In order to conduct the experiment, we accomplished the following: (i) we improved the pointing stability of lasers by eliminating vibration sources; (ii) we invented a new method to align two laser pulses to collide in a small designated region. A small portion of the laser energy split from the main laser was used as a exposure light and the colliding region in the plasma was thereby monitored with a device similar to a microscope. In addition, viewing the scattered light from the region through a top-view monitor was also implemented to achieve colliding.

When two laser pulses collided properly, we observed extreme ultraviolet frequency photons as seen in Fig.4-3. The incident source laser whose wavelength (frequency) was 780 nm (380 THz) was successfully compressed (upshifted) to 13.4 nm(22,300 THz). The number of the reflected photons per unit solid angle is estimated to be 3×10^7/sr, which is 100 times higher than that expected from incoherent Thomson scattering of plasma electrons. In addition to this, we carefully analyzed experimental data, and we conclude that these photons were obtained by reflection from the electron agglomerate formed in the plasma.

This is the first demonstration of the flying mirror concept, confirmed by observing the frequency upshift of the reflected photons. This method will lead to an ultra-high intensity of 10^{29} W/cm^2, where electron-positron pairs would be produced from vacuum. Moreover, because this method also compresses pulse duration, it may help us achieve attosecond X-rays, a field which is just now opening up.

Reference

Kando, M. et al., Demonstration of Laser-Frequency Upshift by Electron-Density Modulations in a Plasma Wakefield, Physical Review Letter, vol.99, 2007, p.135001-1-135001-4.

4-2 Observation of a Key Hydrogen Atom in an Enzymatic Reaction –Neutron Structure Analysis of a Compound Modeling the Reaction Center of [NiFe]Hydrogenase–

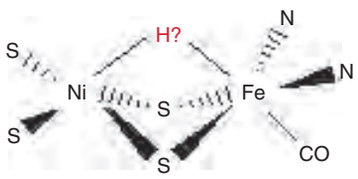

Fig.4-4 Deduced structure of the active site of [NiFe]hydrogenase
The activation center of [NiFe]hydrogenase is thought to have such a Ni-H-Fe structure. S's are sulfur atoms.

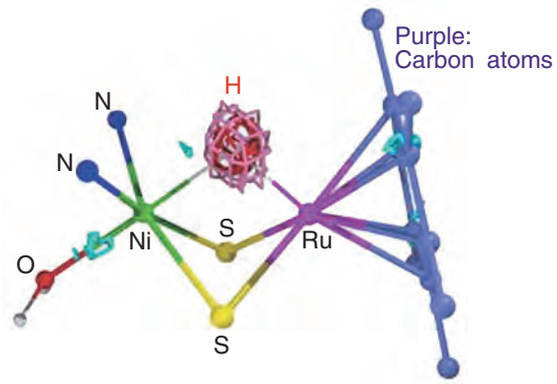

Fig.4-6 The hydrogen atom between the Ni and the Ru atoms observed by neutron diffraction
The red mesh in this figure shows the distribution of negative nuclear scattering length density observed by neutron diffraction (the water-blue mesh shows the positive distribution). In neutron structure analysis, hydrogen atoms are observed as negative distribution. Consequently, a large red mesh between Ni and Ru clearly shows the existence of a H atom. This result shows that this compound has Ni-H-Ru structure.

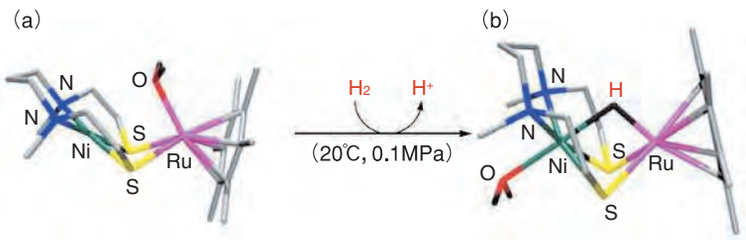

Fig.4-5 Reaction of the model compound of [NiFe]hydrogenase
The reaction from (a) to (b) is similar to the enzymatic reaction of [NiFe]hydrogenase, and (b) is similar to the reaction center of [NiFe]hydrogenase shown in Fig. 4-4 (only Fe was replaced by Ru). Thus, (b) can be considered a compound modeling the reaction center of [NiFe]hydrogenase.

Hydrogenases are bacterial enzymes that catalyze the activation of H_2 into two protons (H^+) and two electrons (e^-). Their structure when they are active in this enzymatic reaction has been attracting much attention since this would elucidate the reaction mechanism. Though a Ni-H-Fe structure, a nickel atom (Ni) and an iron atom (Fe) bridged by a hydrogen atom as shown in Fig.4-4, has been proposed as a possible structure, such a structure has not been observed.

Recently, Prof. Ogo's group at Kyushu University successfully synthesized a model compound with reactivity similar to the reaction center of a [NiFe]hydrogenase, [NiFe]Hase, by using ruthenium (Ru) instead of Fe as shown in Fig.4-5. Whether this compound has a Ni-H-Ru structure or not is important for determining the activation structure of the [NiFe]Hase and to elucidate the mechanism of the enzymatic reaction. However, observation of the hydrogen atom is difficult by the usual structure analysis method, X-ray diffraction, and consequently the Ni-H-Ru structure had not been observed.

Thus, JAEA carried out single crystal neutron structure analysis of this model compound using the "BIX-3" diffractometer at "JRR-3" reactor. A neutron is well scattered by a hydrogen atom and thus a neutron beam is suited for observation of hydrogen atoms. We measured the strength of 10161 diffraction spots in 9 days of measurement and successfully observed the hydrogen atom between the Ni and the Ru atoms as shown in Fig.4-6. Consequently, this model compound was confirmed to be the first compound which has a Ni-H-Ru structure, which indicates that the activation site of the natural [NiFe]Hase has a similar Ni-H-Fe structure.

This result may lead to development of new hydrogen activation catalysts to produce hydrogen energy resources. This research was carried out by Kyushu Univ., JST, Osaka Univ., Univ. of Hyogo and JAEA and published in Science in 2007. JAEA carried out the structure analysis by neutron diffraction.

Reference

Ogo, S., Ohhara, T. et al., A Dinuclear Ni(μ -H) Ru Complex Derived from H_2, Science, vol.316, 2007, p.585-587.

4-3 Why Do Heavy Ions Have Great Effect on a Cell? Chemistry Elucidates the Reason

–Quantitative Analysis of Reactive Species Which Induce DNA Damage–

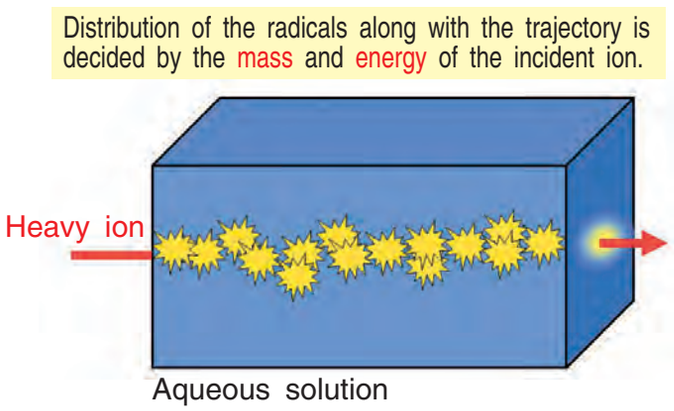

Fig.4-7 Radicals generated along heavy ion trajectory in water
A heavy ion deposits its kinetic energy densely along its trajectory to produce reactive species. Their distributions are decided by the mass and specific energy of the incident ion. Moreover, reactive species react and diffuse with time.

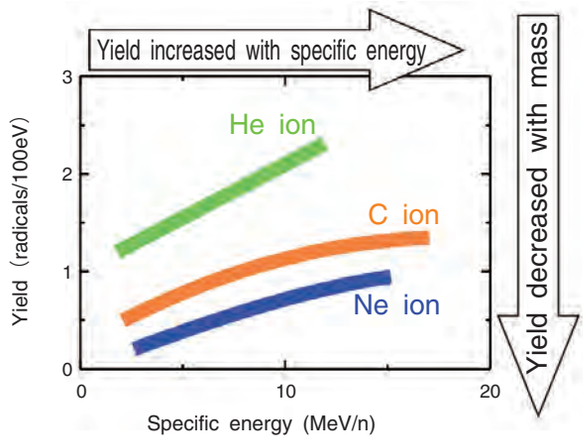

Fig.4-8 Dependence of yield of hydroxyl radicals on specific energy and mass of incident ion
Yields of hydroxyl radicals increased with the specific energy for each ion, but decreased with the mass of each ion at the same specific energy.

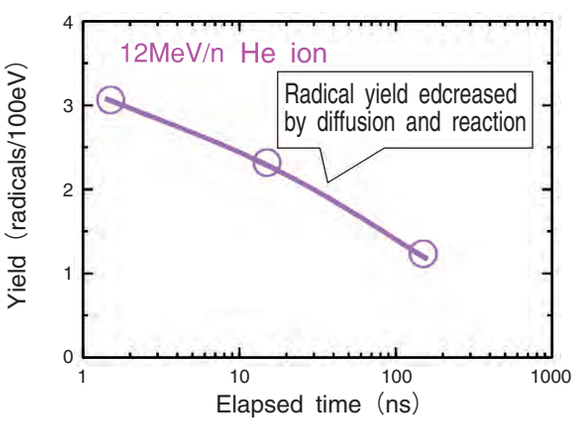

Fig.4-9 Yield of hydroxyl radicals decreased with elapsed time just after helium ion irradiation
Yield of hydroxyl radicals decreased in ns time scale, with diffusion and reaction of the radicals. The same tendency was observed in other energies and ions.

High energy heavy ions are used for plant breeding and cancer treatment. The heavy ion can produce highly reactive species (e.g. hydroxyl (OH) radical) with a different distribution from that of conventionally used radiation, such as γ-rays, in a cellular tissue, i.e. an aqueous solution, as shown in Fig.4-7. Although the characteristics of the heavy ion irradiation effects can be explained in terms of LET (linear energy transfer) in many cases, one cannot explain the spatial distribution of the reactive species using LET. Moreover, the reactive species diffuse and react with time. Since the OH is considered the most important basic radical for radiation chemistry research, we estimated the yield of the OH radicals based on the mass and energy of the incident ion, and the elapsed time.

We irradiated aqueous phenol solution with heavy ions, changing the mass and energy systematically, and estimated the OH radical yield from the yield of reaction products of phenol. As a result, the yield of the OH radicals increased with the specific energy in the case of each ion, but decreased with the mass of the ion at the same specific energy as shown in Fig.4-8. The yield decreased with elapsed time (Fig.4-9). These results can be derived from the initial distribution of the reactive species around the heavy ion trajectory, and subsequent diffusion and reaction of the radicals.

Presently, we are constructing a time resolved optical measurement system. We will thereby increase the reliability of data about the radical yield, and observe directly reactions of radials with biomolecules.

Reference

Taguchi, M. et al., Yield of OH Radicals in Water under Heavy Ion Irradiation. Dependence on Mass, Specific Energy and Elapsed Time, Nuclear Science and Techniques, vol.18, issue 1, 2007, p.35-38.

4-4 Biodegradable Elastic Gel from Cellulose Derivatives
–Combination of Radiation-Induced Crosslinking and Aggregation–

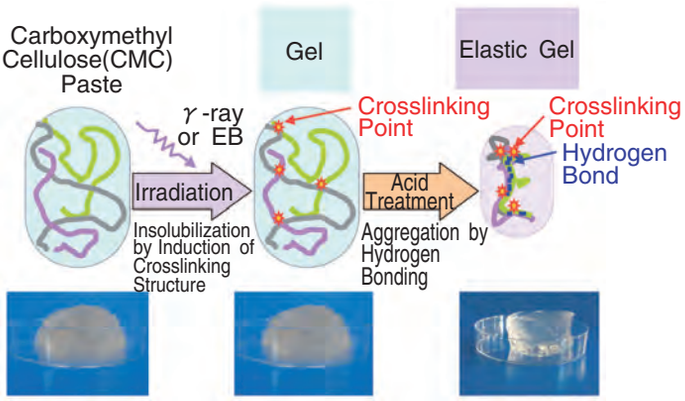

Fig.4-10 Preparation of biodegradable elastic gel
10wt% or higher aqueous solution of water-soluble carboxymethylcellulose is formed into a gel by γ-ray or electron beam irradiation. Rubbery elasticity can be given to the radiation crosslinked gel by immersion in acid solution.

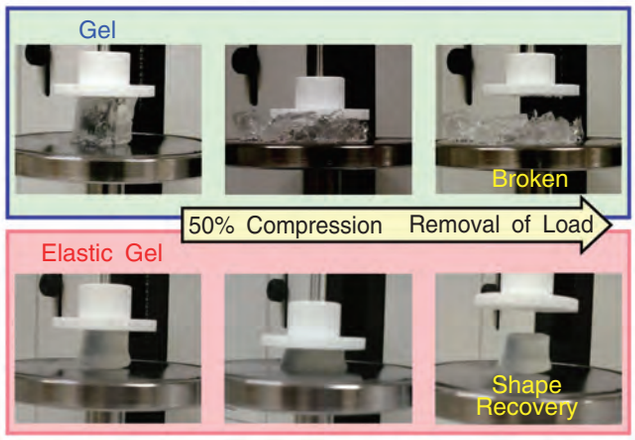

Fig.4-11 Mechanical property of biodegradable elastic gel
At 50% compression, the carboxymethylcellulose gel cross-linked by radiation disintegrates into small pieces. On the contrary, the elastic gel given acid treatment does not fall apart, even at 50% compression, and returns to its original shape when the load is removed.

Development of cellulose, the chief material of plants which is produced through growth by photosynthesis, has received considerable attention as a carbon neutral high polymer. Though polysaccharide gel, manufactured from cellulose with crosslinking agents, absorbs hundreds of times its volume of water, its production is discouraged because the crosslinking agents are toxic in general.

To solve this problem, the development of a method to prepare the gel from water-soluble carboxymethylcellulose (CMC) without using a crosslinking agent was attempted. As a result, kneading CMC powder in water at a concentration of more the 10wt% yielded a homogeneous paste, and when the CMC in this condition was irradiated by γ-rays or electron beams, the crosslinking occurred and biodegradable gel was formed. Though the gel prepared by this technique had high water absorbency, the area of its application was very limited as the gel was fragile and brittle when swollen.

To solve this problem, the control of molecular structure is important, and we utilized the molecular aggregation caused by acid treatment to improve gel strength. We were able to make the rubbery elastic gel by immersing radiation-crosslinked CMC in an acid solution (Fig.4-10). The reason for this transformation is that a Na ion, which exists as a counter ion of a carboxyl group in the radiation crosslinked CMC gel, is replaced by hydrogen during immersion in the acid solution. As a result, the electrostatic repulsion power within the CMC molecular chain decreases, and the carboxymethylcellulose molecular chain agglomerates, pulled together by the hydrogen bond. Strong interaction between the molecules ensues. Measuring the thermal decomposition characteristics of the elastic CMC gel, it was found that a broadening and shifting of the peak to a higher temperature due to the decomposition of the CMC occurred only after immersion in the acid solution. This indicates that there is strong intermolecular interaction between CMC molecules.

Though the CMC gel made by the irradiation breaks up at 50% compression as shown in Fig.4-11, the elastic CMC gel does not break and returns to the same shape before it was compressed once the load is removed. The breaking strength of the acid treated elastic CMC gel was 150 times that of the untreated gel ($3N/mm^2$). When the pH is lowered and the processing time of immersion is lengthened, this elastic CMC gel has increased strength and becomes harder, regardless of the kind of the acid. For instance, when the immersion processing is done for four days by using 0.5M hydrochloric acid, it becomes a gel that is about 100 times harder than that of CMC gel formed by radiation-induced crosslinking alone.

Thus, we succeeded in making a novel biodegradable gel with elasticity like rubber by the combination of radiation-induced crosslinking and acid treatment. Therefore, this elastic gel promises to be a new carbon neutral material of plant origin with a wide range of applications for cosmetics, environmental protection, and medical treatment.

This work was supported in part by Japan Science and Technology Agency, and is a product of the Gunma Prefecture Collaboration of Regional Entities for the Advancement of Technological Excellence.

Reference

Takigami, M., Amada, H., Nagasawa, N. et al., Preparation and Properties of CMC Gel, Transactions of the Materials Research Society of Japan, vol.32, no.3, 2007, p.713-716.

4-5 Medical Applications for the Laser-Driven Proton Beam
–High Quality Beam Is Produced with High Conversion Efficiency–

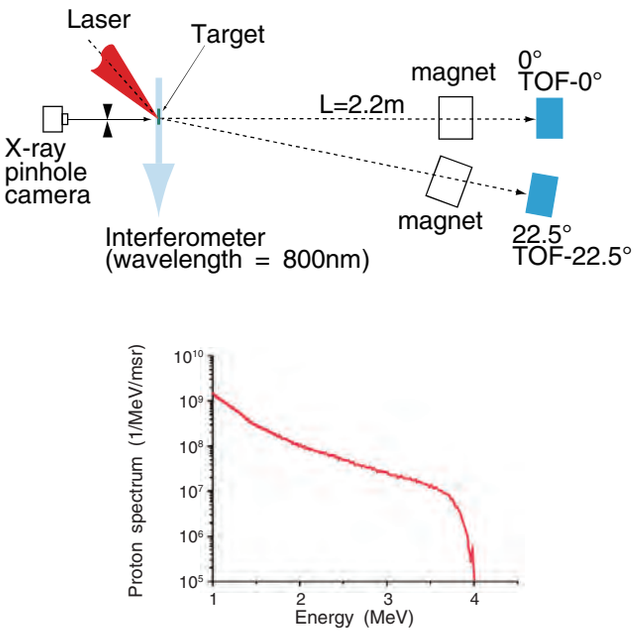

Fig.4-12 Experimental set up and the energy spectrum of the proton beam
The magnet in front of the time-of-flight spectrometer is set there to eliminate background noise from electrons.

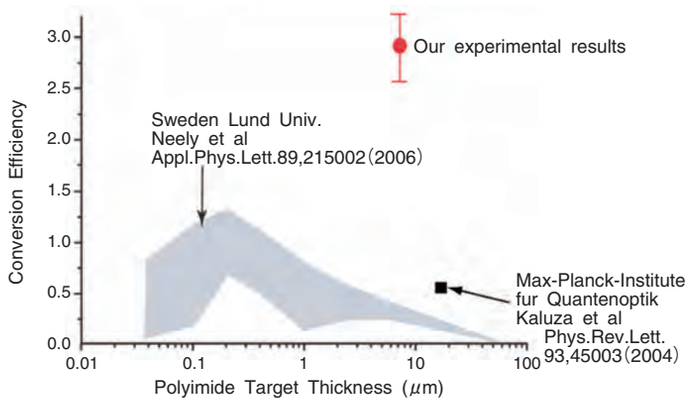

Fig.4-13 The experimental results obtained by the ~1 J class laser system
Our efficiency is higher than those obtained by other groups.

A high energy proton beam is produced by the interaction between a short-pulse high intensity laser and a target material such as metal or plastic. We can down size the accelerator using this laser-driven proton beam, because the laser-driven proton beam has very small (~μm) acceleration field compared with that of the conventional accelerator. However, for the practical use of this laser-driven accelerator in industry or medicine, we have to obtain the necessary proton dose within a limited time period with compact laser system. We have to increase the energy conversion efficiency from laser to proton beam in order to obtain a higher proton number per laser shot. In order to obtain conversion efficiency improvement of more than a few %, a large laser system whose energy is more than a few tens of J is needed. The energy conversion efficiency with a small laser system (~1 J class) is limited to less than 1%.

We have carried out an experiment in collaboration with GIST in Korea, CRIEPI, and ILE. We produced a proton beam with maximum energy up to 4 MeV with good conversion efficiency, by irradiating a polyimide 7.5μm target with laser pulses whose peak intensity and pulse width were 50 TW and 34 fs, respectively, from a compact 1J class laser system (Fig.4-12 and Fig.4-13). The conversion efficiency from laser to proton was more than 3%. The peak current was 0.3 MA, which is more than 2 orders of magnitude higher than those obtained by a conventional accelerator with energy on the order of a few MeV.

This realization of a laser-driven proton beam with high conversion efficiency, will surely contribute to the application of the laser-driven proton beam to medical as well as industrial fields. This increase in the conversion efficiency will lower the quantitative demands made upon the laser (presently laser energy of 10 J, repetition rate of 100 Hz). This makes it easier to reach our goal of realizing a laser-driven proton accelerator.

We have shown that a compact laser system can accelerate the proton beam very efficiently. This paves the way toward the application of the laser-driven proton beam in industrial as well as medical fields. However, problems still remain. First of all, we have to increase the energy of the proton at least to 80 MeV in order to apply the laser-driven proton beam to radiation therapy, if no additional accelerator is attached. In the next step, we have to develop the transport and irradiation system of the proton beam, where the spatial distribution and number of the protons as well as the energy is optimized, in order to supply the necessary and sufficient dose to the diseased part of the patient. We are now developing not only the source of the laser-driven proton but also the transport and irradiation systems, in order to realize the laser-driven proton accelerator.

Reference

Nishiuchi, M. et al., Efficient Production of a Collimated MeV Proton Beam from a Polyimide Target Driven by an Intense Femtosecond Laser Pulse, Physics of Plasmas, vol.15, issue 5, 2008, p.053104-1-053104-10.

4-6 Local Structure in a Material Shrinking with Heat –Broadening of Magneto-Volume Effect (Invar Effect) Caused by Local Lattice Distortion–

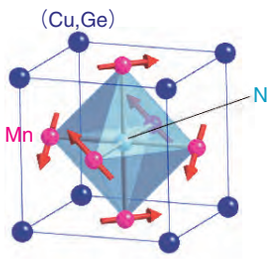

Fig.4-14 Crystal and magnetic structures of $Mn_3Cu_{1-x}Ge_xN$
Cu or Ge atoms form a cube, and Mn atoms locate at the center of each face, forming an octahedron. A N atom locates at the center of the octahedron. Red arrows show the direction of Mn moments.

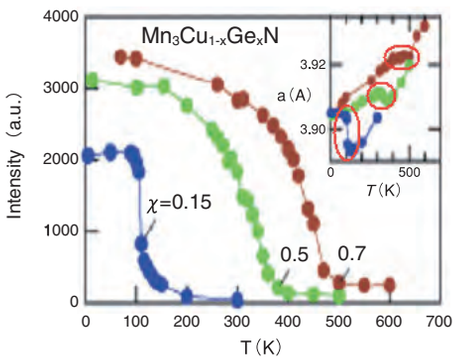

Fig.4-15 Temperature (T) dependences of intensities of magnetic scattering (main panel) and lattice constants (inset) of $Mn_3Cu_{1-x}Ge_xN$(x=0.15,0.5,0.7)
Intensities of magnetic scatterings of samples, whose lattice constants gradually increase in T-region shown by red circle, gradually increase.

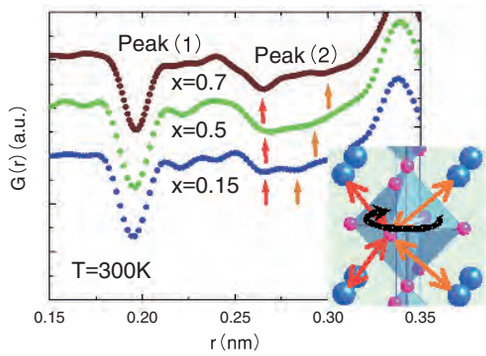

Fig.4-16 Atomic pair distribution function G(r) of $Mn_3Cu_{1-x}Ge_xN$(x=0.15,0.5,0.7) obtained at 300 K (main panel) and the rotation of Mn-octahedron expected from G(r) (inset)
Arrows of peak (2) show atomic correlation between Mn and Cu (Ge). The peak splitting increases with increasing x.

Generally, a material expands with increasing temperature (T). However, some rare materials mysteriously contract with increase in T. One of the origins of such phenomenon is the magneto-volume effect (MVE), in which volume expansion accompanies magnetic ordering with decreasing T. There is a special case of this MVE in which the contraction is gradual with rise in T, the so-called Invar effect. The mechanism for this is not yet clear although it has been studied for about 100 years. According to the study by Takenaka and Takagi of RIKEN concerning the material $Mn_3Cu_{1-x}Ge_xN$ (Fig.4-14), the system with Ge-concentration of x~0.15 exhibits sharp volume contraction with rise in T by MVE, and the volume-change with rise in T becomes gradual with increase in x. At around room temperature, the rate of volume contraction is the largest in the material with x~0.5. In order to investigate the mechanism of moderation of the MVE in this material, we performed neutron powder diffraction measurements.

To study the crystal and magnetic structures of this system including the material with x<0.15 which does not exhibit MVE, we performed neutron diffraction measurement at JRR-3. Only the material with the cubic structure and the arrangement of Mn-moment shown in Fig.4-14 was found to exhibit large MVE. As shown in Fig.4-15, a material with gradually increasing Mn-moment (corresponding to magnetic scattering intensity) exhibits gradual volume expansion.

In this material, crystal and magnetic structures do not change and only T-dependence of magnitude of ordered magnetic moment changes against x. We focused on a possible local lattice distortion caused by Cu and Ge having different atomic sizes. We derived the atomic pair distribution function G(r) from the total scattering measurement made at Los Alamos National Laboratory, to study the local structure. G(r) is shown in Fig.4-16. The peak (1) around 0.19 nm shows the relation between Mn and N atoms, and the peak (2) around 0.28 nm superposes the relation between Mn atoms and the relation between Mn and Cu (Ge) atoms. Peak (1) is a sharp single peak. In contrast, peak (2) splits in to two peaks shown by arrows. The former suggests that the shape of the Mn-octahedron does not change (see inset), and the latter indicates that the rotation of the octahedron causes both short and long distances between Mn and Cu (Ge) atoms. This rotation of the octahedron is not observed in the average structure, because it is not periodic and is due to local lattice distortion. A system with large x and moderate volume-contraction with increase in T exhibits large rotation of the Mn-octahedron, resulting in large splitting of peak (2), as shown by arrows. From these studies, we found that the local lattice distortion strongly correlates with the moderation of MVE, i.e., the Invar effect.

Reference

Iikubo, S., Kodama, K. et al., Magnetovolume Effect in $Mn_3Cu_{1-x}Ge_xN$ Related to the Magnetic Structure: Neutron Powder Diffraction Measurements, Physical Review B, vol.77, no.2, 2008, p.020409-1-020409-4.

4-7 Observation of Electron Dynamics Utilizing Synchrotron Radiation X-ray

–Charge Excitations in Ladder Cuprates by Resonant Inelastic X-ray Scattering–

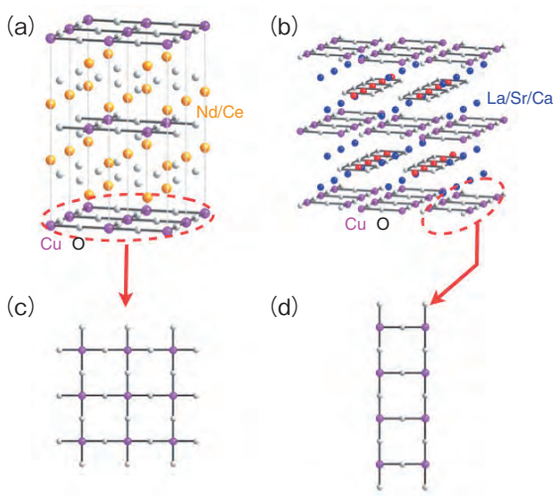

Fig.4-17 Crystal structure of two representative copper oxides and their relevant Cu-O components
(a)$Nd_{2-x}Ce_xCuO_4$ (b)$(La,Sr,Ca)_{14}Cu_{24}O_{41}$ (c)Two-dimensional square lattice (d)Two-leg ladder

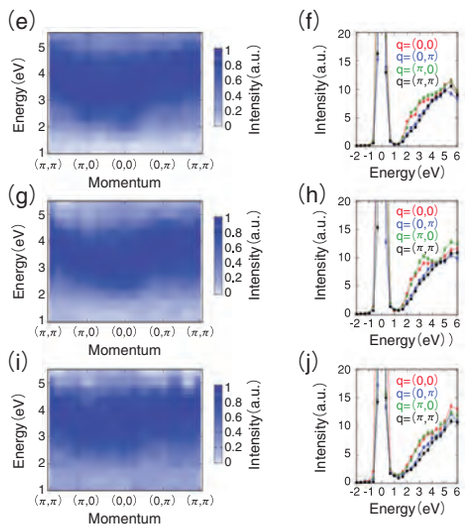

Fig.4-18 Resonant inelastic x-ray scattering spectra of $La_5Sr_9Cu_{24}O_{41}$ [(e), (f)], $Sr_{14}Cu_{24}O_{41}$ [(g), (h)], $Sr_{2.5}Ca_{11.5}Cu_{24}O_{41}$ [(i), (j)]
Momentum q = (q_{rung}, q_{leg}) is reduced in the Brillouin zone of the ladder. Elastic scattering and high-energy excitation above 5 eV are removed in (e), (g), (i). The right column gives representative spectra corresponding to the contour plots in the left column.

One of the important roles of materials science is to understand electronic properties of a material from the investigation of its electronic structure, that is, energy and momentum of the electrons. For this purpose, the photon is a good probe because it is mainly scattered by the charge of the electron. Brilliant x-rays from a large synchrotron radiation facility such as SPring-8 now enable us to measure electronic excitations by so-called inelastic x-ray scattering (IXS). A great advantage of IXS over conventional optical methods is momentum resolution. Furthermore, resonant inelastic x-ray scattering (RIXS), where the incident photon energy is tuned to the electron level of a specific element, has an additional merit of element selectivity.

A main target of our research is strongly correlated copper oxides such as high-T_c superconductors. Fig.4-17(a) shows a representative superconducting copper oxide, $Nd_{2-x}Ce_xCuO_4$, and the playground of the superconductivity is the two-dimensional square lattice shown in Fig.4-17(c). We have reported on $Nd_{2-x}Ce_xCuO_4$ two years ago. Here we present a RIXS study of another copper oxide system, $(La,Sr,Ca)_{14}Cu_{24}O_{41}$, whose crystal structure is shown in Fig.4-17(b). The relevant component of the system is the two-leg ladder in Fig.4-17(d). Superconductivity was also found in the system under high-pressure and it is considered to belong to the second class of superconducting copper oxides which has a different structural component.

Fig.4-18 shows RIXS spectra of three concentrations of $(La,Sr,Ca)_{14}Cu_{24}O_{41}$. The carrier number increases from the top to bottom graphs. The dispersive feature at 2-4 eV is an excitation between the Cu 3d orbital split by the strong Coulomb repulsion and the O 2p orbital. Energy-momentum dependence of the excitation is almost independent of the carrier number, which is a characteristic of the two-leg ladder. In contrast, it is dependent on the carrier number in the square lattice. The continuum excitation at 1-1.5 eV is related to the dynamics of the mobile carriers in the ladder and its intensity is proportional to the carrier number in the ladder.

These detailed studies give fundamental information of the electronic structure which is necessary to construct a model of the superconductivity.

In both the square lattice and two-leg ladder, a charge ordered state where mobile carriers stop their motion and align periodically was found at some concentrations. Whether the charge order is cooperative or competitive with superconductivity is an important issue. The next aim of our RIXS studies is to detect the electron dynamics in the charge ordered state.

Reference

Ishii, K. et al., Momentum Dependent Charge Excitations of Two-leg Ladder: Resonant Inelastic X-ray Scattering of $(La,Sr,Ca)_{14}Cu_{24}O_{41}$, Physical Review B, vol.76, no.4, 2007, p.045124-1-045124-7.

4-8 Observation of Curious Long-Period Structures in Metal Hydride

–A Clue to Understand the Hydrogen-Metal Interactions and Their Role–

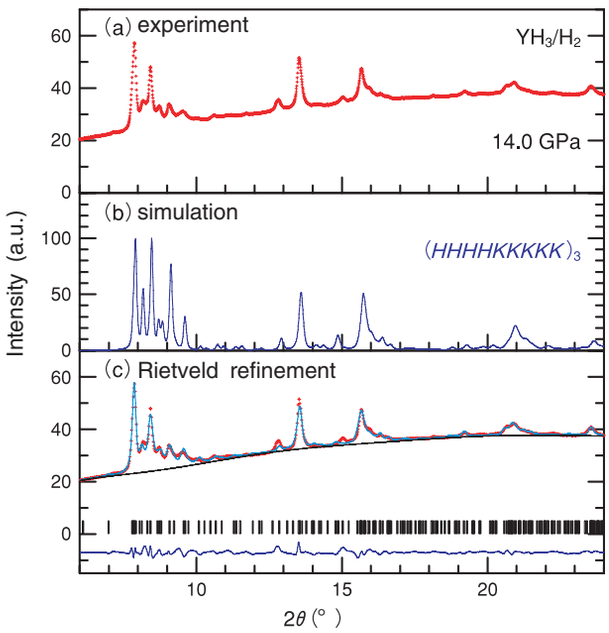

Fig.4-19 X-ray diffraction patterns of YH_3
(a) X-ray diffraction pattern of YH_3 measured at 14.0 GPa.
(b) Diffraction pattern simulated with a 27-layered long-period structural model.
(c) Result of pattern fitting by Rietveld method.

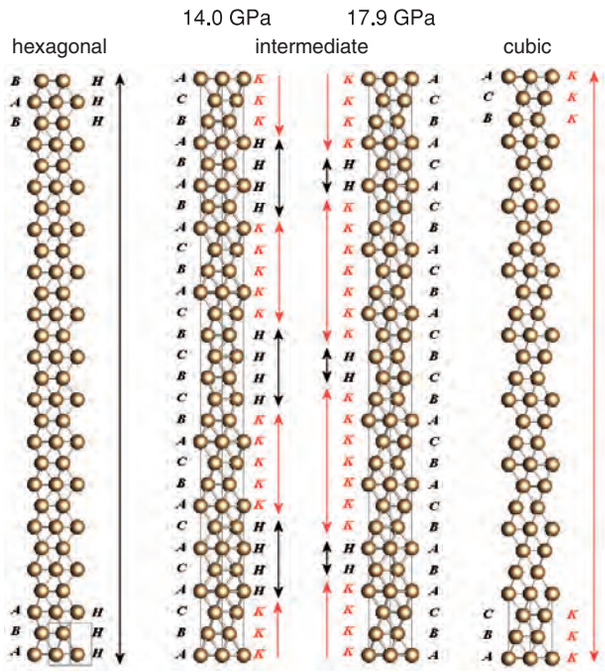

Fig.4-20 Pressure variation of metal lattices of YH_3
From right, low-pressure hexagonal structure, long-period stacking structures at 14.0 and 17.9 GPa, and high-pressure cubic structure.

Hydrogen (H) is the smallest, lightest and chemically active element. Hydrogen reacts with almost all metals and form hydrides, in which hydrogen atoms occupy the interstices of metal lattices. The interstitial H atoms form chemical bonds such as ionic or covalent-like bonds with the surrounding metal atoms and change the lattice structure and electronic state. Crystal structure and electronic state are changed by applying pressure as well. We have investigated the structure of yttrium trihydride (YH_3) under high pressure. YH_3 is an insulator, but was found to become a metal again upon compression beyond 20 GPa. The high-pressure structural study of YH_3 would provide a clue to elucidate the insulator-metal transition in terms of the metal-H and/or H-H interactions.

The process of the pressure-induced hexagonal-cubic transition of YH_3 was investigated by synchrotron radiation X-ray diffraction experiments at "SPring-8". The hexagonal structure gradually transformed into a cubic structure in a wide pressure span from 11 to 20 GPa, while the electronic state changed from insulating to metal. The intermediate state while in the above pressure range has been interpreted as the coexistence of the low-pressure hexagonal and high-pressure cubic phases. However, we have found that the intermediate state was a single phase and their diffraction patterns were well reproduced by models with long-period stacking structures of Y metal layers. Fig.4-19 shows (a) a measured high-resolution diffraction pattern, (b) a pattern simulated with a long-period model, and (c) the result of profile fitting analysis. The long-period structures consisted of Y-metal layers periodically arranged in *ABA*-type (*H*-type) and *ABC*-type (*K*-type) stacking sequence. The 14.0-GPa structure of a unit cell containing 27 layers was characterized as consisting of three sub unit cells, each having a 4-*H* and 5-*K* layer sequence, which were stacked up along the 3-fold axis. The17.9-GPa structure was described with the 27 layers as well but here the sub unit cells consisted of a 2-*H* and 7-*K* layer sequence (Fig.4-20). The *K*-type component increased in number gradually with increasing pressure, and eventually became the only type. Such structural transition does not occur in Y metal containing no H atoms. The interstitial H atoms likely played a dominant role in the formation of the long-period structures.

Reference

Machida, A. et al., Long-period Stacking Structures in Yttrium Trihydride at High Pressure, Physical Review B, vol.76, no.5, 2007, p.052101-1-052101-4.

4-9 A Breakthrough in Development of High-Temperature Polymer Electrolyte Membrane Fuel Cells
–Successfully Making a Highly Heat-Resistant Proton-Conductive Aromatic Polymer Electrolyte Membrane–

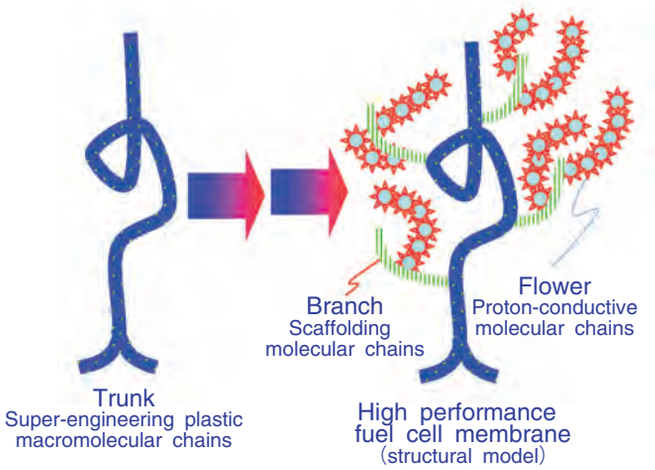

Fig.4-21 Schematic diagram for the development of high-performance fuel cell membranes by radiation grafting method
Scaffolding molecular chains (branches) were grafted to a highly heat-resistant super engineering plastic macromolecular chain (trunk), followed by radiation grafting of the functional molecular chains (flower), so that a number of proton conductive molecular chains were introduced into the membrane.

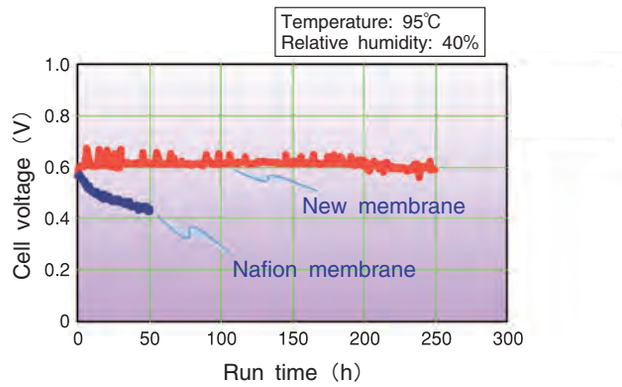

Fig.4-22 Fuel cell performance of new polymer electrolyte membranes operated under high temperature and low humidification
Operating the fuel cell under high temperature and low humidification, the prepared radiation-grafted polymer electrolyte membranes exhibited fuel cell performance better than that of commercial Nafion membrane.

The polymer electrolyte membrane fuel cells are promising electric power sources for home cogeneration and automobiles. To enhance the fuel cell performance and catalyst utilization efficiency, and to simplify the cooling system, it is desired that the fuel cell be operable at high temperature and low humification. However, although the commercial perfluorinated polymer electrolyte membranes, such as Nafion membranes, have excellent performance below 80°C and with full humidification, performance deteriorates remarkably above 90°C or at relative humidity below 50%. Therefore, development of a new polymer electrolyte membrane that can be used for thousands of hours under high temperatures and low humidification has been widely pursued recently.

To meet the demand for high temperature fuel cells, we used a thermally stable engineering aromatic polymer as the base film to develop a polymer electrolyte fuel cell membrane. In this study, the typical super-engineering film polyetheretherketone (PEEK) was chosen as the base film, and a styrenesulfonic ethyl ester (ETSS) monomer was radiation-grafted to this. The ETSS-grafted PEEK film was hydrolyzed to obtain the desired high performance polymer electrolyte membrane. By means of this new method, the PEEK-based polymer electrolyte membrane was directly prepared without a severe sulfonation reaction using a strong acid. Consequently, the intrinsic properties of PEEK were maintained and the resulting polymer electrolyte membrane was very tough, suited for application in fuel cells.

However, because of the low grafting activity of the PEEK chains (trunks), the ETSS monomer (flowers) was difficult to attach to the PEEK trunks in the desired amounts. Therefore, we designed a branch which could be easily attached to the trunks and easily graft with ETSS flowers. We found that the divinylbenzene (DVB) can serve as this branch well, allowing many flowers to be radiation grafted to the PEEK trunks. As a result, new polymer electrolyte membranes with high proton conductivity and highly thermal durability were successfully developed (Fig.4-21).

The new polymer electrolyte membrane was tested in a fuel cell under high temperature and low humidity (cell temperature, 95°C; 40% relative humidity). For comparison, the Nafion membrane was also tested under the same conditions. It was confirmed that the new membranes exhibited higher cell performance than the Nafion membrane. The membrane durability was evaluated in a fuel cell operated at a fixed current density of 0.3 A/cm^2. The Nafion membrane cannot withstand such a high temperature and low humidity, its voltage drastically dropping in a short operation time due to the deterioration-induced crossover of the fuel across the membrane. In contrast, the developed new polymer electrolyte membranes had significantly higher durability and stability. The voltage of the fuel cell was almost unchanged after the initial 250 h of operation, and was estimated to be stable for more than thousands of hours under this high temperature and low relative humidity (Fig.4-22).

In conclusion, it was possible to develop a polymer electrolyte membrane for a fuel cell which has high performance under high temperature and low humidification, by radiation grafting techniques. Development of such a highly stable and durable polymer electrolyte membrane is a big breakthrough for the practical application of fuel cells using hydrogen as the fuel.

Reference
Chen, J. et al., Fuel Cell Performance of Polyetheretherketone-based Polymer Electrolyte Membranes Prepared by a Two-step Grafting Method, Jounal of Membrane Science, vol.319, issues 1-2, 2008, p.1-4.

4-10 Strain Measurement on Rebars in Reinforced Concrete –Application of Neutron Diffraction to Nondestructive Strain Measurement–

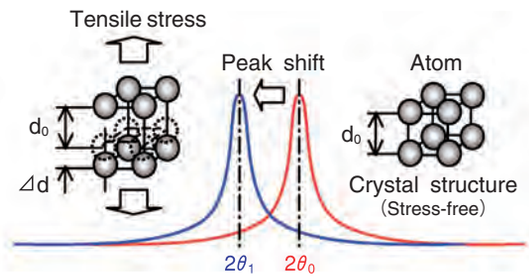

Fig.4-23 Principle of neutron strain measurement
Lattice strain can be measured by observing change in diffraction angle, 2θ, which is due to change in lattice spacing.

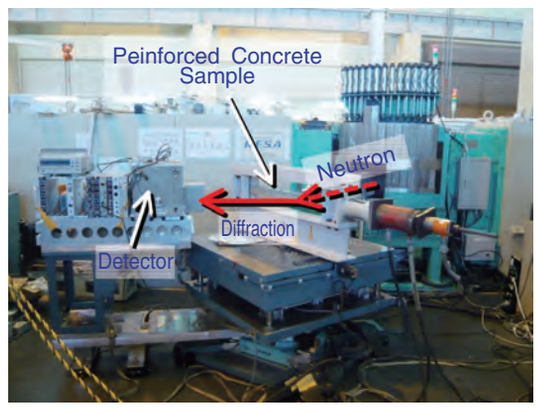

Fig.4-25 Layout of neutron strain measurement system
Neutrons irradiate the rebar through the concrete, and then the diffractions from the rebar are detected by the neutron detector.

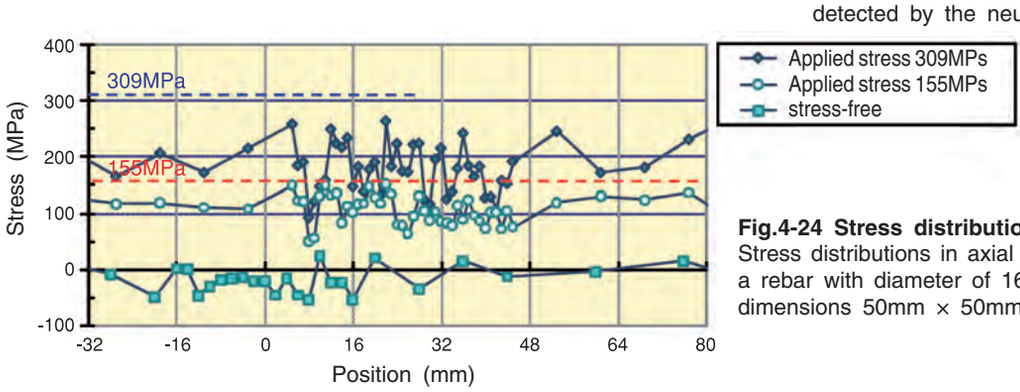

Fig.4-24 Stress distributions on the rebar
Stress distributions in axial direction (loading direction) on a rebar with diameter of 16mm embedded in concrete of dimensions 50mm × 50mm × 800mm.

It is already known that the performance of a reinforced concrete structure is affected by the bond condition between the rebar and concrete, and this bond condition has been evaluated by evaluating the strain on the rebar. In general, strains on the rebar have been measured using strain gauges; however, waterproofing treatment and wiring of the strain gauges affect the bond condition, and strain gauges discretely set on the rebar cannot measure strain distributions in detail. On the other hand, the neutron diffraction method, which is nondestructive and non-contact, can measure the lattice spacing of crystalline materials (Fig.4-23), and residual stresses and strains inside materials at a depth on the order of centimeters can be evaluated from the change in lattice spacing with the spatial resolution on the order of a few millimeters. Although the water in hydrated cement and the evaporated water in the concrete structures would decrease the neutron intensity due to high absorption by hydrogen atoms, drying the water in the concrete makes it possible to measure the strains on the rebar in concrete with the size of 50mm to 100mm square.

Fig.4-24 shows the lattice stress distribution on a rebar in concrete, derived from measurements by the neutron diffraction method. The residual stress distributions in this figure were measured along the rebar under uniaxial tensile stress of 155 MPa and 309 MPa, as well as the stress-free condition, as shown in Fig.4-25. Stress transferred to the rebar increased with an increase in the applied stress, though it was less than the applied stress because stress was shared with the concrete. Moreover, dispersion of stress around cracks was observed due to loss of adhesion there and also due to stress concentration around rebars. These results clearly indicate that the neutron diffraction method enables detailed measurement of stress distribution on the rebar.

As indicated above, the neutron diffraction method is expected to make possible measurement of the detailed residual stresses on the rebar nondestructively and also to measure the stress distributions around cracks in the concrete which cannot be measured by strain gauges. There is a possibility that the neutron diffraction method will gives us new knowledge in the structural engineering field.

Reference

Kanematsu, M., Noguchi, T., Yasuda, M., Suzuki H., Nondestructive Stress Measurement of Rebar using Neutron Diffractometer “RESA”, Proceedings of Annual Meeting of Japan Concrete Institute, Fukuoka, Japan, 2008, p.775-780, in CD-ROM (in Japanese).

4-11 Compact and Low Noise Ultra-High Intensity Laser –Good Prospects for a Laser Driven Proton Accelerator for Cancer Therapy–

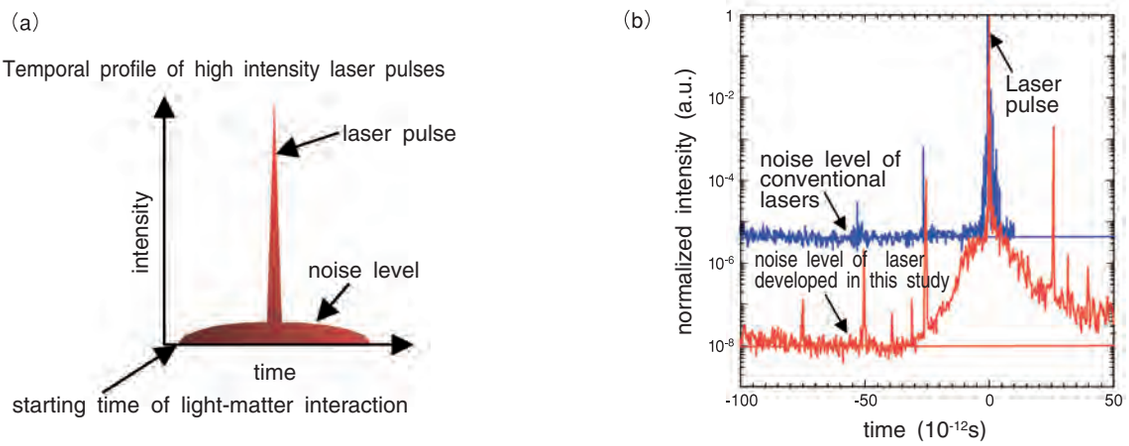

Fig.4-26 Temporal contrast of laser pulse
The output laser pulse has a noise component. The temporal contrast is defined to be the ratio of the intensity of the noise to the peak intensity of the laser pulse and is plotted as "normalized intensity". The contrast is improved by over 2 orders in magnitude with our laser system (red curve) compared to conventional systems (blue curve).

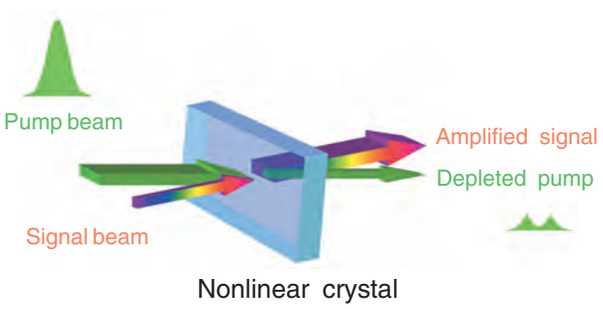

Fig.4-27 Conceptual diagram of Optical Parametric Chirped-Pulse Amplification (OPCPA)
The OPCPA scheme amplifies a frequency stretched "signal" pulse when a pump beam and a signal beam are present in a nonlinear crystal.

Ti:sapphire crystal is widely used as the lasing medium of choice for high intensity lasers. However, this material also causes critical technical problems such as unwieldy equipment size and unacceptably large noise levels which means low temporal contrast (Fig.4-26). Here, the contrast is time-dependent and defined as the ratio of the intensity of the noise to the peak intensity of the main pulse. Typically, terawatt (TW, 10^{12} W) Ti:sapphire laser amplifiers themselves require a space of a few meters square and have a contrast of ~10^{-6}. Therefore, at high intensity, the noise level can exceed the ionization threshold of a target, which can destroy or significantly modify the laser-plasma interaction processes. For the laser driven accelerator, the accelerated energy is limited by the noise level.

In order to solve these problems, we have improved the optical parametric chirped-pulse amplification (OPCPA) technique (Fig.4-27). The OPCPA affords significant reduction in the noise level compared with conventional systems because the amplification occurs only within the time of the pump pulse. For shorter pump pulse durations, the amplification time width is shorter, minimizing the noise amplification, and allowing high contrast. For the OPCPA we have (1) improved the pump-to-signal efficiency by increasing the spatial overlap between pump and signal beams and (2) added more precise control of amplification gain and spectrum by the use of multiple stages. By using these techniques, it is possible to increase the contrast and reduce the size of the high intensity laser.

This improved OPCPA laser facilitates a decrease in optical component size by at least an order of magnitude and at least a two order of magnitude improvement in contrast. With this compact system, a peak power of 3 TW was realized. This is the world's highest power compact OPCPA laser. These improvements in the high intensity laser technology are expected to make possible medical applications that use laser driven accelerators for therapy, and industrial technology.

Reference
Kiriyama, H. et al., High-energy, High-contrast, Multiterawatt Laser Pulses by Optical Parametric Chirped-pulse Amplification, Optics Letters, vol.32, no.16, 2007, p.2315-2317.

4-12 Mechanism for Biological Sensing of Ionizing Radiation –The Role of γ Subunit of G Protein in *Caenorhabditis elegans*–

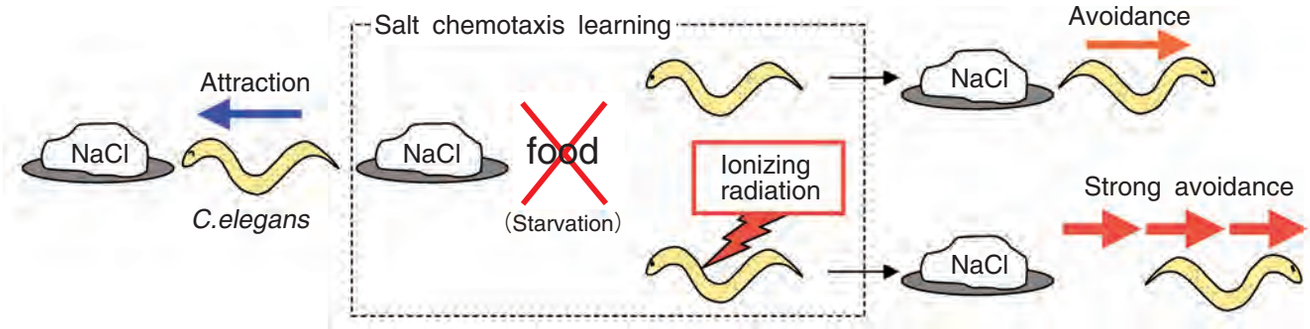

Fig.4-28 Salt chemotaxis learning in *C. elegans* and radiation effects
C. elegans is normally attracted to NaCl (salt), but the presentation of NaCl in the absence of food decreases its attraction to NaCl. The behavioral change from attraction to avoidance is the "salt chemotaxis learning", which is enhanced by ionizing irradiation.

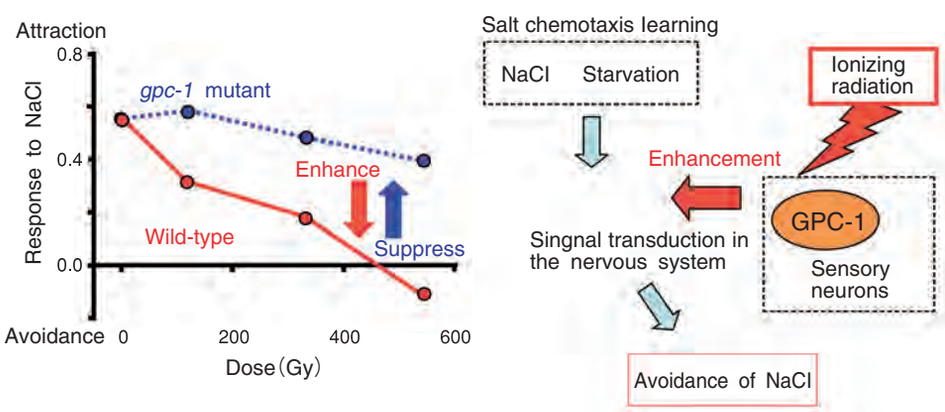

Fig.4-29 Radiation responses and the mechanism
Acute exposure to ionizing radiation induced an additional decrease in attraction to salt in the transition stage of the salt chemotaxis learning. The ionizing radiation induced additional decrease in attraction is significantly suppressed in the *gpc-1* mutant, which was defective in GPC-1 (one of the two γ subunits of the heterotrimeric G-protein). This suggests that ionizing radiation behaves as a modulator in the salt chemotaxis learning via *C. elegans* GPC-1.

Immediately after the discovery of ionizing radiation (IR), it was employed for medical uses as a roentgenography since it has permeability. At present, IR is an indispensable tool for a medical treatment, and has other uses. On the other hand, the biological effects of IR on humans have been studied and accumulated. Recently, effects of IR on the nervous system are drawing attention in the medical and space research fields. An important issue for medicine is the IR-induced suppression of adult neurogenesis in the hippocampus, where neurons are continuously born throughout life and which is an integral site for learning and memory. In space science, acute IR-induced learning impairment and abnormalities in the nervous system are seen as important potential risks associated with interplanetary space missions.

The research background made us to examine the effects of IR on learning using the nematode *Caenorhabditis elegans*. *C. elegans,* which is used for study of Alzheimer disease, is an attractive multi-cellular model organism for neurosciences because the connections in its neural network are completely known and has many genes similar to human genes. From experiments with salt chemotaxis learning, we found that only in the transition stage of learning, exposure to an acute dose of IR immediately induced an additional decrease (avoidance) of salt-attraction (Fig.4-28). To investigate the cause of radiation effects, we used a mutant with a deletion of gene. Finally, we found that IR-induced additional avoidance of NaCl was significantly suppressed in the *gpc-1* mutant (Fig.4-29), which was defective in GPC-1 (one of the two γ subunits of the heterotrimeric G-protein). It suggests that IR modulates the signal transduction in the nervous system of *C. elegans* via specific sensory neurons, and so qualitatively and quantitatively alters the salt chemotaxis learning.

In future, we will study the molecular mechanism of IR sensing in the sensory neurons and the effect of signals induced by IR in the nervous system of *C. elegans.*

Reference
Sakashita, T. et al., Modulatory Effect of Ionizing Radiation on Food-NaCl Associative Learning: the Role of γ Subunit of G Protein in *Caenorhabditis Elegans*, FASEB Journal, vol.22, no.3, 2008, p.713-720.

5 Nuclear Safety Research

To Support Safety Regulations and to Ensure Nuclear Safety and Confidence

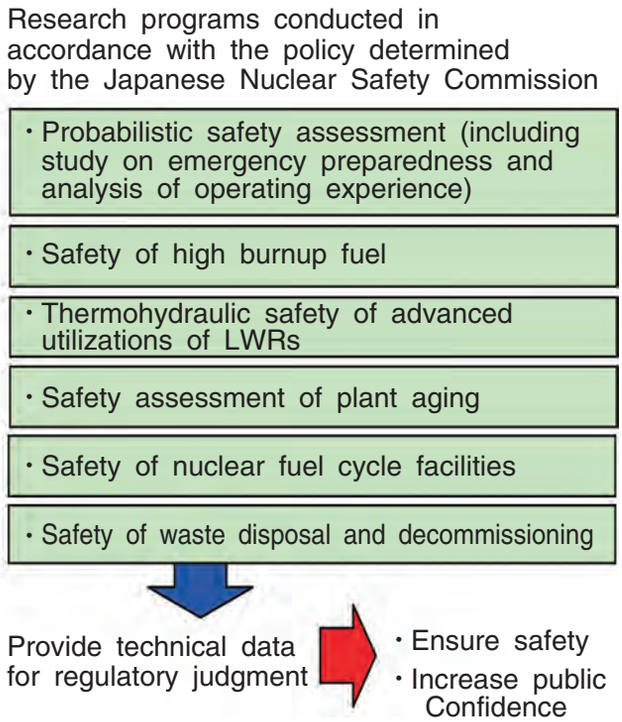

Fig.5-1 Major Subjects and Tasks of Safety Research

The latest scientific and technical knowledge is essential for the development and improvement of the safety guidelines and criteria with which the regulatory authorities perform safety regulation to assure the safety of nuclear installations.

The Nuclear Safety Commission (NSC) proposed a "Prioritized Plan for Nuclear Safety Research" in July 2004, to be carried out in order to meet the future regulatory needs. The main tasks expected of us are shown in Fig.5-1.

The results of nuclear safety research contribute to the maintenance and improvement of safety of the nuclear facilities and also to fostering public confidence in nuclear safety.

Furthermore, we are supporting the regulatory body Nuclear and Industrial Safety Agency (NISA) and the Japan Nuclear Safety Organization (JNES) by conducting research on various technical issues in safety regulation which they have contracted us to do.

The programs specified in the NSC's prioritized research plan and these contracts with the regulatory bodies are steadily providing a wide spectrum of useful results. The following paragraphs briefly describe the current status of research and new results from the programs shown in Fig.5-1.

The program on probabilistic safety assessment (PSA) is developing PSA methodologies for nuclear fuel cycle facilities and studying effective uses of risk information for safety regulation and management. The research program on emergency preparedness is applying the methodologies of PSA and environmental consequence analysis to the development of guides for decision making in various emergencies, including action levels, area, and timing of protective actions. Analysis of operating experience aims to obtain lessons from incidents that have occurred in nuclear facilities. An analysis of reported events of primary water stress corrosion cracking (PWSCC) provided information useful for early detection of PWSCC (Topic 5-1).

For the study of high burnup fuel safety, the FEMAXI-6 code for simulation of fuel behavior under normal operation was improved for application to MOX fuel and was tested by comparison with an experiment (Topic 5-2). A test at the nuclear safety research reactor (NSRR) simulating a reactivity initiated accident (RIA) clarified the fission gas release behavior in fuel pellets of high-burnup fuel (Topic 5-3)

In the study of safety assessment on advanced uses of light water reactors, tests at the Large Scale Transient test Facility (LSTF) under the international collaboration with the OECD/NEA are in progress and have produced test data useful for diagnosis of accident conditions and validation of analysis codes (Topic 5-4). A new measurement system for rapid boiling behavior in coolant channels in fuel bundle was developed and obtained test data for validation of RIA analysis codes (Topic 5-5).

For research on structural integrity assessment of reactor components, data on the neutron irradiation embrittlement mechanism such as intergranular embrittlement were obtained. The data suggested that the effect of phosphorus (P) impurities is not significant even with high values of neutron fluence. Moreover, we proposed a modified "Master Curve" method for fracture toughness evaluation of reactor pressure vessel steel, that enables a conservative fracture toughness estimate considering intergranular embrittlement (Topic 5-6).

For research on safety evaluation of nuclear fuel cycle facilities, we performed tests of the degree to which fission products in spent fuel reduce reactivity (burn up credit), and using this data examined the accuracy of the computation analysis used in criticality safety assessment of spent fuel storage facilities (Topic 5-7).

In the field of radioactive waste disposal and facility decommissioning safety research, we developed procedures to derive the upper bound of radioactivity concentration for three disposal methods of transuranium (TRU) wastes: trench disposal, concrete vault disposal and intermediate depth disposal. Calculation results of these procedures were incorporated in a report by the nuclear safety commission and in the ordinance of Ministry of Economy, Trade and Industry in 2008 that prescribed requirements on disposal of TRU wastes (Topic 5-8).

For the safety assessment of geological disposal of high-level radioactive waste (HLW), we developed a computer code for prediction of long-term performance alteration of compacted bentonite that covers the metal container encapsulating the HLW (Topic 5-9).

5-1 To Learn from Operating Experience
–Analysis of Primary Water Stress Corrosion Cracking Events at PWRs–

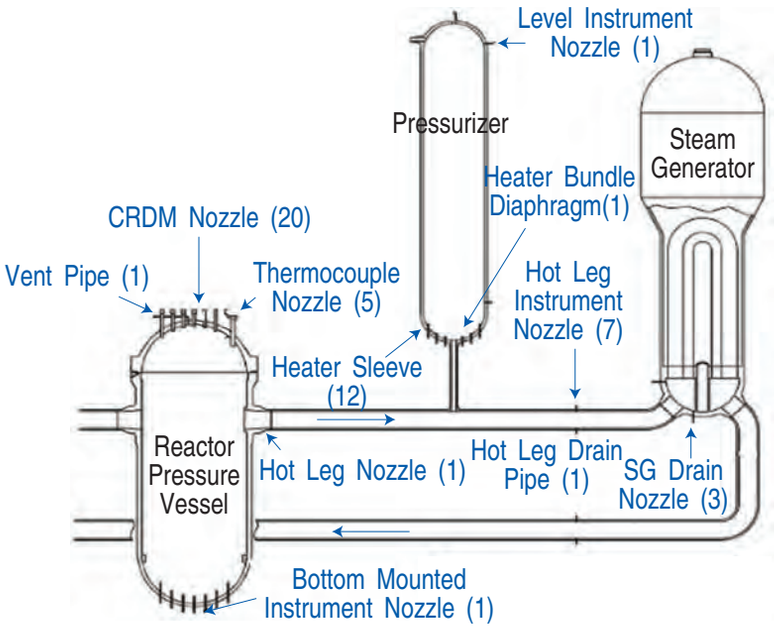

Note) The number in parentheses means the number of applicable LERs. There are some LERs that include degradations of two or more RCPB components.

Fig.5-2 Summary of Reactor Coolant Pressure Boundary Components with PWSCC Observed
Although primary water stress corrosion cracking (PWSCC) has been observed since early 1990's, it was not then recognized as an urgent issue for reactor safety. However, recently several significant degradations originating from PWSCC in the reactor coolant pressure boundary (RCPB) components have been observed at U.S. PWR plants. We analyzed the U.S. experience with alloy 600 degradation by reviewing licensee event reports (LERs) from 1999 to 2005 to examine trends of such events mainly focusing on affected components, characteristics of cracking, and inspection approaches for detecting the PWSCC. This figure provides a summary of locations where PWSCC was observed. As shown in this figure, PWSCC was found to have occurred in the RCPB components exposed to the high temperature environment, such as the control rod drive mechanism (CRDM) nozzles on reactor vessel head, and thus high temperature condition is one of the factors causing high susceptibility to PWSCC.

It is worldwide recognized that it is important to learn from operating experience in all technologies. In the field of nuclear technology, nowadays, regulatory authorities and industries have been actively carrying out analysis of incidents to identify their causes and to feed back the lessons learned to the design, operation and maintenance of installations on an international basis.

Since a severe accident at a nuclear installation, in particular a nuclear power plant, could cause serious damage to the environment as well as the surrounding populace, it is generally considered essential to eliminate potential or latent causes that could lead to such an accident in advance. Therefore, it is necessary to collect and analyze event information to consider corrective actions for preventing recurrence of the event. Further, it is important to continuously conduct such activities. At JAEA, such activities have been carried out for some time, and the results from these activities have been provided to the regulatory authorities and utilities in Japan.

Fig.5-2 illustrates an example of results from analysis of recent events which occurred at nuclear power plants. This analysis was carried out on the events involving primary water stress corrosion cracking (PWSCC) observed in the reactor coolant pressure boundary components such as the reactor pressure vessel (RPV) and reactor cooling system (RCS) piping.

Should the RPV or RCS piping break, resulting in a loss-of-coolant-accident (LOCA), the capabilities of core cooling and confinement of radioactive materials would be degraded. To obtain insights useful for preventing such a serious condition from occurring, we analyzed PWSCC events focusing on where PWSCC was observed, a method which could detect PWSCC, and so on. The results from this analysis revealed that PWSCC tends to occur at alloy 600 components exposed to relatively high temperature, such as control rod drive mechanism (CRDM) nozzles and pressurizer heater sleeves. In addition, it was shown that depending on the component affected, the non-destructive examination such as ultrasonic testing and/or eddy current testing is generally needed to detect and/or confirm the PWSCC , as well as visual inspection and different repair techniques should be applied. These results have been published to provide the relevant regulatory authorities and industries in Japan with the lessons learned and insights gained that seem useful for the early detection of PWSCC at nuclear power plants.

Reference

Takahara, S., Watanabe, N., Trending Analysis of Incidents Involving Primary Water Stress Corrosion Cracking on Alloy 600 Components at U.S. PWRs, Nippon Genshiryoku Gakkai Wabun Ronbunshi, vol.5, no.4, 2006, p.282-291 (in Japanese).

5-2 Simulation of MOX Fuel Irradiation Behavior for LWRs –Analysis of MOX Fuel Behavior in Halden Reactor by FEMAXI-6 Code–

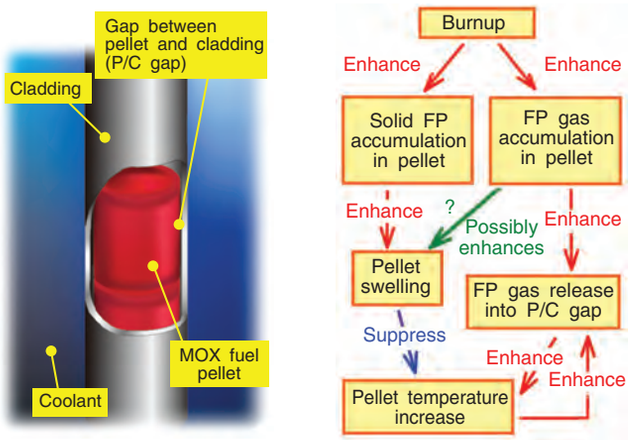

Fig.5-3 Burnup-induced phenomena in a fuel rod
FEMAXI-6 simulates behavior of one fuel rod. Fuel burnup induces pellet swelling, fission product (FP) gas accumulation, and its release to P/C gap. These phenomena interact with each other as shown above. This indicates that FP gas at the grain boundary can promote pellet swelling, which is usually induced by solid FP accumulation.

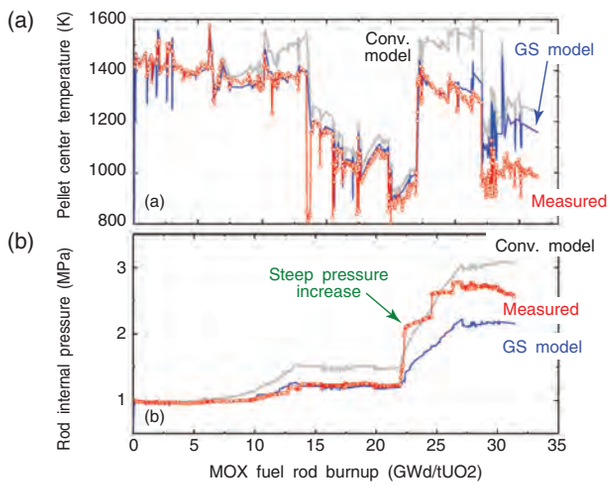

Fig.5-4 Comparison between measurements and calculations
(a) Calculated pellet temperature agrees with the measurement especially in the GS model, supporting the gas-induced swelling theory. (b) Calculation cannot reproduce the steep pressure increase satisfactorily. More accurate treatment of FP gas behavior is needed.

In nuclear reactors, energy is produced via fission reactions of Uranium (U) or Plutonium (Pu) in fuel pellets. This is the so-called “burnup” process. Because a variety of phenomena take place along with burnup, and these interact in a complicated manner as shown in Fig.5-3, computer simulation is indispensable to predict such fuel behavior. We have developed a high burnup fuel behavior analysis code, FEMAXI-6, in order to understand the behavior of high burnup fuels for reliable safety evaluation. As extensive use of U-Pu Mixed Oxide (MOX) fuels in LWRs is planned now, we have improved FEMAXI-6 to achieve more accurate prediction of high burnup MOX fuel behavior.

Some thermal and mechanical property models for MOX pellets were implemented to properly calculate pellet temperature, which is the most important factor influencing total fuel behavior. The next factor to be treated carefully is the effect of fission product (FP) gas which is accumulated inside the pellet grain or at the grain boundary. The latter, intergranular gas bubble growth, can enhance pellet swelling, and for this a new gas-induced swelling model (GS model) was implemented. With the improved version of FEMAXI-6, the behaviors of the MOX fuels irradiated in the Halden (Norway) reactor were analyzed.

Fig.5-4(a) shows changes in pellet center temperature during irradiation. Calculations successfully reproduced the measurement, especially in the GS model calculations. As pellet swelling is enhanced in the GS model, pellets more easily contact the cladding than in the conventional model (Conv. model) which does not consider the gas effect. This P/C contact enhances heat transfer and lowers pellet temperature. The agreement between the GS model and measurement supports the gas-induced swelling theory.

Fig.5-4(b) shows changes in the fuel-rod internal pressure. The steep increase indicates an appreciable FP gas release, which also implies that there was a large accumulation of FP gas at the pellet grain boundary before the sudden release. The deviation of the calculation results from the measurement is, therefore, mainly attributable to underestimation of intergranular FP gas inventory. As such deviation could affect prediction of pellet temperature in higher burnup cases, more accurate treatment of FP gas behavior is needed.

The present improvement enabled more accurate prediction of MOX fuel pellet temperature. A new model to calculate grain boundary FP gas inventory is under development. FEMAXI-6 is an open code and is extensively used for research and safety evaluation. The next release is planned at the end of FY2008 (to be shown at http://www.rist.or.jp/nucis/).

Reference

Udagawa, Y. et al., Analysis of MOX Fuel Behavior in Halden Reactor by FEMAXI-6 Code, Journal of Nuclear Science and Technology, vol.44, no.8, 2007, p.1070-1080.

5-3 Does Pellet Microstructure Change Affect Fuel Behavior during a RIA ?
–Fission Gas Release in High Burnup BWR Fuel under RIA Conditions–

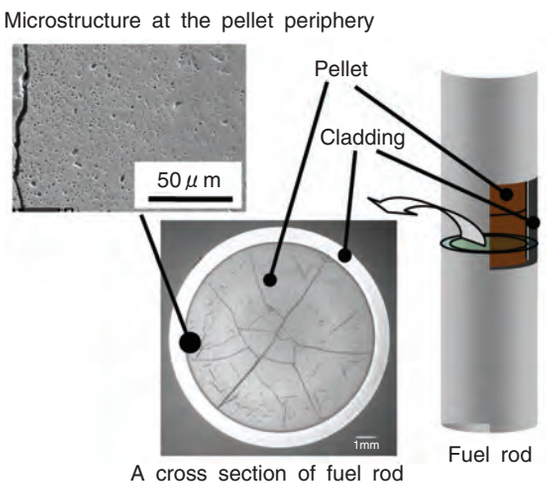

Fig.5-5 Crystal structure of fuel pellet before power burst test
A cross section of high burnup fuel pellet was observed by an optical microscope and scanning electron microscope (SEM). Fine fission gas bubbles of high density precipitated at the pellet periphery than in the center and middle, and the fabricated microstructure was lost in the periphery.

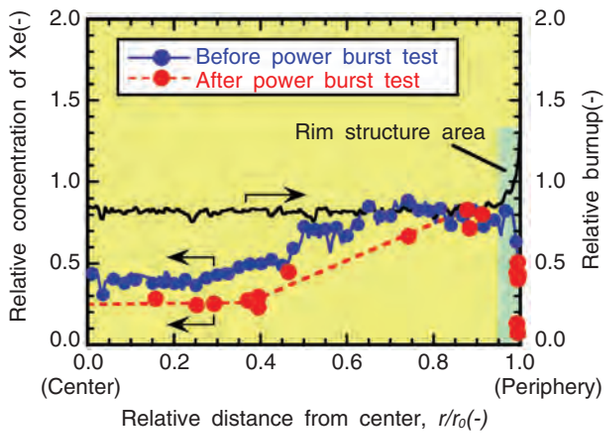

Fig.5-6 Comparison of radial Xe concentration profiles
Pulse operation of the Nuclear Safety Research Reactor (NSRR) can simulate safely a Reactivity Initiated Accident (RIA) which is envisioned in light water reactors. Comparing Xe concentration profiles which were measured before and after a power burst test, decrease of Xe concentration is seen in the rim structure, but this was negligible. Since the Xe concentration substantially decreased in the region between the center and mid-radius of pellet, it is considered that most fission gas was released from this region.

Extending the utilization period of reactor fuel, i.e. burnup extension, is progressing in stages, for the efficient use of natural resources and the reduction of fuel cycle cost. With increase in fuel burnup, more fission products accumulate in the fuel pellet, and cladding corrosion worsens. Accordingly, fuel safety with high burnup must be confirmed under accident conditions as well as under normal operation conditions.

At the periphery of a high burnup pellet, the microstructure is different from that at the time of pellet fabrication (Fig.5-5). This microstructure is called rim structure, and high pressure fission gas is accumulated in the bubbles generated in this region. In the case that the accumulated fission gas is released during a reactivity initiated accident (RIA), pellet temperature increase and the cladding deformation which is caused by additional fission gas release would occur due to the degradation of the heat conduction between pellet and cladding. These phenomena may affect the fuel rod safety. Consequently, the investigation of the effect of rim structure formation on fission gas release behavior under an RIA is an important subject of study.

A test rod was prepared from a fuel rod with high burnup after use in a commercial reactor, and power burst tests simulating a RIA were carried out at the NSRR with the test rod. In one of the post irradiation examinations (PIEs), the amount and composition of the fission gas released during the power burst test were investigated. Fig.5-6 shows the radial concentration profile of fission gas (Xe) which was measured by electron probe micro analysis (EPMA). Comparing the data obtained after power burst test with those before power burst test, it is seen that the Xe concentration decreased in the region between the center and mid radius region, while it hardly changed at all at the pellet periphery where the rim structure formed. The amount of the fission gas released during the power burst test can be evaluated from the difference of the Xe concentration before and after the test, shown in Fig.5-6, and this evaluated value is comparable with the value obtained from the PIE. In consideration of the grain boundary separation which was observed in the mid-radius region, it is found that most fission gas was released from the grain boundary in the mid-radius region, and that fission gas in the rim structure was hardly released at all during the power burst test.

The result of this study shows that the amount of fission gas released during a RIA is barely affected at all by rim structure formation, important information for analyzing fuel behavior during a RIA.

Reference
Amaya, M. et al., Fission Gas Release in BWR Fuel with a Burnup of 56GWd/t during Simulated Reactivity Initiated Accident (RIA) Condition, Journal of Nuclear Science and Technology, vol.45, no.5, 2008, p.423-431.

5-4 Reactor Instruments to Prevent PWR Severe Accident
–LSTF Test to Estimate Usefulness of Core Exit Thermocouple (CET)–

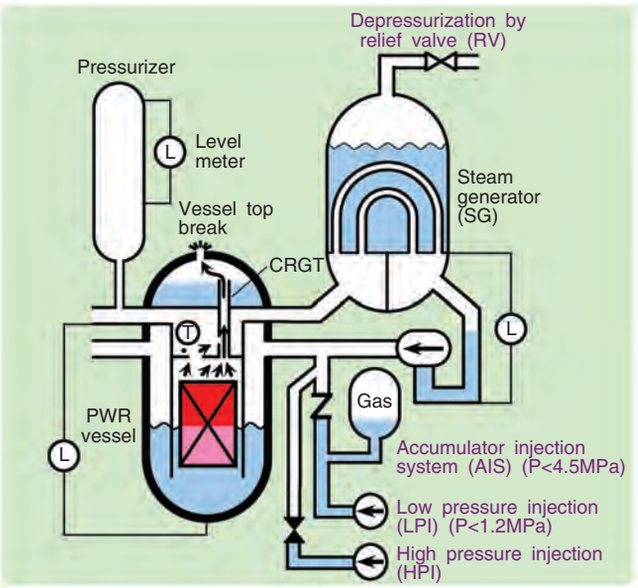

Fig.5-7 CET validation in a PWR top break LOCA test
LSTF is the largest PWR simulator in the world, with full-height and 1/48 volume scaling. A top break test was performed, motivated by an incident of significant wall thinning around the control rod penetration nozzle at pressure vessel head of Davis Besse reactor (see Topic 5-1). Capability of the CET ("T" in Fig. 5-7) to detect core overheating in case of an HPI failure was examined. The test revealed that the CET capability was influenced by three-dimensional steam flow from the core toward the CRGT inlets as well as their location around the CRGT.

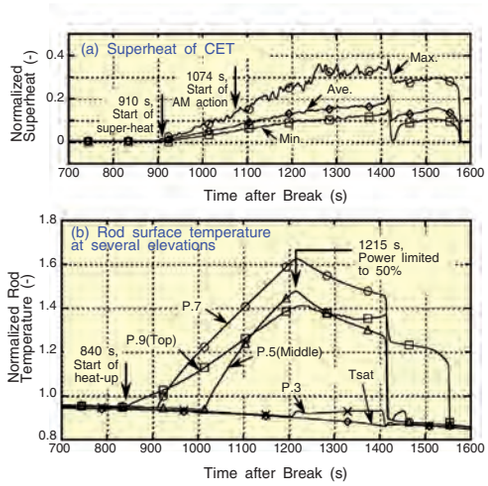

Fig.5-8 Maximum steam superheat detected by CET (a) was later and lower than superheat of rods in core (b)

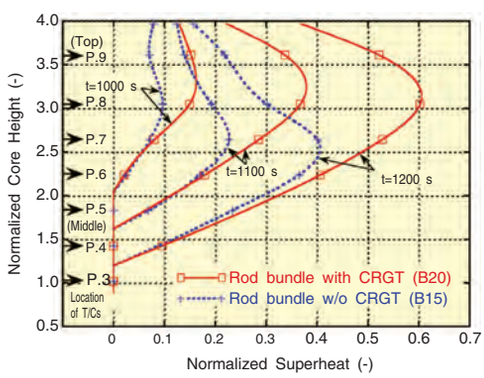

Fig.5-9 Comparison of axial steam temperatures in two rod bundles with and without CRGT at the core exit
Temperature profiles significantly changed with CRGT.

We conducted a Large Scale Test Facility (LSTF) test simulating a pressurized water reactor (PWR) loss-of-coolant accident (LOCA) caused by a small break at the vessel top under assumption of the total failure of high pressure injection (HPI) system (Fig.5-7). This test was part of the OECD/NEA ROSA Project which is an international cooperative study on reactor safety and advanced code development, one goal being the validation of a core exit thermocouple (CET) to detect core overheating and give a cue to start steam generator depressurization, an accident management (AM) action.

The CET detected superheated steam temperature, but this was 70 s later than the start of core superheating, and there was a further delay of 160 s to detect the temperature at which AM action is started, 623K. Thus, a large temperature difference was found between the CET and the hottest fuel rod (Fig.5-8). We found two reasons for this. One was the cooling effect of structural metals on uprising steam. The second one, specific for this test, was that steam flow convergence into the control rod guide tube (CRGT) inlet (Fig.5-7) induced three-dimensional steam flow in the core. In fact, steam temperatures in upper part of a high power bundle without a CRGT (B15) were significantly lower than those in B20 bundle with CRGT, suggesting colder steam inflow from the periphery following after the hot steam that went to a neighboring bundle with a CRGT (Fig.5-9). The CET installation outside the CRGTs may have caused further discrepancy from the hot core.

We showed that such CET response was possible in actual PWR operation, and furthermore demonstrated the usefulness of alternative indexes measured by water level meters (3 kinds; "L" in Fig.5-7).

OECD/NEA has just started study of CET effectiveness in PWRs. (This paper contains findings of the OECD/ROSA Project with its consent for publication.)

Reference

Suzuki, M. et al., Performance of Core Exit Thermocouple for PWR Accident Management Action in Vessel Top Break LOCA Simulation Experiment at OECD/NEA ROSA Project, Proceedings of 16th International Conference on Nuclear Engineering (ICONE16), Orlando, Florida, USA, 2008, ICONE16-48754, 11p., in CD-ROM.

5-5 Measurement of Rapid Boiling and Vapor Void Behavior in Coolant among Fuel Rods
–Toward Improved Prediction of Power Increase during RIAs–

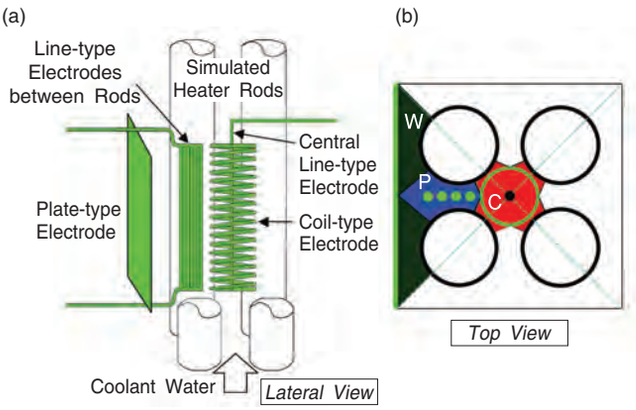

Fig.5-10 Layout and measurement area of impedance type void fraction meter
Measured impedance between inserted electrodes and simulated fuel rods also serving as electrodes is converted into void fraction. The void fractions of central area (C), inter-rod area (P) and near-wall area (W) are measured by measuring the impedance between coil and central line electrodes, between inter-rod line electrodes and rods, and between plate electrode and rods, respectively.

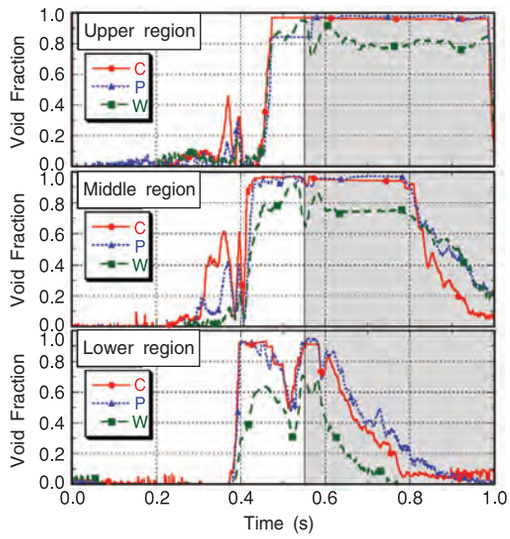

Fig.5-11 Time histories of void fraction in each measurement area
Simulated fuel rods were heated during the period of the unshaded area. Abrupt void fraction increase was delayed in the near-wall area. Location where the abrupt increase in void fraction occurs first varies depending on the conditions.

Recently, high burn-up fuels are being introduced in light water reactors (LWRs), making it possible to produce a larger amount of energy and utilize resources efficiently. However, it may cause the degradation of fuels due to the greater change of material composition with higher burn-up. To ensure the reactor integrity in an accident situation, LWRs are designed to satisfy regulatory criteria with a certain safety margin. Our research aims at contributing to more realistic evaluation of the safety margin of boiling water reactors (BWRs) during reactivity initiated accidents (RIAs), in which nuclear reaction is abruptly enhanced due to sudden extraction of control rods resulting in a rapid increase of core power.

In the BWR core, fast neutrons created by the nuclear reaction are decelerated by surrounding water to become thermal neutrons which sustain the chain reaction. Thus, the most favorable condition for nuclear reactions is where the fuels are fully surrounded by single-phase water. In the current safety assessment of RIAs, the power increase of the core is evaluated under such a condition. But in reality, the water around the fuels boils to generate vapor voids in the water. As the voids lower the amount of water around the fuels, the nuclear reaction becomes less active; the core power decreases by the feedback of negative void-reactivity. Therefore, the safety margin can be more realistically evaluated by taking the void-reactivity feedback into account. However, because of difficulties in the void behavior measurement under such rapid power increase conditions during RIAs, technical knowledge necessary for the evaluation of the void-reactivity feedback has been limited. We thus developed a fast-response measurement technique of the volume fraction of voids (void fraction), installing electrodes in a test flow channel having four simulated fuel rods as shown in Fig.5-10 and conducting a series of experiments simulating RIA conditions.

The void fraction meter utilizes the property of water that electrical impedance increases with the void fraction. The electrical impedance measured between several pairs of electrodes is converted into a local void fraction in the flow channel. Since the geometry of the test flow channel is complex, several types of electrodes including coil, line and plate types were installed in various spatial arrangements, and the combination of the electrodes was rapidly switched. The void fraction meters were placed in three regions along the flow direction (upper, middle and lower regions). In each region, the void fraction was measured in the central area (C), an inter-rod area (P) and a near-wall area (W). The changes in void fraction under conditions simulating the rapid heat generation of a RIA with a heating duration of 0.55 s are shown in Fig.5-11 as an example. It is clearly indicated that the variation of the void fraction strongly depends on the location in the channel. We conducted a number of experiments varying the heat generation rate and the temperature and velocity of water. The measured results form a valuable database to improve the prediction accuracy of the void fraction under RIA conditions. We made efforts further to improve the predictive capability of numerical analysis codes using the database, aiming at technical support of the national safety regulations.

This study was performed under a contract between Nuclear and Industrial Safety Agency (NISA) of the Ministry of Economy, Trade and Industry (METI) of Japan and JAEA.

Reference

Satou, A. et al., Study on Transient Void Behavior During Reactivity Initiated Accidents Under Low Pressure Condition – Development and Application of Measurement Technique for Void Fraction in Bundle Geometry – , Journal of Power and Energy Systems, vol.1, no.2, 2007, p.154-165.

5-6 Estimating Fracture Resistance of Reactor Pressure Vessel Steels –Estimating Toughness against Combination of Cleavage and Intergranular Fracture–

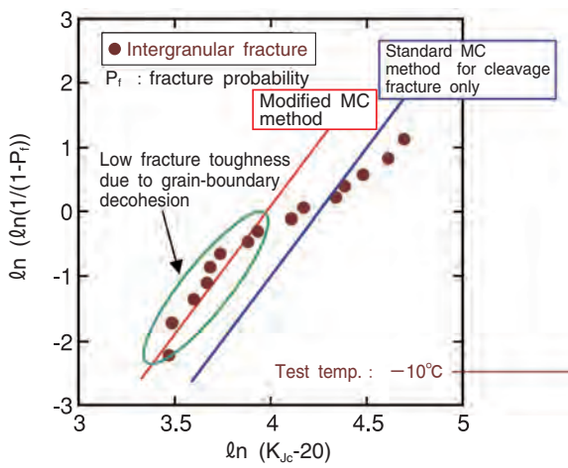

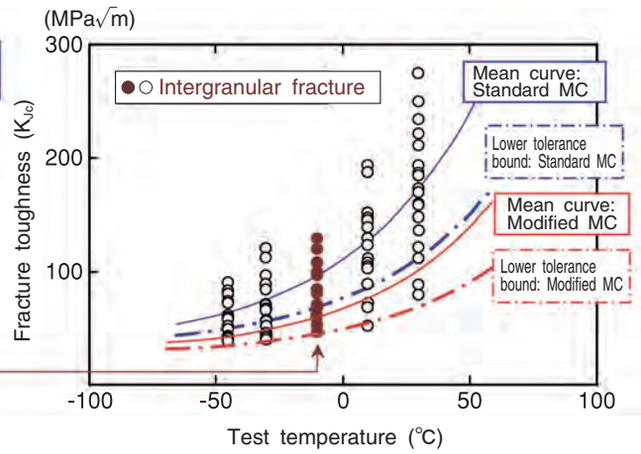

Fig.5-12 A Weibull plot of fracture toughness of intergranularly brittle material
The distribution of fracture toughness (K_{Jc}) values indicating grain boundary decohesion does not follow the linear regression defined in the standard method for cleavage fracture. A modified method is needed to estimate lower K_{Jc} values.

Fig.5-13 Temperature dependence of K_{Jc} values for the intergranularly brittle material together with the Master Curve
The K_{Jc} values are beyond the lower tolerance bound. The modified method enabled us to estimate lower K_{Jc} values due to intergranular fracture.

The reactor pressure vessel (RPV) is one of the most important safety-related structural components, because it has no redundancy and its failure is not considered in the design of the reactor. There is concern is that because the portion of the RPV surrounding the core region called “beltline” is exposed to neutron irradiation, the RPV material will be degraded (irradiation embrittlement). The effect is manifested by an increase in yield strength, a decrease in ductility, and degradation of toughness which are monitored by surveillance tests during plant operation. In the technical evaluation of every nuclear power plant whose operating period reaches 30 years, the irradiation embrittlement upon 60-years operation at high neutron fluence is estimated to ensure the structural integrity of RPV. One of possible types of embrittlement by such high neutron fluence is intergranular embrittlement caused by grain-boundary phosphorus (P) segregation. The P segregation is promoted by neutron irradiation and the presence of P weakens the cohesive strength of grain-boundaries, leading to embrittlement through intergranular fracture. How to estimate fracture toughness for the materials exhibiting intergranular fracture is one of the issues.

For fracture toughness evaluation of RPV steels, extensive efforts have been made to achieve direct determination of fracture toughness (K_{Jc}) in the ductile-to-brittle transition temperature region, using the so-called the “Master Curve” (MC) method. This estimates the fracture toughness versus temperature curve from a test at one temperature. Since fracture initiation is assumed to be cleavage in the MC method, it is questionable whether the method is applicable to materials subject to intergranular fracture.

The K_{Jc} values of the material exhibiting a mixed mode fracture of intergranular and cleavage due to intergranular embrittlement exhibit a large scatter. A Weibull plot of K_{Jc} values is shown in Fig.5-12, together with the data fitting denoted as a blue line by the standard MC method. The figure clearly indicates that the distribution of K_{Jc} values does not follow the linear regression defined in the standard method. It seems that the distribution of K_{Jc} values is from an inhomogeneous material creating two distributions of fracture toughness. This feature becomes more pronounced with increase in P concentration at the grain-boundaries. Since fracture toughness depends on the type of brittle fracture which initiates at the crack front, the obtained K_{Jc} values may follow the dual fracture toughness distributions of cleavage and intergranular fracture. We applied a modified MC analysis to the estimation of intergranular fracture by censoring the upper K_{Jc} data in Fig.5-12. The test temperature dependence of K_{Jc} is shown in Fig.5-13. The solid and dashed blue lines represent the mean curve and lower bound for fracture, respectively. The dependence of material subject to intergranular fracture as well exhibits low K_{Jc} values below the lower tolerance bound of brittle fracture. The modified method enables a more conservative fracture toughness estimate, as shown by the solid and dashed red lines in Fig.5-13.

Reference

Nishiyama, Y., Onizawa, K. et al., Phosphorus Segregation and Intergranular Embrittlement in Thermally Aged and Neutron Irradiated Reactor Pressure Vessel Steels, Journal of ASTM International, vol.4, issue 8, 2007, p.12, Paper ID JAI100690.

5-7 Taking Advantage of Spent Fuel Being Harder to Make Critical than Fresh Fuel
–Acquisition of Verification Data for Burn Up Credit Analysis Methods–

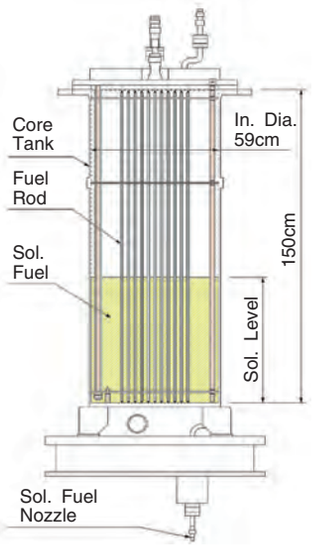

Fig.5-14 Heterogeneous system consisting of fuel rods and solution fuel
There were 333 uranium dioxide fuel rods arrayed at 1.5-cm intervals in a cylindrical core tank. Uranyl nitrate solution was fed from the bottom, and the level of the solution when it became critical was measured.

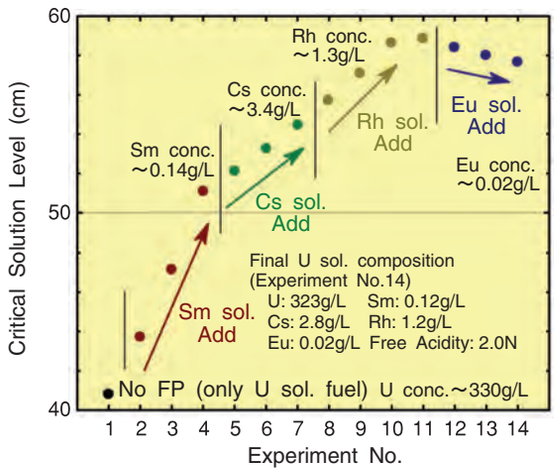

Fig.5-15 FP elements addition and critical level increase
As Sm, Cs and Rh were added in sequence to the uranium solution fuel, neutron absorption increased and critical solution level became higher. Although Eu was also added, the effect of reduced concentration of Sm etc. due to increase of total solution volume overcame the effect of increased Eu concentration, and critical solution level decreased.

In a nuclear reactor, nuclear burn of fuel proceeds with fission chain reaction, and thus fissile material such as uranium is depleted and fission products (FP) accumulate. Because both such changes hinder the chain reaction, spent fuel is by its nature harder to make critical than fresh fuel. The so-called "introduction of burn up credit" quantitatively evaluates this nature which enables handling of larger quantities of spent fuel in transportation, storage, reprocessing, etc. without danger of critical accidents

Up to now in Japan, there has been no example of burn up credit introduction considering of FP accumulation although there is one considering fissile material depletion. To quantitatively evaluate the FP accumulation effect, it is necessary to accurately estimate both the amount of FP in spent fuel and its negative effect on criticality.

Precise measurement of the negative effect of FP was conducted at the Static Critical Experiment Facility (STACY) in the Nuclear Science Research Center. Simulating the dissolving process of a reprocessing facility, where the advantage of burn up credit introduction is large, uranium solution fuel (^{235}U 6wt%) was fed through a bottom nozzle to a core tank in which uranium fuel rods (^{235}U 5wt%) were arrayed (Fig.5-14) and the critical level of the solution was measured. Natural elements of samarium (Sm), cesium (Cs), rhodium (Rh) and europium (Eu) were added in that order to the solution so that their final concentrations became equivalent to that produced by the power generation of 30 GWday per 1-t uranium. As a result, criticality was harder to reach, i.e., critical solution level was raised as shown in Fig.5-15.

Effect on criticality is expressed as change of neutron effective multiplication factor k_{eff} (k_{eff} is the change rate of the number of neutrons mediating chain reactions. k_{eff} is 1.0 at criticality). The effects of each element per unit concentration were estimated to be -3293 ± 40 ¢/(g/L) for Sm, -26.5 ± 1.4 ¢/(g/L) for Cs, etc. ("¢" is a unit of k_{eff} change; 7.6×10^{-5} for this experiment.)

Multi-group cross sections based on the nuclear data library JENDL-3.3 were produced by the SRAC code, and k_{eff}s were calculated by the TWODANT code. Computation analysis of the effect of each element based on the k_{eff} s agreed well with the measurement for Eu but gave slightly larger values than measurement for Sm, Cs, and Rh. Although the calculation was significantly larger than the measurement uncertainty only in the case of Sm, it should be noted that estimation by computation only may result in a larger negative effect than in reality.

Thanks to recent developments, the perturbation method now can be used with Monte-Carlo codes such as MCNP and MVP, so that the effect on criticality can be calculated, which should be validated with this measurement results. It is also necessary to improve accuracy of the post irradiation examination (PIE) to measure the amount of FP in actual spent fuel.

This report includes results of experimental and computational studies performed under a contract with the Ministry of Education, Culture, Science and Technology of Japan.

Reference

Tonoike, K. et al., Benchmark Critical Experiments and FP Worth Evaluation for a Heterogeneous System of Uranium Fuel Rods and Pseudo FP Doped Uranium Solution, Proceedings of 8th International Conference on Nuclear Criticality Safety(ICNC 2007), Russia, 2007, p.222-227.

5-8 Evaluating the Radioactivity Concentration of Radioactive Wastes below Which They Can Be Disposed
–Dose Calculation to Derive the Upper Bound of Radioactivity Concentration in Disposal of Transuranium Wastes–

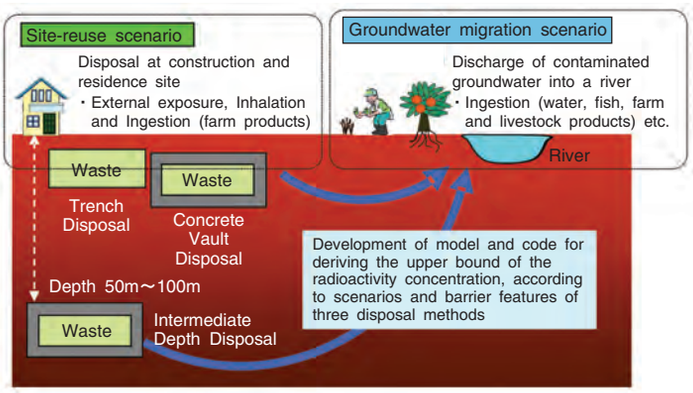

Fig.5-16 Scenarios and exposure pathways used to derive upper bound of radioactivity concentration in disposal
We developed an assessment code (GSA-GCL ver. 2) to derive the upper bound of radioactivity concentration for three disposal methods: trench disposal, concrete vault disposal and intermediate depth disposal. This code supports the dose estimation for the exposure pathways of a site-reuse scenario and of a groundwater migration scenario.

Table5-1 Recommended values of upper bound of radioactivity concentration for 3 disposal methods
We calculated exposure doses resulting from three disposal methods for low-level radioactive wastes. Based on the results, the NSC decided the upper bounds, considering both easiness of measurement of radioactivity concentration and concentration distribution of radioactive waste to be disposed of.

Radionuclide	Recommended Values of Upper bound of Radioactivity Concentration(Bq/ton)		
	Trench Disposal	Concrete Vault Disposal	Intermediate Depth Disposal
C-14	—	1E+11	1E+16
Cl-36	—	—	1E+13
Co-60	1E+10	1E+15	—
Ni-63	—	1E+13	—
Sr-90	1E+07	1E+13	—
Tc-99	—	1E+09	1E+14
I-129	—	—	1E+12
Cs-137	1E+08	1E+14	—
α-radionuclide＊	—	1E+10	1E+11

(＊)The values of upper bound for radionuclide emitting α radiation are represented as those for Am-241 for trench disposal and Np-237 for intermediate depth disposal, respectively.

The upper bound of radioactivity concentration during disposal means the maximum concentration of radionuclides of waste repository allowable in a license application for that repository. In Japan, there are three concepts for methods of disposing of low-level waste categories: near surface disposal without an artificial barrier (trench disposal), near surface disposal with an artificial barrier (concrete vault disposal), and intermediate depth disposal. The Nuclear Reactor Regulation Law has not been amended to set the upper bound of the radioactivity concentration for each of these disposal methods of transuranium (TRU) wastes. We developed an assessment code (GSA-GCL ver. 2) to derive the upper bound of radioactivity concentration for TRU wastes, according to geological and artificial barrier features in three disposal concepts. This code supports the dose estimation for the exposure pathways in two typical scenarios: (a) the site is a residential area and (b) the groundwater from the site is discharged into a river (Fig.5-16). We specified important radionuclides and their dose levels based on calculations using our code, setting appropriate geological and artificial barrier conditions for each disposal method. These dose estimations were adopted in the report published by the Nuclear Safety Commission (NSC); "Upper Bounds of Radioactive Concentration in Burial of Low-Level Radioactive Solid Waste (in Japanese), May 2007". In this report, the NSC recommended upper bound values considering both ease of measurement of the radioactivity concentration and the variation in concentration of radioactive waste to be disposed of (Table5-1). Their recommended values were prescribed by ordinance of Ministry of Economy, Trade and Industry in 2008. This work was performed by JAEA under contract with Nuclear and Industrial Safety Agency in Ministry of Economy, Trade and Industry.

References

Takeda, S. et al., Estimation of Radioactivity Concentration Limit for Trench Disposal of Transuranium and Uranium Wastes (Contract Research), JAEA-Research 2008-044, 2008, 64p. (in Japanese).
Takeda, S. et al., Estimation of Radioactivity Concentration Limit for Intermediate Depth Disposal of Transuranium and Uranium Wastes (Contract Research), JAEA-Research 2008-045, 2008, 60p. (in Japanese).
Sawaguchi, T. et al., Estimation of Radioactivity Concentration Limit for Concrete Vault Disposal of Transuranium and Uranium Wastes (Contract Research), JAEA-Research 2008-046, 2008, 62p. (in Japanese).

5-9 How Long Does a Repository Confine Radionuclides?
–Modeling of Long-Term Alteration of Bentonite Buffer Material–

Fig.5-17 A conceptual view of high-level radioactive waste (HLW) disposal system
Vitrified HLW is encapsulated in an iron container (overpack), surrounded by engineered buffer material (bentonite) and placed in a shaft contained in stable bedrock. Cement is used for mechanical support of the shafts, but it causes surrounding water to become highly alkaline, which is likely to deteriorate the properties of the bentonite buffer over a long period.

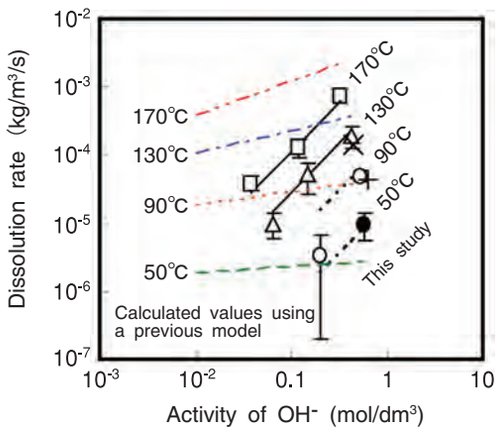

Fig.5-18 Dissolution rate of montmorillonite in highly alkaline solutions
The dissolution rate of montmorillonite, the main constituent of bentonite, was investigated using compacted bentonite. The dependence of the rate on activity of hydroxide ions, a_{OH}-, and on the temperature is shown here. There is higher dependence on a_{OH}- than a model based on results of experiments using pulverized bentonite. The rate is sensitive to the alkalinity.

In the Japanese program, high-level radioactive waste (HLW) is vitrified, encapsulated in a metal container called overpack, surrounded by engineered bentonite buffer material, and placed in a repository cut out from stable bedrock as shown in Fig.5-17. Cement is expected to be applied for the mechanical support of the repository.

Besides its mechanical buffer function, bentonite prevents groundwater from intruding into the waste and retards radionuclide movement outwards by adsorbing them. It is necessary to estimate the long-term changes of such properties of bentonite confining long-lived radionuclides in HLW.

Radioactive decay of radionuclides in HLW increases the temperature of the surrounding bentonite up to 90ºC right after the emplacement, and an alkaline environment is likely to be induced by the cement used in the repository. The temperature and alkaline condition possibly accelerate alteration of bentonite.

Because the radionuclide confining property of the bentonite arises from its main constituent montmorillonite, dissolution of montmorillonite in contacting groundwater results in deterioration of the confinement. Several researchers have obtained the dissolution rates of pure pulverized montmorillonite in free water with high water/solid-ratio, which are far from the repository condition where bentonite is in a compacted state. The property of water filling the narrow pore spaces (porewater) in the compacted bentonite may be different from that of free water. We performed the dissolution experiments of montmorillonite in a compacted state simulating the repository condition.

The dissolution rate of montmorillonite we obtained was a function of activity of hydroxide ions, a_{OH}- (mol/dm^3), and temperature, T (K), as shown in Fig.5-18. The rate, R_A (kg/m^3/s), could be formulated as:

$$R_A = 3.5 \times 10^3 (a_{OH}\text{-})^{1.4} \exp(-51000/RT) [\text{kg/m}^3\text{/s}]$$

where R is the gas constant. The dissolution rate obtained for a compacted state has a higher dependence on the a_{OH}- than that of previous models that were based on high water/solid-ratio dissolution experiments using pulverized materials.

The a_{OH}- of porewater is an important factor determining the dissolution rate, and this is determined by both chemical reactions with minerals and mass transport. We developed a coupled mass-transport/ chemical-reaction code for predicting the a_{OH}- and the long-term alteration of the bentonite.

Further investigation is necessary to understand the mechanisms of the dissolution of compacted montmorillonite and to verify the model by comparing results of the model calculation with laboratory experiments or field observations.

Reference
Yamaguchi, T. et al., Experimental and Modeling Study on Long-Term Alteration of Compacted Bentonite with Alkaline Groundwater, Physics and Chemistry of the Earth, vol.32, no.1-7, 2007, p.298-310.

6 Advanced Science Research

Advanced Basic Research to Create the Future

In the Advanced Science Research Center, new frontier research of nuclear energy and ionizing radiation expected to bear fruit in the future is conducted to discover new principles and phenomena, and furthermore to create new materials and technologies. In order to achieve these aims, we have four basic policies; (1) to pursue research for which the high level research capability (researchers and facilities) in JAEA is effectively used and which is difficult to do in other research organizations, (2) to achieve results before the rest of the world does, (3) to nurture a new basic research area until it becomes fruitful, (4) to explain and apply the research, thus fulfilling our responsibility to society, in conformity with the Third Science and Technology Basic Plan.

The following research is going on: nuclear physics and nuclear chemistry of superheavy elements, the nuclear shell structure, reaction dynamics and electrochemistry using heavy-ion beams of accelerators; synthesis of uranium and transuranium compounds and measurement of their macroscopic quantities and electronic structure, clarification of magnetic structure, magnetic excitation, and the mechanism of superconductivity using NMR, μSR, neutron scattering, and theoretical methods; design of novel materials using mega-gravitation and nano-particle deposition, topmost surface studies using bright and coherent positron beams; elucidation of the interaction mechanism of heavy elements and ionizing radiation within living cells by spectroscopy, and studying the primary and fundamental processes in the interactions of ionizing radiation with matter.

In order to promote this research, we are collaborating with other research sections in JAEA, and several international collaborations are ongoing. In addition, we accept new research subjects based on public suggestions within the framework of the Reimei Research Promotion project of JAEA.

Superheavy Element Nuclear Science

Recoil mass separator for experimental research on fusion reaction mechanisms to produce super-heavy elements by bombarding deformed nuclei with heavy-ion beams from JAEA tandem-booster accelerator.

Extreme Environment and Substance Science

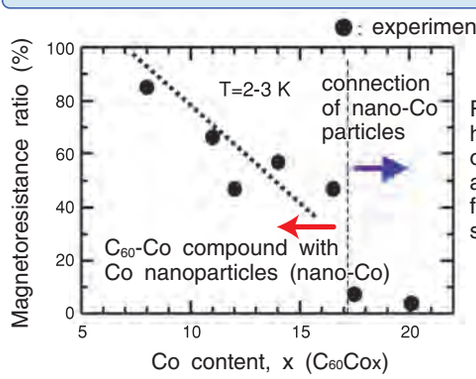

Research of new hybrid materials of organic molecules and transition metals for highly functional spintronics.

Finding of anomalously large tunnel magnetoresistance effect (~90%) not predicted by existing theory

Actinide Material Science

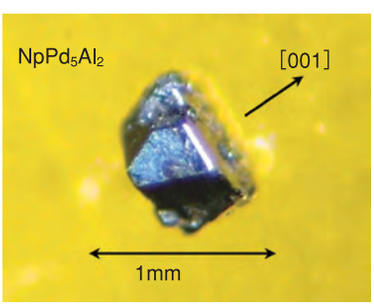

Discovery of the first Np-based heavy fermion superconductor with large upper critical magnetic field (500,000 times of the geomagnetism)

$NpPd_5Al_2$ high quality single crystal

Material and Life Sciences

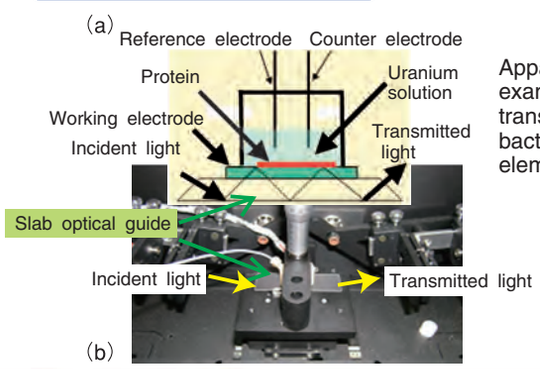

Apparatus for examining electron transfer between bacteria and heavy elements.

Fig.6-1 Four Research Fields and Collaboration in Advanced Science Research Center

6-1 Chemical Characterization of Superheavy Elements –Fluoride Complexation of Element 104, Rutherfordium–

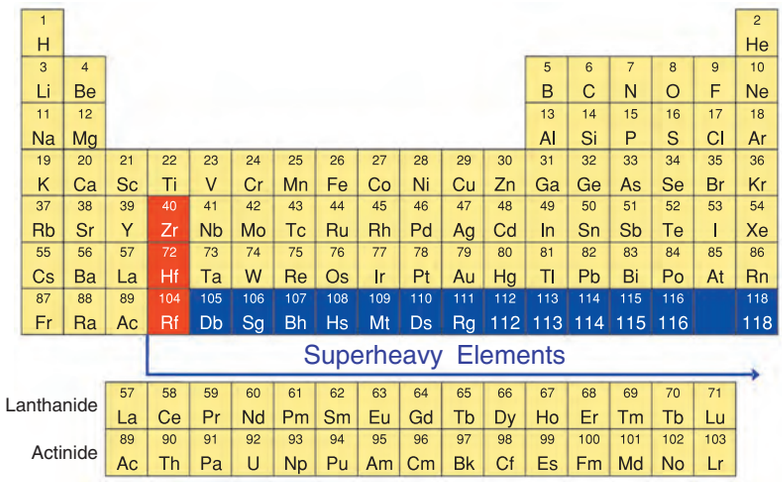

Fig.6-2 Periodic table of the elements
Superheavy elements are represented by blue panels. Group-4 elements studied in the present work are indicated by red panels. (Superheavy Elements beyond element 112 have not been formally recognized yet.)

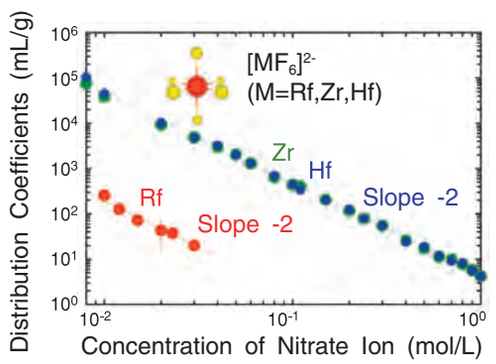

Fig.6-3 Variations of distribution coefficients (K_d) of rutherfordium (Rf), zirconium (Zr) and hafnium (Hf) as a function of the concentration of the nitrate ion
The K_d values of Rf, Zr and Hf are indicated by red, green, and blue circles, respectively.

Superheavy elements with atomic numbers ≥ 104 are currently placed on the uppermost end of the periodic table as shown in Fig.6-2. Chemical properties of lighter elements arranged in the same columns of the periodic table show gradual variation, and those of superheavy elements are theoretically expected to have greater deviations among homologues due to strong relativistic effects on their electronic structure.

In the present study, we studied anion-exchange behavior of element 104, rutherfordium (Rf) in hydrofluoric acid and nitric acid (HF/HNO_3) mixed solutions. The Rf atoms were produced in the nuclear reaction between a ^{248}Cm target and ^{18}O beams delivered from the JAEA tandem accelerator. It was clarified for the first time that the properties of fluoro complexes of Rf are significantly different from those of its lighter homologues Zr and Hf.

In Fig.6-3, the variations of distribution coefficients (K_d) of Rf, Zr and Hf are shown as a function of the concentration of the nitrate ion. K_d is the concentration ratio of the element in the resin phase to that in aqueous solution; larger K_d shows stronger adsorption on the resin. The K_d values of Rf, Zr and Hf decreased with increase in the concentration of the nitrate ion. These decreasing trends indicate that the nitrate ions entering in the binding sites of the anion-exchange resin drive the anionic fluoride-complexes of Rf, Zr, and Hf out of the resin into the aqueous solution. The slopes in the logarithmic plot of K_d vs. the concentration of the nitrate ion are -2 for all the elements. These -2 slopes show that the anionic fluoride-complexes have the same -2 charges, clearly demonstrating that Rf forms a hexafluoro complex, $[RfF_6]^{2-}$, as do Zr and Hf. It was also found that the K_d values of Rf are smaller than those of the homologues by about 2 orders of magnitude. We further investigated the variation of the K_d values depending on the concentration of the fluoride ion to understand the difference in the K_d values. We then found that about 2 orders of higher concentration of the fluoride ion is necessary to form $[RfF_6]^{2-}$ than that to form $[ZrF_6]^{2-}$ and $[HfF_6]^{2-}$. It was thus understood that the difference in K_d between Rf and its homologues in Fig.6-3 results from the fact that Zr and Hf have completely formed hexafluoro complexes while the Rf complex is incomplete at the concentration of fluoride ions used.

This suggests that Rf^{4+} has a larger ionic radius than Zr^{4+} and Hf^{4+} because formation of fluoro complexes of the group-4 elements depends on the ionic radii of the tetravalent ions. An ionic radius of Rf would be influenced by the relativistic effects that change the electronic structure of Rf. Although it has not so far known how relativistic effects change the ionic radii, the present result is a key to solve the question.

Reference

Toyoshima, A. et al., Hexafluoro Complex of Rutherfordium in Mixed HF/HNO_3 Solutions, Radiochimica Acta, vol.96, no.3, 2008, p.125-134.

6-2 Heavy Fermion Superconductivity in Neptunium Compound –A New Material Advances Actinide Science–

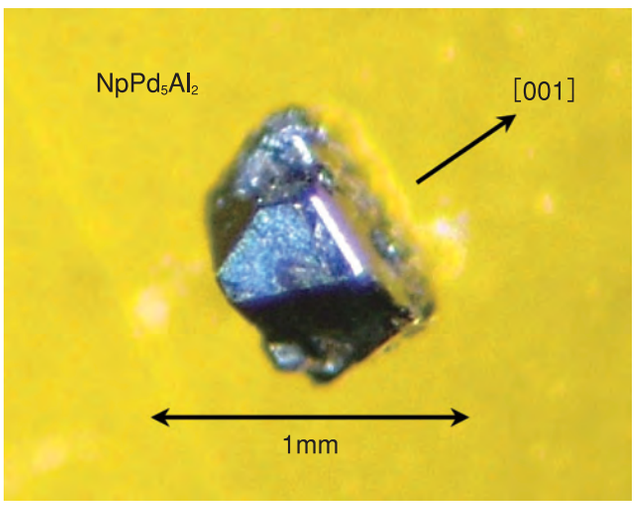

Fig.6-4 Photograph of $NpPd_5Al_2$ single crystal

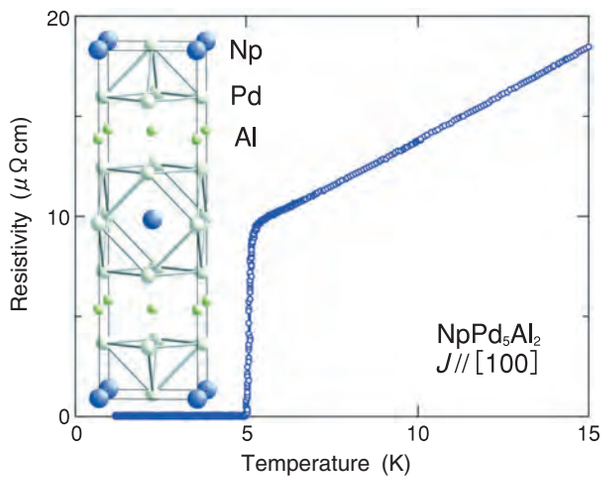

Fig.6-5
$NpPd_5Al_2$ crystallizes into a body-centered tetragonal lattice. Np is surrounded by Pd atoms. Electrical resistivity goes to zero at 5 K, demonstrating superconductivity.

Actinide elements such as uranium (U), neptunium (Np), plutonium (Pu), which are used as nuclear fuels, are very important materials in atomic energy science and technology. At the same time, these elements and their compounds have also attracted attention for their novel physical properties, because 5f electrons in actinides sometimes exhibit novel magnetic and/or superconducting behavior. While uranium compounds with less radioactivity have widely been investigated, the solid-state science of transuranium compounds including neptunium and plutonium began rather recently. The discovery of plutonium-based superconductor $PuCoGa_5$ in 2002 has demonstrated that many new compounds as well as unknown scientific phenomena might be hidden in actinide compounds.

In 2007, we found a new neptunium-based superconductor (Fig.6-4). The occurrence of superconductivity in neptunium compounds is very surprising because they often exhibit strong magnetism, which usually destroys superconductivity. The detailed characterization of the new compound has shown that it has the composition $NpPd_5Al_2$ and crystallizes into a tetragonal crystal structure (Fig.6-5).

The discovery of $NpPd_5Al_2$ stimulated scientists in this field, leading to the discovery of several new rare-earth and actinide compounds with the same structure.

5f electrons in actinide elements change their behavior depending on the chemical or physical environment surrounding them. In particular, plutonium exhibits multiple structural phase transitions among six different crystal structures with increase in temperature from room temperature to its melting temperature. No other elements behave in such a way. The discovery of $NpPd_5Al_2$ demonstrates that discovering "new materials" by providing a new environment for actinide elements can lead to discovery of new phenomena. We hope that the present actinide material research will aid in deeper understanding of physical behavior of actinides.

This work has been performed in collaboration with Tohoku University and Osaka University.

References

Aoki, D., Haga, Y. et al., Unconventional Heavy-Fermion Superconductivity of a New Transuranium Compound $NpPd_5Al_2$, Journal of the Physical Society of Japan, vol.76, no.6, 2007, p.063701-1-063701-4.

Haga, Y. et al., Crystal Structure and Magnetic Properties of the New Ternary Actinide Compounds $AnPd_5Al_2$ (An = U,Np), Journal of Alloys and Compounds, vol.464, 2008, p.47-50.

6-3 Microscopic Investigations of Uranium and Trans-Uranium Oxides
–Nuclear Magnetic Resonance Studies of the Electronic States–

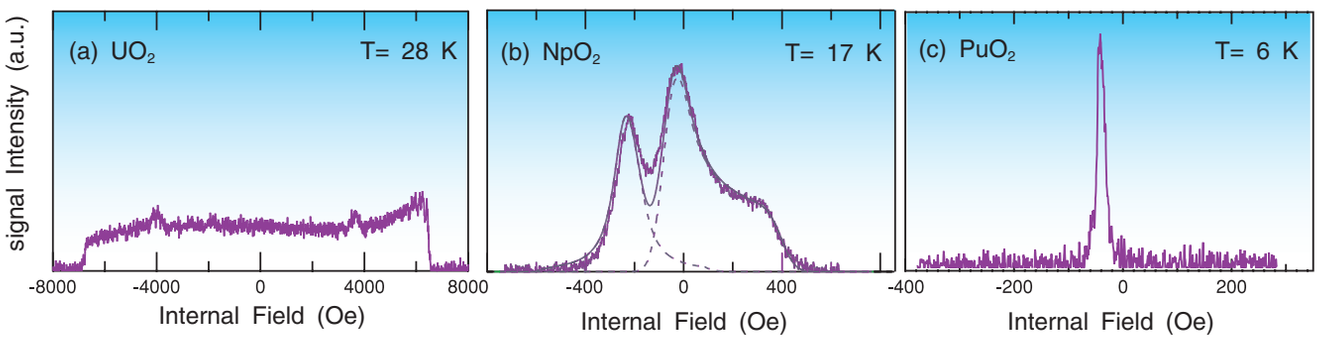

Fig.6-6 ^{17}O-NMR study of UO_2, NpO_2 and PuO_2
The transverse axis shows an internal field at oxygen sites induced by f-electron spins. The vertical axis shows signal intensity, which is proportional to the number of oxygen ions responding to that internal field.

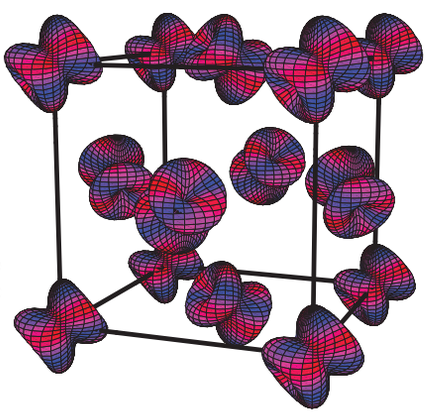

Fig.6-7 Magnetic octupolar ordering in NpO_2
Colors indicate the weights of spin up (red) and down (blue) states. The spin is distributed anisotropically according to the anisotropic charge distribution, and the electronic state of each Np ion has a finite magnetic octupole moment.

To understand macroscopic properties of materials, it is essential to understand their electronic properties from a microscopic viewpoint. Recently, we have carried out a series of nuclear magnetic resonance (NMR) studies for actinide oxides (AnO_2 : An= U, Np, Pu, Am, etc). The microscopic NMR data make a clear distinction between their electronic properties at low temperatures.

Fig.6-6 shows the ^{17}O-NMR spectra observed in UO_2, NpO_2 and PuO_2, respectively. There is a marked difference in the width and shape of the spectra. For UO_2 (a), we have obtained a broad spectrum with a rectangular line shape. This characteristic line shape indicates the existence of a large internal filed at oxygen sites due to the ordering of magnetic dipoles. On the other hand, the spectrum for NpO_2 (b) broadens rather moderately, as compared with that for UO_2, while it exhibits a complex structure. The electronic ground state of NpO_2 had remained a mystery for many years. Our recent NMR study on a single crystal has revealed the occurrence of a novel magnetic octupolar ordering in the ground state (Fig.6-7). Finally, we have observed a narrow spectrum for PuO_2 (c). This confirms that a nonmagnetic electronic ground state is realized even at the low temperature of 6K.

The actinide dioxides discussed here are all insulators with the same cubic crystal structure. Even though, these materials exhibit a variety of electronic states at low temperatures. Why they are so different?

All the actinide ions in AnO_2 have the same tetravalent state. Therefore, the number of localized f-electrons per ion is two for U^{4+}, three for Np^{4+} and four for Pu^{4+}. In addition, due to the strong spin-orbit interaction, the f-electrons carry multipole degrees of freedom: dipole, quadrupole, octupole, etc. The available multipoles on each material are dependent on the number of the f-electrons as well as the symmetry of crystal. A variety of physical phenomena result from a variety of available multipoles in AnO_2.

AnO_2 represents perhaps the most studied series of any actinide compounds. From a chemical and industrial perspectives, this interest has stemmed from their use as nuclear fuels. Nowadays, however, AnO_2 is also an important series of materials to promote a better understanding of the fundamental physics of multipoles. We are now preparing to advance our NMR study to AmO_2 as a joint work with Tohoku University.

Reference
Tokunaga, Y. et al., NMR Studies of Actinide Dioxides, Journal of Alloys and Compounds, vol.444-445, 2007, p.241-245.

6-4 Atomic Scale Observation of Metal Degradation –Development of a Positron Scanning Microscope–

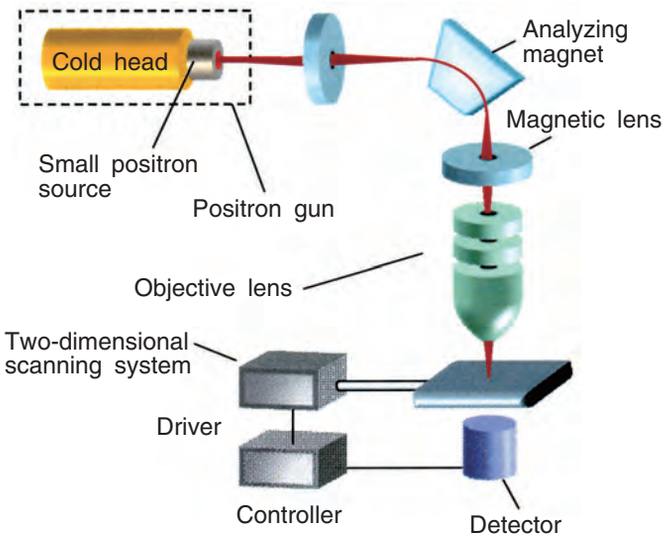

Fig.6-8 Schematic drawing of the positron microbeam apparatus
Positron beam from the source is focused by the objective lens. Synchronizing the measurement of γ-rays and stage scanning, distribution of atom vacancies beneath the surface is obtained.

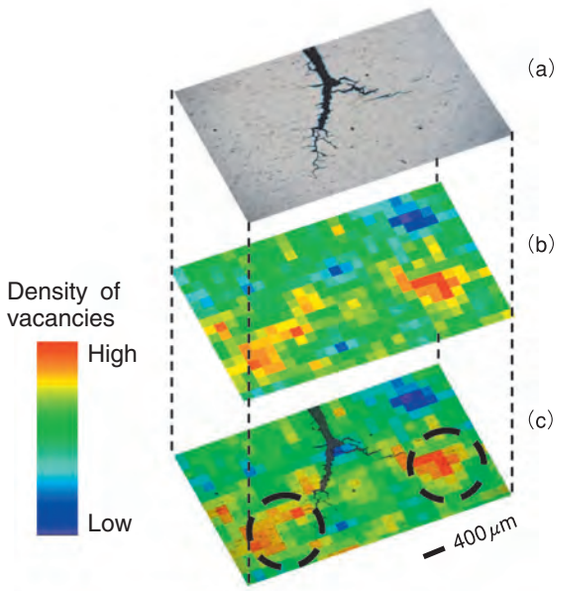

Fig.6-9
(a) Optical image of the stress corrosion cracking of stainless steel.
(b) The spatial distribution of atom vacancies.
(c) Overlapped image of (a) and (b). Atom vacancies appear before the crack grows.

Positron annihilation method is a powerful tool to detect atom vacancies in solids. This technique is based on the unique property of positrons. That is, positrons get trapped by atom vacancies and annihilate with electrons to emit γ-rays. By measuring the annihilation γ-rays, vacancy defects are characterized. To implant positrons into a specimen at a controlled depth, positron beams are used. The diameter of a conventional positron source is, however, rather large and hence it is difficult to focus the beam down to a few microns. This means that measurement of vacancies in a specific area is impossible. In this study, we newly developed a positron source which is suitable for the formation of well-converged beam. Employing an objective lens, we succeeded in focusing a positron microbeam to a diameter of 1.9 microns. Using this microbeam, we can inject positrons in a certain small area only and evaluate vacancy type defects in that specific region. Moreover, combining a stage controller which can aim the beam at an arbitrary place on a sample, we constructed a scanning positron microscope which can obtain distributions of vacancy type defects beneath the surface (Fig.6-8).

Using this positron microscope, degradation of materials can be diagnosed through the observation of defects on the level of atom vacancies. Stainless steel, which is hard to corrode and tough is widely used as a structural material of nuclear power plants. The interior of the nuclear reactor is a severe environment, with high temperature, high pressure, and high radiation dose. In such extreme conditions, stress corrosion cracking (SCC) may occur. In order to secure the safety of nuclear reactors, understanding of detailed mechanism of crack progress is required. Using the positron microscope, we observed the tip of a crack formed in stainless steel by stress corrosion in an environment simulating a nuclear reactor (Fig.6-9). We then found that the density of atom vacancy type defects increased at the region beyond the tip of the crack. This is the world's first observation of atom vacancy type defects being formed before a crack grows.

Thus, the positron microscope can offer original information about atom vacancy type defects which are undetectable by conventional devices, such as the optical microscope and the electron microscope.

Present study is the result of "Innovative Nuclear Research and Development Program" entrusted to "Japan Atomic Energy Agency (JAEA)" by the Ministry of Education, Culture, Sports, Science and Technology of Japan (MEXT).

Reference
Maekawa, M. et al., Development and Application of Positron Microprobe, 17th Iketani Conference "Doyama Symposium on Advanced Materials", Transactions of the Materials Research Society of Japan, Tokyo, Japan, vol.33, issue 2, 2008, p.287-290.

6-5 Biological Effects of Clustered DNA Damage
–Mutation Induction by DNA Lesions in Close Proximity–

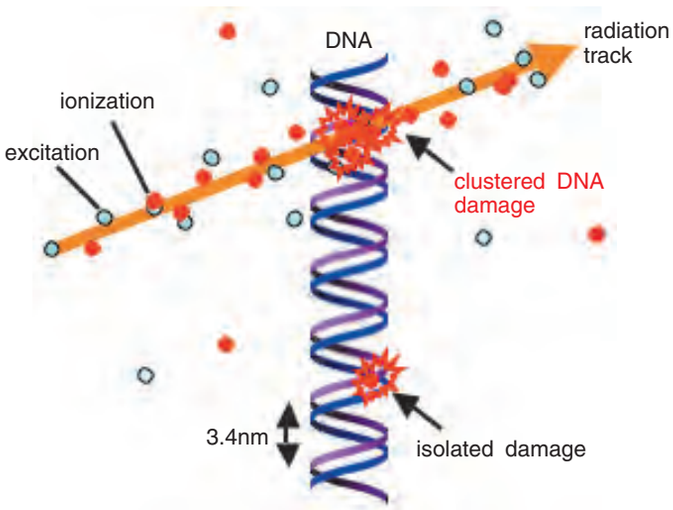

Fig.6-10 DNA damage by ionizing radiation
DNA is damaged due to ionization or excitation caused by radiation. Clustered DNA damage would be produced where the density of ionization/excitation is high, whereas the isolated damage would be generated where it is low.

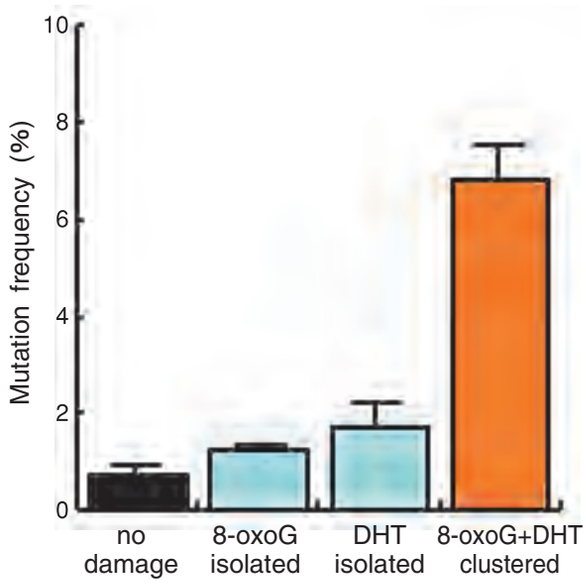

Fig.6-11 Induced mutation frequency by cluster DNA damage
Using a newly developed mutation detection system to observe effects of synthetic DNA lesions, it was found that the mutation frequency was higher at the cluster DNA damage than that at isolated lesions.

Exposing cells to ionizing radiation leads to lethality, mutation induction, and carcinogenesis. These biological effects of radiation are considered to result from various chemical alterations (DNA damage) induced in DNA. Various types of DNA damage are induced by radiation, such as “base damage” where the base of DNA is damaged, “DNA strand break” where DNA helix is broken, and so on. On the other hand, it has been known for a long time that certain chemical agents generate same kind of DNA damage with those induced by radiation. However, it was pointed out that the biological effects of chemical agents are not as significant as those of ionizing radiation even when an equivalent number of lesions are induced. In order to explain this seemingly contradictory outcome, an idea of “clustered DNA damage” was proposed. Clustered DNA damage is a type of damage in which multiple DNA lesions are induced within a region of a few nm (Fig.6-10). It is assumed that dense ionization and excitation in or around the DNA caused by radiation leads to clustered DNA damage, and that, as a result of its low reparability, the biological effect of radiation becomes substantial. Although results indicating the presence of clustered DNA damage have been accumulated, there was no experimental evidence on whether clustered DNA damage is relevant to biological consequences. This was because it is difficult to relate the effect of clustering of damage with biological effects, as ionizing radiation induces various kinds and numbers of damage in DNA at random positions. In order to overcome this difficulty, we have devised and developed an experimental system using model cluster damage composed of several artificially-synthesized base lesions positioned at close proximity. With this method, it has become possible to examine the biological effects of defined types, numbers, and positions of damage. Our experiment reveals that the clustered DNA damage including two base lesions (8-oxo-7,8-dihydroguanine (8-oxoG) and dihydrothymine (DHT)) is more mutagenic than isolated lesions (Fig.6-11). It is experimentally demonstrated, for the first time, that base lesions at close proximity enhance the mutagenic potential. This result confirms the biological significance of clustered DNA damage and will provide important implications for the fields of biological application of radiation, such as risk assessment, radiotherapy of cancer, and mutation breeding.

Reference
Shikazono, N. et al., The Roles of Specific Glycosylases in Determining the Mutagenic Consequences of Clustered DNA Base Damage, Nucleic Acids Research, vol.34, no.13, 2006, p.3722-3730.

Formation of Basis for Nuclear Energy R&D, and Creation of Innovative Nuclear Energy Utilization Technology

The nuclear science and engineering R&D activities at the Japan Atomic Energy Agency have the four roles shown in Fig.7-1. In order to fulfill these roles, research in nuclear data and reactor engineering, fuels and materials engineering, environment and radiation science, and nuclear applied heat technology is being conducted.

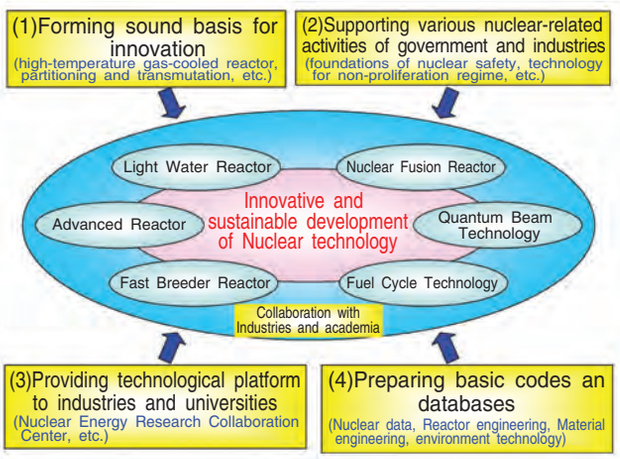

Fig.7-1 Roles of Nuclear Science and Engineering Research

Nuclear data and reactor engineering

Various types of research are being performed to investigate the feasibility of advanced nuclear systems and to establish the basic technology for these systems. Development of nuclear data evaluation codes in Topic 7-1 and measurements of nuclear data are continuing, and the JENDL Actinoid file 2008, which can predict FBR neutronic characteristics with higher precision, was completed. The extended bias factor method was established to evaluate nuclear design accuracy based on multiple criticality experiments and to identify new experiments needed for achievement of the required accuracy. Detailed two-phase analysis codes processed with supercomputing technology as well as model experiments for code validation are being developed to establish new thermal design methods for advanced nuclear systems. Topic 7-2 describes a three-dimensional thermal-hydraulic measurement to build a detailed database for code validation. Basic studies on transmutation of long-lived nuclides are being conducted so as to reduce the burden of radioactive waste management.

Fuels and materials engineering

Basic studies on advanced nuclear fuel and cycle technology and the degradation of nuclear power plant materials are being made. In the advanced nuclear fuel cycles, minor actinides (MA), which are classified as high level radioactive wastes in the current nuclear fuel cycle, are expected to be recycled to reduce the burden of waste disposal. To develop this technology, it is required to understand and control behavior of MA in the system. We are, therefore, performing R&D on separation technology of actinides and fission products, such as high decontamination (high purity) uranium separation by mono-amide extractants, together with fabrication technology and property measurements of MA-bearing fuels (Topic 7-3). Moreover, R&D is being carried out on irradiation effects of materials for nuclear reactors, the corrosion damage mechanism of stress corrosion cracking of reactor structural materials, and the corrosion mechanism of reprocessing plant materials. Topic 7-4 describes the result of recent research on stress corrosion cracking mechanisms.

Environment and radiation science

R&D on environmental behavior of radionuclides (Fig.7-2), utilization and detoxication techniques of wastes, and advanced analytical and monitoring techniques for ultra-trace amounts of substances in the environment are being carried out, together with R&D on fundamental mechanisms of biological radiation effects, dose assessment, and a shielding calculation technique for various radiations. Topic 7-5 describes development of a radionuclide database which enables accurate dose assessment on a gene level. Topic 7-6 describes the only environmental sample analysis method which can determine ^{235}U enrichment in micro-particles, a safeguard technology without mass spectrometry.

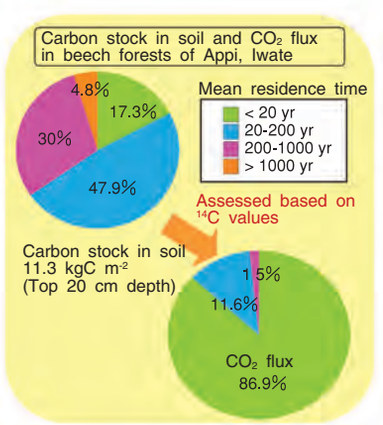

Fig.7-2 Carbon Cycle in Forests
Flux of CO_2 released from soil was assessed by detecting ^{14}C from nuclear weapons testing. These results will contribute to research for elucidating the role of forests as release and absorption sources of CO_2.

Nuclear applied heat technology

To expand nuclear energy application to heat utilizing industries, we are continuing extensive R&D for high-temperature gas-cooled reactor (HTGR) technology and for an HTGR-heated hydrogen production system. Through the first 30 day full power operation of the High Temperature Engineering Test Reactor (HTTR), the HTTR fuel exhibited excellent fission product retention. Moreover, we are performing R&D for an advanced core characteristic evaluation technique based on the HTTR data, for higher fuel burn-up and long-life graphite structure. Topic 7-7 describes the development of ZrC coated fuel particles. For hydrogen production, research for a higher efficiency thermo-chemical IS process (Topic 7-8) is being carried out, together with research into concentration of hydrogen iodine using a polymer electrolyte demarcation membrane, corrosion resistant materials, use of glass lining for hot section piping, and an indirect measuring method of composition of the sulfuric acid and hydrogen iodide solution.

7-1 Compilation of Reliable Nuclear Reaction Data –Development of Comprehensive Code for Nuclear Data Evaluation, CCONE–

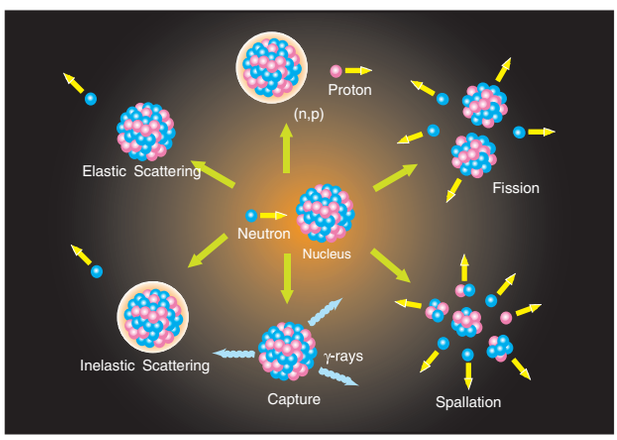

Fig.7-3 Types of nuclear reactions

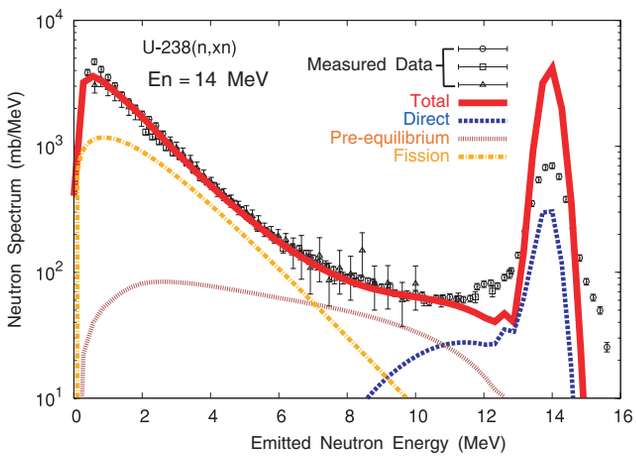

Fig.7-4 Comparison of calculated and measured neutron spectra

Reactor designs, shielding analyses, and safety evaluations of criticality etc. need precise prediction of neutron behavior. The neutron behavior is determined by nuclear reactions (Fig.7-3) of the nuclei which make up the materials used. The probability of a nuclear reaction is determined by nuclear cross section. The data related to nuclear reactions like cross section are called nuclear reaction data. Reliable nuclear reaction data are indispensable for accurate reactor design and other applications. The nuclear reaction data and other data such as half-lives of radioactive nuclides are broadly called nuclear data, and they are the basis for planning nuclear applications. Neutron reaction data are especially important for reactor applications. Reliable reactor designs and safety analyses depend on the reliability of the basic nuclear data used.

Activities to provide reliable nuclear reaction data have continued from the early days of nuclear development. The nuclear reaction data are based on theoretical models and measurements, and they are required to cover neutrons in the energy range from thermal (0.025 eV) to high energy produced by fission (~ 10 MeV) in their effects on all used materials to understand the neutron behavior in a reactor. The number of naturally occurring stable isotopes which make up materials amounts to over 220 and the measurement of these over the full energy region is difficult. The measured data and the theoretical models are appropriately combined to provide all the needed nuclear reaction data. As there is no single theoretical model applicable to this wide energy region, various kinds of nuclear models have to be used to predict the nuclear reactions. This procedure requires much effort to keep consistency among the model calculations.

We have developed a comprehensive code for nuclear data evaluation, CCONE, which maintains this consistency. As the code uses an object-oriented programming language, it is easy to calculate the neutron and γ-ray spectra emitted by complicated reactions producing many nuclei by dynamically treating them as objects. The code has been tested for the nuclear data of thorium, uranium and plutonium isotopes and its accuracy has been confirmed. Fig.7-4 shows the energy spectrum of neutrons emitted after impinging on uranium-238. Although the spectrum consists of many nuclear reaction processes (direct, pre-equilibrium, fission processes; the total spectrum is their composite), the calculation by CCONE agrees well with the measured data. This code is to be used for future nuclear data evaluation to provide reliable nuclear reaction data. The development of CCONE was honored with a Special Award and Award for Distinguished Technology by the Atomic Energy Society of Japan in March, 2008.

Reference

Iwamoto, O., Development of a Comprehensive Code for Nuclear Data Evaluation, CCONE, and Validation Using Neutron-Induced Cross Sections for Uranium Isotopes, Journal of Nuclear Science and Technology, vol.44, no.5, 2007, p.687-697.

7-2 Detailed Measurement of Boiling Flow –Monitoring 3D Change of Vapor / Water Distribution by Neutron Beam–

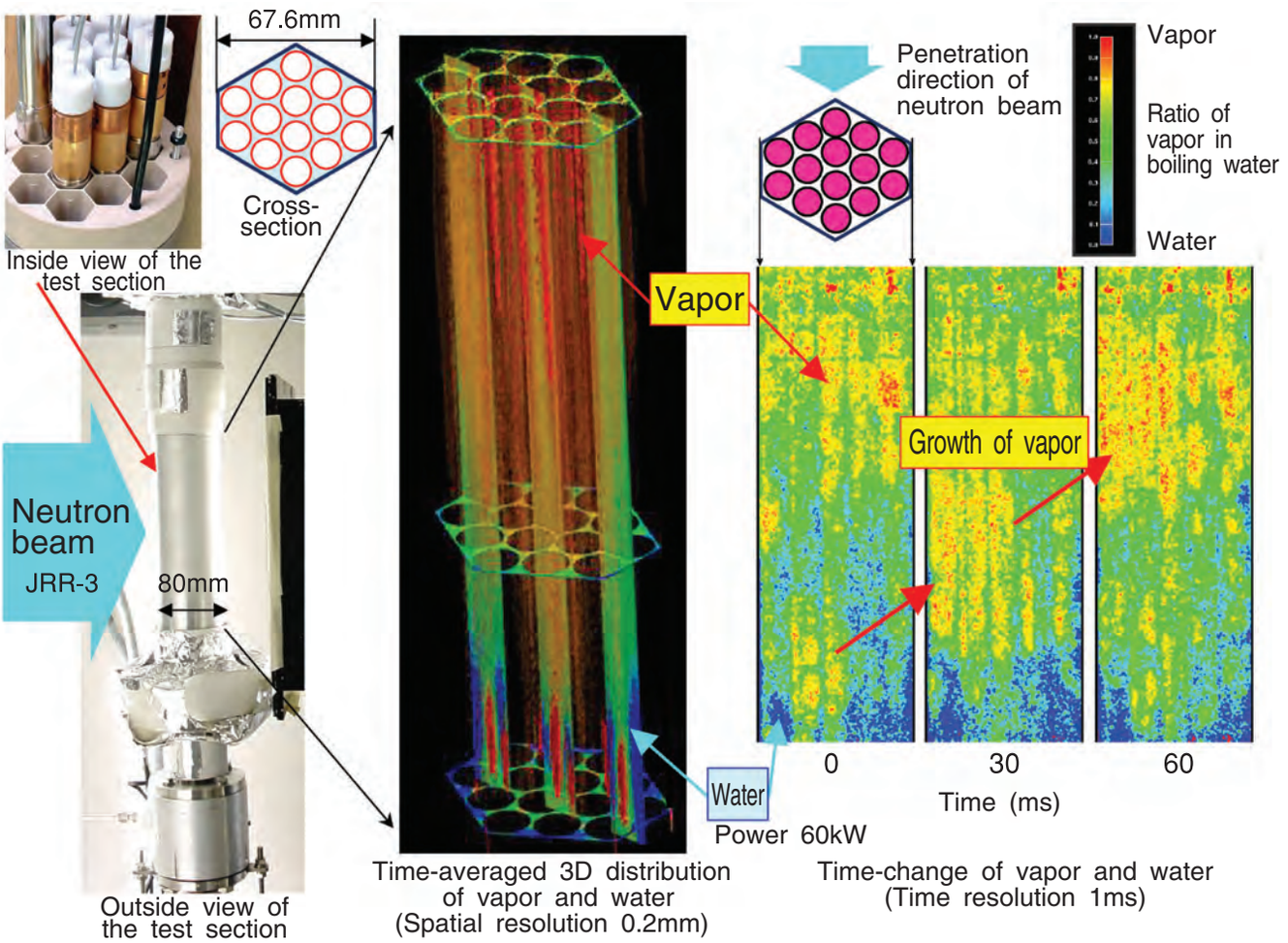

Fig.7-5 Measuring 3D changes of vapor/water distribution in the heated rod-bundle by neutron beam
Changes in spatial distribution of boiling flow in the fuel assembly of a water-cooled breeder reactor affect the cooling performance of the nuclear reactor. In this study, we developed a technique by which we can measure the changes in spatial distribution of vapor and water, using a neutron beam.

One of the important considerations in the design of the water-cooled breeder reactor is the estimation of cooling limit of a fuel assembly. Since the cooling performance depends on the distribution of water and vapor, we need high definition data in order to understand the flow behavior between rods and thereby estimate the cooling limit. However, it is difficult by traditional measurement techniques to measure the flow distribution in a heated bundle. Thus, we developed a new technique which can measure in detail the distribution of boiling flow, using a neutron beam which has a high sensitivity to water. We carried out tight-lattice 14-rod bundle experiments using "JRR-3" as the neutron source (Fig.7-5). The aim of the experiments was to measure the changes in spatial distribution of vapor and water in the heated rod bundle. This is a new technique combining neutron radiography and computed tomography. We can understand the high definition 3D distribution of vapor in boiling flow. We also measured the flow behavior. It was found from the visualization with the time resolution of 1ms that the vapor accumulation point which was observed in 3D data was washed away by cooling water periodically. These results were of use not only for advancing our understanding of various phenomena but also for the verification of advanced thermal hydraulic codes.

This page contains some results obtained by the project "Development of Fuel Assembly for Very High Burn-up Water-cooled Breeding Reactor" entrusted from the Ministry of Education, Culture, Sports, Science and Technology of Japan.

Reference

Kureta, M., Experimental Study of Three-Dimensional Void Fraction Distribution in Heated Tight-Lattice Rod Bundles Using Three-Dimensional Neutron Tomography, Journal of Power and Energy Systems, vol.1, no.3, 2007, p.225-238.

7-3 Demonstration of Excellent Thermal Properties of Minor Actinide Nitride Fuel
–High-Quality Thermal Conductivity Data of MA Nitride Obtained from Small Samples–

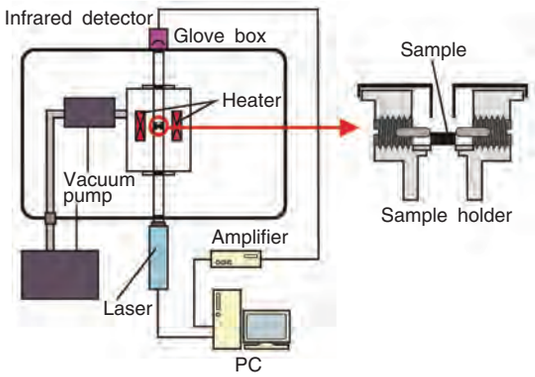

Fig.7-6 Schematic diagram of the thermal diffusivity measurement apparatus
In the glove box, the oxygen and moisture contents were controlled to less than two and three ppm, respectively.

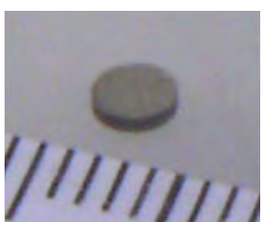

Fig.7-7 Sintered AmN disk sample
The sample color was black. The diameter and thickness were about 3 mm and 0.6 mm, respectively.

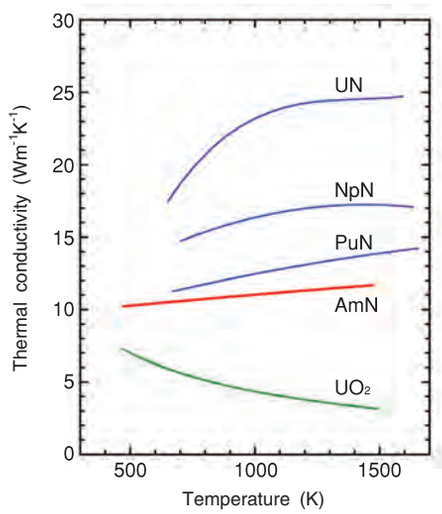

Fig.7-8 Thermal conductivity of AmN corrected to theoretical density, together with those for UN, NpN, PuN and UO_2
Thermal conductivity of AmN was smaller than UN, NpN and PuN, but larger than UO_2.

The spent fuels arising from nuclear power plant contain minor actinides (MAs:Np,Am,Cm) which are long-lived radioactive nuclides, and thus, the management of MA is a key issue for sustainable nuclear energy use. To solve this problem, the technology of partitioning and transmutation of MA, which can significantly reduce the heat generation and radiotoxicity of high level radioactive waste, has been examined. Among various fuel types, nitride fuel is one of the candidates for MA-bearing fuels for transmutation because of its high melting point, good thermal conductivity and mutual solubility.

Facing this task, it is important to obtain thermal property data such as heat capacity and thermal conductivity to design the MA-bearing fuels. However, the thermal properties of MA nitrides are little known due to their high specific radioactivity and the high reactivity with water and oxygen. Thus, we installed a laser flash apparatus in a glove box with a highly-purified argon gas atmosphere (Fig.7-6) for thermal diffusivity measurement and a drop calorimeter for heat capacity measurement. These apparatuses enabled us to obtain high-quality thermal property data of MA nitrides.

The diameter of the MA nitride disk sample prepared by the carbothermic reduction of MA oxide was about 3 mm (Fig.7-7). With this small disk and its fragments, we measured the thermal diffusivity and heat capacity, respectively.

We have measured the thermal properties of various MA nitrides. As an example, the results of thermal conductivity measurement of AmN is here described. It was found that the thermal diffusivity of AmN tended to slightly decrease with increasing temperature and the heat capacity of AmN was nearly the same as other actinide nitrides. The thermal conductivity of AmN, which was determined from the thermal diffusivity, heat capacity and bulk density, tended to slightly increase with temperature in the temperature range from 473 to 1473 K (Fig.7-8). It was also found that the thermal conductivity of AmN was smaller than UN, NpN and PuN, but larger than UO_2. Thus, in this study, the advantage of MA nitride fuel was confirmed in view of its thermal properties. In addition, we have been measuring the thermal expansion of MA nitrides by high temperature X-ray diffraction analysis.

The present study was carried out within the task "Technological development of a nuclear fuel cycle based on nitride fuel and pyrochemical reprocessing" entrusted from the Ministry of Education, Culture, Sports, Science and Technology of Japan.

Reference

Nishi, T. et al., Thermal Diffusivity of Americium Mononitride from 373 to 1473 K, Journal of Nuclear Materials, vol.355, issues 1-3, 2006, p.114-118.

7-4 New Approach for Testing Aging of Reactor Structural Materials –Study of Stress Corrosion Cracking (SCC) Mechanisms Using Electron Backscatter Diffraction (EBSD) in Mesoscale Analysis–

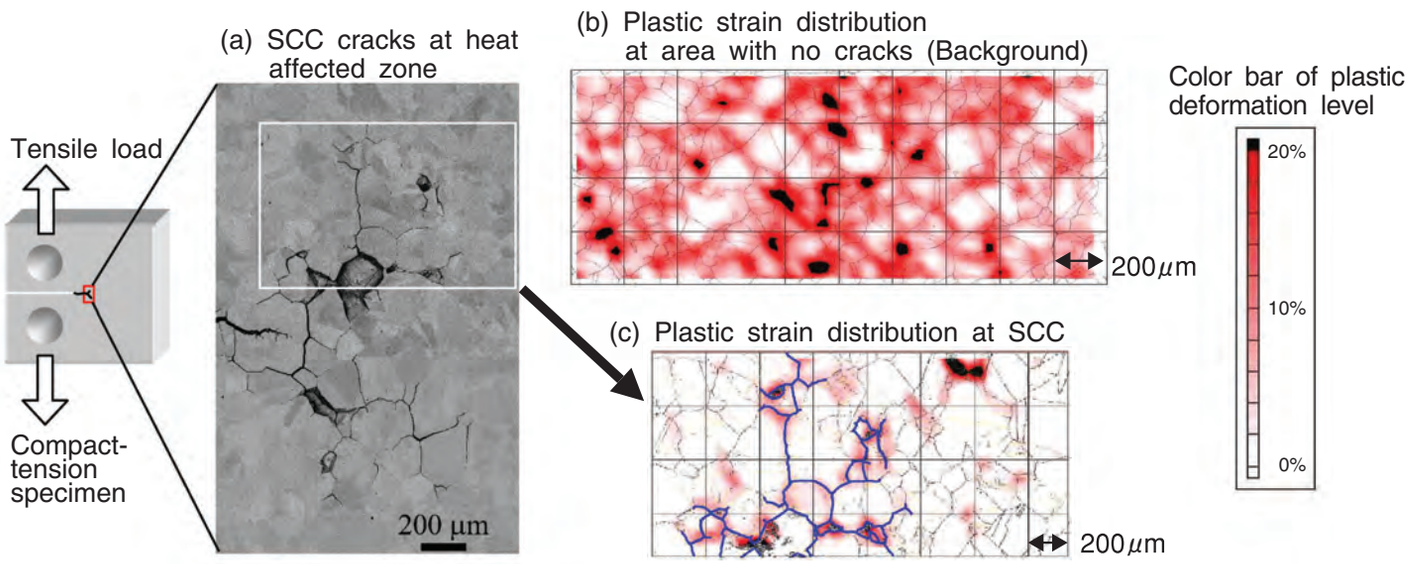

Fig.7-9 (a) Intergranular type SCC in compact-tension specimen, (b) plastic strain distribution at no crack area, and (c) at SCC area
In area (c), background strain was subtracted; blue lines indicate SCC cracks.

Austenitic stainless steels and nickel base alloys are used as structural materials of primary loop recirculation (PLR) pipes and shrouds/core barrels in light water reactors (LWRs). These steels and alloys are susceptible to SCC which is one of the quasi-brittle fracture modes. SCC was observed in the structural materials of LWRs after long term operation. Estimation of SCC initiation and growth behavior is important for preventive maintenance of LWRs.

The mechanisms of SCC are not clear yet. Recently, the following results on macro- and microscopic scale SCC have been obtained, but the mechanism relating the microscopic phenomena to macroscopic phenomena is still unknown. On the macroscopic scale, crack growth rate of SCC increases with increase in the materials' hardness and the stress intensity factor at the crack tip. The effect on hardness induced by irradiation damage was equivalent to that induced by cold work and welding processes. On the microscopic scale, segregation and precipitation are induced by heating during the welding process, and the effects of neutron irradiation are observed at grain boundaries (GBs). The segregation and precipitation are affected by the grain boundary character. SCC occurred also in low-carbon stainless steel which had no Cr depletion at GBs. Change of deformation mode from uniform to localized occurs in the grain matrix of irradiated materials.

We developed a new experimental technique using an EBSD in order to determine the properties of grain boundaries with and without crack propagation and plastic strain distribution near cracks. Fig.7-9 shows plastic strain near SCC cracks measured by this new technique in a compact-tension heat-hardened zone of a real size mock-up PLR pipe joint which is made of low carbon stainless steel. It was revealed in the heat affected zone that the plastic strain near grain boundaries reached about 15% and was much higher than that in the grain matrix (Fig.7-9(b)). When SCC occurred in such hardened stainless steel, additional plastic strain (about 10%) was observed along the SCC cracks (Fig.7-9(c)). The plastic strain gradient became very steep at the crack tip. It is likely that this steep strain gradient is one of the causes of SCC in low carbon stainless steel.

This pioneering work enables us to study the mechanism of SCC on a mesoscale and to model the SCC initiation and propagation behavior. We will improve prediction of aging degradation of reactor structural materials by means of multi-scale modeling.

Reference

Kaji, Y., Miwa, Y. et al., Multi-scale Analysis of Deformation Behavior at SCC Crack Tip (II) (Contract Research), JAEA-Research 2007-008, 2007, 69p. (in Japanese).

7-5 Advancement of Nuclear Medicine Dosimetry –Development of a Radionuclide Database Applicable to Microdosimetry in Subcellular Dimensions–

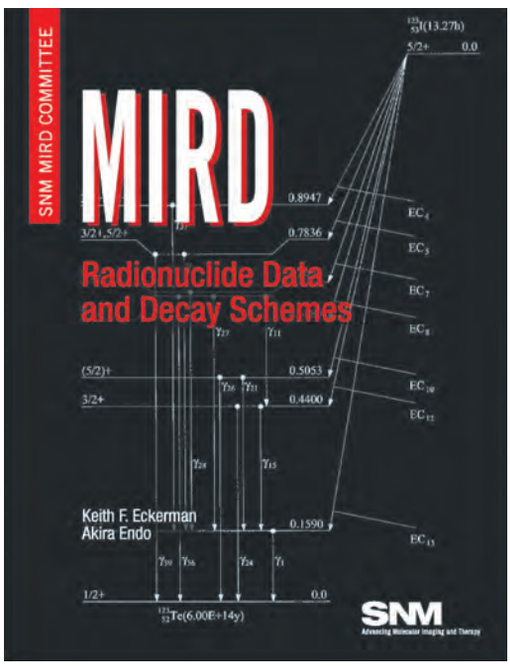

Fig.7-10 Radionuclide data book
"MIRD: Radionuclide Data and Decay Schemes, 2nd Edition" published by the Society of Nuclear Medicine (Reprinted by permission of the Society of Nuclear Medicine)

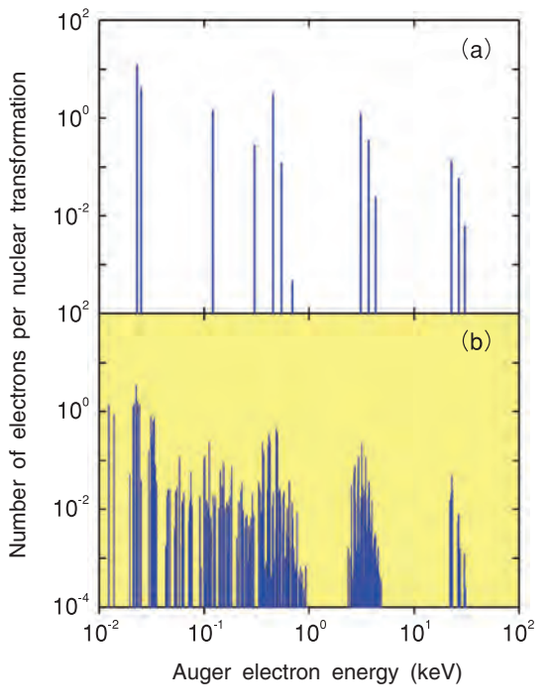

Fig.7-11 Improvement of resolution of Auger electron spectrum of ^{125}I
(a) First Edition (b) Second Edition

Nuclear medicine has been widely used as a safe and painless technique to diagnose and treat disease using small amounts of radiopharmaceuticals labeled with ^{99m}Tc, ^{123}I, ^{67}Ga, and so on. In diagnostic and therapeutic nuclear medicine, radiation dose to patients from radiopharmaceuticals is evaluated to perform appropriate examination while avoiding unsafe radiation exposure. We have updated a radionuclide data book entitled "MIRD: Radionuclide Data and Decay Schemes" (published in 1989) used for nuclear medicine dosimetry and have completed its Second Edition (Fig.7-10) with the cooperation of the Medical Internal Radiation Dose (MIRD) Committee of the Society of Nuclear Medicine (SNM), a leading organization in nuclear medicine research.

In the Second Edition, the data of Auger electrons emitted from radiopharmaceuticals have been enhanced so that microdoses can be calculated. Several radionuclides used as radiopharmaceuticals decay by electron capture and/or internal conversion and emit a number of low-energy Auger electrons as a consequence of these decay processes. These low-energy Auger electrons deposit their energy over ranges with subcellular dimensions (nm ~ μm) in the human body and cause severe biological damage by DNA strand break. To evaluate DNA damage, we have developed a computer code EDISTR04 which calculates detailed spectra of Auger electrons emitted from all radiopharmaceuticals by electron capture and internal conversion (Fig.7-11). Using this code, we have developed a database concerning 333 radionuclides for radiation dosimetry calculation. These radionuclides include the 242 nuclides addressed in the First Edition and an additional 91 nuclides for future use in nuclear medicine.

Radiation dosimetry methods and related data developed by SNM comprise the standard methods used in the field of nuclear medicine. This new radionuclide database also will be used for radiation dosimetry to improve and develop diagnostic and therapeutic methods in nuclear medicine.

Reference

Eckerman, K. F., Endo, A., MIRD: Radionuclide Data and Decay Schemes, 2nd Edition, The Society of Nuclear Medicine, 2008, 671p.

7-6 Selective Detection of Ultra-Fine Particles Containing Highly Enriched Uranium

–Development of an Environmental Sample Analysis Method for IAEA Safeguards–

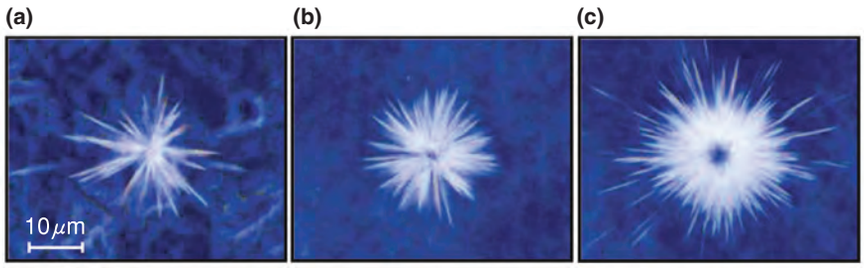

Fig.7-12 Microscopic images of FTs created by uranium particles: (a) natural, (b) 10% enriched, (c) 85% enriched

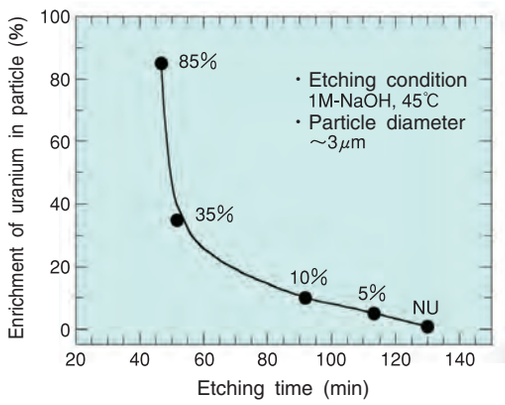

Fig.7-13 Correlation between the time until a fission track appears by etching and the enrichment of uranium in particle

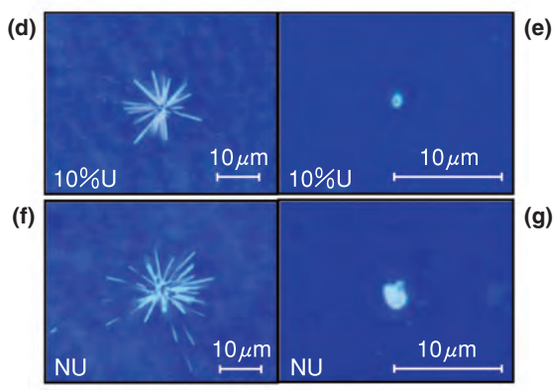

Fig.7-14 Microscopic images of FT morphologies (d, f) and of uranium particles (e, g) corresponding to the FT

Environmental sample analysis technique was adopted by the International Atomic Energy Agency (IAEA) as a new technique for the strengthened safeguards system to detect undeclared nuclear activities. In the technique, particle analysis, which measures isotope ratios of uranium and/or plutonium in individual particles, is an effective tool for safeguards because the particle analysis can surmise the history of the nuclear activities in the past.

The particle analysis by a fission track (FT) technique combined with thermal ionization mass spectrometry (TIMS) can measure the isotope ratios of uranium particles smaller than one micrometer in diameter (equivalent to about 4 pg for uranium). Fig.7-12 shows the microscopic images of FTs of uranium particles with different enrichment irradiated with thermal neutrons. By observing the FTs, a particle containing fissile materials can be detected with high sensitivity from an environmental sample taken from nuclear facilities.

The number of FTs is dependent on the size as well as the ^{235}U enrichment of uranium particle. The etching rate of FTs by the uranium particle increases with the ^{235}U enrichment of uranium particles in the case of irradiation with a fixed neutron fluence. This implies that the detection of uranium particles with a specific enrichment is possible by controlling the etching time. Fig.7-13 shows the correlation between the time until a fission track appears by etching and the enrichment of uranium in particle. The etching time to detect the FT becomes shorter with increase in ^{235}U enrichment. This result indicates, for example, that the uranium particles with an enrichment of more than 25% and 10% will be detected mainly by the etching time is set to 60 min and 100 min, respectively.

In the case of a mixture of highly enriched uranium particles with small size and lowly enriched particles with large size, it is difficult to distinguish between the two solely by controlling the etching time. The size of both the particles is compared in this case. When the numbers of FTs are comparable, it is clear that the smaller particle has the higher enrichment (Fig.7-14). In the real sample containing particles of various sizes, we analyze the particles which made size distribution uniform roughly by a suction filter.

Comparing the FT morphology and the particle size enables the screening of the uranium particles according to their enrichment. Particularly, even when uranium particles with a higher ^{235}U enrichment are scarce in a myriad of uranium particles, it is possible to detect them reliably. The uranium particles detected are transferred onto a TIMS filament, and the isotope ratios are measured precisely. The FT-TIMS method developed has attracted the attention of IAEA as a strong tool for safeguards.

Reference

Lee, C. G. et al., Development in Fission Track-Thermal Ionization Mass Spectrometry for Particle Analysis of Safeguards Environmental Samples, Journal of Radioanalytical and Nuclear Chemistry, vol.272, no.2, 2007, p.299-302.

7-7 Improving Performance of Very High Temperature Reactor Fuel
–Development of ZrC Coated Fuel Particle–

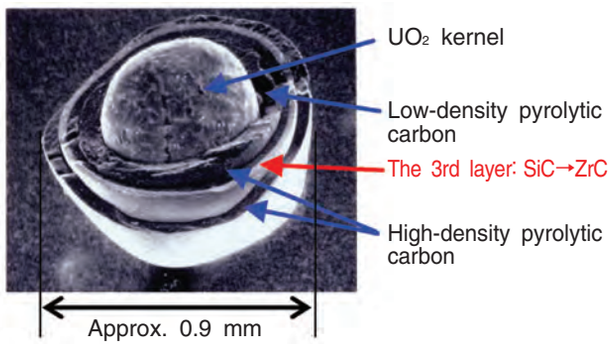

Fig.7-15 Structure of the coated fuel particle
The tiny coated fuel particle is used as HTGR fuel, and consists of a uranium dioxide (UO_2) kernel and four thin ceramic coatings.

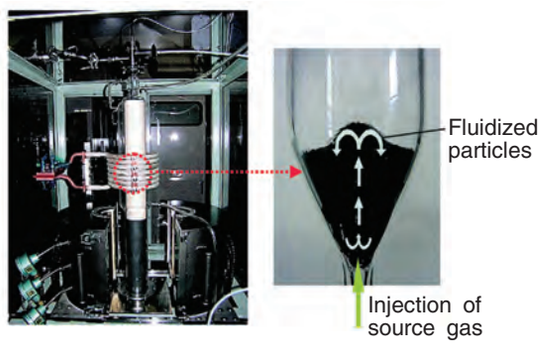

Fig.7-16 ZrC coater
Inside the coater, ZrC is applied by chemical vapor deposition on particles fluidized by the coating material gases, zirconium bromide and methane, at over 1300°C.

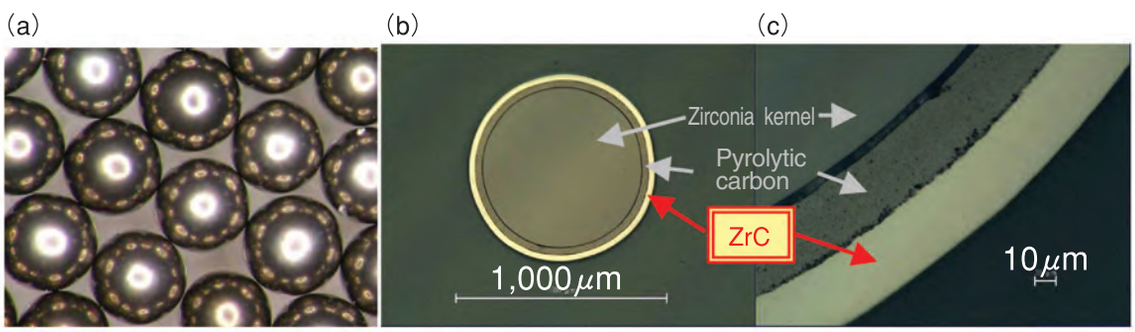

Fig.7-17 Photos of ZrC coated particles, (a) appearance and (b)(c) cross sections
A ZrC coating layer with C/Zr atom ratio of 1.00 was successfully deposited after coating tests using dummy zirconia particles with weight close to UO_2 fuel particles and after developing inspection techniques for ZrC stoichiometry etc. Advanced techniques to coat pyrolytic carbon and ZrC successively are being developed.

The High Temperature Gas-cooled Reactor (HTGR) has inherent safety features with heat output of nearly 1000°C which has prospects to be utilized for hydrogen production and high efficiency power generation. The Very High Temperature Reactor (VHTR) is evaluated highly worldwide, and is a principal candidate for the Generation-IV reactor systems.

The HTGR fuel uses coated fuel particles made with refractory ceramics as shown in Fig.7-15. Silicon carbide (SiC) coated fuel particles were installed in the High Temperature Engineering Test Reactor "HTTR". We are developing zirconium carbide (ZrC) coated fuel particle as an alternative to SiC coated fuel to take advantage of ZrC's excellent properties. ZrC has a higher melting point than the temperature of SiC decomposition and higher chemical stability against metallic fission products such as palladium than SiC. ZrC is expected to be applied as the VHTR fuel, which will be used under high temperature and extended burnup conditions. On the other hand, for ZrC coated fuel particle to have optimum performance, stoichiometric ZrC, whose quantity ratio of Zr to C is 1, should be deposited. We have constructed a ZrC coater (Fig.7-16) applying an original fabrication technique using zirconium bromide and methane gases, and also developed ZrC layer inspection techniques.

At first, non-uniform stripes were observed in the deposited ZrC. It was found by transmission electron microscopy observation that segregated excess free carbon made the non-uniformity. Uniform ZrC was successfully deposited by controlling ZrC depositing temperature to be 1300-1400°C in order to prevent excessive pyrolysis of methane. In parallel, a method to measure ZrC stoichiometry was newly developed by conducting both inductively coupled plasma - atomic emission spectrometry and infrared absorption spectrometry, enabling measurement of C/Zr atom ratio with high accuracy on the order of 0.01. Finally, the fabrication conditions for high quality stoichiometric ZrC as shown in Fig.7-17 were successfully determined. Now we are accumulating data for designing a future commercial ZrC coater (kg-batch scale), and are irradiating ZrC samples in a US research reactor to study the performance of ZrC under irradiation. The present study is the result of "Research and development for advanced high temperature gas cooled reactor fuels and graphite components" entrusted to the Japan Atomic Energy Agency by the Ministry of Education, Culture, Sports, Science and Technology of Japan.

Reference

Ueta, S. et al., Development on Fabrication and Inspection Techniques for the ZrC-coated Fuel Particle as an Advanced High Temperature Gas Cooled Reactor Fuel, Hyomen, vol.46 ,no.4, 2008, p.222-232 (in Japanese).

7-8 For Efficient H_2 Production Using IS Process –Success in Measuring SO_2 Pressurization Effect on the Bunsen Reaction–

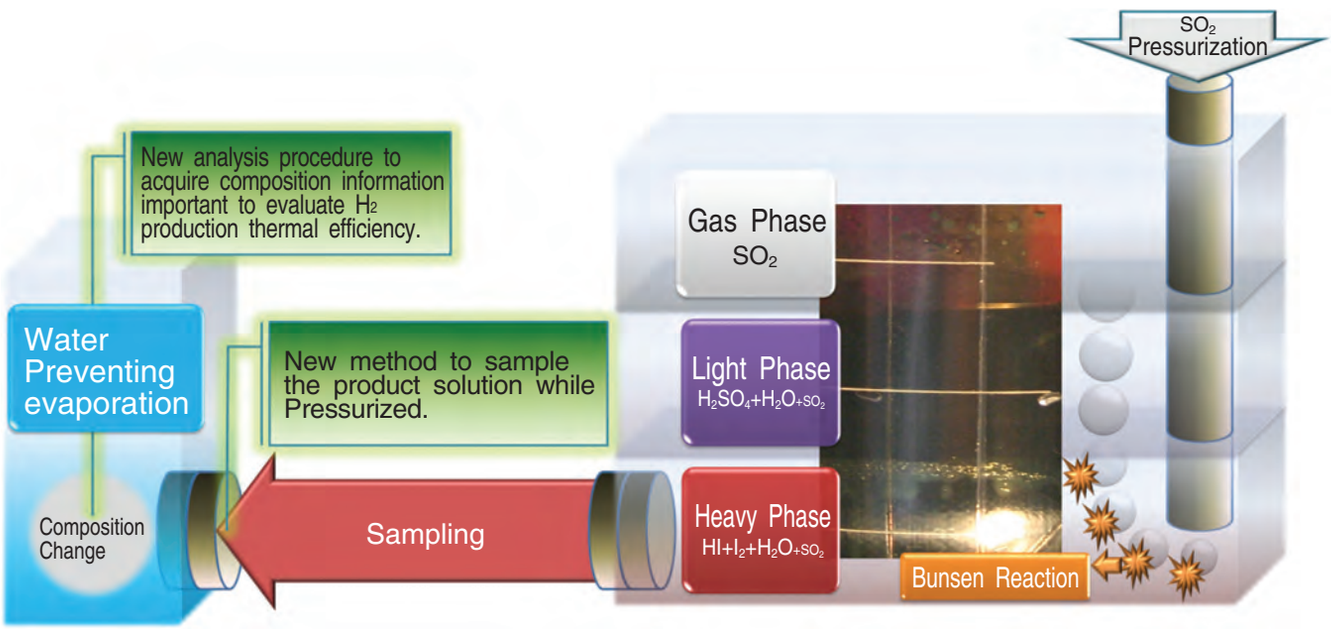

Fig.7-18 Outline of the method to measure SO_2 pressurization effect on the product of the Bunsen reaction
The Bunsen reaction is the most complicated reaction in the IS process and a key reaction for improving the efficiency of the H_2 production process. In this reaction, SO_2 gas contacts with a mixture of water and iodine, generating sulfuric acid and hydrogen iodide. The product solution separates into a light phase and heavy phase spontaneously.

We are investigating a large scale hydrogen (H_2) production method, the IS process, using a High Temperature Gas-cooled Reactor (HTGR) as the heat resource. By using the IS process which is a thermo-chemical reaction cycle using Iodine (I) and Sulfur (S) as recycling agents, H_2 can be obtained from H_2O without emitting CO_2.

The following reaction is the Bunsen reaction which is one of the major reactions in the IS process.

$$SO_2+I_2+2H_2O \rightarrow H_2SO_4+2HI$$

By obtaining a highly concentrated solution of sulfuric acid (H_2SO_4) and hydrogen iodide (HI), we can reduce the separation energy of H_2SO_4 or HI from H_2O and other impurities, which is essential for high thermal efficiency of the IS process. From Le Châtelier's principle, by increasing the iodine (I_2) concentration and the partial sulfur dioxide (SO_2) pressure, the reaction equilibrium shifts to the product side. We have found that increasing the I_2 concentration is effective, but it has been a problem how to measure the SO_2 pressurization effect.

There was no indirect measurement method suited to this pressurized system, because of I_2 dissolving in the product solution (the heavy phase, Fig.7-18). Even in the case of direct composition analysis using sampling method, it was the problem that the components dissolved in the product solution dissipated into the atmosphere during sampling and the composition change due to the reaction between the product solution and the water to prevent evaporation of the product solution.

We developed a new method of direct composition analysis by which we could sample the product solution while maintaining the reaction conditions including the high pressure. To deal with the composition change caused by water, we devised an analysis procedure of the post-reaction composition to acquire the composition information needed to evaluate the H_2 production thermal efficiency.

With this method, we can easily search for favorable reaction conditions for obtaining more concentrated product solution and thus accelerate the development of an efficient H_2 production process.

Reference

Nakajima, H., Imai, Y. et al., Effect of Sulfur Dioxide Partial Pressure on the Reaction of Iodine, Sulfur Dioxide and Water, Kagaku Kogaku Ronbunshu, vol.33, no.3, 2007, p.257-260 (in Japanese).

Promotion of Nuclear Fuel Cycle Development and Technical Co-operation with Industry

We are carrying out research and development of the nuclear fuel cycle, specifically such activities as examination of mixed oxide (MOX) spent fuel for reprocessing and development of technology for vitrification of high-level radioactive waste, to support and promote reprocessing and plutonium recycling in Japan.

Moreover, in our technical co-operation with the nuclear fuel cycle private business of Japan Nuclear Fuel Ltd. (JNFL) at Rokkasho village, Aomori Prefecture, we are providing technology transfer of results of our research and development, dispatching our engineers and training their engineers, etc. as requested by JNFL, to ensure that their business progresses satisfactorily.

1. Reprocess technology development

We began examination of reprocessing of the "FUGEN" reactor MOX type B spent fuel which has higher plutonium content and higher burn-up than the fuel which has been reprocessed since February 2007 at Tokai Reprocessing Plant (TRP). We obtained various data on dissolving processes, undissolved residue, solvent degradation, etc. of MOX spent fuel (Fig.8-1). We will be organizing these data, and reconsidering our plans for examinations after FY 2009 based on evaluation of the earthquake resistance improvement measures carried out at TRP.

To develop technology for vitrification of high-level radioactive waste, we obtained data on stable operation of the melter during the manufacturing of vitrified canisters. We are executing research and development concerning an advanced vitrification melter which is to have long life. We made a small test melter in FY 2007 and will test it in order to set specifications for a commercial melter in the future.

To develop technology for reduction and stabilization of low-level radioactive waste, we examined cement solidification of simulated low-level liquid waste, and clarified the solidification conditions suited to various kinds of waste fluid. Moreover, we carried out tests of nitrate decomposition of low-level radioactive liquid waste containing nitrates, and gathered data concerning the decomposition performance etc. of reductants, confirming their applicability.

In addition, we are making arrangements with related organizations for examination of light-water nuclear reactor high burn-up spent fuel reprocessing to upgrade reprocess technology for high burn-up of fuel.

2. Technical co-operation

(1) Technical co-operation for uranium enrichment business

We are carrying out technical co-operation with JNFL for their R&D of a super-efficient new material centrifuge, sharing our uranium enrichment technology.

We will continue to execute technical co-operation with JNFL necessary for the introduction of this super-efficient new material centrifuge into the Rokkasho Enrichment Plant.

(2) Technical co-operation for reprocessing business

We are carrying out technical co-operation, such as dispatch of our engineers who have operation experience at TRP, and extra funding for operation and management of the vitrification facility etc. to support smooth execution of the tests for activation of the Rokkasho Reprocessing Plant JNFL which have been going on since March 2006.

(3) Technical co-operation to MOX fuel fabrication business

We are adjusting our engineer dispatch plan with JNFL for operation of a MOX fabrication facility, a permit for which JNFL has applied.

(4) Other technical co-operation

We dispatch our engineers upon request of the Nuclear Material Control Center, and provide technical co-operation concerning nuclear material control in Rokkasho district.

Moreover, we are offering our technical information to JNFL, based on the "Agreement of technical co-operation concerning technological proposals for the NFRC construction as part of the GNEP plan of the United States" concluded with JNFL in June, 2007.

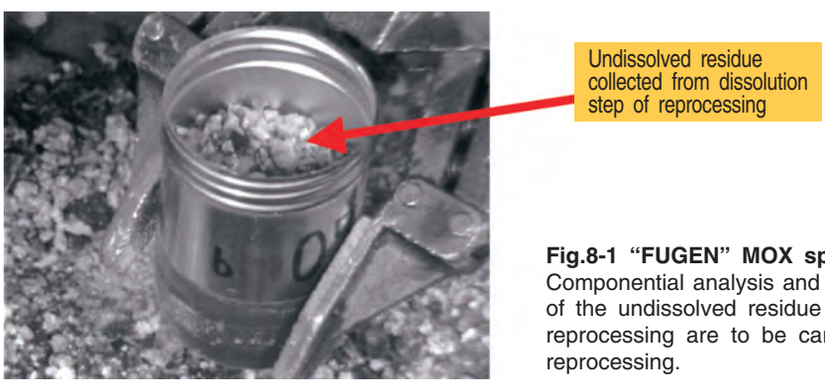

Fig.8-1 "FUGEN" MOX spent fuel reprocessing test
Componential analysis and grain degree distribution measurement of the undissolved residue collected from the dissolution step of reprocessing are to be carried out for data on MOX spent fuel reprocessing.

8-1 Vitrification Melter Improvement –Development of Long-Life High Level Radioactive Liquid Waste (HLW) Vitrification Melter–

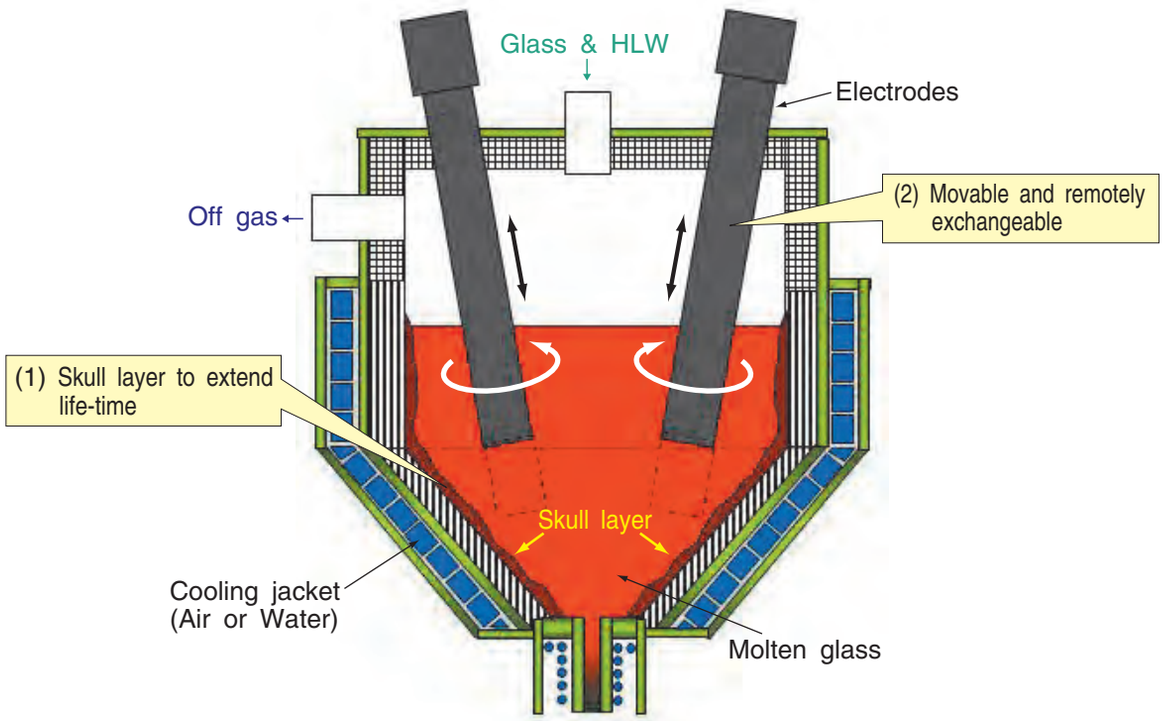

Fig.8-2 Outline of advanced melter and development objectives
To extend vitrification melter life-time from 5 years of the current design base to 20 years, corrosion rate must be decreased drastically. (1) Skull layer formation technology and (2) Movable and remotely exchangeable electrodes are introduced for this purpose.

In a vitrification melter, borosilicate glass cartridges filled with high level radioactive liquid waste (HLW) are fed directly into a melter and melted at high temperature around 1150°C. Thus, the refractory melter wall is gradually corroded by the high temperature glass.

The Tokai Vitrification Facility (TVF) melter is designed to be exchanged every five years because of corrosion of its electrodes and refractory wall.

The objective of this development is to extend vitrification melter life-time from the 5 year standard upon which current design is based to 20 years to reduce the economic burden of high level radioactive waste management, by applying advanced technologies (Fig.8-2).

Development of a new long-life vitrification melter for this purpose is focused on establishing measures for preventing corrosion of the refractory and electrode, and preventing accumulation of noble metal particles at the bottom of the melter.

The new melter wall structure, which forms a skull layer (a solid glass layer or low-temperature high viscosity melted glass layer) on the wall by cooling the wall, is being considered as a measure against refractory wall corrosion. To prevent electrode corrosion, a “commutative electrode structure” is being considered. This structure avoids fixing the current electrodes within the refractory wall by inserting them from the top of the melter in an exchangeable configuration.

Moreover, basic tests of the corrosion rate are being carried out for data on candidate materials for the refractory and the electrode.

In the advanced melter, good drainage of noble metal will be attained by special temperature control of melted glass in the lower part of the melter. Viscosity of glass changes according to glass temperature and concentration of noble metal. Thus we are continuing to gather basic data in our laboratory. In a normal condition, glass temperature of a conical chamber decreases as the radius decreases. To drain noble metal smoothly, higher glass temperature along the wall of conical part than inside is necessary. Glass viscosity along wall then becomes lower than that of glass near the center, resulting in flow of accumulated noble metal rich glass along the wall and out of the melter. We call this temperature distribution mode the “reverse viscosity operation mode”.

We started advanced melter development in 2005 and will promote melter design and related R&D activity until 2008, aiming to determine the most feasible melter concept design.

Reference

Aoshima, A. et al., Vitrification Experience and New Technology Development in Tokai Vitrification Facility, Proceedings of European Nuclear Conference 2007(ENC2007), Brussels, Belgium, 2007, 5p., in CD-ROM.

8-2 Developing to LLW Encapsulation Stage for Disposal –Future Planning of LLW Treatment at the Tokai Reprocessing Center–

Fig.8-3 The low level radioactive waste treatment facility (LWTF)
2 underground stories and 5 above-ground stories of 2,400m² (40m × 60m); Reinforced concrete structure. Solid waste is treated above ground and effluent is treated in the basement.

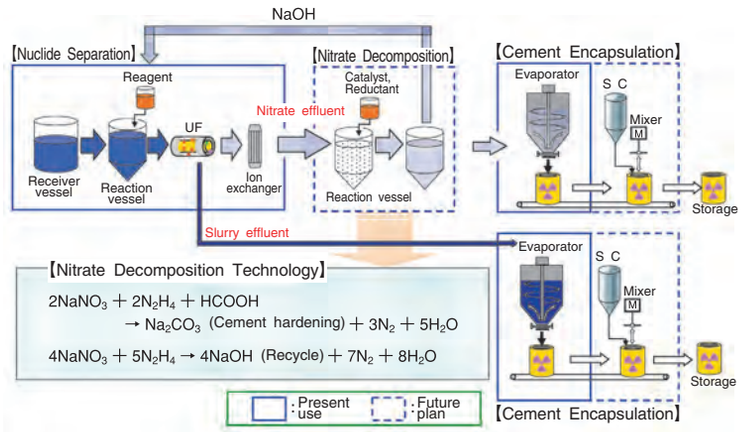

Fig.8-4 Present and future procedure of LLW treatment

The Low Level Radioactive Waste Treatment Facility (LWTF) was completed on September 2006 after about 4.5 years of construction (Fig.8-3). The role of LWTF is to demonstrate treatment technology for solid and effluent LLW. This section describes the effluent treatment, comprising Nuclide Separation, Hardening with Cement, and Nitrate Decomposition, the last two technologies to be installed in the future (Fig.8-4) .

1. Development of Nuclide Separation Technology

In the Nuclide Separation Process, the nuclide and salt in the effluent are separated prior to the cement hardening to reduce the cost of disposal. Following the Nuclide Separation, almost all the waste is converted into a nitrate effluent with a low radioactivity. The amount of slurry effluent with high radioactivity that will require disposal deep underground is reduced to about 10% of the original waste. In consideration of the chemical behavior of each nuclide, the following processes were incorporated in the Nuclide Separation.

(1) Radio-iodine is precipitated as Silver Iodide (AgI) by adding Silver Nitrate ($AgNO_3$) and separated from the effluent with an Ultra-Filtration Membrane (UF) whose pore diameter is several tens of Å.

(2) α nuclides such as Pu and β γ nuclides such as Ruthenium are co-precipitated with Iron Hydroxide (FeO(OH)) by adding Ferric Nitrate ($Fe(NO_3)_3$), and separated from the effluent with a UF membrane.

(3) Highly soluble materials like Cesium are adsorbed after ion exchange performed with $[TiO(CO_3) / TiO(ONa)_2]_n$ and $K_2Co[Fe(CN)_6]$.

2. Development of Cement Hardening Technology

Each of the liquids produced during separation of each nuclide is evaporated to adjust the water volume and mixed with cement by In-drum Mixing. The cement used is “SC,” slag based cement. SC has ability to encapsulate the waste at high loading in aptly short time. SC has proved to be capable of uniform solidification when nitrate effluent is mixed in up to 50 wt% in a beaker. In these cases, adequate compressive strength over 10MPa was achieved. Further 200 ℓ trials have been performed, measuring the strength and density. It was found in these tests that the nitrate effluent was uniformly solidified.

3. Development of Nitrate Decomposition Technology

A high concentration of $NaNO_3$ is contained in the effluent. Density of nitrate in the disposal environment has to be kept appropriately low. To solve this problem, we plan to decompose the sodium nitrate by a Catalyzed Reduction Process using a metal catalyst and reductant (hydrazine (N_2H_4) and formic acid (HCOOH)). Sodium Hydroxide (NaOH) is generated with decomposition of $NaNO_3$. The NaOH is then recycled as a reagent, which is expected to reduce the encapsulated waste. The process has been demonstrated to be capable of decomposing over 90% of the nitrate in a $NaNO_3$ solution whose concentration is about 4.7mol/ ℓ . Further study is necessary to optimize the operating conditions and to improve the catalyst life-time, enabling practical applications.

Reference

Saito, Y. et al., Development of New Treatment Process for Low Level Liquid Waste at Tokai Reprocessing Plant, Proceedings of International Symposium on Radiation Safety Management 2007 (ISRSM2007), Daejeon, Korea, 2007, p.275-280.

Aiming at Establishment of Rational Process for Radwaste Management

A well-planned, rational, and safe execution of decommissioning and radwaste treatment/disposal is one of our major missions, and these are goals of our midterm plan. In addition, promotion of the disposal business of radwaste arising from our research activities and those of universities, institutes and industrial facilities etc. is specified as another of our missions in the amendment to the law governing us on June 2008.

Because great cost is required to accomplish these missions, research and development (R&D) for cost effective measures is called for. We therefore are pursing R&D aiming at establishment of a rational process for decommissioning and treatment/disposal of radwaste as shown in Fig.9-1. In addition, specific technologies have been developed at each site suited to those nuclear facilities.

The major progress in 2007 was as follows.

R&D for Decommissioning

Prototypes of an engineering system to plan decommissioning of nuclear facilities and of an evaluation system to provide safety clearance for wastes were constructed.

At the Fugen reactor site, an evaluation method was verified for residual radioactive inventories of core components (Topic 14-1). The technique of uranium removal using IF_7 was developed at the Ningyo-toge site (Topic 14-11). An all-at-once removal technique was applied to the waste storage tanks at the Tokai site.

R&D for Waste Treatment

A decontamination technique using supercritical carbon dioxide fluid to remove plutonium from radwaste has been studied. Furthermore, we are developing a calcination technique to remove the vinyl bag packing waste and a reduction method using a precious metal catalyst for denitration of TRU waste.

A waste data management system using input such as waste identification was studied, and a model database for Nuclear Science Research Institute was developed.

R&D for Waste Disposal

For simple and rapid analysis of radionuclides in radwaste, a method was developed for rapid determination of ^{89}Sr and ^{90}Sr in liquid waste using a Sr extraction disk and β-ray spectrometer (Topic 9-1).

Evaluation of radioactive characteristics of waste from a nuclear reactor and safety evaluation of the uranium waste disposal process are in progress. For the long term safety evaluation of disposal of uranium waste, exposure doses were evaluated in the cases of topography or sea level change caused by geologic upheavals or climate change. It was found that the exposure dose would be relatively high if there were upheaval or erosion.

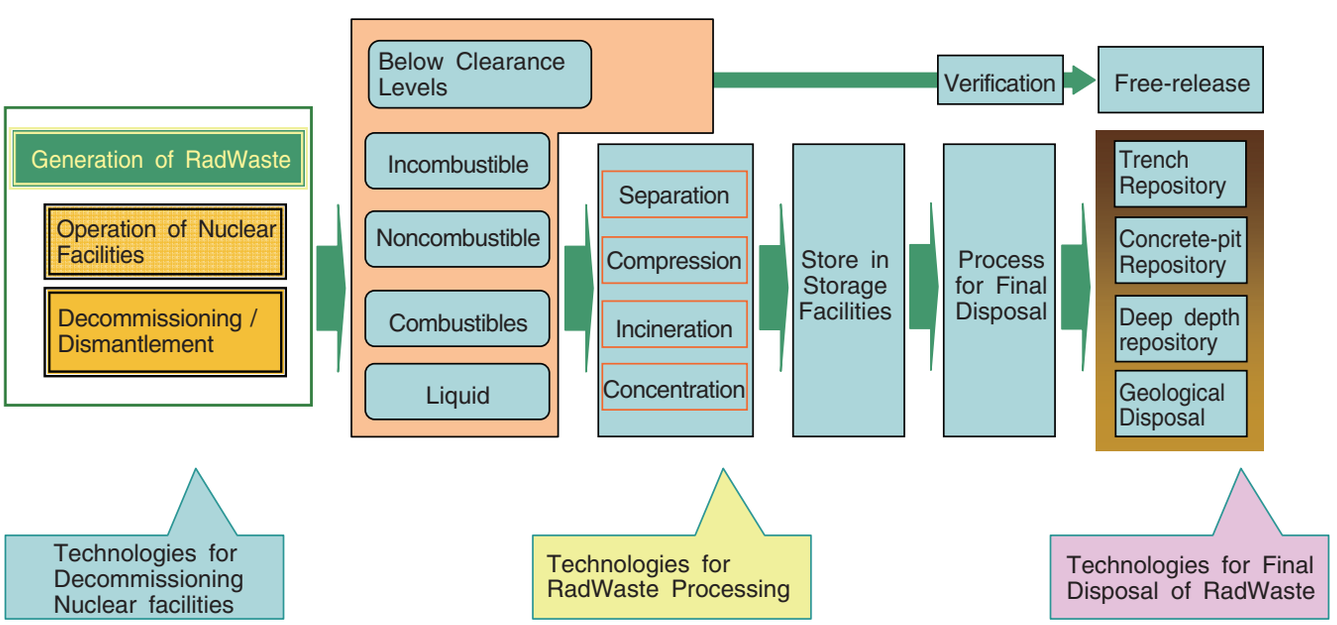

Fig.9-1 R&D Subjects in Decommissioning and Radwaste Processes from Generation to Disposal

9-1 Determination of ^{90}Sr in Radioactive Waste –Development of Rapid and Simple Method for Evaluation of Radioactivity Inventories in Waste–

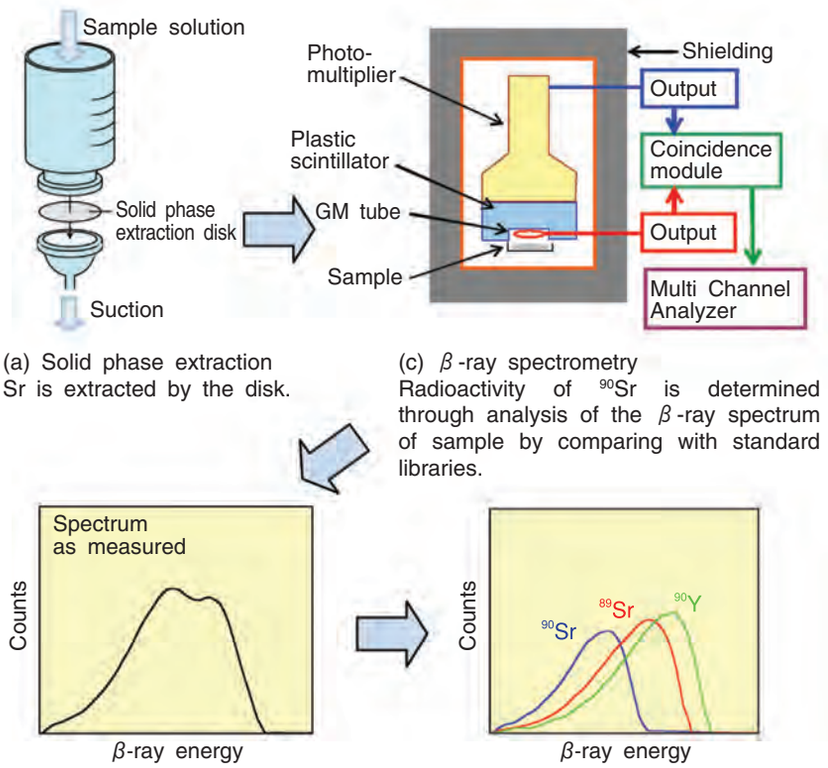

(a) Solid phase extraction
Sr is extracted by the disk.

(c) β-ray spectrometry
Radioactivity of ^{90}Sr is determined through analysis of the β-ray spectrum of sample by comparing with standard libraries.

(b) β-ray measurement
When the scintillation pulses are sorted by a multi-channel analyzer using a coincidence module, a β-ray spectrum without influence of γ-rays is obtained.

Fig.9-2 Rapid and simple ^{90}Sr determination method

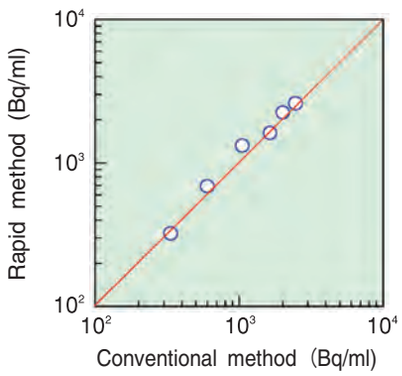

Fig.9-3 Comparison between ^{90}Sr values found by conventional and rapid methods
The amount of ^{90}Sr in actual radioactive liquid waste determined by the two methods were in agreement with each other.

For proper disposal of radioactive waste packages generated from various research facilities, an evaluation of radioactivity inventories in the waste packages is indispensable. In order to establish a practical and reliable verification method, we are currently collecting data concerning radioactivity concentrations in radioactive wastes before processing.

^{90}Sr is one of the most important nuclides from the viewpoint of safety assessment of the radioactive waste disposal process. Since ^{90}Sr emits only β-rays when it decays, nondestructive measurement cannot be done. In a conventional method, Sr is separated by ion-exchange chromatography or a precipitation method. After the Sr fraction reaches radioactive equilibrium with ^{90}Y, the daughter nuclide of ^{90}Sr, the ^{90}Sr is separated and quantified. The tedious and time-consuming chemical separation in this method is a major problem.

Therefore, we developed a new rapid and simple determination method for ^{90}Sr in radioactive wastes. In this method, ^{90}Sr in the waste sample solution is quickly separated by a solid phase extraction disk (Fig.9-2(a)). After the extraction, radioactivity of ^{90}Sr is also quickly determined through analysis of the β-ray spectrum of the sample by comparing with predetermined standard libraries (Fig.9-2(b),(c)). This method was successfully applied to the determination of ^{90}Sr in liquid waste from nuclear research facilities.

The values of ^{90}Sr determined by the rapid method were compared with the results of the conventional method, and they were in agreement with each other (Fig.9-3). As a result of our development work, separation of ^{90}Y after reaching radioactive equilibrium was no longer needed. The time for the ^{90}Sr determination was shortened to be less than one-third to one-fifth of the conventional method.

Reference
Kameo, Y. et al., Rapid Determination of ^{89}Sr and ^{90}Sr in Radioactive Waste Using Sr Extraction Disk and Beta-ray Spectrometer, Journal of Radioanalytical and Nuclear Chemistry, vol. 274, no.1, 2007, p.71-78.

10 Collaboration on Basic Nuclear Engineering

Promotion of R&D to Meet the Demands of Industry and Academia

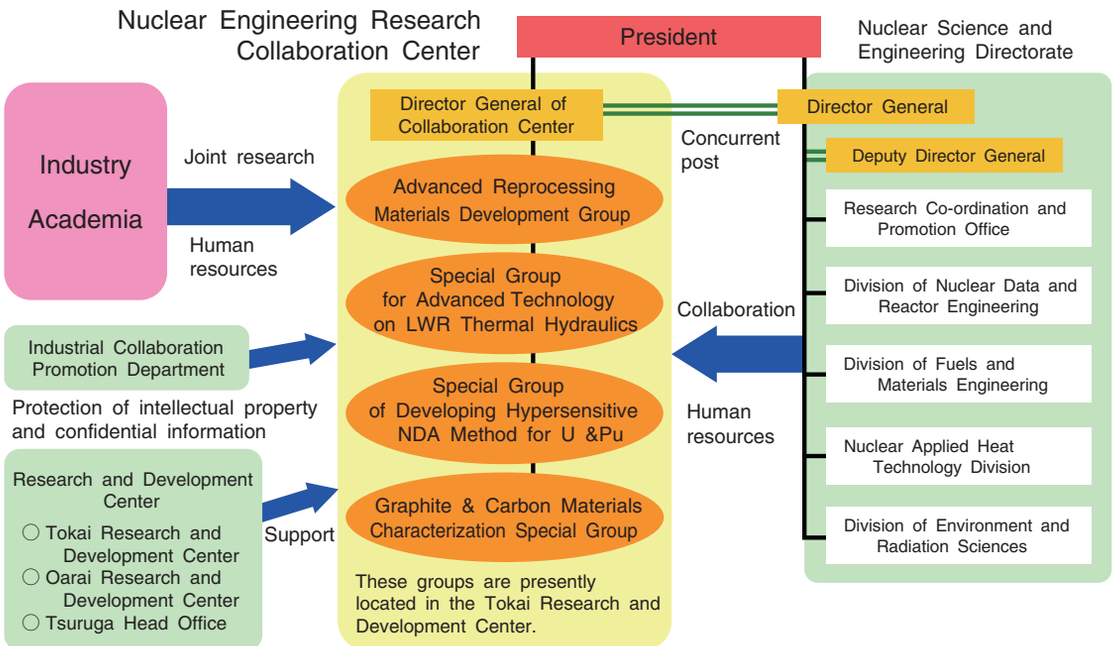

Fig.10-1 Nuclear Engineering Research Collaboration Center and Related Organizations

JAEA has been promoting joint research and development with industry and academia and has made its nuclear facilities and experimental apparatuses available to meet their needs. This collaboration is done under the auspices of the Nuclear Engineering Research Collaboration Center (NERCC), established in 2005 and supported mainly by the Nuclear Science and Engineering Directorate, as shown in Fig.10-1. NERCC provides a platform for joint research and development of innovative nuclear technology. The platform manages specific technology groups established in collaboration agreements with university and industry partners interested in collaboration, cooperation, technology transfer, etc. Four technology groups, organized by researchers and experts of universities, industries, and JAEA, are presently active.

The Advanced Reprocessing Materials Development Group has succeeded through cooperation with Kobe Steel, Ltd. in making original extra high purity (EHP) alloys by cold crucible induction melting (CCIM) for Ca/CaF reduction and then electron beam cold hearth refining (EB-CHR). The EHP alloys have demonstrated excellent resistance against grain boundary attack in a severe reprocessing environment and good weldability, as reported in Topic 10-1. The trial melting of several hundred kg has determined the necessary conditions to limit harmful impurities entering the EHP alloys to less than 100 ppm, even if nuclear facility grade scrap is used as raw materials.

The Special Group for Advanced Technologies for LWR Thermal-hydraulics is conducting mock-up tests in collaboration with an industry partner to attain improved information management. The Special Group for Developing Hypersensitive NDA Method for U&Pu has invented a fast neutron direct interrogation method, by which distributions of U and Pu in the interior of the waste matrix can be measured with more than 100 times higher sensitivity than by conventional methods. The group is cooperating with IHI Ltd. in R&D to make this method practicable by improving detection accuracy and sensitivity. Additional ongoing R&D collaboration with IHI Ltd. and Tokyo University aims at applying the method to detect nuclear material hidden in personal luggage.

The Graphite & Carbon Materials Characterization Special Group conducts material development for HTGRs and is developing an irradiation material database and evaluation method in cooperation with Toyo Tanso Co. A goal is to extend the lifetime of in-core materials for the VHTR. 3D- X-ray CT of fine-grained graphite of 20 μm grain size with high magnification (Fig.10-2) was achieved. This image technique can be used for irradiated graphite evaluation.

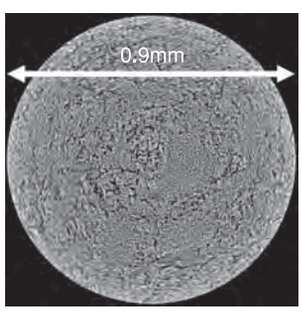

Black:pore Gray:crystal

Fig.10-2 X-ray CT image for IG-110 graphite

10-1 Development of Extra High Purity Stainless Steel (EHP Alloy) with High Corrosion Resistance in Severe Environment

–Excellent Grain Boundary Corrosion Resistance of EHP Alloy under Boiling Nitric Acid–

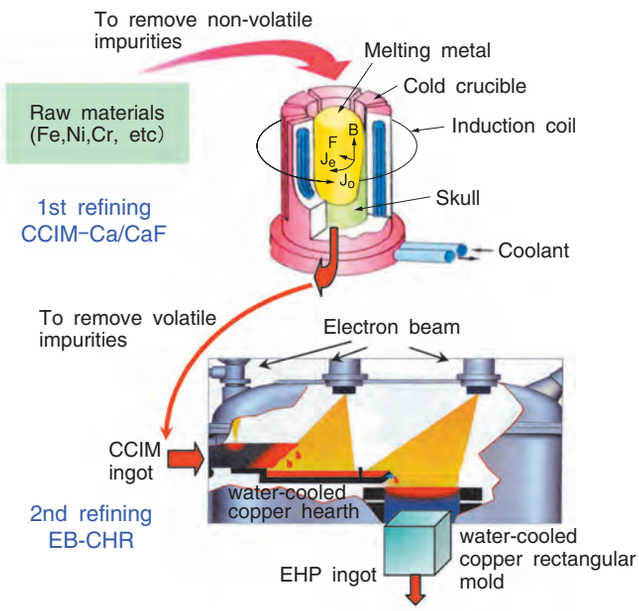

Fig.10-3 Multiple refining technology for EHP alloy
EHP alloy with harmful impurities limited to less than 100ppm was produced by a cold crucible induction melting (CCIM) for Ca/CaF reduction and an electron beam cold hearth refining (EB-CHR).

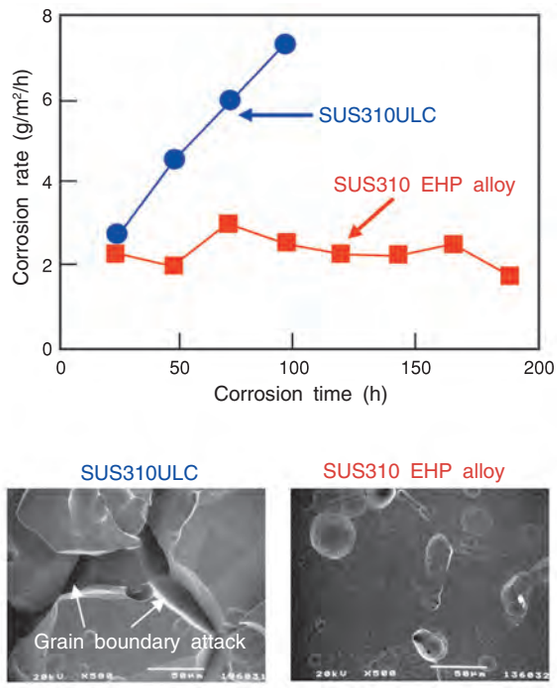

Fig.10-4 Results of the corrosion test in the boiling nitric acid
SUS310 EHP alloy showed excellent resistance against grain boundary corrosion compared with conventional SUS310ULC.

The development of high performance next generation nuclear energy systems is expected to place priority on global warming and effective utilization of resources. In these systems, fuels of high burnup light water reactors and of fast breeder reactors must be stored. Therefore, it is necessary to develop the stainless steels with higher corrosion resistance more than the current materials for reprocessing plants.

The life of stainless steels for reprocessing plants mainly depends on resistance to grain boundary corrosion. Grain boundary corrosion is local corrosion which starts at inclusions or at grain boundaries. We carried out the fundamental research of an Extra High Purity alloy (EHP alloy) in which impurities are reduced to the lowest practical level. For practical use of EHP alloy, the development of commercial refining technology with high quality and low cost is necessary. Thus, we are developing new EHP alloy multiple refining technology and evaluation jointly with Kobe Steel, Ltd. The technology comprises cold crucible induction melting (CCIM) for Ca/CaF reduction and electron beam cold hearth refining (EB-CHR) as shown in Fig.10-3. Non-volatile impurities are removed by CCIM and then volatile impurities are removed by EB-CHR. Moreover, an intermediate product with rectangular cross section can be directly produced using a water-cooled copper rectangular mold. In trial melting of several hundred kg, EHP alloy whose total harmful impurities were less than 100 ppm was produced even if nuclear facility grade scrap was used as raw materials.

Fig.10-4 shows results of a corrosion test in boiling nitric acid which simulated the environment of a reprocessing plant. The specimens tested were the conventional SUS310ULC (Ultra Low Carbon) and the present SUS310 EHP alloy. Grain boundary corrosion was observed on the surface of SUS310ULC, causing the corrosion rate to be accelerated greatly. On the other hand, the corrosion rate of SUS310 EHP alloy was approximately constant and showed excellent resistance against grain boundary corrosion. It was confirmed that EHP alloy is unaffected by boiling nitric acid. As the weld cracking resistance of EHP alloy was improved by removal of harmful impurities, EHP alloy can be used as a welding material.

The study was carried out as part of the “Research and Development of Nitric Acid Resistant Material Technology Applicable to the Next Generation of Reprocessing Equipment” entrusted by the Ministry of Education, Culture Sports, Science and Technology of Japan.

Reference

Ioka, I. et al., Susceptibility of Intergranular Corrosion for Extra High Purity Austenitic Stainless Steel in Nitric Acid, Proceedings of 16th International Conference on Nuclear Engineering (ICONE16), Orlando, Florida, USA, 2008, ICONE16-48776, 5p., in CD-ROM.

11 Photo-Medical Research Cooperation

Aiming at Creating a Photo-Medical Industrial Valley Lasers in Medicine

This project aims to develop a much more compact cancer diagnosis and treatment instrument using ion beams driven and controlled by high intensity laser technology.

JAEA has successfully proposed this novel project to the Ministry of Education, Culture, Sports, Science and Technology (MEXT), seeking the creation of a "photo-medical industrial valley" base in FY 2007.

In October 2007 we established the Photo-Medical Research Center (PMRC) as a chief directorate and central control "hub" for developing a network for cooperation with industry and universities, and to promote this new endeavour.

With the possibility of compact laser-driven treatment facilities being built within the next 10-15 years, we envision that the world will have much greater access to hadron cancer therapy, for which the global demand is continuing to grow.

Promotion of PMRC is fundamentally based on the development of industrial laser technologies for ion acceleration and companion development of related applications such as endoscopy.

The cooperative organization with ten partners and their roles are shown in Fig.11-1. The innovations for which the creation of "Photo-medical industrial valley" is intended are shown in Fig.11-2.

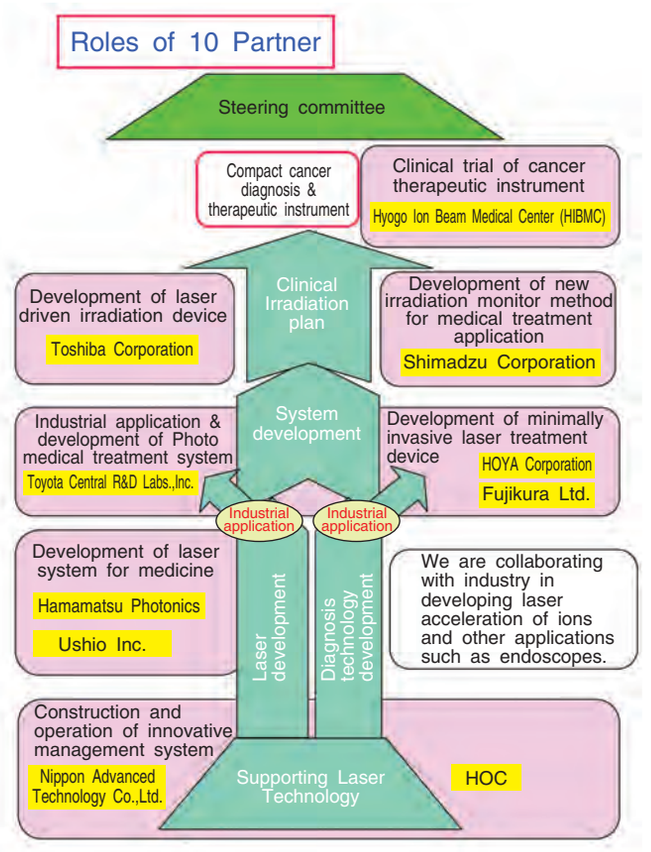

Fig.11-1 PMRC Partners and Their Roles

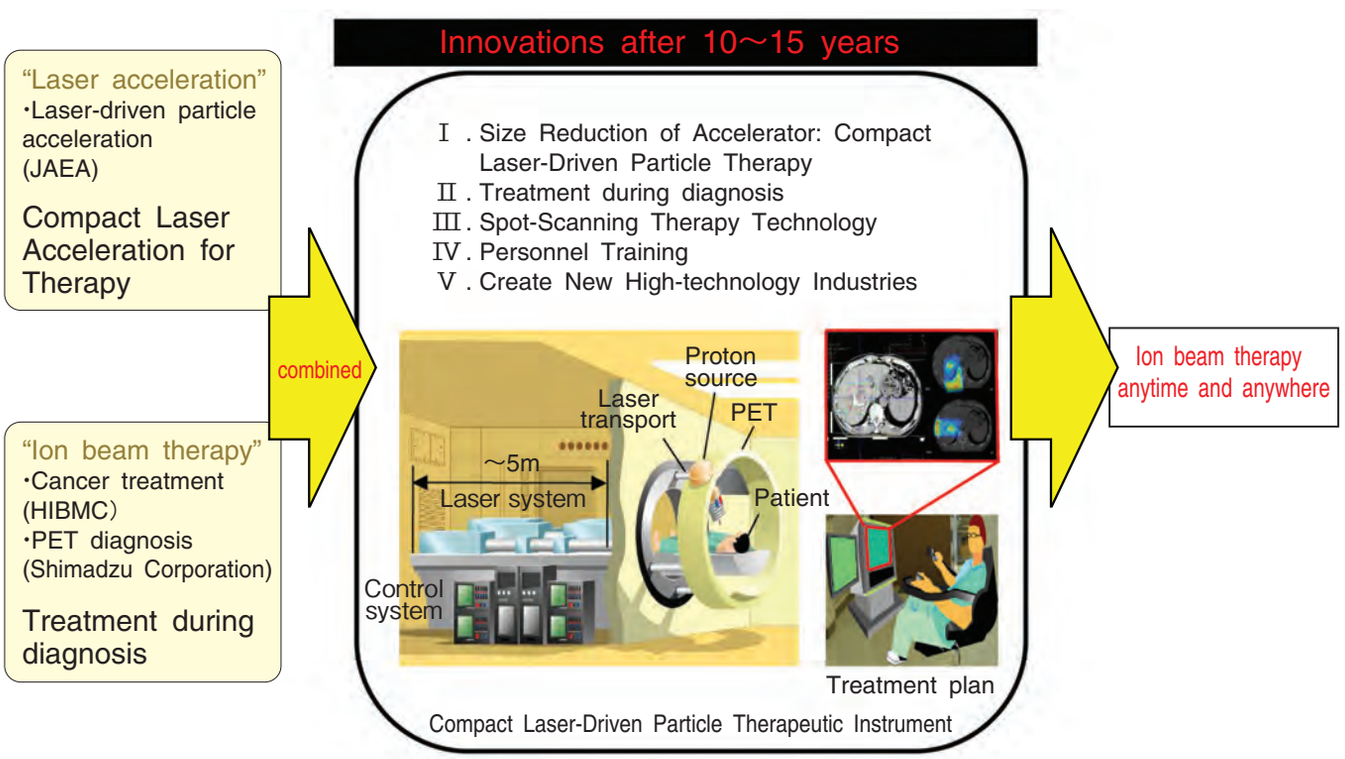

Fig.11-2 Concept of the Desired "Photo-Medical Industrial Valley"

11-1 Ion Acceleration from Near-Critical Density Plasma Produced by Lasers
–Proposal of a Novel Ion Acceleration Method for Cancer Therapy–

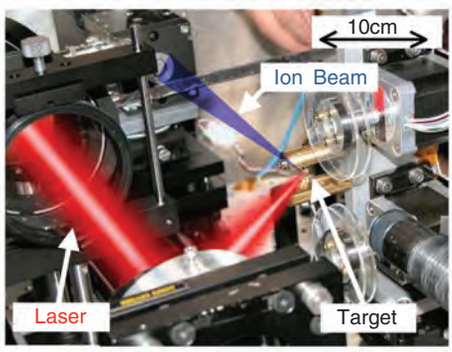

Fig.11-3 Laser ion accelerator
A laser pulse is focused onto a thin-foil target with intensity exceeding 10^{18} W/cm^2, which generates high-density plasma at the focal spot. This plasma produces a MeV-scale proton beam.

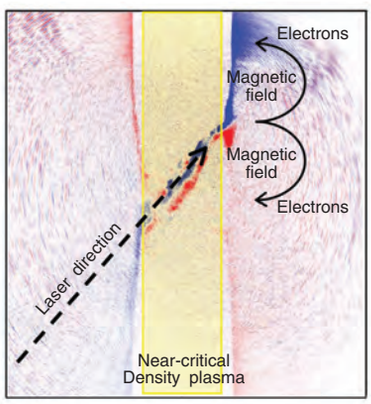

Fig.11-4 A novel mechanism of ion acceleration
A laser pulse can invade into a near-critical density plasma target, and the laser energy is efficiently converted into electron kinetic energy.

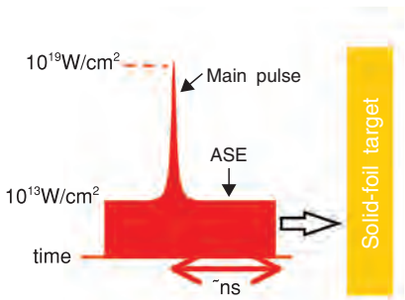

Fig.11-5 Near-critical density plasma production method
A solid foil target is converted into near-critical density plasma by the amplified spontaneous emission (ASE) light preceding the main laser pulse.

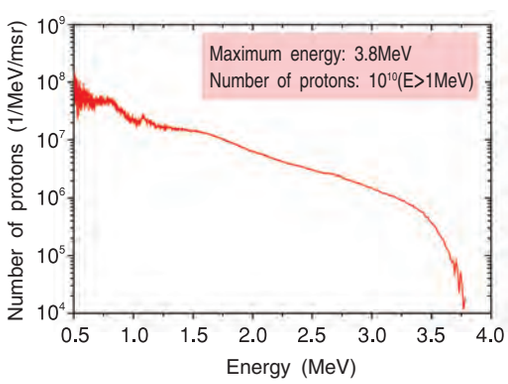

Fig.11-6 A proton energy spectrum
We have successfully obtained protons of 3.8 MeV maximum energy.

When a laser pulse is focused onto a thin-foil target with intensity exceeding 10^{18} W/cm^2, high-intensity plasma is induced at the laser focal spot, generating several kinds of radiation including high-energy ions. By using this phenomenon of laser-ion acceleration, conventional ion accelerators, that have lengths of tens of meters, can be replaced by a compact apparatus as shown in Fig.11-3. The Photo-Medical Research Centre (PMRC) aims to develop a compact and novel laser-driven ion accelerator for cancer therapy.

Recently, we proposed and demonstrated experimentally a new method of laser-ion acceleration by which laser pulse energy can be converted more efficiently into ion kinetic energy. The method is based on creation of a near-critical density plasma target. In the case of a usual solid target, the target surface can reflect a large part of the laser pulse energy. By contrast, a laser pulse can penetrate into a near-critical density plasma target (Fig.11-4), where laser energy is efficiently converted into electron kinetic energy. The vortex of moving electrons thus created generates a magnetic field on the target rear surface and sustains an electrostatic ion-accelerating field. A solid foil target is converted into near-critical density plasma by the part of the light pulse that precedes the main high intensity laser, amplified spontaneous emission (ASE) (Fig.11-5).

In experiments we have generated protons with maximum energy of 3.8 MeV. Fig.11-6 shows the proton energy spectrum, which also shows that approximately 10^{10} protons are generated by a single laser shot. Higher-energy protons will be achieved by optimizing the target density through control of the ASE intensity and duration.

This work is supported by Special Coordination Funds for Promoting Science (SCF) provided by the Ministry of Education, Culture, Sports, Science and Technology of Japan.

Reference

Yogo, A. et al., Laser Ion Acceleration via Control of the Near-Critical Density Target, Physical Review E, vol.77, no.1-2, 2008, p.016401-1-016401-6.

11-2 One Optical Fiber Can Both Observe and Treat –Development of Extra-Fine Endoscope with Laser Radiation Function–

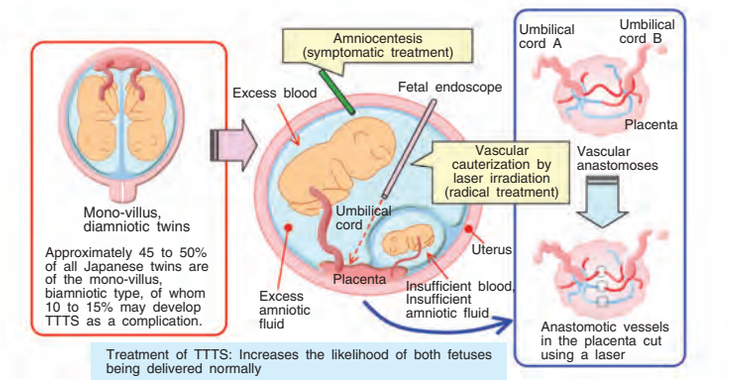

Fig.11-7 Example of congenital disease: Twin-to-Twin Transfusion Syndrome (TTTS)
In TTTS, the blood vessels to twins become connected inside the placenta, resulting in one twin receiving less blood than the other. If left untreated, there is a 70% or greater probability that one or both fetuses will die. A radical treatment is vascular cauterization method by laser irradiation (FLP).

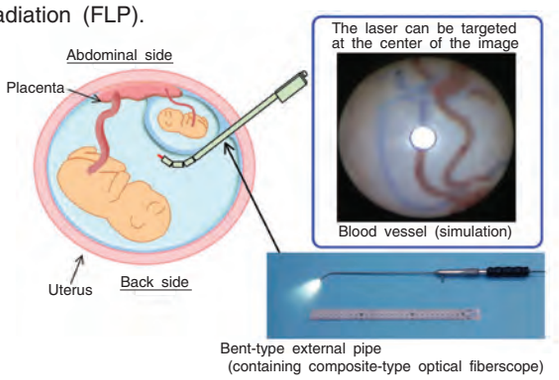

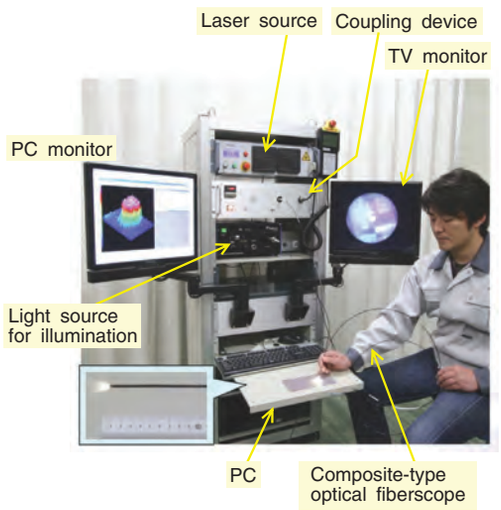

Fig.11-8 Extra-fine endoscope having a laser radiation function
We produced a trial system which performs laser radiation and observation at the same time by one optical fiberscope with an outside diameter of 2 mm.

Fig.11-9 Technology that enables placenta treatment at all positions
This device enables treatment even if the placenta is in front.

Twin to twin transfusion syndrome (popular name TTTS) is one of the congenital diseases that twins develop in utero. This disease that only occurs in cases consisting of two amnions and one placenta (mono-villus diamniotic twins) requires highly advanced medical treatment. In the case of normal mono-villus diamniotic-twins, each blood vessel is connected to the placenta and the balance of blood circulating through each is good. When blood flow between twins becomes unbalanced, and blood continues flowing to only one fetus, TTTS develops. A laser treatment method while observing with an endoscope (popular name FLP) recently is attracting attention as a radical therapy of TTTS, (Fig.11-7).

However, experience in FLP treatment is superficial nationwide, and the reality is that there are only a few hospitals nationwide that can perform FLP treatment. In addition, there are the following problems because this treatment is intended for a fetus floating in the uterus (in amniotic fluid) which is a small space; (1) the definite vascular configuration (a map) of connection to the placenta is not clear, (2) the distance between the tip of the optical fiber and a blood vessel is not clear, (3) quantitative determination whether the bloodstream is stopped or not is not possible, (4) the endoscope image is narrow, and (5) it is hard if the placenta is in front of the fetuses (placenta previa). Advanced technical progress and a highly skilled doctor are necessary to do such an operation with the conventional endoscope.

Therefore to make a contribution to FLP treatment, by utilizing a composite-type optical fiber by which observation and laser irradiation are possible in one optical fiber at the same time, we produced a device which promises to solve the problems with the conventional endoscope (Fig.11-8). We note that this device was created as a spin-off from development of a robot for inspecting and maintaining nuclear fusion reactors.

In this system, the middle of an image can be laser-irradiated, and there are functions to measure the distance to an object and blood quantity/flow speed. This allows laser radiation to be applied precisely, safely and comparatively easily. This instrument has potential for prenatal surgical treatment of the congenital disease mentioned above. In addition, this makes laser radiation easy even in the case of placenta previa (Fig.11-9). Furthermore, because the diameter of the hole (possibly through the abdomen) can be reduced by reducing the endoscopic external diameter to as little as 2 mm, we can expect that the burden to a mother's body will be reduced greatly (Minimally Invasive Treatment). The efficacy of this system has already been confirmed in animal experiments. We are proceeding with development for clinical applications now.

Reference

Oka, K., Development of Extra-fine Endoscope Having a Laser Radiation Function -We Apply It to Prenatal Treatment-, Energy Review, vol.27, no.7, 2007, p.7-10 (in Japanese).

Atomic Energy Research by Computational Science
–Establishment of Advanced Technology for Atomic Energy R&D–

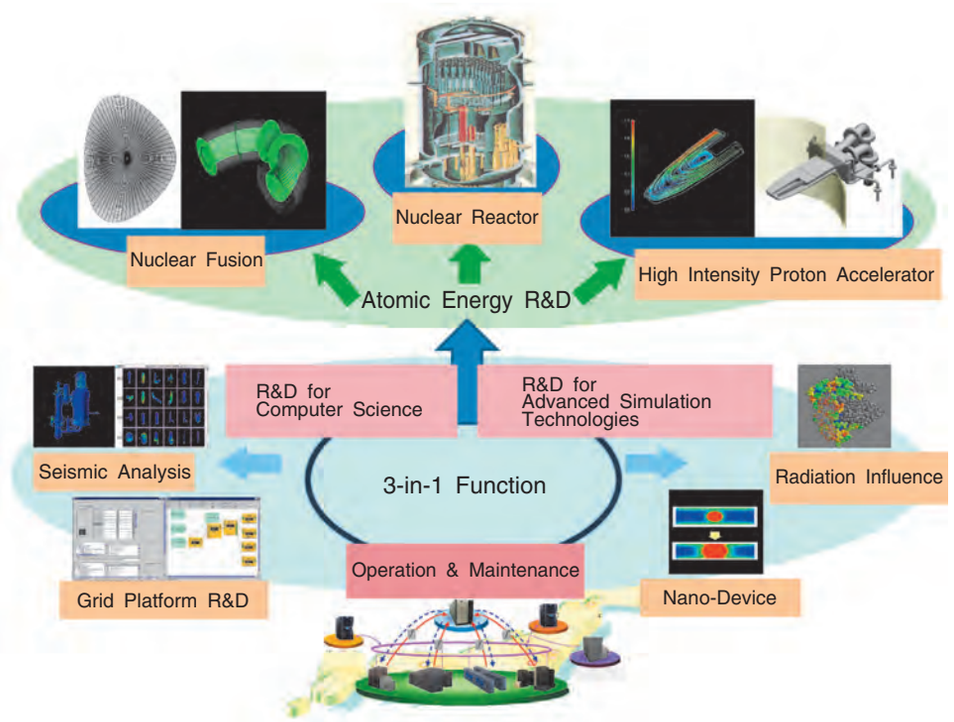

Fig.12-1 Computational Science in Atomic Energy Related Fields
The CCSE is carrying out three-fold coordinated R&D in advanced computational science: for computer science, for advanced simulations, and for better operation/maintenance of computer systems.

For the increased safety of atomic energy, we are carrying out R&D of computational science which could be used with theoretical and experimental advances to predict the safety state of an entire nuclear facility. Computational science is a third method along with "theory" and "experiment" to pursue R&D, and is currently expanding to new fields such as global warming predictions. Further development of computational science is expected also in the field of atomic energy.

The Center for Computational Science and e-Systems (CCSE) promotes three missions, "R&D for computer science to allow computational scientific research in the atomic energy field and to promote cooperative research", "R&D for advanced simulation technologies to make predictions with higher accuracy" and "operation & maintenance of computer systems allowing active research with the guaranty of information security" as depicted in Fig.12-1.

Presently, we are tackling the following seven topics in a mid-term plan to promote innovative atomic energy research and to drive domestic R&D in the computational science field; "distributed parallel computing through grid technology", "vibration simulator of an entire nuclear facility", "mechanisms of crack-propagation in nuclear reactor materials and of rim-structure formation in UO_2 nuclear fuel", "nano-scale device development for atomic energy", "multi-scale modeling incorporating micro to macro level simulations", "development of databases for genome analysis" and "tools for studying DNA/RNA repairing proteins".

CCSE has actively participated in various national projects. For instance, we participated in an ITBL (Information Technology Based Laboratory) project from FY2001 to FY2005, which was one of the e-Japan priority policy programs. In this project, we collaboratively constructed a virtual supercomputer consisting of distributed supercomputers. ITBL shares computer capacity of 60 TFLOPS (from 17 supercomputers) with 11 research communities in 64 research institutes and is continuously supporting their research activities. We also contributed to the "Development & Application of Advanced High-Performance Supercomputer" project through computational science technologies cultivated in the atomic energy field.

We are also promoting international cooperation with the United States (2institutes), Germany (3) and France (5) in order to share in worldwide leading edge research on computational science for the atomic energy. Simulation and modeling technology has been selected as a one area of the Global Nuclear Energy Partnership (GNEP) activities of Japan and the United States, and we are cooperating with this partnership.

CCSE will keep accelerating computational science R&D in the field of atomic energy.

12-1 Computational Nuclear Power Plant Modeling and Structural Integrity Assessment

–3-D Vibration Simulator for Predicting Dynamic Behavior of Nuclear Power Plants–

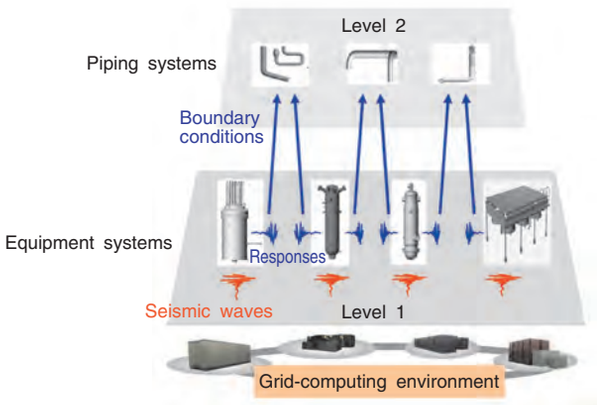

Fig.12-2 Hierarchization in assembly structural analysis by finite element method
Analysis using the conventional finite element method has a computational limit in terms of data capacity when modeling an object because the method treats the object as a continuum structure. We propose a procedure that mitigates this problem by dividing the object into several parts. This figure shows an example of how hierarchization is used to decrease the scale of analysis by dividing the entire system into two levels. Specifically vibrations of the equipment system and piping system are handled separately, and the interaction between these data sets is considered.

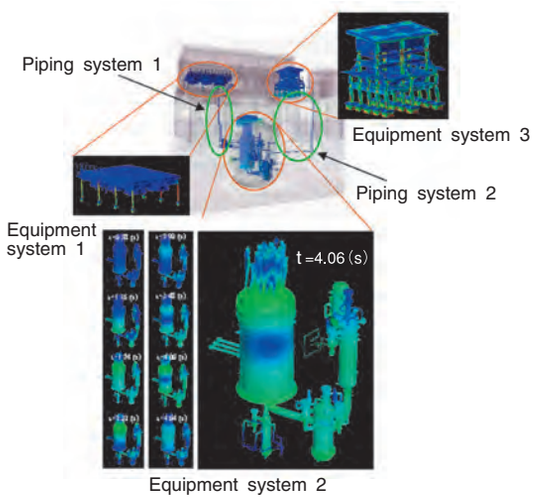

Fig.12-3 Vibration analysis of entire nuclear power plant by hierarchization
Vibration responses of three level-1 equipment systems (equipment systems 1, 2, 3) were calculated and then, the responses at the boundary between the equipment and piping systems were input to two level-2 piping systems (piping systems 1, 2) as boundary conditions. The vibration responses of the two piping systems were calculated to realize vibration analysis of the entire nuclear plant.

There is much concern with validation of the structural integrity of nuclear power plants, especially in earthquake-prone nations, due to the recent occurrence of several large earthquakes. In conventional structural design, the equipment and building constituting a plant have been modeled individually in comparatively simple approximations based on past experience and testing. It is, however, required to treat the plant in its entirety and in more detail in order to analyze the structural integrity of the plant consisting of many parts.

The CCSE of JAEA has been conducting studies using a three-dimensional vibration simulation technique to evaluate the structural integrity of nuclear power plants using the latest computational techniques. In the Hanshin-Awaji Earthquake, a recent large-scale earthquake, physical phenomena such as local deformations caused by the interaction between parts were observed which cannot be easily understood by conventional part analysis techniques. We are trying to understand these interactions between parts by using a three-dimensional vibration simulation technique to model and study the entire structure.

Thus far, we have developed a data processing technique called assembly structural analysis method for plants, comprising more than 10 million parts. We have also developed a procedure to model an entire structure using a grid computing approach, because a single supercomputer cannot process the huge data required for modeling. An assembly structural analysis method can be used to generate model data for each part and assemble them in a way similar to how real structures are manufactured into a finished structure; this method is expected to solve the problem presented by huge data. We have developed a prototype of a vibration simulation system by combining these techniques, and began numerical experiments to analyze the structure of the main facilities of the "High Temperature Engineering Test Reactor (HTTR)" at the Oarai Research and Development Center of JAEA. As a first step, we succeeded in performing a static analysis of HTTR.

It is necessary to perform iterative calculations that consider sequential state changes of extremely large components in order to realize vibration analysis of an entire nuclear power plant; this has proved difficult using conventional analytical techniques due to the scale of the problem and the computational time required. Therefore, we proposed a hierarchized assembling structural analysis method to mitigate the problems. In hierarchization, components are classified suitably into units, for example into those serving a common function, and these units are first processed separately. Fig.12-2 shows an example of a nuclear plant system that is classified into two levels, equipment systems and piping systems; the plant is analyzed by considering the interaction between these two levels.

The work of calculation of the structural model with approximately 180 million degrees of freedom was distributed optimally among several supercomputers and was simplified by hierarchizing the input data, as shown in Fig.12-3. We succeeded in conducting a vibration analysis of HTTR, although the model did not include inner structures, using a prototype of a three-dimensional vibration simulation system. Compared with conventional analysis, the data size and processing time were reduced to less than one-third and one-tenth respectively. This result increases the possibility of performing detailed vibration analysis of an entire nuclear power plant having more than 1 billion degrees of freedom.

Reference

Nishida, A. et al., Numerical Simulation System "Three-Dimensional Virtual Plant Vibration Simulator" for Nuclear Plants by Using Assembled Structural Analysis, Nippon Genshiryoku Gakkai Wabun Ronbunshi, vol.6, no.3, 2007, p.376-382 (in Japanese).

12-2 Suppressing Bubble-Induced Material Damage by Gas Bubbles –Numerical Study of the Damage Suppression Effect of Bubble Injection–

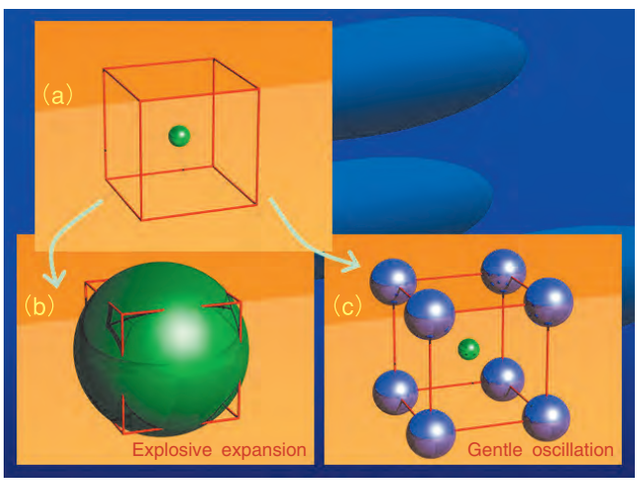

Fig.12-4 Suppressing bubbles' destructiveness by injecting gas bubbles
When subjected to a sudden pressure change, liquid mercury is ruptured and tiny bubbles emerge (the green sphere in (a)). These bubbles will expand (b) and collapse violently, causing significant material damage. Bubble injection is a technique to suppress this violent motion by injecting gas bubbles (the blue spheres in (c)) into liquid mercury.

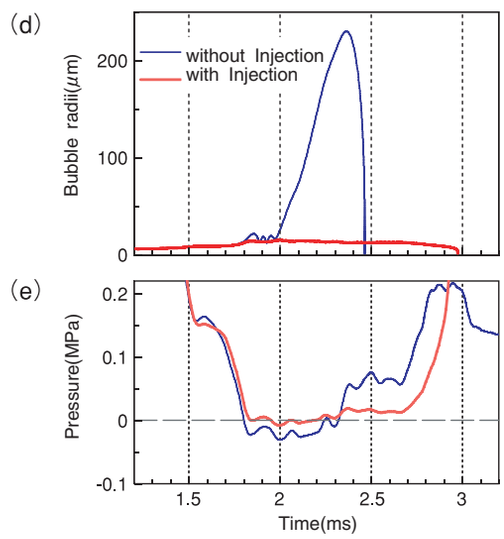

Fig.12-5 Bubble radii (d) and pressure (e) in mercury without (blue) and with (red) injected bubbles as functions of time
This numerical result reveals that the injected bubbles suppress the violent motion of the emerged bubble and reduce the negative pressure in liquid mercury. This is closely consistent with our experimental findings, and elucidates the fundamental mechanism of damage suppression.

We are now developing an intense pulsed neutron source using a MW-class proton accelerator and liquid mercury as part of the J-PARC project. Using this facility, leading-edge research on, e.g., high-T superconductors and DNA will be performed in the near future.

In this "Big Science" facility, tiny bubbles, smaller than 1 mm, are posing a serious problem. The facility produces neutron beams by breaking mercury nuclei with energetic protons, at which moment a large amount of energy is released and a sudden pressure change occurs in mercury. The pressure change ruptures the mercury and there many bubbles emerge. The bubbles are so violent, causing significant material damage on the metal vessel. To suppress this damage that reduces the lifetime of the facility and limits the output energy, we are now developing several techniques.

One of them is "Bubble Injection," in which gas bubbles are injected into flowing liquid mercury (Fig.12-4). To realize this technique, several issues must be resolved such as the development of an injection method (Topic 14-5) and clarifying the physical effect of the injected bubbles (this article). Our recent investigations have verified the effectiveness of this technique. Fig.12-5 shows the dynamics of a bubble which has emerged, calculated numerically using a theoretical model that takes the interaction with the injected bubbles into account. With no bubble injection (the blue curve), the emerged bubble expands explosively and then collapses very violently: such an aggressive bubble is certain to cause material damage. With bubble injection, on the other hand, the bubble becomes very gentle, as shown by the red curve.

From this numerical result we found that the change in bubble dynamics was caused by positive pressure waves emitted by the injected bubbles, which reduce the negative pressure in mercury (the lower panel of Fig.12-5) that drives the bubble expansion. This is the hidden function of bubble injection.

This work was partly supported by a Grant-in-Aid for Young Scientists (B) (No. 17760151).

References

Ida, M. et al., Direct Observation and Theoretical Study of Cavitation Bubbles in Liquid Mercury, Physical Review E, vol.75, no.4, 2007, p.046304-1-046304-7.
Ida, M. et al., Suppression of Cavitation Inception by Gas Bubble Injection: A Numerical Study Focusing on Bubble-bubble Interaction, Physical Review E, vol.76, no.4, 2007, p.046309-1-046309-10.

12-3 Large-Scale Conformational Change of a Protein Elucidated by Computer Simulation
–Molecular Mechanism of Cell Adhesion Protein Integrin–

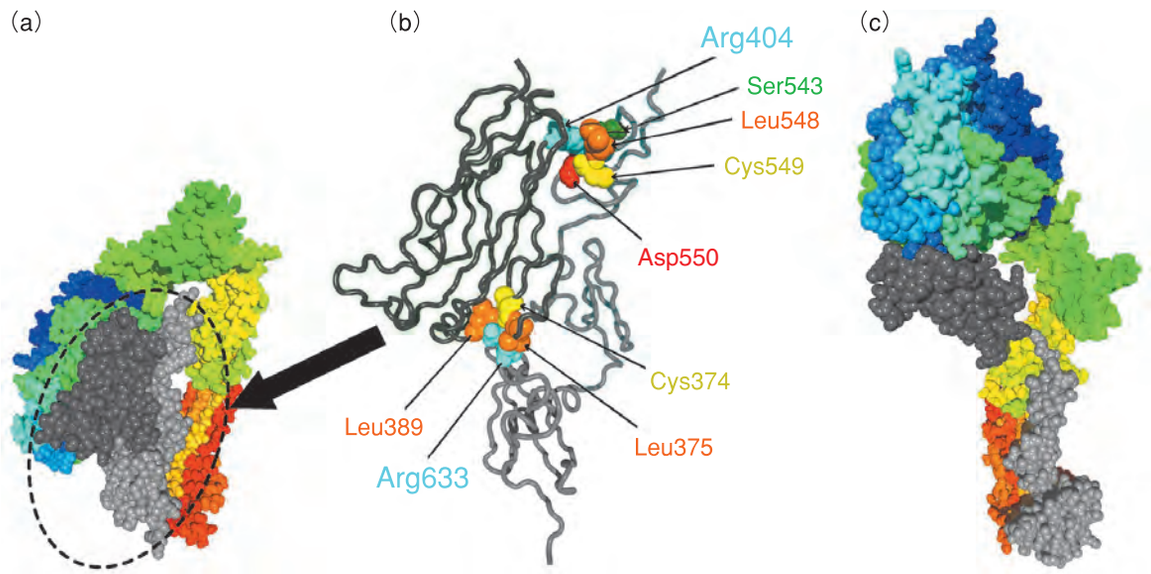

Fig.12-6 (a) and (b) X-ray crystal structure of integrin $\alpha V \beta 3$; (c) computer model of the extended conformation
(a) 3D structure of integrin solved by X-ray crystal structure analysis: ball model of the molecule when "bowing down".
(b) A Magnified tube model of part of the integrin structure. Important amino-acid residues are shown by ball model and their names are shown.
(c) Extended conformation of integrin obtained by computer simulation of large-scale conformational change.

Cells in multicellular organisms such as humans are usually not in isolation, but they are bound to each other directly or indirectly through an extracellular matrix. In this binding, cell adhesion proteins, which exist on the cell surface, are involved. Integrin is a type of cell adhesion protein, and a variety of integrins with different functions and structures have been identified.

Some kinds of integrins are known to be normally in an inactive state changing to an active state only when necessary. Integrin α IIb β 3, which exists abundantly on the cell surface of a blood platelet, is one of them. When we bleed, this integrin changes to an active state to promote the platelet aggregation and stop the bleeding. Large-scale conformational changes of integrin (Fig.12-6 (a),(c)) are considered to be involved in this activation.

We made computer simulations to study the mechanism of the large-scale conformational change of integrin α V β 3, which is similar to integrin α IIb β 3 and whose structure was determined by X-ray crystal structure analysis at the atomic level. Among ~1500 amino-acid residues which constitute the protein, we found that two amino-acid residues play important roles in the conformational change (Arg633 and Arg404 in Fig.12-6 (b)). That is, we found that the conformational change occurs more easily if the interactions of these amino-acid residues with nearby residues are eliminated in the simulations. This computational result suggests that these amino-acid residues work as switches for the conformational change. The residues had not been recognized as important, but experiments performed by our co-worker demonstrated that the mutation of these residues activates integrin, thereby verifying our simulation results.

Heart attacks and strokes, which are the major causes of death for Japanese people, are caused by the formation of the blood clot at undesirable locations in the body. For the development of a cure for these deceases, many researchers are focusing on integrin, which is involved in the formation of the blood clot. Our discovery about this protein will be helpful in advancing this development.

Reference
Matsumoto, A. et al., Key Interactions in Integrin Ectodomain Responsible for Global Conformational Change Detected by Elastic Network Normal Mode Analysis, Biophysical Journal, vol.95, no.6, 2008, p.2895-2908.

12-4 Development of Steel Impurity Behavior Simulation Technology
–Estimation of Impurities in Materials Based on Thermal Desorption Gas–

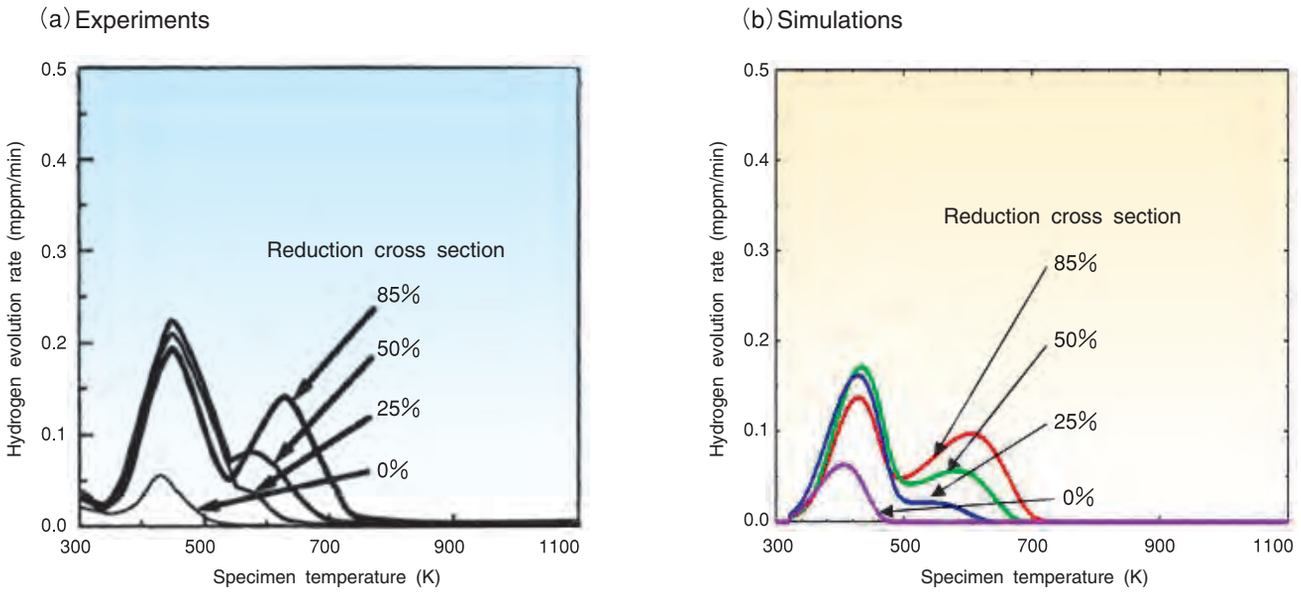

Fig.12-7 Comparison of the hydrogen desorption profile of deformed eutectoid steel: (a) Experiment results (b) Simulation results
The numerical model simulates one peak at the low temperature side, which may relate to hydrogen desorption from defects of vacancy or dislocation, and the other peak at the high temperature side, which may be due to an increase in phase interfaces caused by the cold drawing.

Steel is a basic structural material which is used for various constructions. Steel material inevitably includes impurities and defects disrupting the crystal structure. which are vacancies, dislocations, grain boundaries, phase interfaces, and inclusions. Hydrogen, the smallest and lightest element, also enters into materials from the environment as impurities. Furthermore hydrogen seriously changes the mechanical properties of materials by migrating and combining with defects. The change of mechanical properties causes the degradation of material strength. Therefore, the estimation of the hydrogen and defects within materials is an important issue.

Defects in the steel lattice structure are called trapping sites because they capture hydrogen migrating from the defect-free crystalline regions. Type of defects can be distinguished by their differing energy for capture of hydrogen. Defects with deep energy valleys trap hydrogen strongly and defects with shallow energy valleys trap hydrogen weakly. Thus, the former defects release hydrogen at higher temperature, and the latter defects release at lower temperature. Inferring from this property, if there is a peak of desorbed hydrogen from a specimen heated at a constant rate, one can regard the hydrogen of the peak as being released from the defects with a specific trapping energy. Therefore, we can determine the type and amount of defect in the specimen, the trapping energy of the types of defects, and the amount of trapped hydrogen by analyzing the profile representing the relation between specimen temperatures and desorbed hydrogen. This analysis is called thermal desorption analysis. In order to estimate these quantities and the relation between them, we developed a numerical model of the hydrogen desorption process and tried to simulate the hydrogen desorption profile obtained by the thermal desorption analysis. Our model computes the equilibrium state between the hydrogen in trapping sites and the hydrogen in surrounding regions at each temperature, and regards hydrogen in the surrounding regions as desorbed hydrogen that produces the profile, though in practice hydrogen in the surrounding regions diffuses within materials. This model of the hydrogen desorption process is based the assumption that hydrogen migration is very fast in the defect-free crystalline regions.

As shown in Fig.12-7, our numerical model simulates very well the actual hydrogen desorption profile of eutectoid steel, which indicates several types of defects distinguished by different trapping energy. This successfully simulated profile has two peaks, which was difficult for previous models to reproduce, and allow us to estimate the amount of defects and trapped hydrogen and the trapping energy of the defects of each peak. This simulation also may suggest experimental conditions which will isolate the peak of a specific defect.

This idea and technique can also be applied to the estimation of helium in steel materials. The estimation of the amount of defects and trapped impurities, and the trapping energy of defects should be of use for research into the mechanical property change that causes embrittlement or hardening of nuclear steel materials.

Reference

Ebihara, K. et al., Modeling of Hydrogen Thermal Desorption Profile of Pure Iron and Eutectoid Steel, ISIJ International, vol.47, no.8, 2007, p.1131-1140.

Development of Technology for Nuclear Nonproliferation, Foundation of Peaceful Use of Nuclear Energy

We have two primary missions regarding nuclear nonproliferation. One mission is to support the government in developing nonproliferation-related policies through research and study. The other mission is to support government and international organizations by developing nuclear nonproliferation technology. Other important missions of JAEA are to support denuclearization, nuclear material control by the facility using it, and human resource development.

Policy Research and Study

"Modelling the nonproliferation process in Japan", and "Improving Trustworthiness and Transparency of Peaceful Use of Nuclear Energy in Asia", based on in-house technical knowledge.

In 2007 we comprehensively reviewed Japan's current nuclear nonproliferation efforts with regard to items such as guarantee of peaceful nuclear use by domestic laws and regulations, ensuring transparency of plutonium use, export control, sensitive technology control, physical protection /nuclear security, and safeguards measures, and also considered concrete cooperative arrangements with the countries in Southeast Asia where introduction of nuclear power generation is likely. Moreover, in support of the Japanese government, we investigated fuel supply guarantees and nuclear nonproliferation strengthening, which are international issues.

Development of technology for nuclear nonproliferation

Development of an advanced safeguards system which will provide effective and efficient safeguards for the future Fast Breeder Reactor fuel cycle is underway. In collaboration with the U.S. as part of GNEP, cooperative research plans for next generation safeguards measures/physical protection have been discussed at a working group level.

Regarding environmental sampling for safeguards, we are performing further development of the fission track-thermal ionization mass spectroscopy method with which a uranium particle less than 1 μm can be detected.

We have started demonstration tests of a new color surveillance camera with high resolution, as a technical development for improvement of the reliability of, and confidence in, peaceful use of nuclear energy.

We also contribute to international activities such the Generation IV Atomic Energy International Forum, and we are performing research on evaluation methodology for the proliferation resistant features of future nuclear cycle systems.

Support of Denuclearization

We have been developing technology with contributes to disarmament and denuclearization of the world, in particular cooperative research with Russia to use surplus nuclear weapons plutonium as MOX vipac fuels in fast breeder reactors. The effectiveness of this method was recognized by both the U.S. and the Russian Federation, and both countries issued a joint statement that this application of plutonium in the fast breeder reactor BN600 has been approved.

In support of the CTBT (Comprehensive Nuclear-Test-Ban Treaty), at Tokai laboratory we continue to perform precise analysis of environmental samples collected at radionuclide monitoring stations throughout the world.

We have started provisional operation of the Takasaki and Okinawa monitoring stations after certification by the CTBT Organization. Operation of those stations is treated as provisional operation until CTBT enters into force, but it actually has reached the stage of full-scale operation with completion of all planned R&D.

At the National Data Center located in the Nuclear Science Research Institute in Tokai, we continued development and upgrade of software for γ-ray spectrometry, β-γ coincidence data analysis for radioxenon, a database system, and source location estimation of radionuclide release using an atmospheric transport model.

Nuclear Material Management

We have been making technical contributions to IAEA safeguards implementation by conducting several technical development projects in cooperation with the U.S. Department of Energy. We have also cooperated in domestic and international personnel training.

From the results of our long-term environmental durability tests of intruder automatic detection systems performed in order to strengthen physical protection, we identified causes of problems arising upon long term outdoor use and countermeasures therefore. We have verified that this is an effective system which can quickly detect and automatically monitor suspicious persons, if there is proper installation position of surveillance cameras and setup of effective detection rules, etc.

We have examined the medium-to-long term nuclear materials transportation plans of each project of JAEA for possible problems. Also, we have started negotiation with U.S. DOE on a contract for spent fuel transportation from research reactors. Moreover, in our development of a MOX powder transportation container, we carried out handling tests at a facility and heat transfer tests using a prototype container.

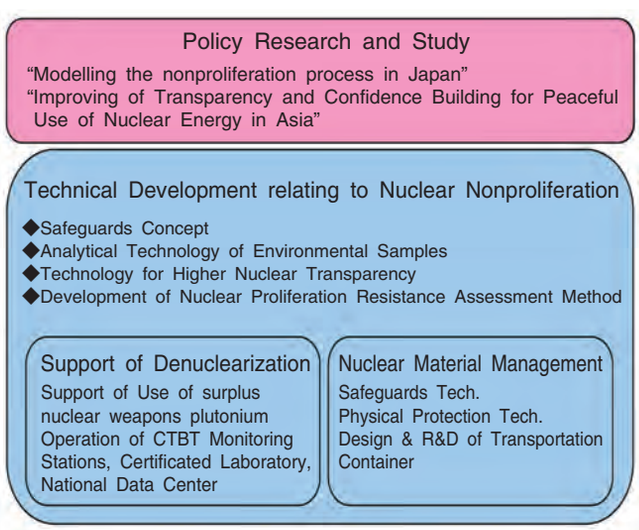

Fig.13-1 Research Activities of Nuclear Nonproliferation Science Technology

13-1 Nuclear Proliferation-Resistance and Safeguards for Future Nuclear Fuel Cycle

–Study of the Evaluation Technique and Criteria of Nuclear Proliferation Resistance–

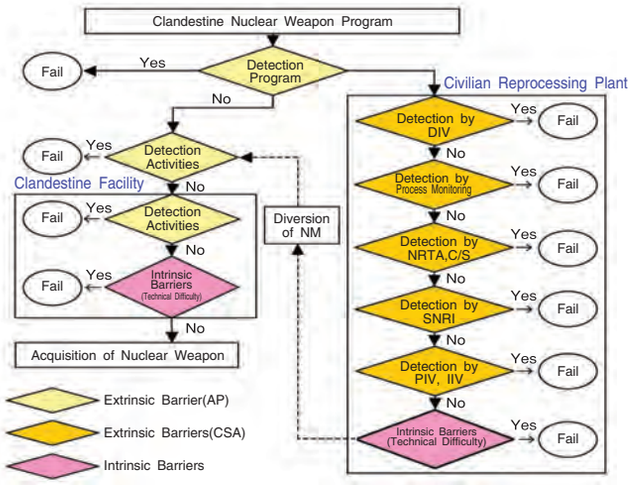

Fig.13-2 Proliferation resistance of future reprocessing plant (Extrinsic barriers, intrinsic barriers)

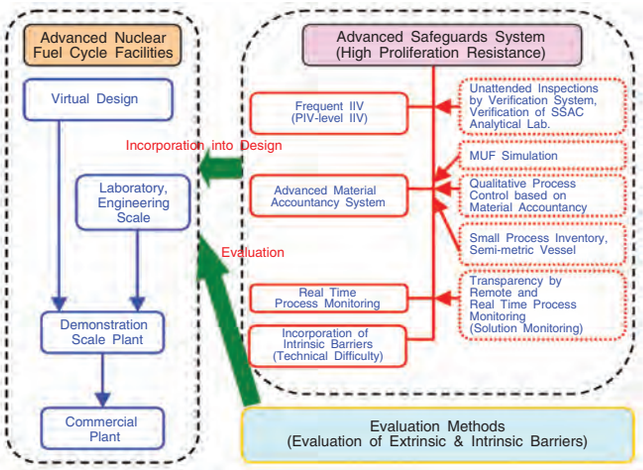

Fig.13-3 Incorporation of advanced safeguards system into design of NFC (Future reprocessing plant)

The demand for peaceful use of nuclear power is remarkably increasing, in particular in order to ensure global energy security and prevent global warming. A future nuclear fuel cycle (NFC) (i.e. fast neutron reactor fuel cycle) must recycle a much larger amount of plutonium than at present, which raises nuclear security issues (prevention of nuclear proliferation). In this context, for the future NFC, very robust measures for nuclear security, namely nuclear proliferation-resistance (PR), have to be taken in advance. A proliferation resistant NFC will impede diversion of nuclear materials by host states into nuclear explosive devices or other weapons. It is said that PR should be supported both by intrinsic features of nuclear energy system and extrinsic measures. International safeguards are very reliable and effective for early and timely detection of diversions of nuclear materials, but intrinsic features of the future NFC also have to be investigated at the same time to establish very robust nuclear security. We are developing reasonable PR measures (intrinsic features and extrinsic measures) for the future NFC. Here we explain briefly an example of our study results for a next generation reprocessing plant, including ways for improvement of technologies for detection of diversion (safeguards) and deterrence of diversion. Also, we summarize requirements for the future reprocessing technologies to have PR.

As proliferation threats, acquisition (diversion) of nuclear material by states, misuse of NFC facilities, withdrawal from NPT and theft of nuclear material by terrorist groups are mentioned. The effects of the extrinsic measures (extrinsic barriers) and intrinsic features (intrinsic barrier) on these threats are shown in Fig.13-2.

Extrinsic measures (IAEA safeguards), based on comprehensive safeguards agreement (CSA) and additional protocol (AP), are very effective for timely detection of diversion of nuclear material for clandestine weapon programs, because they establish many checkpoints. This is proved by the fact that so far no state which has entered into CSA and AP has attempted a clandestine weapon program. For realization of the future NFC with very heavy plutonium recycling, it is essential that extrinsic measures maintain high level detection capability.

To deal with the threat of a state's withdrawal from NPT or theft of nuclear material by terrorist groups, intrinsic features (technical & material barriers) are useful. The next generation reprocessing (advanced aqueous reprocessing) technology which is proposed in the FaCT project, features the requirement of technically difficult plutonium separation, due to minor actinide (MA) and fission product (FP) content in plutonium, making diversion less attractive. These intrinsic barriers are very effective for preventing a state from withdrawing from NPT.

We are proposing following requirements those make the future NFC technologies have higher proliferation-resistance, based on the results of our study. These requirements should be considered in designing the next generation reprocessing plant (Fig.13-3).

1. Frequent PIV (Physical Inventory Verification)-level IIV (Interim Inventory Verification); Implementation of frequent IIV close to PIV level in addition to PIV (once a year) in order to make MUF (Materials Unaccounted For) value low
2. Advanced nuclear material accountancy; Introduction of small process inventory based on semi-metric vessel procedures / Systemized material measurement / Creating quantitative modes for process control based on material accountancy
3. Real time process monitoring (Improvement of detection capability); Real time material accountancy with advanced solution monitoring / Detection of change of operation conditions (including acid content)
4. Incorporation of intrinsic barriers; Application of technology not readily capable of plutonium separation / Treatment resulting in less attractive plutonium mixed with MA and FP.

In order to establish a system concept of the future NFC which will be internationally accepted and has economic rationality, it is very important to combine extrinsic measures (safeguards) and intrinsic features properly. Also, explaining the concept to the world is important. For this purpose, it is necessary to participate in international non-proliferation activities such as INPRO and GEN-IV to set up internationally-accepted PR evaluation methodologies and PR norms.

In our study, so far we have investigated minimum conceptual requirements of proliferation-resistance. Hereafter, we need to investigate them in further detail.

Reference

Senzaki, M., Kuno, Y. et al., Proliferation Resistance of Next Generation Nuclear Energy Systems, Nippon Genshiryoku Gakkaishi, vol.50, no.6, 2008, p.368-373 (in Japanese).

14 Development of Experimental Techniques / Facilities at JAEA R&D Centers

We have been promoting a wide range of R&D activities systematically by coordinating between R&D sectors, including the R&D Directorates whose activities have been described in previous chapters and 12 R&D Centers located in various locations in Japan.

The R&D Directorates of JAEA have been promoting R&D for their respective purposes with the experimental equipment/facilities at each R&D Center. The R&D Centers have not only been operating and managing various types of equipment/facilities but have also been working on innovations and improvements for them, and in addition have themselves been developing experimental techniques, management techniques and equipment/facilities necessary for the various R&D projects of JAEA.

This chapter introduces the developments which have been made over recent years at each R&D center.

Tsuruga Head Office

In "MONJU", a "Function Confirmation Test" to confirm the performance and function of the facility which was modified to prevent sodium leakage, was completed in August, 2007, and a "Plant Confirmation Test" to check the entire function of the plant is being performed. In March, 2008, a report on the reevaluation of the seismic safety of "MONJU" was submitted to the national authority in light of the revised Regulatory Guide for Renewing Seismic Design. As a result of a false sodium leakage alarm which occurred in March, 2008, all of the sodium leakage detectors have been inspected.

In "FUGEN," the spent fuel has been shipped out, and heavy water has been collected/shipped out however, after the decommissioning project was approved in February, 2008, the "Fugen Decommissioning Engineering Center" was reorganized to play a leading role in decommissioning projects. During the modification construction, the facilities and equipments with relatively low levels of radiation, and non-contaminated facilities and equipment are being dismantled.

"Fugen Decommissioning Engineering Center" Reorganized February, 2008

Tokai Research and Development Center, Nuclear Science Research Institute (NSRI)

In research reactor JRR-3, a high performance vessel is being developed to increase the intensity of a cold neutron beam. In JRR-4, the technology to increase the efficiency of dosimetry is being developed, in response to the demand for the increased usage of medical irradiation at the boron neutron capture therapy (BNCT). The technology for a Tandem Accelerator is being developed to achieve a higher performance of an ion source. Also, in the Facility of Radiation Standards, the facility for monoenergetic neutron calibration is being developed, to perform energetic experiments of neutron monitors.

In addition, based on an external research fund which was started in 2007, irradiation technology of a 12 inch silicon ingot is being developed in JRR-4 and JRR-3.

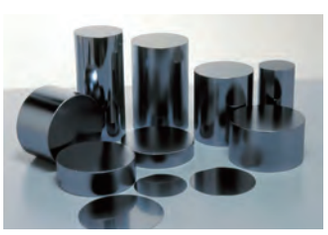

Silicon Ingots and Silicon Wafers (upper)
Equipment for Neutron Transmutation Doping of Silicon Ingot in JRR-3 (left)

Semiconductors with uniform resistivity can be made by adding ^{31}P evenly by nuclear transmutation of ^{31}Si, and is widely used for thyristors to control high-voltages and high currents, CCD for video cameras and other devices.

Tokai Research and Development Center, Nuclear Fuel Cycle Engineering Laboratories

In the Tokai Reprocessing Technology Development Center, a reprocessing test of spent MOX fuel was conducted by using about 3.1 t of fuel from "FUGEN". The research and development of the vitrification technology to decrease and stabilize the generation of waste which occurs in the tests was performed. In the Plutonium Fuel Development Center, a fuel production technology development test, and a physical characteristics measurement for the melting point and thermal conductivity of MOX pellet was performed for future FBR utilization.

In April, 2008, based on the cooperation agreement between the U.S. Department of Energy (DOE) and JAEA, a cooperation agreement for the purpose of personnel training in the nuclear fuel cycle field was concluded at the Nuclear Fuel Cycle Engineering Laboratories and the Oarai R&D Center with the Idaho National Laboratory (INL). Hereafter, an assignment of personnel for training and education, and the exchange of information will be carried out based on this agreement.

Conclusion of Cooperation Agreement Ceremony with INL
Shigeo Nomura (right) Director General, Nuclear Fuel Cycle Engineering Laboratories (JAEA)
David J. Hill (center) Deputy Laboratory Director for Science & Technology, INL
Hiroshi Hiroi (left) Director General, Oarai Research and Development Center (JAEA)

J-PARC Center

In Japan Proton Accelerator Research Complex (J-PARC), the building for three facilities for accelerators and a Material and Life Science experimental facility (MLF) were completed and trial operations are progressing for proton beam transportation. Particularly, in October, 2007, the acceleration of a beam by a Linac was successfully accelerated to 3 GeV by a 3-GeV synchrotron. Also, on May 22, 2008, the revolution control of an incidence beam was succeeded by a 50-GeV synchrotron, and on May 30, 2008, the generation of a neutron by a nuclear spallation reaction was successful in the MLF. The beam intensity will be increased further by the end of December, 2008, to start using MLF.

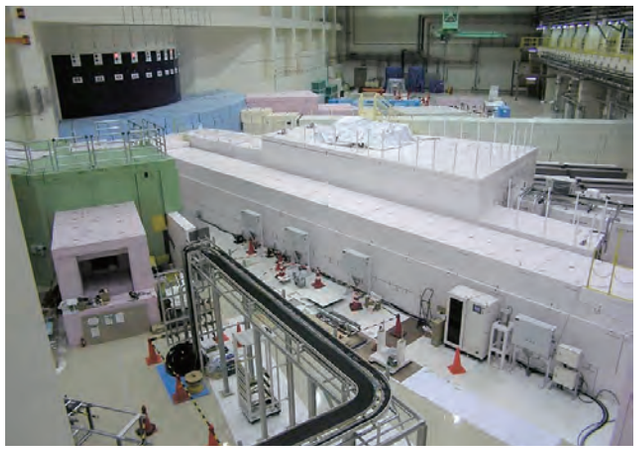

Neutron beam lines now under construction in MLF (J-PARC) Photo May 30, 2008

Oarai Research and Development Center

Regarding the R&D for the Fast Reactor Cycle Technology Development Project "FaCT", the irradiation tests for FBR high burn-up fuel and minor actinide containing fuel were performed in the experimental fast reactor "JOYO" and the post irradiation examination facilities. The experimental researches have been also carried out in the water and sodium test facilities.

"JOYO" completed a highly advanced project (MK-III) which improved the irradiation capability by about four times more than in the past, and the results of the FBR cycle research using "JOYO" were accepted. As a result, "JOYO" received the "2008 Minister of Education, Culture, Sports, Science and Technology Award" in the science and technology field (Research Dept.).

The refurbishment of the Japan Materials Testing Reactor (JMTR) was started for the restart in 2011. In May, 2007, the High Temperature Engineering Test Reactor (HTTR) achieved the first 30 days continuous operation with a nuclear reactor exit coolant temperature of 850 degrees C.

Also the development of the hydrogen production technologies with an iodine-sulfur process and with a thermochemical-electrolysis hybrid cycle has progressed.

HTTR Central Control Room

Naka Fusion Institute

Naka Fusion Institute in close cooperation with Fusion R&D Directorate, are aiming for the utilization of fusion energy. As well as fusion plasma research and fusion engineering research, the project to upgrade JT-60 is ongoing as a part of the Broader Approach Activities, to support and perform supplemental research for the International Thermonuclear Experimental Reactor (ITER)(to be built in France). In order to broadly introduce the forefront of nuclear fusion R&D, facility tours have been implemented often for local junior high school students and high school students from across the country (Super Science High Schools). Also, the facility is open to the public in October every year.

Junior high-school students marveling at the characteristics of a synthetic diamond, which is used for a plasma heating device at ITER

Takasaki Advanced Radiation Research Institute

The Takasaki Advanced Radiation Research Institute of JAEA opens the Takasaki Ion Accelerator for Advanced Radiation Application (TIARA), which consists of four ion accelerators, an electron accelerator, and gamma irradiation facilities, to be used by JAEA and any organization to perform R & D on biotechnology, new functional and environment-friendly materials, radiation effects of materials and quantum beam analysis. In 2007, the supply of a heavy ion micro beam of a several hundred MeV class was started in the experiment for the evaluation testing of radiation resistance of semiconductor and radiation effect study for living cells. The development of a high speed single ion hit technology at 10 hits per second or more is also progressing.

Divergence defining slit for formation of a heavy ion micro beam of a several hundred MeV class

Kansai Photon Science Institute

In the Kizu district, research on advanced lasers with a sub-petawatt laser oscillation output, and the oscillation of an X-ray laser with a output wavelength of about 10 nm have been performed and are progressing satisfactorily. In the research for laser utilization, the generation of semi-monochromatic electrons, high energy ion generation and basic research for medical applications are being researched.

The new project, the creation of a “Photo Medical Industrial Valley”, which had been proposed in the "Formation of creative base for innovations integrating frontier fields" program funded by the Special Coordination Funds for Promoting Science and Technology, commissioned by the Ministry of Education, Culture, Sports, Science and Technology (MEXT) of Japan, was commissioned in 2007. The Photo-Medical Research Center was established for this project in October, and activities for the creation of a “Photo Medical Industrial Valley” were started in collaboration with industries and universities in the Keihanna region, which extends over Kyoto, Osaka, and Nara prefectures, and is a new base of culture, science, and research in the 21st century.

JAEA Kansai Advanced Relativistic Engineering LASER System (J-KAREN)

In the Harima district, various researches such as the treatment of spent-nuclear fuel using synchrotron radiation in SPring-8, and the superconductivity of a uranium compound are being researched. In addition, four dedicated beam-lines commonly used in the facility are available for use by any organization.

Horonobe Underground Research Center

As a part of the research and development program on the geological disposal of high-level radioactive waste, the Horonobe Underground Research Center, a division of the Japan Atomic Energy Agency, is implementing the Horonobe Underground Research Laboratory Project (Horonobe URL Project) with the aim of investigating sedimentary rock formations.

Regarding the construction of URL in 2007, the derrick facilities used to excavate the shafts and pithead heater facilities for the entrances of tunnel were constructed, and the excavation of ventilation shafts reached 161 m, and 110 m for the East shaft.

In addition, a pilot boring survey was conducted for the purpose of estimating the amount of groundwater that would flow into the tunnel during excavation, and to predict the point of flow.

Winter view of the Horonobe Underground Research Laboratory from the viewing platform of the Public Information House

Regarding the above ground facilities, the construction of the Public Information House (Yume Chisoukan) of the Horonobe URL center was finished in May, and was opened in June 30. In December, the number of visitors reached 10,000.

Regarding the construction of URL in 2008, the ventilation shaft, excavation of the east shaft and the drilling of a portion of the horizontal shaft continued to be constructed, and the waste water treatment facility will be extended. A pilot boring survey near the ventilation shaft, and joint researches with the other research institutes will also be continued.

Regarding the above ground facilities, the construction of the International Communication House as the base of international exchange activities for domestic and international researchers will be started.

Tono Geoscience Center (TGC)

In the R&D to provide the scientific and technical basis for safe geological disposal of high-level radioactive waste, the R&D for investigation technology to characterize the deep geological environment mainly crystalline rock (Granite), a wide of range of engineering for deep underground application and the long term stability of the geological environment are being researched. In FY 2007, a drift was completed at GL-200m level, and the shaft has reached GL-231.2m in the construction of the Mizunami Underground Research Laboratory(MIU). This research is being performed in close collaboration with universities and scientific institutions, both in Japan and abroad. In order to promote a mutual understanding, TGC holds project explanation meetings for the local residents and municipalities, and openly accepts site tours of the facility. More than 3,000 visitors have visited MIU in the past year, and have experienced underground research first-hand.

Geological mapping at the bottom of main shaft

Ningyo-toge Environmental Engineering Center

The Ningyo-toge Environmental Engineering Center has been developing a dry decontamination technology using an Iodine heptafluoride (IF_7) gas as a part of the decontamination technology R&D for uranium enrichment facilities.

In 2007, to promote the optimization of the decontamination processing condition, such as flux velocity, and flow rate, the decontamination time was reduced to more than half the time when compared to the start of operation.

The preparation for the decontamination of a single type centrifugal separator cascade will continue to be promoted.

In addition, the dismantling of a Refinement and Conversion facility was started and is in full scale, and is the first nuclear fuel facility in Japan. The facility dismantling data will be provided for the “Decommissioning Engineering System Database”.

The Ningyo-toge Mine continues to perform technology development for the mining complex

Decommissioning status of the Refinement and Conversion facility

Aomori Research and Development Center

The Aomori office in the Rokkasho area and the Mutsu office were unified and reorganized as the Aomori research and development center in April, 2007.

In the Rokkasho area, the construction of research facilities for Broader Approach (BA) activities was started in March, 2008. The BA program is a joint implementation program between Europe and Japan which will be advanced in parallel with the ITER project which just started in France.

In the Mutsu area, a radioactivity related database for a clearance evaluation system, a practical decommission method for the nuclear ship “Mutsu” related facilities, and an ultra low level measurement and related techniques about C-14 and I-129 by accelerator mass spectrometer (AMS) are being developed. “The 3rd symposium on marine environmental sciences” was held at Mutsu to disclose information to the local residents, and “The 1st JAEA Tandetron AMS utilization workshop” was held to exchange information between AMS users.

In order to propagate and to deepen the community’s understanding of the Broader Approach activities, a billboard was put up on the site in June, 2007.

14-1 Evaluation of Radioactive Inventory in Nuclear Facility for Its Decommissioning

–The Applicability of a Radioactive Inventory Evaluation Technique for "FUGEN" Verified–

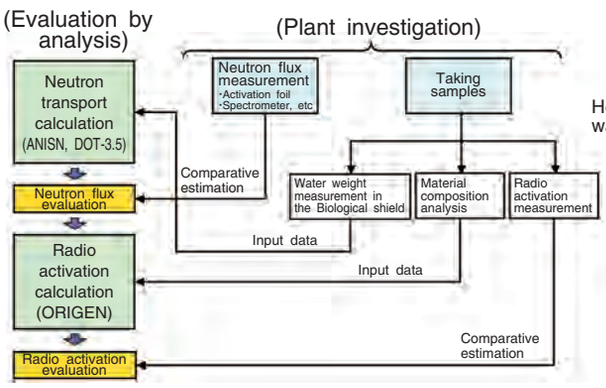

Fig.14-1 The estimation technique of radio-activation in "FUGEN"
The neutron flux is estimated from measurements and calculations, and then, the radio-activation is calculated with the ORIGEN code using it. We had been acquiring data on neutron flux, material composition, and water content in concrete during the reactor operation period in order to calculate the radio-activation. We also had been measuring radio-activation. We verified the validity of our technique by comparing those data with calculation data.

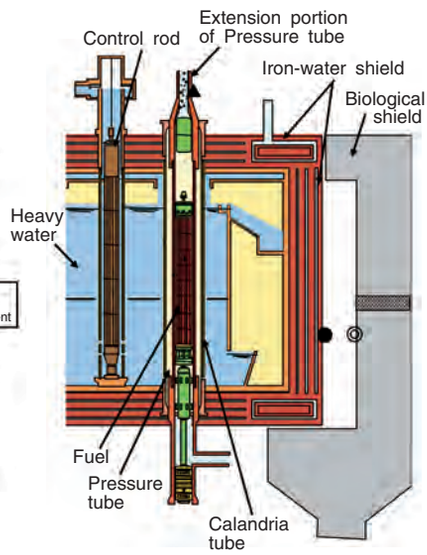

Cross-section of reactor core of "FUGEN"
Note; ▲●◎ indicate the measurement positions of activation foil, and ▩ indicates the sampling point of concrete specimens.

(a)Measurement data of Activation foil

Evaluation at the Extension portion of Pressure tube(▲position)

(Bq/g)

	Co-60	Au-198
measurement data	8E+02	3E+04
calculation data	1E+03	4E+04

Evaluation at the Iron-water shield's surface (●position)

(Bq/g)

	Co-58	Co-60	Au-198
measurement data	6E+01	1E+04	3E+05
calculation data	2E+02	1E+04	7E+05

Evaluation at the biological shield's surface (◎position)

(Bq/g)

	Co-58	Co-60	Au-198
measurement data	8E+01	1E+04	3E+05
calculation data	2E+02	1E+04	7E+05

(b)Measurement data of concrete specimen in the Biological shield

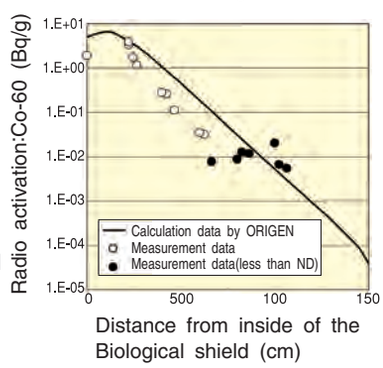

Fig.14-2 Comparison between calculated and measured radio-activation values

When we carry out the decommissioning of the "FUGEN" reactor, it is important that the safety assessment of the public exposure dose, the evaluation of radioactive waste amount and the planning of an appropriate method and procedure for dismantlement are based on an accurate radioactive inventory.

The radioactive inventory evaluation consists of (1) evaluation of the radio-activation on the structural materials such as reactor cores, caused by the neutron irradiation during reactor operation and (2) evaluation of the corrosion layer adhering to the equipment and piping, etc. in which there are substances which were in the coolant water and were radio-activated in the reactor core.

The radio-activation of many parts can be evaluated by analysis following the flow of "Evaluation by analysis" in Fig.14-1. However, "FUGEN" is a complicated pressure tube type reactor different from a light water reactor, and its neutron behavior near the reactor can be complicated. Thus, it is necessary to understand the neutron flux distribution accurately before analyzing the radio-activation, and to evaluate the appropriateness of the result. We acquired as much data as possible of the element composition, neutron flux, and the radio activation in investigation of "FUGEN", and we compared those with the evaluations made by analysis (Fig.14-1).

In "FUGEN", the radio-activation calculation was analyzed by dividing the reactor into the core structure area and the shielding area surrounding reactor core.

The radio-activation measurement was carried out as follows. A high pressure tube test piece irradiated for a certain period in the core structure area during the reactor operation was measured. Also, many Activation foils set around the reactor core in the shielding area and irradiated for a certain period during the reactor operation were gathered and measured. Moreover, after reactor shutdown, pieces of concrete were taken from the Biological shield and were measured.

The analytical data values were almost equal or more conservative than the measurement data in all cases. Thus, the validity of our evaluation method was confirmed (Fig.14-2). This technique was applied to the radioactive inventory evaluation in the "Decommissioning plan of FUGEN" (authorized on February 12, 2008), and the public exposure and the amount of generation of waste were evaluated appropriately from these results. Moreover, this technique will also be applicable to the safety clearance evaluation of the waste surrounding the nuclear reactor after dismantling which had been exposed to neutrons.

Reference
Kitamura, K. et al., Evaluation of Radioactive Inventory for Fugen's Decommissioning, Hoshasen, vol.34, no.1, 2008, p.53-63 (in Japanese).

14-2 Achieved Utilization of Short-Lived Radioactive Nuclei Beams
–Development of Ion Sources for Radioactive Nuclei–

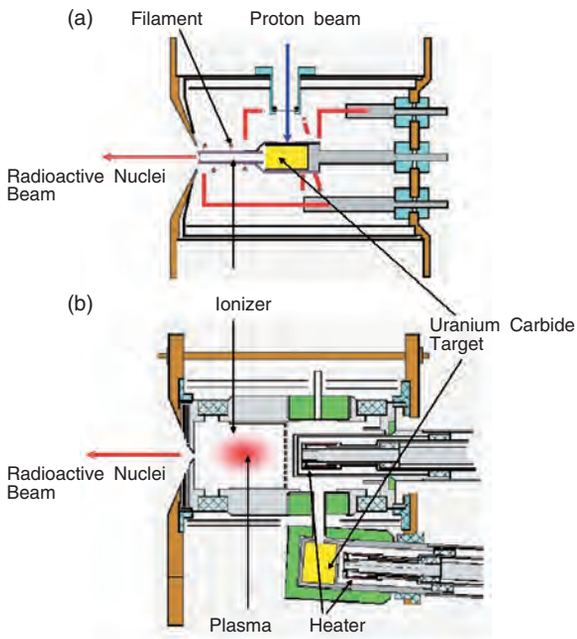

Fig.14-3 Schematic view of Ion sources for Radioactive Nuclei
Two types of integrated uranium target-ion source systems were developed that are considered to be chemical properties of elements.
(a) Surface ionization type ion source (operated at ~2300°C): Ionized by the interchange of electron at the heated metal surface on the inner wall of the ionizer.
(b) Low-pressure arc-discharge ion source (operated at ~1500°C): Ionized in plasma created in an ionizer by an arc-discharge.

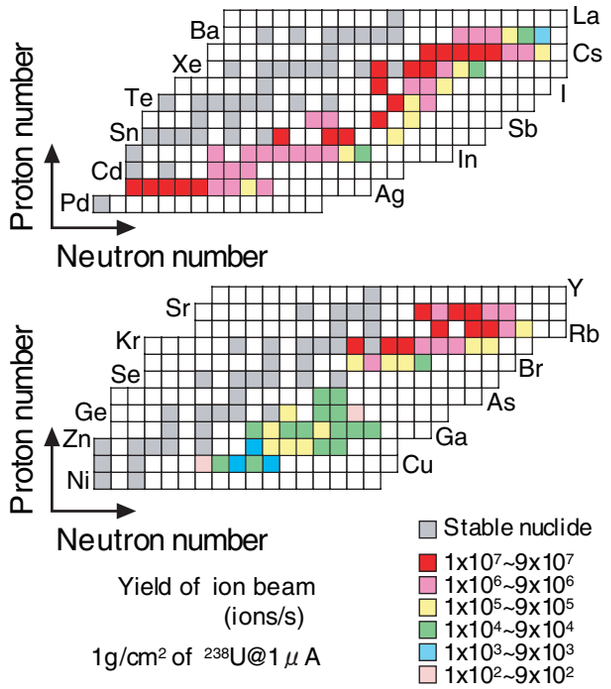

Fig.14-4 Beam intensities of the nuclei successfully ionized
We succeeded in the ionization of neutron rich nuclei with 19 elements and 105 nuclei, that were produced in a proton induced uranium fission.

We are developing ion sources to ionize radioactive nuclei, which do not occur naturally, for acceleration by a radioactive nuclei beam accelerator in the facility of the JAEA tandem accelerator. Radioactive nuclei of about 40 elements and 400 nuclei are produced at a time when uranium is bombarded by a proton beam. For an effective acceleration of these nuclei, the diffusion/evaporation should be fast from the uranium target and ionization at once, because most of these nuclei are in minute amounts and short-lived, as half-life is less than a few seconds. Therefore, we developed a unique uranium target and two types of ion sources for radioactive nuclei that are considered to be chemical properties of these elements.

The more the weight of the uranium is increased, more radioactive nuclei in the target was obtained. However the diffusion/evaporation of the fission products becomes slower if a highly-condensed target is made. In addition, the target should be raised to a high temperature to accelerate the speed of the diffusion/evaporation. Therefore, we made a uranium carbide target, which has a chemical stability at a high-temperature on a graphite fiber, so that the amount of uranium (~800 mg/cm^2) was maintained. This uranium target has a large surface area and fast diffusion/evaporation speed of the fission products.

High ionization efficiency is required for the ion source for radioactive nuclei that are produced in minute amounts. It is impossible to ionize every element with one type of ion source produced in the reaction of proton induced uranium fission. Therefore, two types of integrated uranium target-ion source systems were developed that are considered to be chemical properties of elements. It is suitable that the surface ionization ion source (Fig.14-3 (a)) to ionize alkali, alkaline-earth and rare-earth elements that have a low ionization potential. We developed an ion source that could operate at 2300°C to obtain high ionization efficiency.

The low-pressure arc-discharge ion source (Fig.14-3(b)) is suitable for the ionization of gaseous elements, Kr and Xe, and volatile elements such as Sn, In, Ag and Cu. We built a heater to maintain a high-temperature of the uranium target on the ion source. This modification made it possible to efficiently transfer radioactive nuclei from the target to the ionization chamber.

Using these ion sources, 105 isotopes in 19 elements produced in the proton induced fission of uranium have been provided to the radioactive nuclei beam accelerator with maximum yield of 10^7 ions/s as shown in Fig.14-4. With these radioactive nuclei beams, advances are expected in the studies of synthesis of elements in the universe and structural analysis of materials.

Reference
Osa, A. et al., Ion Source Development for the On-line Isotope Separator at JAEA, Nuclear Instruments and Methods in Physics Research B, vol.266, issues 19-20, 2008, p.4394-4397, DOI: 10.1016/j.nimb.2008.05.063.

14-3 Study on Basic Properties for Establishment of a Fast Reactor Cycle System
–Melting Temperatures and Phase Diagram of MOX Fuel–

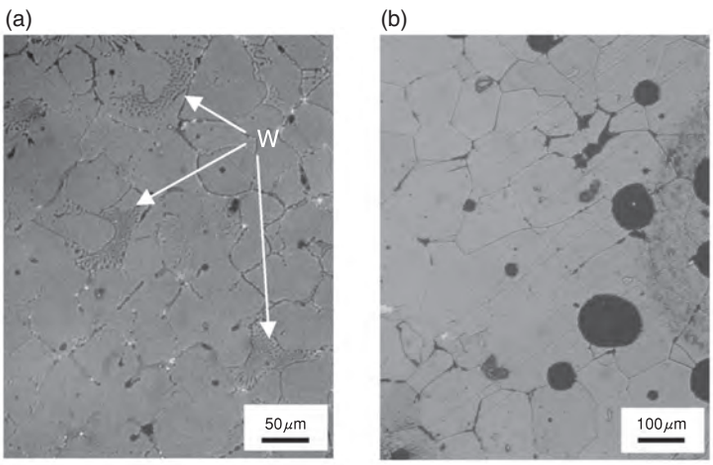

Fig.14-5 Microstructures of heated MOX with 40% Pu content
(a) The sample was encapsulated in W and heated to 2963K. Precipitates of W metal and Pu oxide were observed by electron probe micro analyses in the grain boundary.
(b) The sample was heated to 2978K using a W capsule with a Re inner. Grain growth was observed, and there was no trace of melting.

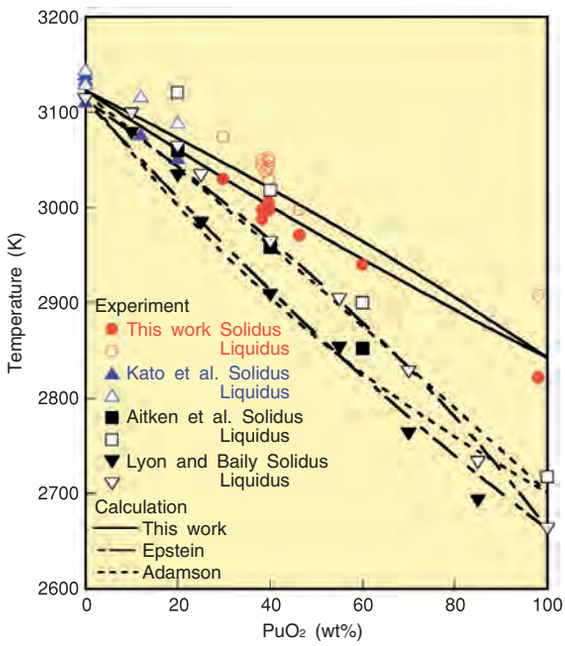

Fig.14-6 Solidus and liquidus temperatures in the UO_2-PuO_2 system

It is essential that nuclear fuels are operated in an undamaged condition during their entire lifetime. Therefore, the maximum temperature of the fuel is limited by the melting temperature of MOX.

JAEA has developed a fast reactor recycle technology. As a part of the development, the basic properties of uranium and plutonium mixed oxide (MOX) fuels that are used as fuel in the fast reactor have been studied. The melting temperature of MOX fuels was measured during the period of 1960-1970's as functions of Pu content and O/M ratio, and their phase diagram was evaluated. Unfortunately, analyses of the melted samples were not performed in those studies. As a result, the measured melting temperature of the actual compounds is unreliable.

In this study, the melting temperature was investigated by a new measurement technique using a W capsule with a Re inner. It was found that the previously obtained data was not correct, because a reaction between the sample and the W capsule material occurred and the compound which formed affected the melting. The melting temperature of MOX fuels was determined to be a function of the Pu content and O/M ratio, and the phase diagram of the UO_2-PuO_2 system was revised for the first time in about 40 years.

Fig.14-5 (a) and (b) show the microstructures of the heated MOX fuel with about 40% Pu content. The sample shown in Fig.14-5 (a) was encapsulated in W and heated to 2963K, which was the method used in the conventional melting temperature measurements. The sample was transformed into a block, and the precipitates of metallic W and Pu oxide were observed in the grain boundary. A reaction occurred when the MOX fuels contained more than 30% Pu.

The sample shown in Fig.14-5 (b) was heated to 2973K inside a W capsule with a Re inner. Grain growth was observed, but no traces of melting, such as deformation was seen. These observations show that the previously obtained data is not correct, and a reaction between the MOX and the W capsule material occurred and affected the melting measurements.

The melting temperature was determined by the thermal arrest method which was observed in the heating curve when a sample melted. Fig.14-6 shows the measurement results of solidus and liquidus temperatures which were measured by using the W capsule with a Re inner. The measurement results were evaluated by the ideal solution model, and the phase diagram of the UO_2-PuO_2 system was revised. The calculated results represented the experimental data with an accuracy of ±20K. It was found that the solidus temperatures of fast reactor MOX fuels were 50-100K higher than the existing data had shown.

Reference

Kato, M. et al., Solidus and Liquidus Temperatures in the UO_2-PuO_2 System, Journal of Nuclear Materials, vol.373, issues 1-3, 2008, p.237-245.

14-4 Basic Knowledge on Treating Various Wastes Generated from Pyro-Reprocessing
–Recovery of Actinides from Solid and Liquid Wastes–

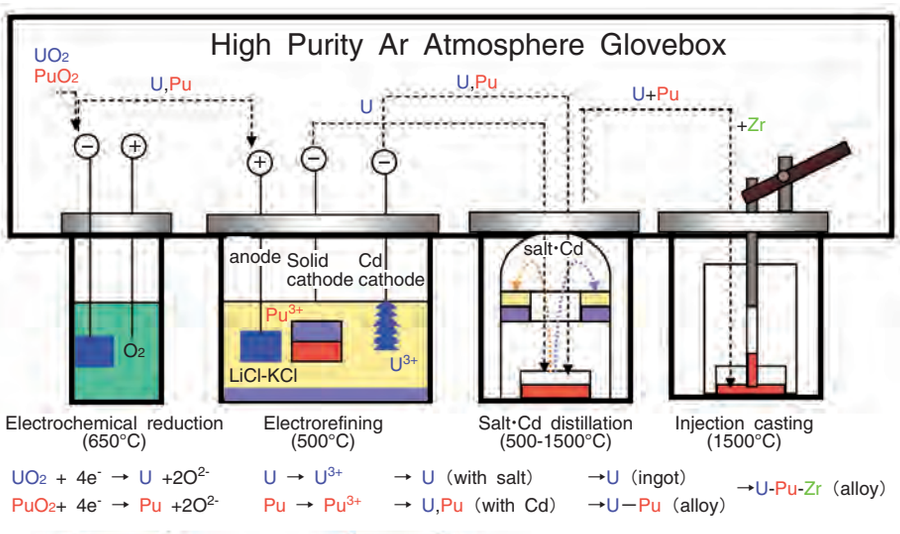

Fig.14-7 Outline of main pyro-reprocessing steps
Electrochemical reduction:
Oxide spent fuel is reduced to a metal form by the electrochemical procedure in the lithium chloride (LiCl) molten salt.
Electrorefining:
Uranium (U), and plutonium (Pu) were recovered by the electrochemical procedure in lithium chloride-potassium chloride (LiCl-KCl) eutectic molten salt for separating from fission products.
Distillation:
Removal of adhered salt and cadmium from a recovered U, Pu, and U-Pu metal ingot was obtained.
Injection casting:
Injection casting of U, Pu to form a metal fuel.

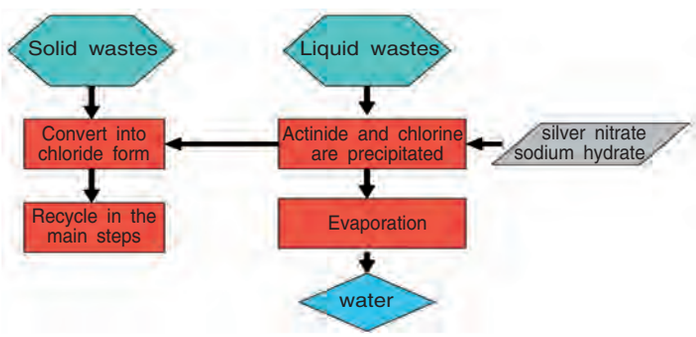

Fig.14-8 Flow chart of waste processing
Procedure for recycling of actinide from solid and liquid wastes in pyro-reprocessing.

The pyro-reprocessing (Fig.14-7) is one of the advanced technologies for the separation of actinide elements from spent nuclear fuel. The elements are electrochemically separated in a molten salt medium unlike the conventional aqueous-reprocessing, which is basically performed in nitric acid and an organic solvent medium. Since actinide elements are naturally recovered together in the pyro-reprocessing, this process has a superior resistance to the nuclear proliferation. Moreover, this process is expected to enhance the economical potential of nuclear fuel reprocessing, because the process itself is quite simple when compared to the conventional aqueous-reprocessing. Concerning the wastes from the pyro-reprocessing, some of the waste might contain significant amounts of actinide elements. It is believed that the recovery of these actinide elements enhances the potential of the pyro-reprocessing in regards to the efficient utilization of nuclear resources and reduction of environmental impact.

The actinide in the chemical formation such as oxide, which can not be treated in a normal process (Fig.14-7), is included in the solid wastes of the residue from the electrodes and sediments. On the other hand, the process operation of the pyro-reprocessing requires a chemical analysis in each step in order to control the process condition. Various liquid wastes containing actinide elements are generated from the analysis. A procedure is being developed to recycle the actinide elements from these wastes.

By conversion of the solid wastes to a chloride form, the actinide elements in the solid wastes can be put back into the pyro-reprocessing. The solid wastes was poured into a LiCl-KCl molten salt, which is the same mixture as the agents currently used in the electrolytic refining process, and a chlorination reagent (zirconium chloride) was gradually added to the LiCl-KCl molten salt. Most of actinide elements were successfully converted to a chloride form after sufficient reaction time (about 10 hours). As for the liquid wastes, the separation method by evaporation was investigated. The actinide elements were recovered as a residue. Since the liquid wastes contain chlorine which causes corrosion of equipments and harmful cadmium, it is necessary to prevent these substances from converting to water which is separated from the residue. These elements are removed by precipitation by using silver nitrate and sodium hydrate before the evaporation. The actinide elements in the residue are also converted to a chloride form as mentioned above.

We have not only been studying the main steps of pyro-reprocessing but also, the incidental technology such as waste treatment (Fig.14-8), in order to realize the pyro-reprocessing for the advanced nuclear reactor fuel. This study is being performed in the Chemical Processing Facility (CPF) in collaboration with Central Research Institute of the Electric Power Industry.

Reference

Nakayoshi, A. et al., Basic Knowledge on Treating Various Wastes Generated from Practical Operation of Metal Pyro-reprocessing, International Symposium on EcoTopia Science (ISETS07), Nagoya, Japan, 2007, p.1062-1066, in CD-ROM.

14-5 Development of Damage Reduction Technique on Mercury Target for the Spallation Neutron Source
–Visualization of the Bubble Formation Behavior in Mercury–

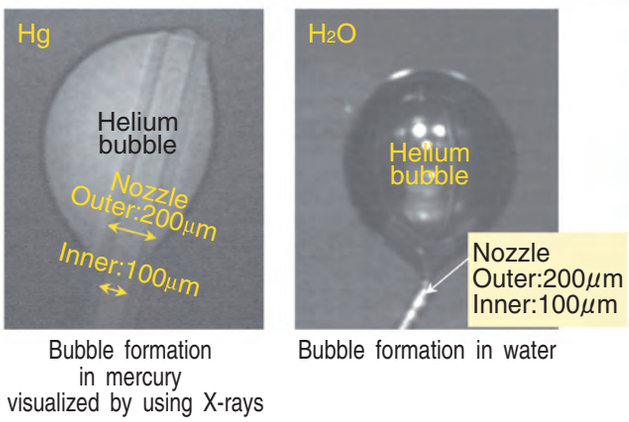

Fig.14-9 Visualization of Bubble Formation Behavior
The bubble formation behavior in opaque mercury was visualized by using high intensity X-rays. The bubble formed around the tip of the nozzle in mercury because of the poor wettability of the mercury while the bubble formed from the tip of the nozzle in water.

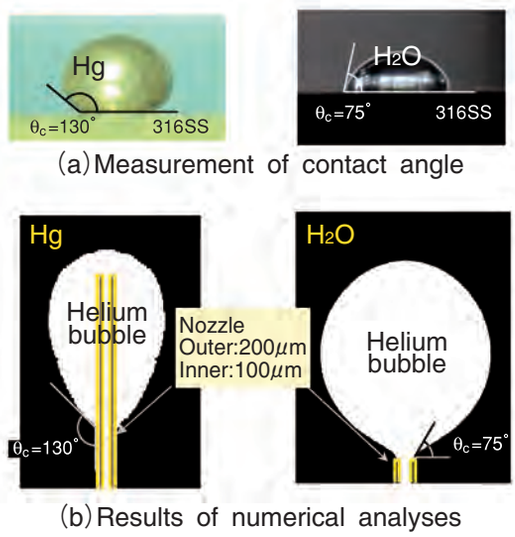

Fig.14-10 Measurement of Wettability and Prediction of Bubble Formation Behavior by Numerical analyses
Contact angles, θc, which are a parameter to express the wettability between the liquid and nozzle material were measured. The results of the numerical analyses clearly represented the visualizing test results by using the measured contact angles in the analyses.

In the materials and life science experimental facility of "J-PARC", innovative sciences in the materials and life science fields will be developed by using high intensity neutrons from a MW-class spallation neutron source. Liquid mercury is used as the target material to produce neutrons by the spallation reaction from a viewpoint of heat removal. However, pitting damage degrades the target structural material, which is caused by pressure waves generated in rapid heating while the proton beam bombards the mercury. To improve the endurance of the mercury target and to use it under a high power proton beam, it is essential to reduce the pressure waves which cause the pitting damage. We aimed for a technique that would reduce the pressure wave by injecting helium gas bubbles into the mercury, because the gas bubbles act as a cushion.

It was predicted that the pressure wave would be reduced by half by injecting 0.1 Vol.% of tiny bubbles of 100 μm in diameter (microbubbles). The reduction mechanism of the pitting damage by the injection of microbubbles is being considered in corporation with CCSE.

To understand the bubble formation behavior in mercury and to develop the technique for injecting the microbubbles into mercury, we tried visualizing bubble formation behavior in opaque mercury by using X-rays. Although it was difficult to visualize the behavior clearly because the absorption rate of the X-rays is high in mercury, the visualization of the bubble formation behavior was successful by increasing the transmission of X-rays using high intensity X-rays in "SPring-8", and optimizing the thickness of the mercury. Fig.14-9 shows the bubble formation behavior while helium gas was injected into stagnant mercury from a narrow nozzle (inner diameter: 100 μm, outer diameter: 200 μm) when compared with the case in water. In water, the bubble formed from the tip of the nozzle, but in mercury, the helium gas flows to the boundary between the mercury and the nozzle wall because of the poor wettability of the mercury as shown in Fig.14-10 (a), and the bubble formed around the tip of the nozzle.

The numerical analysis became a useful tool to predict the bubble formation behavior in opaque mercury. It was confirmed that the numerical analysis represented the visualized results by considering contact angle, which is a parameter to express the wettability as shown in Fig.14-10.

Hereafter, a bubble injecting device to apply the practical mercury target will be considered to improve the endurance of the mercury target.

Reference
Kogawa, H. et al., Effect of Wettabitlity on Bubble Formation at Gas Nozzle under Stagnant Condition, Journal of Nuclear Materials, vol.377, issue 1, 2008, p.189-194.

14-6 Measuring Displacement and Vibration of High Temperature and High Radiation Components Using Optical Fiber
–Development of Fast Reactor Integrity Monitoring Technology–

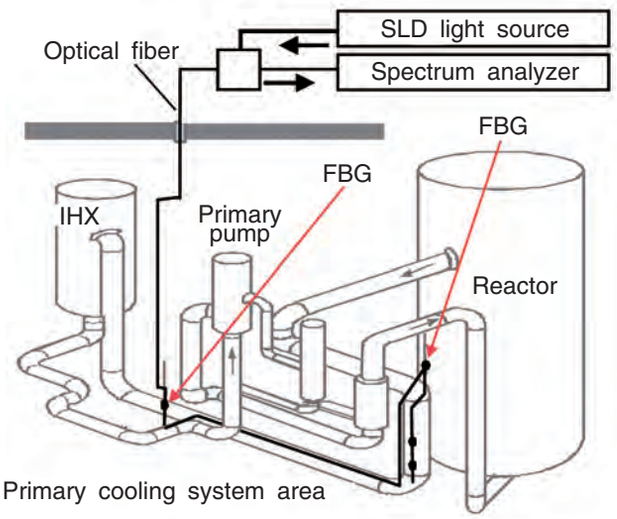

Fig.14-11 Experimental setup of measurement system using optical fiber in the "JOYO" primary cooling area
A few FBGs were combined into a single fiber, and mounted on the piping supports. In the measurement, a wideband light was injected into the optical fiber, and then the wavelength of reflected light from FBGs was scanned with a spectrum analyzer.

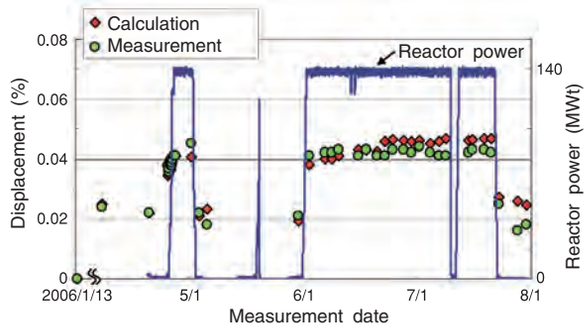

Fig.14-12 Measured displacement of the piping support by FBG
Displacement following reactor power was successfully measured.

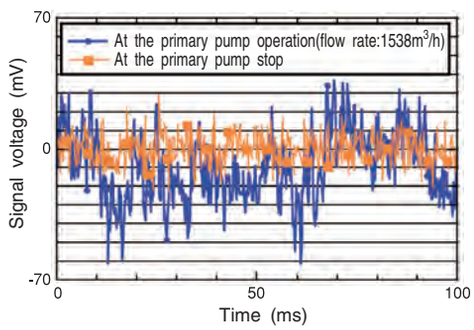

Fig.14-13 Measured vibration of the piping support by FBG
Vibration changes with the primary pump operation were successfully measured.

In the sodium-cooled fast reactor (SFR), circulating pumps and several piping support systems were installed around the primary cooling system piping. How to efficiently and accurately measure the displacement and vibration in high temperature and high radiation components is important, in order to monitor the SFR structural integrity. In the experimental fast reactor "JOYO", displacement and vibration measurements of the primary cooling system were carried out using Fiber Bragg Grating (FBG) to resolve this challenging issue (Fig.14-11).

FBG is an optical fiber sensor, which reflects light at a specific wavelength. Temperature variations or displacement applied to the FBG causes the reflected wavelength to shift. The FBG is a simple instrument, because several FBGs can be combined in a single fiber.

Displacement can be evaluated from a wavelength shift $\Delta\lambda_1$ of the FBG with both-ends fixed. However, $\Delta\lambda_1$ includes a wavelength shift $\Delta\lambda_2$ due to temperature variation. This becomes to be a source of displacement measurement error. Therefore, $\Delta\lambda_2$ of an FBG with one end fixed for detecting only temperature variation was eliminated from $\Delta\lambda_1$. The measured displacement matched the calculation based on the thermal expansion. The measured result indicates that thermal displacement of a piping support was accurately measured (Fig.14-12).

Vibration can be measured as a high frequency displacement. A faster vibration, however, cannot be measured by a spectrum analyzer, because its sampling time is in the order of seconds. In the measurement, the reflected wavelength shift was converted into light magnitude using an optical filter, and then the voltage signal corresponding to the displacement was obtained using a photo diode. This enables a high speed measurement of the vibration. Signal fluctuation at the primary pump operation was larger than when the pump was stopped. The measured result indicates that vibration due to the pump operation was successfully measured (Fig.14-13).

The measurements were successfully conducted with no degradation of the optical fiber up to an accumulated γ-ray dose of 4×10^4Gy, corresponding to 120 effective full power days of operation. The measured results demonstrated that the FBG is suitable for the monitoring of the SFR structural integrity.

Reference
Matsuba, K., Ito, C. et al., Development of Fast Reactor Structural Integrity Monitoring Technology Using Optical Fiber Sensors, Journal of Power and Energy Systems, vol.2, no.2, 2008, p.545-556.

14-7 Material Research for Transmutation of LLFP in a Fast Reactor
–Irradiation Test of $^{11}B_4C$ as a Neutron Moderator–

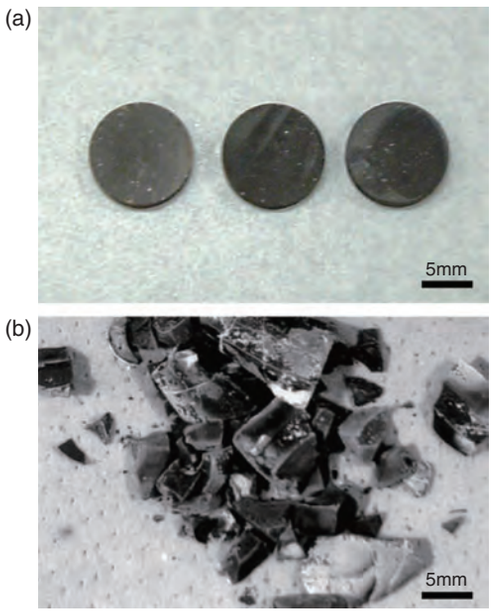

Fig.14-14 Appearance of (a) Irradiated $^{11}B_4C$ and (b) $^{10}B_4C$ at around 500°C
An irradiated $^{10}B_4C$ pellet was broken, and the $^{11}B_4C$ pellet kept the same shape as before being irradiated.

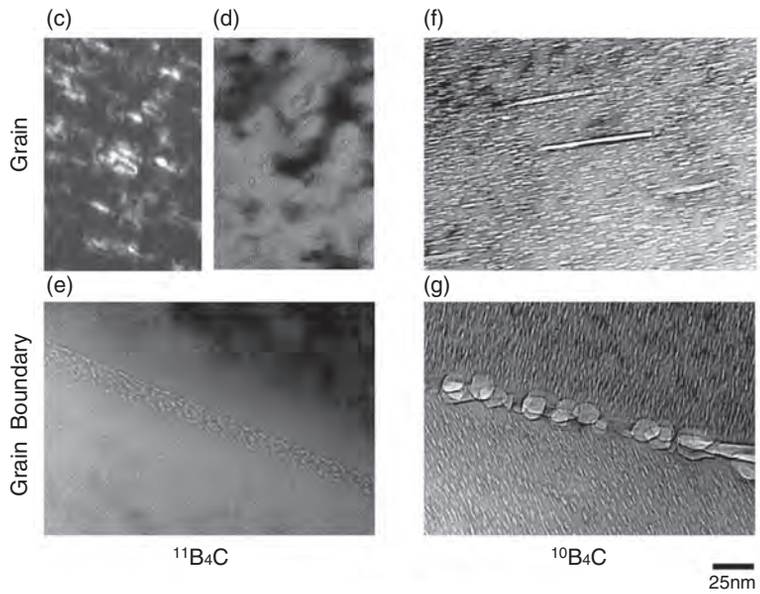

Fig.14-15 Microstructure of irradiated $^{11}B_4C$ and $^{10}B_4C$
Irradiation defects in $^{11}B_4C$ microstructures. Micro dislocation loops (c), bubbles (d). Small helium bubbles (e) were gathering in the grain boundary of $^{11}B_4C$. Helium (He) bubbles (f) were gathering in high density on the grain in $^{10}B_4C$. Large bubbles (g) grew around grain boundaries in $^{10}B_4C$.

It is difficult to store high level waste that contains long-lived fission products (LLFP). Transmutation of LLFP, which changes them into short lived or stable nuclides, is a solution. Thermal reactors are efficient for LLFP transmutation, but fast reactors also have possibilities for it by modifying a fast neutron into a thermal neutron. $^{11}B_4C$ was fabricated from concentrating ^{11}B in natural boron carbide. Both hydride and $^{11}B_4C$ are candidates to be moderators. It is possible to raise the efficiency by loading LLFP as a target with the moderator, in order to transmute LLFP in the fast reactor. The slow-down power of $^{11}B_4C$ is lower than hydride. $^{11}B_4C$ has an advantage in the thermal design, because the boron carbide has been stabilized to the melting point chemically, while the hydride dissociates the hydrogen when it reaches a high temperature.

Hydride and $^{11}B_4C$ were irradiated in Phenix, a fast reactor in France. We have many irradiation experiences with $^{10}B_4C$ as an absorber material. $^{10}B_4C$ was fabricated from concentrating ^{10}B. He was produced by a ^{10}B (n, α) ^{7}Li reaction. A B_4C pellet was sintered for irradiation. The He stored in it and changed into He bubbles. These bubbles caused the pellets to crack, which is a bad effect for materials stability. The volume of He generated in $^{11}B_4C$ was expected to be about 1/100 in comparison with that in $^{10}B_4C$.

In this study, $^{11}B_4C$ was irradiated at 530°C to 1.9×10^{26} n/m^2 (E>0.1 MeV), and $^{10}B_4C$ was irradiated at 800-900°C to 3.1×10^{26} n/m^2 (E>0.1 MeV). Afterwards, a post irradiation experiment was performed. The $^{10}B_4C$ pellet was difficult to be divided around 700-800°C. Then, the $^{11}B_4C$ was specially irradiated at 530°C. The irradiated sample became very brittle. Therefore, a test piece of irradiated $^{11}B_4C$ was prepared by ion-milling method in full detail.

In Fig.14-14, the appearance of $^{11}B_4C$ and $^{11}B_4C$ after irradiation is shown. In Fig.14-15, the microstructure of $^{11}B_4C$ and $^{10}B_4C$ after irradiation is shown. In the $^{11}B_4C$ grain, large bubbles of a high-density were observed compared to $^{10}B_4C$. In the grain boundary, additional large bubbles were observed in the grain. It was considered that in the $^{11}B_4C$, the growth of the bubble was slow, and the nucleation frequency is also low. From the observation results, it was confirmed that $^{11}B_4C$ was stable under the moderator service conditions. In the future, a more detailed microstructure observation will be performed.

Reference
Donomae, T. et al., Neutron Irradiation Effects on $^{11}B_4C$ and Recovery by Annealing, Nippon Seramikkusu Kyokai Gakujutsu Ronbunshi, vol.115, no.1345, 2007, p.551-555 (in Japanese).

14-8 Contribution to "ITER" by Technical Development of Post Irradiation Examinations
–Remote-Handling Type Welding / Processing Techniques for Irradiated Materials–

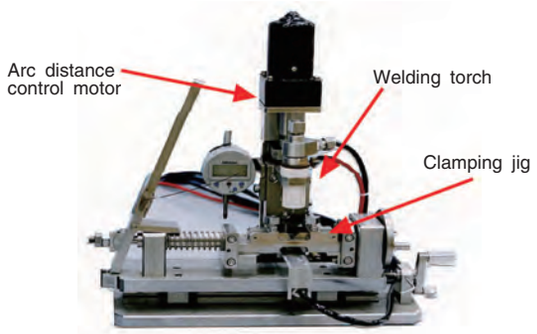

(a) TIG-welding machine
By using a manipulator for remote-handling, it is easy to clamp the specimens onto the welding machine, to adjust the welding position and to adjust the gap distance between the torch and the specimen.
A narrow heat affect zone (HAZ) in the welded specimen can be achieved by a clamping jig with high thermal conductivity.

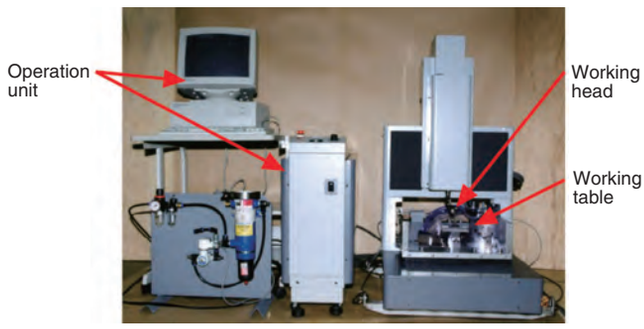

(b) Processing machine
By using a manipulator for remote-handling, it is easy to fix the specimen onto the remote-controlled NC lathe. This machine warrants the high accuracy of processing, the same as the out of the hot cell processing.

Fig.14-16 Technical development of a remote-handling type welding/processing machines

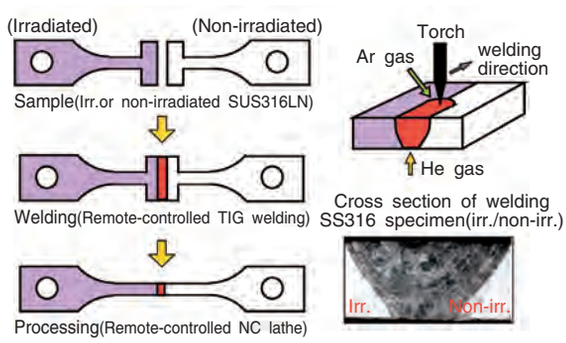

Fig.14-17 Welding/processing procedures for fabrication of test specimens
The weldment specimen was fabricated from irradiated and non-irradiated specimens by remotely handled welding/processing machines in a hot cell. The plate type specimen with a tab was chosen, and the conditions for welding and processing were determined. By applying this technique, data can be obtained from the specimens after re-irradiation.

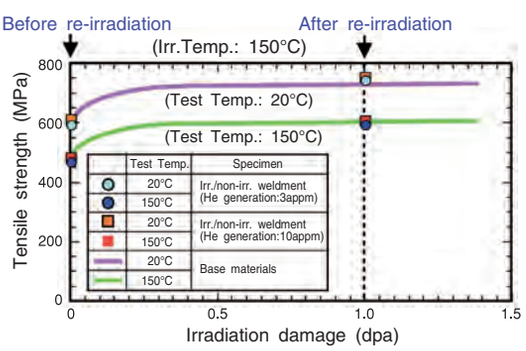

Fig.14-18 Neutron irradiation test results of welding material before and after irradiation
Neutron re-irradiation tests on SS316LN weldment specimens, joined with irradiated and non-irradiated materials, were performed. From the results of a mechanical property test, it was clarified that the tensile strength of the weldment specimens is the same as that of the base materials.

For maintenance and/or replacement of the fusion blanket, new cooling pipes for the blanket will be joined by welding to the existing cooling pipes irradiated by high energy neutrons. Therefore, it is necessary to evaluate the effect of helium generation by neutron irradiation on the mechanical properties of the weldment. In this study, all the work from the welding and processing of test specimens, to the installation of the specimens into the irradiation capsule, were performed in the hot cell by remote handling. Therefore, the remote-handling welding/processing machines, and the assembling procedure of the irradiation capsules were developed based on the experiences of the post irradiation examinations in the Japan Materials Testing Reactor (JMTR) hot laboratory.

The remote-handling type Tungsten inert gas (TIG) welding machine (Fig.14-16 (a)) was developed. In order to evaluate the mechanical properties of the weldment correctly, a plate with a tab where the crater part is able to be removed, was adopted as the shape of the test specimens. On the other hand, the processing machine (Fig.14-16 (b)) with the end-milling type numerical control (NC) lathe was developed. It is possible to fabricate the weldment specimens with high accuracy in dimensions to within 50 μm. These developments for remote-handling techniques enabled a systematic evaluation on the mechanical properties of weldment specimens with irradiated and non-irradiated materials.

Using austenitic stainless steel SS316-LN-IG (IG means "ITER" grade) irradiated up to the "ITER" irradiation conditions in "JMTR", the TIG welding between the irradiated and non-irradiated materials was tested in a hot cell (Fig.14-17). From the test results, it was obvious that the sealed gas and the welding heat affected the welding, as there were defects such as, a crack on the surface and the cross section of weldment, an undercut and insufficient welding. Especially, it was found that when the welding heat input was about 1 to 2 kJ/cm, a good weldment specimen without cracks could be obtained. Furthermore, their welding test specimens were processed as tensile-type weldment specimens, and they were installed onto the irradiation capsule in the hot cell. The neutron re-irradiation test was successful in "JMTR", and the mechanical properties of a re-irradiated weldment was obtained for the first time in the world (Fig.14-18).

Reference

Tsuchiya, K. et al., Effect of Re-irradiation by Neutrons on Mechanical Properties of Un-irradiated/Irradiated SS316LN Weldments, Journal of Nuclear Materials, vol.373, 2008, p.212-216.

14-9 Correlation between the Charge-State and Structure of Fragment Ions for Swift C_3^+ Traversing a Thin Foil
–Study on Interaction between a MeV Cluster Ion and a Matter–

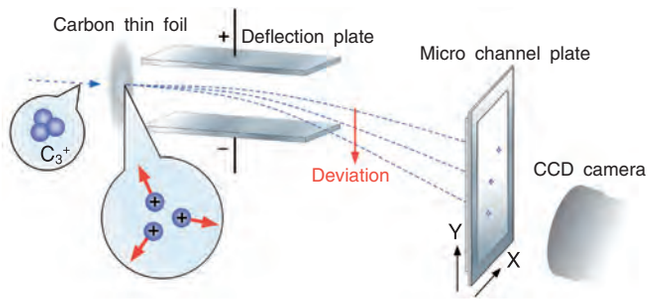

Fig.14-19 Apparatus for simultaneous measurement of charge-state and spatial pattern of a cluster ion
At impingement of a swift cluster ion on a thin foil, its valance electrons are stripped away in a short time, and a rapid explosion process is initiated subsequently by a Coulomb repulsion, which provides a snap-shot of the position of the nuclei in the incident cluster ion. The charge-state of each fragment ion is determined by the position on the MCP, on the basis of the deflected angle relevant to the charge depending mainly on an electrostatic field of the deflection plates.

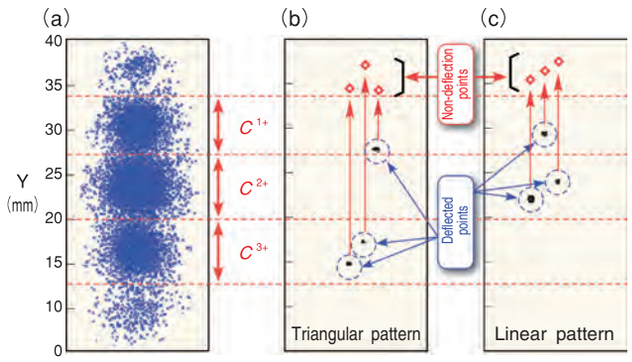

Fig.14-20 Two patterns of correlation of the deflected points and the non-deflection points
The charge-state of each deflected point is identified by the relation between its position and charge distribution on the MCP, as shown in (a). The instance of pattern (b) and (c) shows an almost equilateral triangular pattern and a linear-chain pattern with almost regular intervals, respectively. The blue round symbol shows the original pattern before deflection.

Table14-1 Average charges of the fragment ions arising from the dissociation of a C_3^+ cluster ion passing through a thin carbon foil, estimated experimentally and theoretically

Comparison of cluster structure			Comparison of atomic-position in a liner-chain pattern		
	Linear	Triangle		Center	Edge
Expt.	1.96±0.03	1.89±0.02	Expt.	1.86±0.04	2.01±0.03
Calc.	1.91	1.89	Calc.	1.88	1.93

Studies on material science and biotechnology for various ion beams with an energy ranging from 30 keV to hundreds of MeV are in progress in the Takasaki advanced radiation research institute. Understanding the interaction between an incident ion and a target is indispensable for selection of suitable experimental conditions, i.e., an incident ion species, its energy, and a target, and analyses of experimental results. The interaction for irradiation with mono-atomic ion has been investigated from the early days, and some models have succeeded in explaining most of experimental results. However, various strange phenomena out of such models have been observed for irradiation with a swift cluster ion consisting of a number of atoms for example, secondary-ion or secondary-electron emission.

When a swift cluster ion impinges on a matter, a lot of atoms are brought into a very small volume simultaneously therefore, vicinal fragment ions interact with each other even after the dissociation of the cluster. In this process, a spatial pattern of the cluster constituents could affect their interactions with a matter. The effect of the spatial pattern on charge-state distribution of fragment ions arising from the dissociation of a cluster passing through a thin foil was investigated, to make a new model for the interaction between a cluster ion and a matter.

A new apparatus as shown in Fig.14-19, was developed for the investigation. Ions emerging from a thin carbon foil deflected depending on their charge-state by an electrostatic deflector placed between the foil and a micro channel plate (MCP). A two-dimensional pattern of the deflected ions was observed as luminance points on a fluorescent screen equipped with the MCP. The apparatus enables us to measure the charge-state of each fragment ion of a cluster ion and their spatial pattern, just after emerging from the foil simultaneously, as shown in Fig.14-20. The charge-state distribution of fragment ions of a 3-MeV C_3^+ was measured for different patterns, i.e., a linear-chain pattern and an equilateral triangular pattern after emerging from the foil.

The results are summarized in Table14-1. The cluster average charge obtained for the liner-chain pattern is larger than that for the triangular pattern, and the average charge of two edge-position ions in a liner-chain pattern is larger than that of the middle-position ion. The theoretical average charge of the fragment ions of a C_3^+ ion was calculated considering the effect of the nuclear charge of the other neighboring fragments on the binding energy of the valence electrons, and the spatial pattern of the fragments, a repulsive Coulomb force among the fragment ions, a wake force induced by each fragment and etc., were taken into account in the calculation. The obtained average charges are qualitatively consistent with the experimental results as shown in Table14-1.

Although the measurement of the charge-state distribution of fragment ions have been done by other researchers so far, this is the first time measurements were performed by classifying the special pattern of the fragment ions. The interaction between a swift cluster ion and a matter correlates with the spatial pattern of the constituents in a cluster, which should be demonstrated as one of the most characteristic of the cluster-matter interaction.

Reference

Chiba, A. et al., Average Charge and Its Structure Dependence of Fragment Ions under Irradiation of a Thin Carbon Foil with a 1-MeV/atom C_3^+ Cluster Ion, Physical Review A, vol.76, 2007, p.063201-1-063201-6, DOI:10.1103/PhysRevA.76.063201.

14-10 Reduction of Water Inflow for Continuation of Deep Shaft Excavation

–Development of Grouting Technology at the "Mizunami Underground Research Laboratory"–

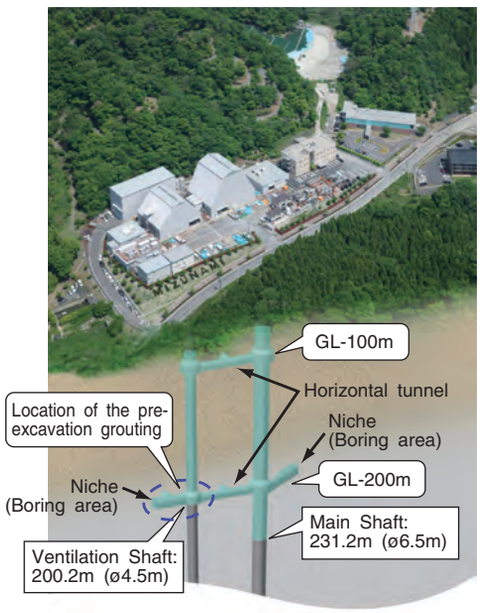

Fig.14-21 Image of the "Mizunami Underground Research Laboratory"
Depth of shafts as of March 15 2008.

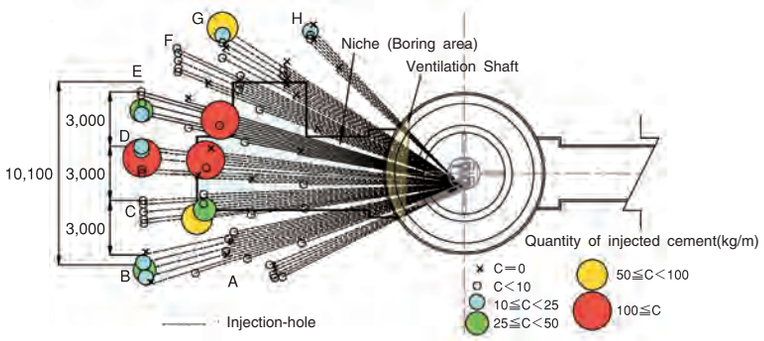

Fig.14-22 Quantity of injected cement per unit length of the pre-excavation grouting at the Ventilation Shaft niche (boring area)
At the end of the Ventilation Shaft niche (boring area), the excavation confirmed a large volume of injected cement.

Fig.14-23 Photograph of cement filled fractures
Red arrow shows cement filled fractures.

The "Mizunami Underground Research Laboratory" (MIU), one of the main facilities in Japan for research and development of the technology for high-level radioactive waste disposal, is being constructed in Mizunami City. Excavation of shafts and galleries is being done to confirm the results of the predictions made in the surface-based investigation phase. As of March, 2008, the excavation of the Main and Ventilation Shafts had reached GL-231.2m and -200.2m (below ground level) (Fig.14-21). Optimization of the costs for treatment of the groundwater as well as reduction of the inflow water volume was required for continuing the MIU excavations. In planning the excavation of the shafts and tunnels below about GL-180m, it was necessary to get more reliable information on the conditions in terms of the rock mass stability and hydrogeology. Therefore, pilot borehole investigations were conducted from the bottom of the shafts. The results indicated that large water inflow could be expected during the excavation around the Ventilation Shaft and the Ventilation Shaft niche (boring area) at GL-200m. In order to reduce the drilling time, procedures for grout injection-hole drilling incorporated the use of a shaft jumbo (blast hole drilling rig) instead of a conventional borehole drill rig. This is one of the engineering techniques tried in the development of the construction procedures. As a result, it was possible for grouting to be accomplished within the planned excavation cycle. The two shafts were extended to GL-200m followed by pre-excavation grouting of the rock mass around the Ventilation Shaft and the planned Ventilation Shaft niche (Fig.14-21). Then, horizontal tunnels were excavated at that level. The pre-excavation grouting around the Ventilation Shaft niche is shown in Fig.14-22.

After the pre-excavation grouting and tunnel excavation, geological mapping was performed to determine the location and extent of the grout penetration. The geological mapping of the tunnels and walls confirmed the successful injection of a large volume of cement into the fractures. An example of a cement filled fracture in the Ventilation Shaft niche is shown in Fig.14-23. The inflow of water through the grouted rock mass was quite small. In areas with a large volume of injected cement, the inflow of water during the excavation was minimal. The grouting procedure using a shaft jumbo for drilling also resulted in a 6% decrease in the excavation cycle time, compared with the use of a conventional boring machine. Constant injection pressure during the last step in the grouting injection cycle prevented cement backflow from the fractures. Pre-excavation grouting will be the standard method for reducing the inflow of water. In this way, construction of the MIU can proceed, while minimizing the cost of water treatment by reducing the inflow of water.

Reference

Kuji, M., Hara, M., Minamide, K., Takeuchi, S., Mikake, S. et al., Pre-excavation Grouting for Reduction of Water Inflow into a Deep Shaft, Proceedings of the 37th Symposium on Rock Mechanics, Dai-37-Kai Ganban Rikigaku Ni Kansuru Shimpojiumu Koen Rombunshu, Tokyo, Japan, 2008, p.251-256, in CD-ROM (in Japanese).

14-11 To Accomplish Decommissioning of Uranium Enrichment Plant Safely and Economically
–System Treatment Chemical Decontamination Technology by Fluoride Gas–

(a) Uranium enrichment plant

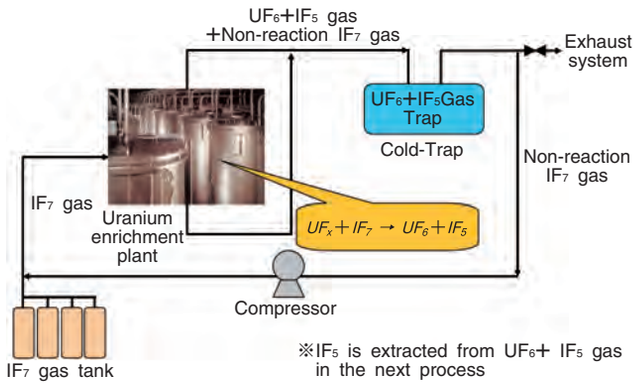

(b) Decontamination method

Fig.14-24 Outline of system treatment chemical decontamination technology

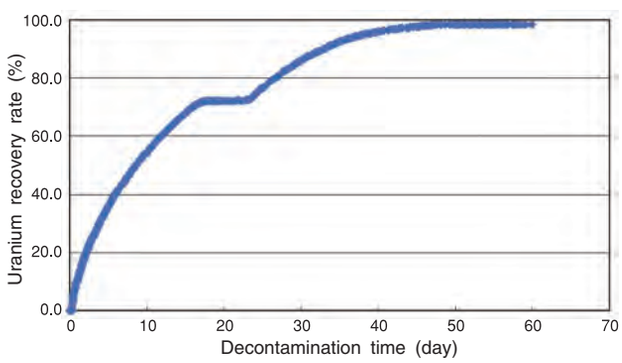

(c) Uranium recovery progress

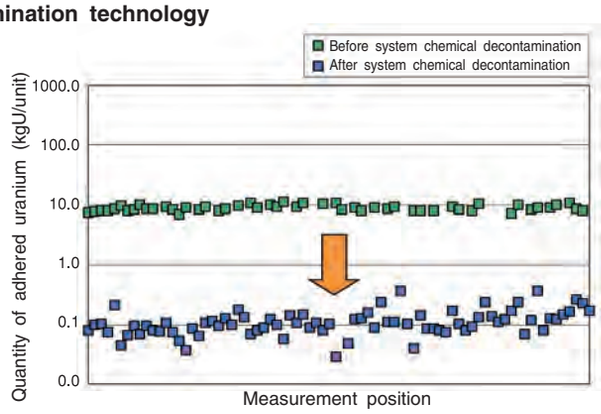

(d) Quantity of adhered uranium

Fig.14-25 Results of system treatment chemical decontamination

The Ningyo-toge Environmental Engineering Center is now entering into the decommissioning stage of the plant. This center has a gas centrifuge uranium enrichment plant, which produced the enriched uranium by supplying Uranium Hexafluoride (UF_6) gas into the cascade for about 10 years. As a result, the uranium compounds have adhered in the equipments of the plant.

Therefore, we have developed the decontamination technology for uranium enrichment plants. The basic policy for this development is to decontaminate equipments in the plant to a level below the clearance level (assumed clearance level: 0.1 Bq/g).

Our decontamination method is performed by the combination of two technologies as follows:

- System treatment chemical decontamination technology
- Sulfuric acid immersing decontamination technology

These are new technologies, and the knowledge has not yet been reported. However, we could reveal that these technologies have a very high decontamination performance through our development.

In this paper, the system treatment chemical decontamination technology is explained.

The main uranium compounds in the uranium enrichment plant are estimated to UF_X ($4 \leq X \leq 5$). We decontaminate the uranium compounds by supplying Iodine Heptafluoride (IF_7) gas into the plant because the UF_X ($4 \leq X \leq 5$) is changed to UF_6 gas and Iodine Pentafluoride (IF_5) gas, by the chemical reaction such as in equation (1). (Fig.14-24)

$$UF_X(s)+IF_7(g) \rightarrow UF_6(g)+IF_5(g) \cdots\cdots\cdots\cdots(1)$$

After the basic experiment, the decontamination of the actual uranium enrichment plant in our center was performed. The following results were obtained.

- Decontamination time was about 60 days.
- About 99% of the uranium compounds in the plant could recovered. (Fig.14-25 (c))
- Average of decontamination level was about 1.0 Bq/g. (Fig.14-25 (d))

As a result, we confirmed that the system treatment chemical decontamination has a very high performance. Therefore, we could obtain the prospect that equipments of the plant are decontaminated below the clearance level by using a combination of the system treatment chemical decontamination technology, and sulfuric acid immersing decontamination technology.

In a few years, the system treatment chemical decontamination technology we have developed will be moved to the uranium enrichment plant of private company's.

Reference

Ema, A. et al., Technology Development of System Chemical Decontamination Using Iodine Heptafluoride Gas -Evaluation of IF_7 Treatment Condition and Uranium Decontamination Result-, JAEA-Technology 2008-037, 2008, 50p. (in Japanese).

14-12 High Precision Measurement of Dissolved Organic Radiocarbon in Seawater

–Development of a Pretreatment Method for AMS Measurement of Dissolved Organic Radiocarbon–

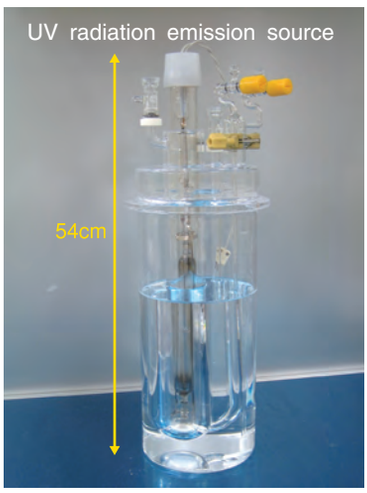

Fig.14-26 DOM oxidation reaction vessel
Four liters of seawater was irradiated with UV radiation, and DOM was oxidized to produce CO_2 in this reaction vessel. The UV lamp is located in the center. During the irradiation, the apparatus is placed in a stainless steel box for ultraviolet shielding.

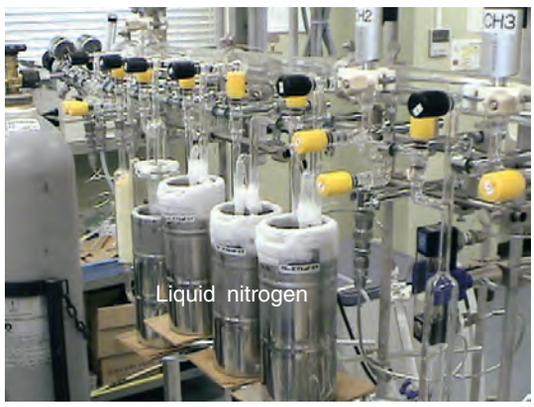

Fig.14-27 CO_2 purification glass line
This is the glass line used to collect and purify the CO_2 emitted from the ultraviolet irradiation step. Liquid nitrogen is used to collect the CO_2.

	Recovery efficiency (%)	pM (%)
1	98	79.3
2	96	78.5
3	98	78.0
4	99	77.4
Mean	98	78.3±0.8

Table14-2 Experimental precision testing using surface seawater
These experiments used surface seawater with a DOM carbon concentration of 64 μM. The recovery efficiency was calculated by the DOM concentration recovered using the method established by this study and 64 μM. pM(%) refers to the proportion of ^{14}C in the sample, if ^{14}C of 1950 is used as the standard (100%).

An Accelerator Mass Spectrometry (AMS) can measure extremely small amounts of long half-life radionuclides with high sensitivity and high precision. An AMS system with the ability to measure radiocarbon (^{14}C) and radioiodine (^{129}I) has been installed in the Mutsu Office of the Aomori Research and Development Center. The characteristics of AMS allow it to be used not only in fields closely related to nuclear power, such as for environmental radiation measurements, but also in various fields such as earth sciences and archaeology.

In recent years, global warming has become a serious problem and a more accurate understanding of the earth's carbon cycle is being sought. Because ^{14}C (half-life 5,730 years) can serve as a time-scale index for this carbon cycle, it can be said that ^{14}C measurements using AMS and building a global scale ^{14}C database is the key to resolving the carbon cycle mechanism. The organic matter fixed by photosynthesis from atmospheric carbon dioxide (CO_2) plays an important role in the carbon cycle. However, ^{14}C research on the portion of organic matter that is in the form of dissolved organic matter (DOM) in seawater has been extremely small compared to ^{14}C research on terrestrial organic matter or particulate organic matter in seawater. This is because the experimental techniques required to measure ^{14}C in DOM in seawater are difficult, as great effort is required for shipboard filtering of large amounts of seawater (4 ℓ), and from samples that contain a salinity more than 10,000 times the concentration of DOM, it is difficult to extract the carbon only for the ^{14}C measurements. Particularly for the ocean around Japan, there are no examples of research. DOM in seawater accounts for about 20% of the organic matter on the earth's surface and more than 90% of the organic matter in the ocean. In terms of carbon, this amount rivals that of atmospheric CO_2. Therefore, it is extremely important when considering the carbon cycle on the surface of the earth. Therefore, there is a great interest from this perspective in the development of AMS measurement methods for ^{14}C in seawater DOM.

To resolve these issues, we have established a method to decompose DOM using ultraviolet (UV) irradiation that can be used with high salinity samples and have combined that with AMS. The two-step decomposition method involves first irradiating DOM samples with UV to produce CO_2 (Fig.14-26) that is then collected and purified (Fig.14-27). Our study of the UV irradiation time enabled the recovery efficiency to exceed 96%. Improvements to the reaction vessel and glass lines allowed exclusion of all CO_2 other than that from the sample, and we were successful in reducing contamination to less than 1% of the sample (world's highest standard). When standard samples of organic matter were decomposed using this method, the results for ^{14}C measurement using AMS had a precision of 0.2% (n = 10). These results mean that it is possible to measure the time scale for DOM with a small measurement error of a decade or so. Experiments with actual seawater showed that an adequate recovery efficiency (98%) was obtained (Table 14-2). Furthermore, for DOM in seawater (oldest samples being about 6,000 years old) that has a low ^{14}C compared to other environmental samples, it was verified that a highly replicable result (0.8%: a period of about 80 years) was obtained.

As DOM affects (and is affected by) all biological activities on the earth, there is interest in this method from researchers in many fields. Measurement of ^{14}C in DOM using this system in addition to contributing to the correct understanding of global warming, may also contribute to fundamental research on next generation resource utilization and environmental forecasting.

Reference

Tanaka, T. et al., Development of Analysis System of Dissolved Organic Radiocarbon and Study on Its Circulation in Sea Water, JAEA-Conf 2008-003, 2008, p.71-74 (in Japanese).

R&D Centers of JAEA

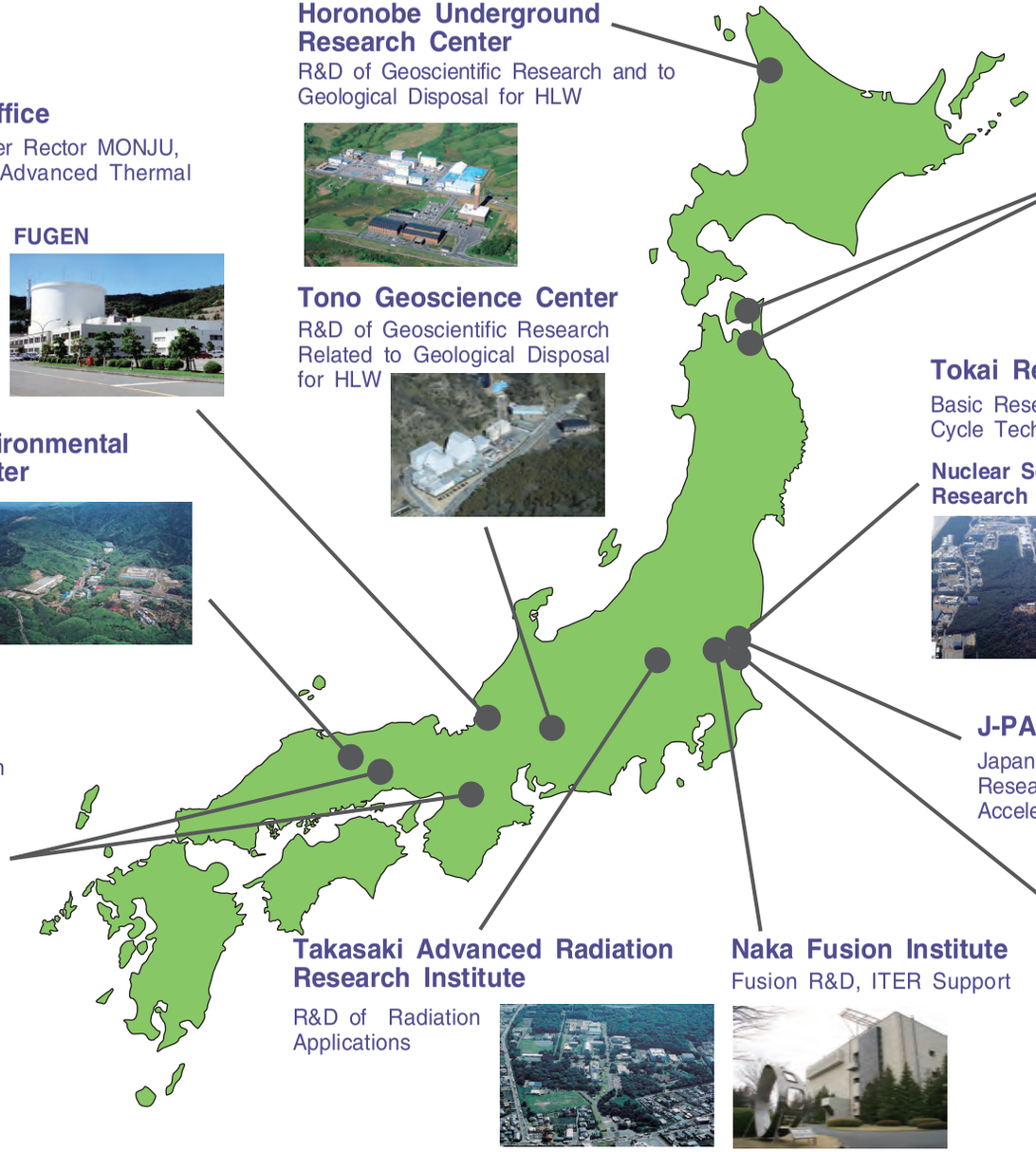

Horonobe Underground Research Center

R&D of Geoscientific Research and to Geological Disposal for HLW

Aomori Research and Development Center

Broader Approach Project, Support for Nuclear Fuel Cycle Business, Decommissioning of Nuclear Ship

Tsuruga Head Office

Prototype Fast Breeder Rector MONJU, Decommissioning of Advanced Thermal Reactor FUGEN

MONJU

FUGEN

Tono Geoscience Center

R&D of Geoscientific Research Related to Geological Disposal for HLW

Ningyo-toge Environmental Engineering Center

Decommissioning of Uranium Enrichment Plants

Tokai Research and Development Center

Basic Research, Safety Studies, Neutron Science, Nuclear Fuel-Cycle Technologies, Rad-Waste Management and Disposal, etc.

Nuclear Science Research Institute

Nuclear Fuel Cycle Engineering Laboratories

Kansai Photon Science Institute

Photon & Synchrotron Radiation Science

J-PARC Center

Japan Proton Accelerators Research Complex, Accelerators and Science

Takasaki Advanced Radiation Research Institute

R&D of Radiation Applications

Naka Fusion Institute

Fusion R&D, ITER Support

Oarai Research and Development Center

Experimental Reactors; JMTR, JOYO, and HTTR, R&D of FBR Cycle System Technology, Irradiation Test Technology, High Temperature Gas Reactor and Hydrogen Production Technology

Japan Atomic Energy Agency —Outline of Organization—

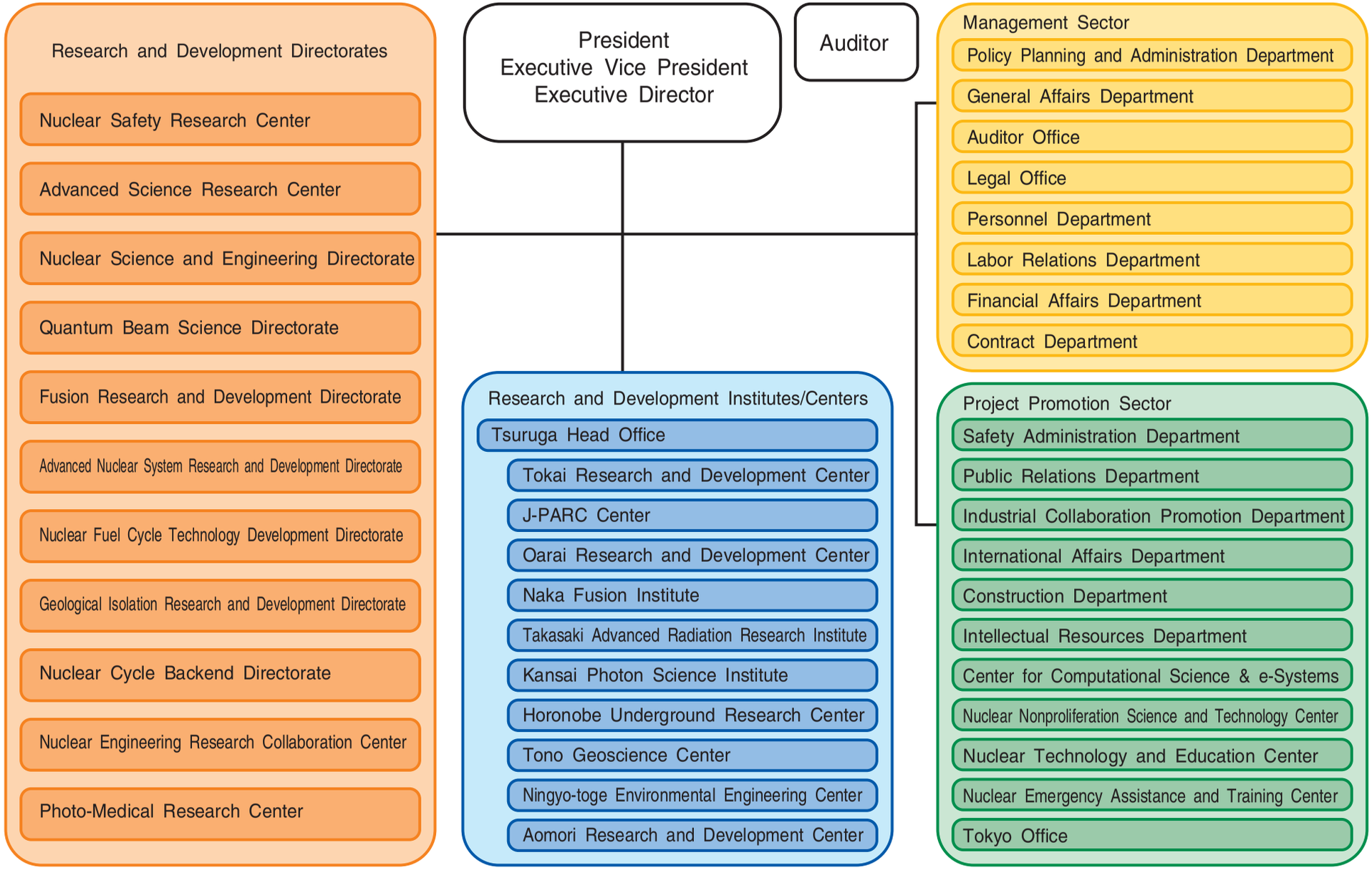

About the Design of the Cover:

The cover is designed to envisage a hopeful future shining in the sky with a blue color derived from the color of the JAEA logo. This is accompanied with white colored hexagons similar to the pattern in a tortoise shell which symbolizes the wish of people for longer lives from ancient times in Japan. Coincidentally, this shape is the same as that of the core fuel assemblies for both the prototype "MONJU" Fast Breeder Reactor, and the High Temperature Test Reactor "HTTR".

The picture in the upper left shows a Compact Laser-driven ion accelerator which has the ability to produce a MeV-energy proton beam. The picture in the lower right circle shows crystals of uranyl nitrate which were extracted by a rotary driven crystallizer.

JAEA R&D Review 2008

Published by Japan Atomic Energy Agency (JAEA)
Editorial Office: Intellectual Resources Section, Intellectual Resources Department
2-4 Shirakatashirane, Tokai-mura, Naka-gun, Ibaraki-ken 319-1195, Japan
Phone: +81-29-282-6387 Facsimile: +81-29-282-5920
e-mail: ird-seika_shi@jaea.go.jp

Japan Atomic Energy Agency